UNIVERSITÀ DEGLI STUDI DI ROMA "FORO ITALICO"
Ph.D. in Human Movement and Sport Science
XXXVIII Cycle

Neuromuscular Mechanisms underlying Motor Coordination in Young and Older Adults during Dynamic Balance Control

Candidate: Imma Ceriello

Supervisor: Prof. Andrea Macaluso

Co-Supervisor: Prof. Valentina Camomilla

Coordinator: Prof. Maria Francesca Piacentini

Sites of Activity: Laboratory of Bioengineering and Neuromechanics of Movement

SSD: BIOS-06/A; IBIO-01/A

ABSTRACT

Dynamic balance control relies on the integration of multisensory inputs, coordinated neuromuscular activation, and whole-body biomechanical organization. Everyday tasks such as upright reaching or rising from a chair challenge these processes by requiring controlled shifts of the center of mass while maintaining postural stability. While it is established that aging diminishes sensory reliability, slows neuromuscular responses, and alters movement strategies, the exact ways these changes affect balance regulation are still not fully understood. Traditional clinical assessments are limited in their ability to capture the underlying neural and modular structure of movement. Therefore, this thesis investigates neuromuscular and kinematic mechanisms that shape balance control across different tasks and age groups.

To address this gap, a series of studies were conducted to examine the structure of muscle synergies, neural coupling via intermuscular coherence, and joint kinematic coordination during functional movements. These complementary investigations shed light on how the central nervous system (CNS) simplifies motor control through modular organization, how neural signals are distributed among muscles, and how the mechanical degrees of freedom of the body are coordinated to perform voluntary destabilizing tasks.

In the first study, muscle synergies underlying multidirectional upright reaching in young adults were assessed. The results revealed direction-dependent yet robust synergies, suggesting that the CNS relies on a stable modular repertoire while flexibly modulating its recruitment depending on task demands.

The second study investigated neural synchronization among trunk and lower-limb muscles during the same multidirectional upright reaching tasks. Coherence patterns varied according to reach direction, revealing direction-dependent adjustments in shared neural inputs and indicating that muscle coordination reflects not only mechanical demands but also centrally driven control strategies.

In the third study, bilateral muscle synergies during a rising-from-a-chair task were analyzed to characterize their relationship with the body center of mass dynamics. Mapping synergy activation to center of mass position revealed functionally interpretable patterns that were independent of movement timing or limb dominance.

The fourth study extended this analysis to older adults performing the same task. Although the spatial composition of synergies remained preserved, aging significantly affected their temporal structure, producing earlier and broader activations. These alterations were

accompanied by changes in center-of-mass–synergy associations, suggesting a shift toward more global and less efficient control strategies.

The fifth study evaluated the effects of aging on synergy organization during multidirectional upright reaching. Older adults showed fewer synergies in tasks with greater mediolateral demands and broader activation profiles, suggesting compensatory strategies to maintain stability.

Finally, the sixth study examined kinematic synergies during multidirectional upright reaching in young adults, identifying consistent coordination patterns across directions that reflect the mechanical principles of whole-body balance regulation.

Collectively, the findings show that while the fundamental structure of motor modules is largely preserved across tasks and age groups, the CNS modulates their recruitment, timing, and neural coupling depending on directional demands, postural complexity, and age-related constraints. Older adults exhibit increased coactivation, reduced modular dimensionality under mediolateral challenges, and temporal broadening of module activity, suggesting a shift from flexible, task-specific control to more generalized and conservative strategies. These results provide new insight into the organization, adaptability, and deterioration of balance-related neuromuscular coordination and suggest potential biomarkers and targets for personalized rehabilitation aimed at restoring efficient postural control.

ABSTRACT (in italiano)

Il controllo dinamico dell'equilibrio dipende dall'integrazione di informazioni multisensoriali, dall'attivazione neuromuscolare coordinata e da un'organizzazione biomeccanica armonica dell'intero corpo. Movimenti quotidiani come il reaching da stazione eretta o l'alzarsi da una sedia mettono alla prova questi meccanismi, richiedendo spostamenti controllati del centro di massa mantenendo al tempo stesso stabilità posturale. Nonostante sia noto che l'invecchiamento comprometta l'affidabilità sensoriale, rallenti la risposta neuromotoria e modifichi le strategie di movimento, l'impatto preciso di tali cambiamenti sui meccanismi di controllo dell'equilibrio rimane non completamente esplorato. Inoltre, gli strumenti clinici tradizionali non permettono di cogliere le strutture neurali e modulari che sottendono il movimento. Da qui nasce l'obiettivo di questa tesi: analizzare i meccanismi neuromuscolari e cinematici che caratterizzano l'equilibrio dinamico in giovani e anziani durante compiti funzionali specifici della vita quotidiana.

A tal fine, sono stati condotti sei studi che combinano l'analisi delle sinergie muscolari, la coerenza intermuscolare e la decomposizione delle sinergie cinematiche. Questo approccio integrato permette di comprendere come il sistema nervoso centrale (SNC) organizzi il movimento in moduli funzionali, come i comandi neurali siano distribuiti tra gruppi muscolari e come i vari gradi di libertà del corpo vengano coordinati durante compiti che richiedono volontariamente una destabilizzazione controllata.

Nel primo studio sono state analizzate le sinergie muscolari coinvolte in compiti di reaching multidirezionale in stazione eretta nei giovani adulti. È emerso un insieme di sinergie stabile, sul quale il SNC interviene modulando l'attivazione in base alla direzione del movimento, a conferma di un repertorio modulare coerente ma flessibile.

Il secondo studio ha invece esaminato la sincronizzazione neurale tra i muscoli del tronco e degli arti inferiori negli stessi soggetti e compiti. I pattern di coerenza variavano in funzione della direzione, evidenziando aggiustamenti negli input neurali condivisi e indicando che il coordinamento muscolare non risponde soltanto alle richieste meccaniche, ma riflette anche strategie di controllo di origine centrale.

Il terzo studio ha analizzato le sinergie muscolari bilaterali durante il compito di alzarsi da una sedia, con l'obiettivo di comprenderne la relazione con la dinamica del centro di massa. L'associazione tra attivazione delle sinergie muscolari e posizione del centro di massa ha rivelato pattern funzionali chiari e interpretabili, indipendenti dal tempo di esecuzione o dalla dominanza degli arti.

Il quarto studio ha esteso lo stesso approccio agli adulti anziani. Sebbene la struttura spaziale delle sinergie risultasse sostanzialmente conservata rispetto ai giovani, l'invecchiamento ha inciso in modo marcato sulla componente temporale, con attivazioni più anticipate e prolungate. Questi cambiamenti erano associati a differenti relazioni tra sinergie e centro di massa, suggerendo strategie di controllo più globali e meno efficienti rispetto ai giovani.

Il quinto studio ha valutato l'effetto dell'età sull'organizzazione delle sinergie durante compiti di reaching multidirezionale. Negli anziani è emerso un numero inferiore di sinergie nei compiti che richiedono un maggiore controllo medio-laterale, insieme a profili di attivazione più ampi. Tali modifiche sembrano riflettere strategie compensative adottate per mantenere la stabilità in condizioni posturali più impegnative.

Il sesto studio ha infine esaminato le sinergie cinematiche nei giovani adulti durante gli stessi compiti di reaching multidirezionale, identificando pattern di coordinazione coerenti tra le diverse direzioni, in linea con i principi biomeccanici che regolano l'organizzazione del movimento e il controllo dell'equilibrio.

Complessivamente, il lavoro mostra che, sebbene la struttura spaziale dei moduli motori sia ampiamente preservata nel corso dell'invecchiamento, è il loro reclutamento temporale, insieme alla distribuzione dei comandi neurali, a modificarsi in relazione alla complessità posturale e alle richieste direzionali, con effetti misurabili sulla cinematica, sulla stabilità e sull'efficacia del movimento. Con l'avanzare dell'età, questi cambiamenti suggeriscono una transizione verso strategie più conservative e meno flessibili. I risultati offrono una comprensione più profonda dell'organizzazione neuromeccanica dell'equilibrio dinamico e indicano potenziali biomarcatori e obiettivi per interventi riabilitativi mirati a preservare o recuperare un controllo posturale efficace.

GLOSSARY

AD: Anterior Deltoid

APAs: Anticipatory Postural Adjustments

APRs: Automatic Postural Responses

BBS: Berg Balance Scale

BF: Biceps Femoris

BoS: Base of Support

biFR: bilateral Functional Reach

C: Muscle Synergy Activation Coefficients

CCI: Co-Contraction Index

CGM: Convolutional Gait Model

CNS: Central Nervous System

CoA: Center of Activation

CoM: Center of Mass

CoP: Center of Pressure

CrossVAF: Cross-Variance Accounted For

$\text{CrossVAF}_{\text{avg}}$: averaged Cross-Variance Accounted For

CS: Cosine Similarity

D: Dominant

D_{max}: Maximum Distance

$\text{Displ}_{\text{CoM}}$: Center of Mass Displacement

DoFs: Degrees of Freedom

EMG: Electromyography

ES: Erector Spinae

FA: Factor Analysis

FR: Functional Reach

FWHM: Full Width at Half Maximum

GastM: Gastrocnemius Medialis

GUI: Graphical User Interface

ICA: Independent Component Analysis

LD: Latissimus Dorsi

LMMs: Linear-Mixed effects Models

LR: Lateral Reach

MMSE: Mini-Mental State Examination

MSE: Mean Squared Error

ND: Non-Dominant

NNMF: Non-Negative Matrix Factorization

PCA: Principal Component Analysis

PiG: Plug-in Gait

PL_{CoM}: Center of Mass Path Length

PL_{CoP}: Center of Pressure Path Length

rmANOVA: repeated measures Analysis Of Variance

RMS: Root Mean Square

RoM: Range of Motion

SD: Standard Deviation

SE: Standard Error

SnPM: Statistical non-Parametric Mapping

Sol: Soleus

SPM: Statistical Parametric Mapping

STS: Sit-to-Stand

TA: Tibialis Anterior

TUG: Timed Up and Go

uniFR: unilateral Functional Reach

unplFR: unplanned Functional Reach

VAF: Variance Accounted For

VL: Vastus Lateralis

W: Muscle Synergy Weights

PART I

1. Introduction

1.1. Research Context and Motivation

Efficient balance control is fundamental to human motor behavior, supporting both stable postures and voluntary transitions that require the body to reorganize its mechanical configuration while maintaining the center of mass (CoM) within safe limits. Everyday tasks, such as reaching, leaning, or rising from a chair, demand finely tuned coordination among sensory processing, neural control, and musculoskeletal function. Such demands require the neuromuscular system to continuously integrate sensory information, adjust motor output, and coordinate multiple joints in a flexible and task-specific manner. Although such processes operate seamlessly in young and healthy individuals, they become increasingly challenged with advancing age. Because these everyday actions are central to functional independence, even subtle changes in balance control can meaningfully affect autonomy, mobility, and quality of life in older adults.

Although many age-related sensory and motor changes have been documented, how these alterations affect the neuromuscular mechanisms that support motor coordination during dynamic balance is still not fully understood. Traditional assessments tend to focus on observable performance limitations, such as reduced stability, slower movements, or shorter reach, but provide limited insight into how the Central Nervous System (CNS) organizes and regulates coordinated movement. As a result, the link between age-related behavioral changes and the underlying neuromechanical processes often remains unclear.

Muscle synergy analysis, intermuscular coherence, and kinematic synergy analysis offer an opportunity to infer the modular and neural architecture of motor control. By reducing complex muscle activations into low-dimensional modules, synergy analysis provides insight into how the CNS simplifies control of redundant musculoskeletal degrees of freedom. Intermuscular coherence reveals frequency-specific synchronization among muscle groups, offering a window into shared neural inputs. Kinematic synergies describe how joints co-vary mechanically to generate functional whole-body movements.

By combining complementary neuromuscular and kinematic analyses across controlled yet ecologically relevant motor tasks, this work seeks to clarify how the CNS organizes movement under varying postural demands, and how these organizational principles evolve with aging.

Understanding the neuromuscular and mechanical structures that support everyday tasks, and how these structures evolve across the lifespan, can provide critical insights into both normative motor control and pathological or age-related deviations.

The motivation of this doctoral work is therefore twofold:

i. to establish a multi-level biomechanical and neurophysiological characterization of dynamic balance control in young adults, and
ii. to determine how aging affects modular coordination, neural coupling, and biomechanical execution.

This framework aims to bridge the gap between understanding functional behavior and its underlying neural mechanisms, providing a foundation for identifying early markers of balance deterioration and guiding targeted rehabilitation interventions.

1.2. Thesis at a glance

The thesis is structured into four main parts, guiding the reader from the theoretical background to the experimental work and its broader implications.

Part I introduces the research context, outlines the motivation behind the work, and presents the overall structure of the thesis. It also reviews the relevant literature, covering the neurophysiological, biomechanical, and methodological foundations necessary to understand the studies that follow. In addition, it provides a general methodological framework, including ethical approval, participant characteristics, and the experimental setups and protocols used across the different studies.

Part II presents the six experimental studies that constitute the core of the thesis. Each chapter includes the study-specific rationale, methods, results, and a dedicated discussion, allowing each investigation to be read both independently and as part of a coherent research trajectory.

Part III provides an integrated discussion that synthesizes the findings across the experimental chapters, highlights the overarching principles that emerge from the collected evidence, and outlines directions for future research.

Part IV presents supplementary materials that support and extend the main experimental work.

This structure is designed to guide the reader from fundamental concepts to specific empirical findings and, ultimately, to a broader interpretation of how the studied mechanisms advance our understanding of dynamic balance control and its alterations with aging.

2. Overview on Postural Control and Balance

2.1. Posture and Balance

Posture can be defined as the spatial organization of body segments in relation to one another and their surrounding environment (Horak & Macpherson, 2011; Massion, 1992, 1994). It represents an active and adaptive process through which the body maintains both stability and readiness for movement (Bouisset & Do, 2008). The continuous regulation of posture ensures that body segments remain adequately aligned for functional actions while counteracting internal and external perturbations that may compromise balance. In this context, posture serves as the foundation upon which all voluntary and automatic motor behaviors are organized.

Postural control may be defined as the act of maintaining, achieving or restoring a state of balance during any posture or activity (Pollock et al., 2000). It encompasses two interrelated objectives: postural orientation and postural equilibrium (Horak, 2006; Horak & Macpherson, 2011). Postural orientation pertains to the alignment of body segments in relation to gravity, the support surface, and external references such as the visual and somatosensory environment. It determines the spatial positioning of the body, thus providing a framework for perception and movement. Postural equilibrium, also referred to as postural stability, may be defined as the capacity of the body to maintain its CoM within the boundaries of its Base of Support (BoS) (Horak, 1987). The BoS corresponds to the area of contact between the body and the support surface, with equilibrium preserved as long as the projection of the CoM remains within this area. Together, orientation and equilibrium facilitate the maintenance of a stable yet adaptable relationship with the environment.

The ability to orient the body concerning gravity, the support surface, visual surroundings, and internal reference frames, along with the capacity to adapt this orientation automatically according to contextual and task-related demands, constitutes a key attribute of postural control. Through the integration of multisensory signals, the CNS ensures that the body remains balanced, aligned, and ready to engage effectively with an ever-changing environment. Somatosensory inputs pertinent to posture include pressure signals from the skin in contact with the support surface, orientation data from muscle proprioceptors and joint receptors, and feedback regarding muscle length, velocity, and force. Such inputs are crucial for generating timely responses to external disturbances. Vestibular inputs primarily contribute to the orientation of the head and trunk relative to gravity, which is particularly vital when the support surface exhibits instability. Visual information supplies knowledge regarding body

sway and orientation within the environment and offers anticipatory cues about potentially destabilizing situations. Vision enhances the capacity to perceive the direction and velocity of sway and enables the individual to understand the body's orientation in relation to both vertical and horizontal visual frames of reference (Horak, 2009). The ability to maintain and adjust balance through this integrated system underlies all functional motor behaviors, spanning from simple stance to complex locomotion and skilled actions, applicable in both stationary and dynamic contexts. Indeed, balance can be conceptualized in both static and dynamic terms. Static balance refers to the maintenance of the body's position when stationary (Kandel et al., 2012), while dynamic balance involves the regulation of the CoM during movement or following perturbations (Horak et al., 1997; D. Winter, 1995). In both scenarios, balance signifies the capacity to produce appropriate and coordinated muscular responses that reposition the CoM over the BoS without excessive sway or loss of alignment. Effective balance control, therefore, necessitates a continual compromise between stiffness and flexibility: the postural system must possess enough rigidity to resist perturbations while simultaneously being compliant enough to allow for efficient movement. This delicate equilibrium underscores the dual function of posture as both a stabilizing and enabling mechanism for motion. In this regard, posture and balance are not passive states, but rather dynamic processes that sustain both stability and mobility, ensuring that the body remains oriented, aligned, and poised for interaction with its surrounding environment.

2.2. Neural Strategies for Maintaining Stability

This dynamic interplay between stability and mobility becomes evident in daily life, where the body must preserve balance while performing purposeful actions. Postural stability is achieved through the coordinated efforts of the CNS, which integrates both anticipatory and compensatory mechanisms that serve to either prevent or correct destabilization. Two fundamental types of postural adjustments can be distinguished: automatic postural responses (APRs), which represent rapid compensatory reactions to external perturbations, and anticipatory postural adjustments (APAs), which occur in preparation for voluntary movements. APRs represent rapid compensatory reactions to unexpected external perturbations and rely predominantly on feedback control mechanisms. These responses are triggered within approximately 100 ms of disturbance onset and involve the coordinated activation of several muscles that generate corrective torques to counteract body motion (Horak, Diener, et al., 1989). In contrast, APAs act proactively, engaging feedforward control to stabilize the body before the onset of a voluntary movement or predictable perturbation

(Bouisset et al., 2000; Massion, 1992). Together, automatic and anticipatory mechanisms ensure that balance is maintained across both predictable and unpredictable conditions, allowing smooth transitions between stability and movement (Latash et al., 2005). Stability is maintained through a dynamic interaction between feedforward and feedback control mechanisms. Feedforward mechanisms use internal models of body dynamics to predict the sensory outcomes of self-generated movements, while feedback mechanisms monitor real-time sensory inputs to identify and correct any deviations from expected states (Horak, 2006). This dual system enables the CNS to minimize response times while remaining adaptable.

The neural architecture supporting these mechanisms is organized across multiple hierarchical levels that operate in parallel. The CNS is conventionally viewed as having three main levels of organization, the spinal cord, brainstem, and cortex, each contributing distinct but interdependent functions (Loram, 2015). The spinal cord provides rapid, short-latency reflex responses that enhance joint stiffness and counteract small perturbations (Prochazka, 2009). At the intermediate level, the brainstem integrates multisensory information and coordinates automatic postural adjustments via the vestibulospinal and reticulospinal pathways, ensuring head–trunk alignment and equilibrium against gravity (Horak & Macpherson, 2011; Takakusaki, 2017). The basal ganglia act as a dynamic gating system for the selection and scaling of postural strategies, while the cerebellum refines motor output through cortico-cerebellar circuits that support predictive control and sensory-based adaptation (Loram, 2015; Takakusaki, 2017). The cerebral cortex, along with subcortical loops from the basal ganglia and cerebellum, provides the highest level of control, supporting a large and adaptable motor repertoire (Loram, 2015). These cortical-subcortical interactions establish a functional hierarchy, facilitating a shift in control from reflexive stabilization to predictive and intentional coordination.

Through the integration of these hierarchical processes, the CNS generates postural strategies that either maintain or restore equilibrium in response to internal or external demands. These strategies can be broadly categorized as fixed-support, wherein the CoM is returned over the existing BoS, and change-in-support, which involves the modification of the BoS through stepping or reaching movements (Horak & Nashner, 1986; Maki & McIlroy, 1997). Within the fixed-support classification, the ankle strategy is predominant for small perturbations on stable surfaces, while the hip strategy is employed when larger or more rapid adjustments are necessary. Importantly, these strategies are not discrete entities; rather, they exist along a continuum, flexibly combined based on the magnitude of perturbation, sensory conditions, and

prior experience. The implementation of these strategies depends on the coordinated activation of multiple muscles.

2.3. Alterations in Balance Control in Older Adults

As individuals age, there is a gradual reorganization of the systems that underpin postural stability. The capacity to maintain and recover balance increasingly diminishes due to the declining reliability of sensory information, the slowing and less coordinated nature of muscular responses, and the heightened demand for cognitive resources. These changes are not merely indicative of the inevitable decline of a single system; rather, they represent the cumulative result of subtle degradations across sensory, motor, and cognitive domains, which collectively alter the dynamics of balance control (Horak, Shupert, et al., 1989; P.-F. Tang & Woollacott, 2004).

One of the earliest and most widespread age-related changes involves the integration of sensory information. The somatosensory system, responsible for detecting body position and motion relative to the support surface, experiences a decline in joint position sense, particularly in the lower limbs (Lord et al., 1991b; Manchester et al., 1989). This reduction in proprioceptive sensitivity diminishes the accuracy of feedback necessary for detecting subtle perturbations, resulting in an increased reliance on visual input (Hay et al., 1996). However, the visual system also deteriorates with age: acuity, contrast sensitivity, and depth perception all decline, and the processing of optic flow slows down (Lord & Ward, 1994; P.-F. Tang & Woollacott, 2004). Furthermore, the vestibular system undergoes age-related degeneration, which leads to a decreased sensitivity to both angular and linear accelerations (Peterka & Black, 1990). Collectively, these sensory changes impair the ability to dynamically reweight sensory inputs. As a result, older adults tend to exhibit slower and less flexible adjustments when switching between sensory cues, particularly in situations of sensory conflict (Woollacott et al., 1986). Alongside sensory decline, there is a gradual deterioration of the neuromotor system (Iosa et al., 2014; Shumway-Cook & Woollacott, 2017; Y.-C. Tsai et al., 2014). This deterioration manifests at various levels, including the progressive loss of skeletal muscle strength (Doherty, 2003; Hortobágyi et al., 1995), altered temporal organization of muscle responses (Y.-C. Tsai et al., 2014), and increased co-activation of antagonist muscles (Papegaaij et al., 2014; Peterson & Martin, 2010). These changes collectively result in less coordinated, slower, and more energy-consuming postural responses. Biomechanical factors amplify these neuromuscular limitations. The restricted range of motion (RoM) constrains the available BoS and limits compensatory movement strategies (Nonaka et al., 2002; Roach & Miles, 1991). When

combined with slowed neuromotor responses, this stiffness causes even minor perturbations to shift the CoM beyond stable limits (S. Clark et al., 2005). Consequently, older adults exhibit greater sway amplitudes, longer recovery times, and less energy-efficient control during both quiet stance and dynamic balance tasks (Maki et al., 1990). Cognitive involvement in postural control also becomes more prominent with age (Melzer et al., 2001). Tasks that previously relied mainly on automatic control now require increased attentional resources (Beurskens & Bock, 2012). Furthermore, emotional and psychological factors, particularly fear of falling, can further alter motor strategies (Lord et al., 1991a; Okada et al., 2001).

In summary, the changes in balance control associated with aging result from a complex interplay of sensory decline, neuromotor deterioration, biomechanical rigidity, and heightened cognitive demand. Together, these processes culminate in slower, less precise, and more energy-consuming control of posture, which increases the risk of falls and diminishes independence. However, current understanding of CNS control of balance in healthy older adults remains limited.

3. Bridging levels of Motor Control

3.1. The Degrees of Freedom Problem: Motor Redundancy

The control of voluntary movement represents the most complex functions of the CNS. Even performing straightforward, daily tasks like reaching for an item or maintaining an upright position necessitates the coordination of many muscles and joints, each with several mechanical degrees of freedom (DoFs). This essential challenge was first articulated by Nikolai Bernstein in his landmark book, *The Coordination and Regulation of Movements* (1967), where he introduced what is known as the "degrees of freedom problem" (Latash, 1993, 2024; Turvey, 1990). Bernstein pointed that the human body has an exceedingly large number of effectors capable of achieving the same motor outcome through countless combinations of joint torques and muscle activations. This motor redundancy suggests that the CNS must choose one specific solution from an infinite array of possibilities to complete a task. To address this issue, Bernstein proposed that the nervous system could manage the complexity of motor control by organizing individual components, muscles, joints, and even motor units, into functional groupings that can be controlled by shared variables. He referred to these functional groupings as synergies. In its most general sense, the term *synergy*, literally "working together", refers to the coordinated activation of multiple elements acting toward a common goal. In this perspective, the CNS does not control each muscle (or joint) individually but rather coordinates

sets of muscles (or joints) as single functional units, which decreases the number of independent variables needed to produce movement. In this manner, the existence of synergies would facilitate control by reducing the dimensionality of the motor command while still allowing for flexibility and adaptability across various motor contexts. This concept of coordinated simplification provided a theoretical resolution to the issue of motor redundancy and directly connects Bernstein's original question regarding redundancy to contemporary theories of muscle synergies.

3.2. Muscle Synergy Theory

The hypothesis of muscle synergies offers a comprehensive framework for understanding how the CNS efficiently manages motor control despite the complexity and redundancy of the musculoskeletal system. Building on Bernstein's concept that the CNS may coordinate groups of effectors using common control variables, this theory suggests that muscles are not activated independently but rather through the recruitment of a limited number of functional modules, or synergies (Bizzi & Cheung, 2013; Latash, 2024; Turvey, 1990). By combining and scaling these modules, the CNS is capable of producing the diverse range of movements observed in humans and animals, all while maintaining computational efficiency and adaptability (d'Avella et al., 2003; d'Avella & Bizzi, 2005; Ting & McKay, 2007).

Muscle synergies are thus conceived as low-dimensional neural constructs that capture the regularities in the co-activation of muscles during various tasks. Typically, a synergy is viewed as a spatial module, a fixed group of muscles that tend to activate collectively, whose contribution to motor output is adjusted over time based on task requirements. The flexible combination of these modules enables the CNS to produce complex, natural, and efficient movements by orchestrating the activity of several muscles simultaneously (Bizzi & Cheung, 2013; Torricelli et al., 2016; Tresch & Jarc, 2009). According to Bizzi and Cheung (2013), the neural basis of muscle synergies can be traced to spinal circuits, where groups of muscles are co-activated via pre-structured networks that act as fundamental building blocks for movement. However, these spinal modules do not function in isolation; their recruitment is continuously influenced by inputs from brainstem and cortical regions, forming an integrated control network that allows for both stability and flexibility in motor behavior. This organization suggests a cooperative hierarchy, where descending motor commands from higher centers engage pre-structured spinal modules, and sensory feedback continuously refines their activation, resulting in flexible and coordinated muscle activity (Cheung et al., 2005; Ting & McKay, 2007).

Consequently, understanding this cooperative hierarchy has motivated the development of quantitative approaches aimed at providing an objective and non-invasive way to evaluate these muscle synergies during different motor tasks. By recording surface electromyographic (EMG) signals, researchers can decompose muscle activations into a smaller set of invariant components that correspond to the underlying neural modules. The most commonly used method is Non-Negative Matrix Factorization (NNMF) (Lee & Seung, 1999) (see **Chapter 7, Section 7.3** for further details). Other factorization techniques such as Principal Component Analysis (PCA), Independent Component Analysis (ICA), and Factor Analysis (FA) have produced comparable decompositions, confirming that the extracted synergies represent consistent and physiologically meaningful features of motor organization rather than methodological artefacts (Tresch et al., 2006).

Over the past two decades, muscle synergy analysis has been widely utilized to investigate spinal modularity and coordination across various motor behaviors (Chvatal & Ting, 2012; d'Avella et al., 2006; Dominici et al., 2011; Ghislieri et al., 2023; Pellegrino et al., 2020; Rimini et al., 2017; Saito, Yokoyama, Sasaki, Matsushita, et al., 2023; Sylos-Labini et al., 2020; Yokoyama et al., 2021; Zhao et al., 2019).

In the domain of postural control, this approach has been particularly informative. Studies on balance have investigated how muscle synergies contribute to automatic postural responses triggered by external or self-generated disturbances while standing (Torres-Oviedo & Ting, 2007, 2010), across different postural configurations including narrow, wide, crouched, and single limb stance (Torres-Oviedo and Ting 2010; Ghislieri et al. 2020), during multidirectional isometric force generation while maintaining an upright posture (Monte et al., 2024), and in a variety of postural responses such as hip, ankle, stepping, and feet in place (Chvatal et al., 2011). Overall, these studies indicated that, as task complexity increases, only minor adjustments occur in the fundamental motor control strategies involved in postural balance. This consistency suggests that the CNS relies on a set of pre-existing synergies that can be flexibly modulated to meet the specific demands of each condition, without the need to generate entirely new motor solutions (Torres-Oviedo & Ting, 2010). Consistent results have been observed in various functional tasks that also challenge postural stability, including sit-to-stand transitions (Ranaldi et al., 2023; Yang, An, Yamakawa, Tamura, Yamashita, & Asama, 2017), gait initiation (Falaki et al., 2023), and stepping reactions (Chvatal et al., 2011; Y. Wang et al., 2017). Extending synergy analysis to everyday motor behaviors may provide new insight into how the CNS flexibly orchestrates muscle synergies to ensure both stability and adaptability. However,

while synergy analysis elucidates the functional organization of movement, it does not fully reveal the neural processes that sustain it. Thus, this perspective lays the foundation for exploring how common neural inputs may underpin motor coordination.

3.3. Intermuscular Coherence

Muscle synergy analysis alone is insufficient for accurately identifying the neural origins of synergy formation. It has been suggested that correlated neural input might serve as the mechanisms through which the CNS organizes the activation of muscles that work together as a synergistic muscle group (Boonstra et al., 2009; Danna-Dos-Santos et al., 2014; Degani et al., 2017; Farmer et al., 2007). This stems from the idea that synchronizing neural oscillations is how the CNS accomplishes extensive integration among its cortical and subcortical components, including those that play a role in the generation and regulation of movement. Intermuscular coherence (EMG-EMG coherence) offers a framework to examine synchronized activity between two electromyographic signal in the frequency domain (Farmer et al., 1993) and can yield insights into shared neural inputs: identifying coherence within specific frequency bands allows inference about the origin and functional role of common neural drives that differ according to the functional demands of the task (Baker et al., 1997). Thus, it provides an indirect assessment of such shared common drive, serving as a valuable method to assess oscillatory coupling and neural synchronization. Intermuscular coherence is typically characterized within four main frequency bands; each associated with specific neural processes. Low-frequency oscillations ranging from 0–5 Hz, defined as the delta band, are associated with the common modulation of motor unit mean firing rates and muscle force production, thus likely reflecting co-modulation of muscle activity (Boonstra et al., 2009; De Luca & Erim, 1994; Kamen & and De Luca, 1992; Lowery et al., 2007; Myers et al., 2004). Oscillatory activity within the alpha band (8–12 Hz) has been linked to physiological tremor (Budini et al., 2014; McAuley & Marsden, 2000) and the engagement of the cortico-reticulospinal pathway (M. R. Baker & Baker, 2003; Charalambous et al., 2024; Conway et al., 1995; Grosse & Brown, 2003). Higher frequency oscillations in the beta (13–35 Hz or 15–30 Hz) and low gamma (35–60 Hz or 30–60 Hz) frequency ranges are related to the functioning of the transcortical pathway and reflect shared corticospinal inputs to the motoneuron pool (Charalambous et al., 2024; Conway et al., 1995; Fisher et al., 2012).

Building on this physiological framework, several studies have applied intermuscular coherence to various postural control tasks, including static stance, unipedal tasks, and forward leaning, providing insights into how the CNS adapts to varying levels of balance challenge under

different conditions and organizes the activation of muscles (Danna-Dos-Santos et al., 2014; García-Massó et al., 2016; Konieczny et al., 2022; Nandi et al., 2019; Noé et al., 2017; Nojima et al., 2020; Tsiouri et al., 2024; Watanabe et al., 2018a, 2018b). Together, these studies show that coherence is sensitive to task difficulty and reflects functional neural coordination that varies across postural and motor behaviors. The majority of studies to-date have focused on trunk and lower limb muscles, particularly ankle plantar- and dorsi-flexor muscles, given their role in maintaining postural stability and controlling body sway (Danna-Dos-Santos et al., 2014; Noé et al., 2017; Watanabe et al., 2018a, 2018b). Robust coherence has been reported between bilateral/unilateral plantar flexor muscles and between agonist–antagonist pairs (e.g., tibialis anterior and plantar flexors) (Boonstra et al., 2015; Degani et al., 2020; Nandi et al., 2019; Noé et al., 2017; Nojima et al., 2020; Watanabe et al., 2018a, 2018b). Coherence between trunk and lower limb muscles has also been observed, underscoring the integration of proximal and distal muscles in balance control (Danna-Dos-Santos et al., 2014; Degani et al., 2017; Noé et al., 2017). While intermuscular coherence has been investigated during isolated postural tasks, compound movements involving dynamic transitions from quiet standing to perturbed or destabilized postures remain largely unexplored. Evaluating intermuscular coherence during these movements could provide key insights on the neurophysiological adaptation of postural control in everyday voluntary movements entailing sudden changes and movement initiation under unstable conditions.

3.4. Kinematic Synergies

Recent research has expanded the concept of synergy beyond muscular coordination to encompass the biomechanical domain, introducing the idea of kinematic synergies. Kinematic synergies refer to stable correlations among joint angles or body segments that reflect the mechanical organization of movement (Grinyagin et al., 2005). These synergies illustrate how different degrees of freedom co-vary to achieve a behavioral goal, complementing the study of muscle synergies that describe how neural circuits activate the musculoskeletal system (Esmaeili et al., 2022). The integration of kinematic and muscle synergy analysis presents a robust framework for investigating the intricate interactions among neural activity, biomechanics, and motor behavior that culminate in coordinated movement.

Over the past two decades, kinematic synergies have gained widespread application in characterizing motor control strategies across various domains, including gait and upper limb movements.

In the field of gait analysis, kinematic synergies have proven instrumental in elucidating the biomechanical functions of muscle synergies underlying locomotion, thereby establishing a one-to-one correspondence between muscle and kinematic synergies during ambulation (Esmaeili et al., 2022). Research indicates that aging significantly alters gait patterns and velocity; however, it does not appear to affect the structural integrity of kinematic synergies (Yamagata et al., 2021). Conversely, a history of falls may modify these patterns, as individuals adopt compensatory mechanisms or manifest a fear of instability (Yamagata et al., 2019). In developmental research, kinematic synergies have aided in monitoring motor growth, revealing age-related asymmetries between limbs that gradually diminish with development, as well as identifying gait imbalances in conditions like Duchenne muscular dystrophy (Xiong et al., 2022, 2023).

In the context of upper limb movements, kinematic synergies have been extracted to characterize reaching behavior and to refine the control mechanisms of assistive and robotic devices. They have offered a compact description of the coordination among fingers and joints, consistent with neuroimaging findings that suggest synergy-based control of the hand is represented in human motor cortical areas (Leo et al., n.d.; Santello et al., 2013). Moreover, empirical studies indicate that lower-order synergies effectively capture primary motion patterns, while higher-order synergies enhance the precision of reaching tasks (S. Tang et al., 2019). Such findings have fostered the development of synergy-based interfaces for exoskeletons and prosthetic control, facilitating more natural and coordinated movements (Garcia-Rosas et al., 2018; Lapresa et al., 2022).

In summary, this body of work suggests that kinematic synergies serve as a unifying principle underlying human movement organization. A comprehensive understanding of their structural characteristics and variability across disparate tasks could provide insights into the mechanisms of motor control, informing advancements in rehabilitation strategies and robotic applications.

4. Dynamic Balance Assessment Tasks

4.1. Functional Reach

Among the various clinical tests used to evaluate postural stability, the Functional Reach (FR) test is one of the most widely adopted tools to assess dynamic balance in both healthy individuals and those with neurological or musculoskeletal impairments. Originally proposed by (Duncan et al., 1990), the FR quantifies the maximum distance an individual can reach

forward beyond arm's length from a fixed standing position without losing balance. The task demands transitioning from a stable upright posture to a forward-leaning position, thus eliciting self-induced perturbations that challenge the ability to control balance dynamically. Duncan and colleagues demonstrated that forward reach distance correlates with the anteroposterior excursion of the center of pressure and provides a precise and repeatable measure of postural stability, with values below six inches being strongly associated with a high risk of falling in older adults (Duncan et al., 1992). Following studies confirmed its clinical practicality and predictive value for physical frailty and fall risk (Tyson & DeSouza, 2004; Weiner et al., 1992).

While the traditional FR test focuses on anterior–posterior stability, several variants have been developed to assess multidirectional balance control, such as bilateral or lateral reaching tasks (S. Brauer et al., 1999; Kage et al., 2009; Newton, 2001; Volkman et al., 2007). In particular, the Lateral Reach test evaluates the medial–lateral component of postural stability by measuring the maximal lateral displacement of the arm abducted at 90°, reflecting the ability to control balance in the frontal plane (S. Brauer et al., 1999; DeWaard et al., 2002). In all variants, reaching strategies are not restricted, leading to different motor control patterns and varying levels of task difficulty.

Despite its simplicity, several authors have questioned whether the reach distance alone adequately represents dynamic balance performance (Wernick-Robinson et al., 1999). The execution of FR involves complex coordination among trunk, hip, leg, and ankle joints, and multiple movement strategies can be used to accomplish the task (Liao & Lin, 2008). Consequently, recent research has extended the traditional FR assessment to include kinematic, kinetic, and electromyographic (EMG) analyses under diverse experimental conditions, such as stable versus unstable surfaces (Ennis et al., 2021), upward (Row & Cavanagh, 2007) or lateral reaches (S. Brauer et al., 1999; DeWaard et al., 2002; Thompson & Medley, 2007), seated positions (Marchesi et al., 2021; Thompson & Medley, 2007), progressive target distances (Bohannon et al., 2020), and different movement speeds (Kozak et al., 2003; Y.-J. Tsai & Lin, 2015). From a kinematic perspective, age-related changes have been observed in the adoption of movement strategies, with older adults tending to combine hip flexion and ankle plantarflexion, while younger adults primarily rely on hip motion (Takasaki et al., 2011). Ghahramani et al. (2022) proposed the chest and pelvis coordination to distinguish age-related changes in the FR execution, while (De Waroquier-Leroy et al., 2014) suggested the pelvic translation as a discriminating element.

From a neuromuscular standpoint, EMG investigations have shown that muscle activation during FR is temporally organized and follows a caudo–cranial recruitment sequence, with initial activation of distal anterior muscles (tibialis anterior, rectus femoris, rectus abdominis, sternocleidomastoid) followed by more proximal and posterior muscles (soleus, hamstrings, erector spinae) (Maranesi et al., 2016a). Other studies have observed increased ankle co-contraction on unstable surfaces, reflecting a compensatory mechanism to enhance balance control (Ennis et al., 2021; Nagai et al., 2011).

Altogether, these findings highlight that the FR and its variants represent ecologically valid paradigms for exploring postural stability, as they reproduce voluntary perturbations similar to those experienced in daily life. Yet, despite the valuable insights gained from kinematic and EMG analyses, the underlying neural organization of muscle coordination during these tasks remains largely unexplored. In this context, the study of muscle synergies provides a promising framework for identifying the fundamental control strategies employed by the central nervous system to maintain stability under different directional and biomechanical constraints, and for revealing adaptations across conditions, ages, and populations.

4.2. Sit-to-Stand

The capacity to transition from a seated position to standing is a fundamental prerequisite for maintaining autonomy in daily life. Impairments in this ability are closely correlated with an elevated risk of falls and diminished functional independence among older adults (Inkster & Eng, 2004). Consequently, the Sit-to-Stand (STS) test has emerged as a widely recognized clinical assessment tool utilized to evaluate lower limb strength, functional capacity, and postural stability (Janssen et al., 2002). This assessment is routinely employed to gauge frailty, balance impairments, and sarcopenia (Shukla et al., 2020), often through standardized protocols such as the 5 Times Sit-to-Stand test (Albalwi & Alharbi, 2023; Csuka & McCarty, 1985) or the 30-Second Sit-to-Stand test (Jones et al., 1999). These protocols assess either the time taken to complete 5 repetitions or the total number of repetitions performed within a 30-second timeframe. Recently, these simple and non-invasive assessments have been augmented by instrumented versions that extract detailed kinematic, kinetic, and EMG data, thereby enhancing their diagnostic precision (Frykberg & Häger, 2015; Kılınç et al., 2023; Ranaldi et al., 2024).

From a biomechanical perspective, the STS movement represents a transitional action that connects a stable, supported sitting position to an upright stance (Yoshioka et al., 2009). This transition involves an initial forward displacement of the CoM, which is achieved by flexing the

trunk toward the thighs, followed by a vertical displacement driven by lower limbs extension to achieve the standing position after leaving the seat (Mathiyakom et al., 2005; Y. -C. Pai & Rogers, 1991; Y. -C. Pai et al., 1994). This holistic action involves intricate coordination among multiple joints and muscle groups to maintain stability and avert backward loss of balance.

The STS movement can be categorized into four primary stages (Galli et al., 2008; Schenkman et al., 1990):

i. Flexion–momentum stage, which begins when the trunk bends forward from a stable sitting position to generate momentum and shift the CoM toward the feet.
ii. Momentum-transfer stage, which starts at seat-off, when body weight is transferred from the chair to the lower limbs and the CoM moves above the base of support.
iii. Extension stage, in which the lower limbs straighten to lift the body. The hip, knee, and ankle extensors contract concentrically to raise the body to an upright position.
iv. Stabilization stage, which occurs once full extension is reached and balance is achieved, marking the transition to steady standing.

Given its multi-joint and whole-body dynamics, the STS movement serves as an insightful model for investigating intersegmental coordination and motor control during self-initiated postural transitions.

Distinct movement strategies have been identified in the execution of the STS task (Hughes et al., 1994). Younger adults frequently employ a momentum transfer strategy, capitalizing on forward momentum to facilitate the vertical rise, whereas older adults are more inclined to adopt a stabilization strategy characterized by a measured forward lean to position the CoM directly above the feet prior to leg extension. Additionally, a hybrid strategy incorporating elements of both extremes has been documented.

Biomechanical studies confirm that aging affects the kinematics and kinetics of standing up. Older adults typically show increased trunk flexion, higher antero-posterior CoM velocity, and greater postural sway during the raising and stabilization phases (Papa & Cappozzo, 2000; Piano et al., 2020; Sadeh et al., 2023). Kinetic studies indicate that aging leads to reduced joint torques and power output, especially at the hip and ankle joints (Y.C. Pai et al., 2006; Sadeh et al., 2023), as well as longer movement durations and lower peak vertical ground reaction force values (T. M. Smith et al., 2020).

Neuromuscular compensations accompany biomechanical changes in STS due to aging. Age-related muscular adaptations during STS movements primarily involve changes in the activation patterns of lower limb and trunk muscles. EMG studies have indicated that older

adults demonstrate earlier and more pronounced activations of the quadriceps, hamstrings, and plantar flexors compared to their younger counterparts, especially around the point of seat-off (Dehail et al., 2007; S. H. L. Smith et al., 2020). This phenomenon is frequently associated with increased co-contraction of agonist-antagonist pairs which enhances joint stiffness and stability but also elevates muscular effort (Roebroeck et al., 1994; Van Der Kruk et al., 2021). Additionally, there are selective shifts in the relative contributions of the hip, knee, and ankle extensors, revealing a greater reliance on hip extensors and plantar flexors to compensate for the diminished strength of knee extensors in aging populations (Caruthers et al., 2016; S. H. L. Smith et al., 2020).

Previous studies have also applied muscle synergy analysis to the STS task to characterize phase-dependent activation patterns and to investigate how the structure or recruitment of synergies is influenced by varying populations and task-specific conditions (An et al., 2013; Hanawa et al., 2017, 2017; Kogami et al., 2021; Ranaldi et al., 2023, 2025; Yang et al., 2017a, 2017b; Yang et al., 2019; Yoshida et al., 2019). Although there are many studies on muscle synergies, only a few have focused on analyzing alterations in muscle synergies in the STS movement of older adults (An et al., 2013; Hanawa et al., 2017; Yang et al., 2017b). Evidence from these studies suggests that age-related differences may manifest as deficient or additional synergies in some elderly individuals (An et al., 2013), or as modifications in the temporal activation patterns while maintaining a largely similar spatial organization of muscle synergies (Yang et al., 2017b).

5. Methodology – General Framework

5.1. Ethical Approval

All the studies received approval from the University Research Committee of the University of Rome “Foro Italico” (CAR 154/2023) on May 4, 2023, and subsequently revised on April 23, 2024 (CAR 154/2023/Rev). Prior to data collection, all participants provided written informed consent, and the study was conducted in accordance with the Declaration of Helsinki as updated in 2024 (World Medical Association, 2025).

5.2. Participants

Nineteen healthy young participants (11 males and 8 females; average age: 27.6 ± 3.1 years; average height: 1.7 ± 0.06 m; average body mass: 65.3 ± 9.0 kg; 2 left-handed and 17 right-handed) and twenty-five healthy older adults (8 males and 17 females; age: 78.8 ± 6.5 years;

height: 1.62 ± 0.1 m; body mass: 70.0 ± 11.7 kg; 2 left-handed individuals and 23 right-handed) without any neurological or musculoskeletal disorders that might influence mobility took part in the study. The handedness was assessed using the Edinburgh Handedness Inventory (Veale, 2014). In the elderly population, additional assessments were conducted to evaluate balance and cognitive function in order to ensure eligibility for participation in the study. Specifically, balance performance was assessed using the Berg Balance Scale (BBS), the Timed Up and Go (TUG) test, and the 6-Meter Walking Test, while cognitive status was evaluated using the Mini-Mental State Examination (MMSE).

5.3. Experimental Setup and Protocols

All measurements were conducted under controlled laboratory conditions to ensure methodological rigor, within a single experimental session to avoid inter-session variability. Participants were instructed to perform the following task blocks:

- Functional Reach tasks, which included unilateral Functional Reach (uniFR), bilateral Functional Reach (biFR), Lateral Reach (LR), and Unplanned Functional Reach (unplFR) blocks.
- 30-Second Sit-to-Stand (STS) tests.

5.3.1. Functional Reach tasks

For all the Functional Reach tasks, including uniFR, biFR, LR, and unplanned FR, participants were instructed to stand barefoot on a stable surface, with their feet positioned at pelvis width to maintain a consistent BoS. Foot placement was marked on the floor using adhesive tape to ensure uniformity of positioning across trials. Each block consisted of 10 repetitions during which participants were instructed to maximize their reach without stepping, lifting their heels, or losing balance. The number of repetitions was selected to ensure a comprehensive representation of the EMG signal variance, allowing for accurate extraction of muscle synergies. The task was performed in a freestanding environment, away from any walls, in accordance with recommended procedures for FR execution (Duncan et al. 1990). In the uniFR and LR tasks, participants used only their dominant arm, while the biFR task required simultaneous reach with both arms. In each repetition, participants began by raising their arm or arms, depending on the task, and extended their reach as far as possible while maintaining balance. After reaching, they returned to the starting position with the arm/s still elevated, then lowered their arm/s back to their side. Participants were also instructed to avoid rotating their torso, bending their knees, or lifting their heels. This approach enabled a more consistent and reliable

assessment of the fundamental components of motor control by reducing the possible different strategies that could be adopted as a way of exploring solutions for the new motor task, rather than meeting functional demands. **Figure 5.1** illustrates a schematic representation of the execution of uniFR, biFR, and LR task.

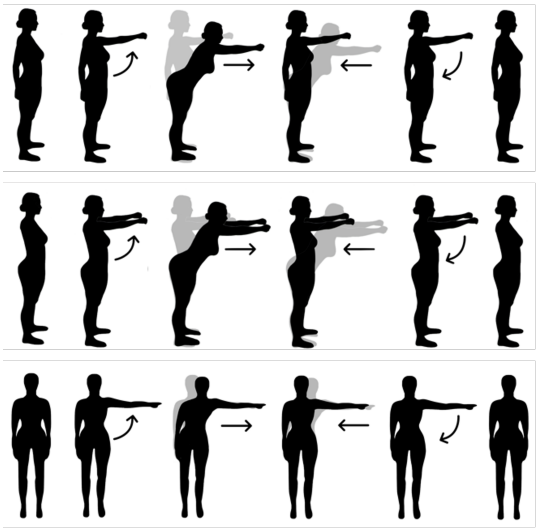

Figure 5.1. Schematic representation of the three different functional reach tasks. Participants performed unilateral Functional Reach (uniFR), bilateral Functional Reach (biFR), and Lateral Reach (LR) conditions. In the uniFR and LR conditions, participants reached using only their dominant arm, whereas in the biFR condition both arms were raised and extended simultaneously. For each repetition, participants raised the arm(s), reached forward or laterally as far as possible while maintaining balance, returned to the starting upright position with the arm(s) still elevated, and finally lowered the arm(s) alongside the body.

5.3.2. Unplanned Functional Reach tasks

Complementing the planned FR conditions, participants undertook one unplFR block. In this instance, participants were not pre-informed of the reaching direction. Visual cues, represented as arrows, were displayed on a monitor positioned directly in front of the participants and generated by a custom MATLAB application (R2022b, The MathWorks Inc., Natick, MA, USA), which randomly presented cues on the screen. This setup required participants to initiate movement based on real-time visual information, engaging unplanned, self-initiated control strategies.

While the unplFR task was fully implemented and integrated into the experimental protocol, the results for this condition are not included in this thesis. Ongoing analyses of the unplanned reaching condition aim to fill the identified gap concerning the impact of non-programmed and unpredictable postural demands, which will be discussed in future perspectives.

5.3.3. 30-Second Sit-to-Stand tests

Participants were instructed to perform three blocks of 30-Second STS tests (Jones et al., 1999), positioning their hands placed on their hips while keeping their elbows pointed outward. Their primary goal was to repeat the movement as many times as possible without any additional guidance. The 30-Second STS Test was administered using a chair without armrests, to avoid

the involvement of the upper limbs, and without a back rest, to prevent the participant from leaning back against it. The seat height was set at 17 inches (43.2 cm) (Shirley Ryan Ability Lab, 2013). Participants were barefoot.

The order of task block presentation was randomized and counterbalanced across participants to mitigate any potential order effects. To address fatigue, participants were allowed 1–2 minutes of rest between blocks. All sessions were closely supervised by a research assistant to ensure adherence to correct execution protocols, and any incorrect trials were repeated as necessary.

5.3.4. Data Acquisitions

A wireless surface EMG system with 16 bipolar channels (MiniWave, Cometa, Bareggio, Italy) was employed to record muscular activity from a total of 16 muscles (8 on each side) at a sample rate of 2 kHz. The EMG electrodes were applied to shaved, abraded, and thoroughly cleaned skin surfaces to record the activity of the following muscles: anterior deltoid (AD), erector spinae (ES), latissimus dorsi (LD), vastus lateralis (VL), tibialis anterior (TA), biceps femoris (BF), gastrocnemius medialis (GastM), and soleus (Sol). The placement of the electrodes followed the recommendations from SENIAM (Surface Electromyography for the Non-Invasive Assessment of Muscles) (Hermens & Merletti, 1996) and Cram's Introduction to Surface Electromyography (Criswell & Cram, 2011). For each participant, the electrode placement remained constant throughout the entire experimental protocol, which facilitated direct comparisons of muscle activity across all tested conditions.

In addition, body motion was recorded at a sample rate of 200 Hz using a 3D motion capture system (VICON®, Oxford Metrics, Oxford, UK) equipped with 9 Vero and Bonita infrared cameras. A total of 61 infrared reflective markers (14 mm in diameter) were used and positioned on both the upper and lower limbs as well as the trunk, in line with the Plug-in Gait Full Body and Convolutional Gait Model 2.5 kinematics models (see **Figure 5.2**).

Two additional force platforms (1 kHz, Bertec, Ohio, USA) were used to record the ground reaction forces during the test.

All data acquisition systems were synchronized through hardware.

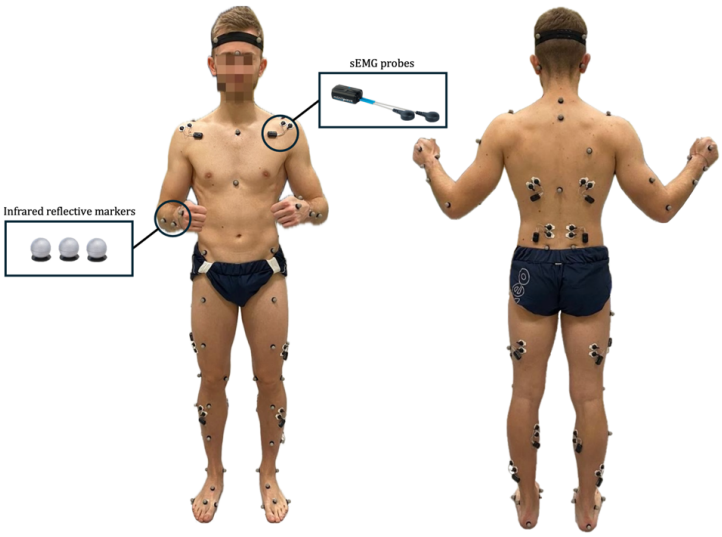

Figure 5.2. Experimental set-up. EMG probes and infrared reflective markers placement for a representative healthy young volunteer. EMG probes are placed bilaterally over 8 key muscles: Anterior Deltoid (AD), Erector Spinae (ES), Latissimus Dorsi (LD), Vastus Lateralis (VL), Tibialis Anterior (TA), Biceps Femoris (BF), Gastrocnemius Medialis (GastM), and Soleus (Sol). The 61 infrared reflective markers are positioned according to the Plug-in Gait and the Convolutional Gait Model 2.5 kinematics models.

5.3.5. Triggered UnplFR Task via Custom MATLAB GUI

A custom MATLAB App Designer application (refer to **Appendix: MATLAB GUI Code**) was specifically created to manage the presentation of unplanned visual stimuli during the unplFR task. This application was designed to work with a Trigger Box that was connected to both the laboratory computer (via USB) and the Vicon Lock system (via analog inputs) (see **Figure 5.3**). The Trigger Box was set up to carry out two related functions:

- Stimulus Control: It sent a digital signal to the MATLAB application through a USB connection. Upon receiving this signal, the application showcased a visual cue on a secondary monitor, indicating the direction of movement required (forward, left, or right).
- Temporal Synchronization: At the same time, the same triggering action produced an analog square-wave signal captured by the Vicon Lock. This signal was essential for accurately timestamping the start of each stimulus within the kinematic data collected by Vicon's Nexus software.

Through this setup, synchronization was completely achieved via the hardware link between the Trigger Box and the Vicon Lock, ensuring that the timing of stimulus onset was directly matched with motion capture data without needing software-based timing solutions.

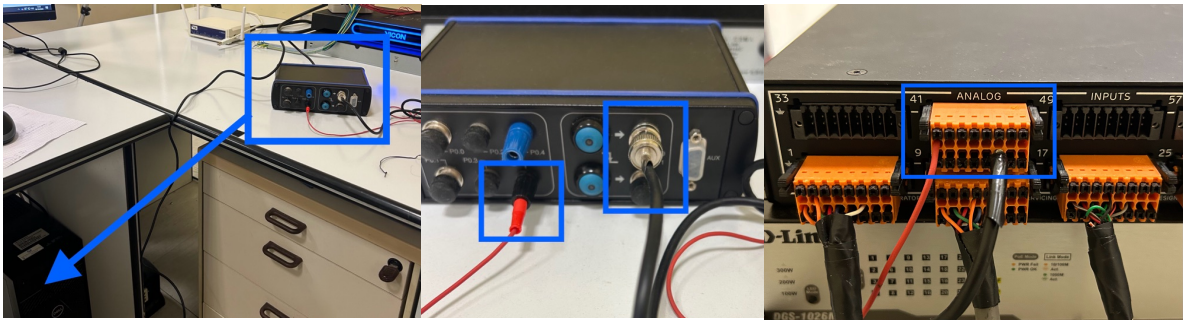

Figure 5.3. Hardware setup used for stimulus triggering and synchronization during the unplanned Functional Reach (unplFR) task. The Trigger Box was connected to the laboratory computer via USB and to the Vicon Lock system via analog inputs.

The MATLAB application was designed for direct communication with the National Instruments (NI) device that controlled the Trigger Box. It consistently monitored the digital input lines for incoming trigger signals and, upon detection, showcased the related visual stimulus in full screen mode on the participant's monitor. When a trigger was detected, the app promptly displayed the corresponding directional image in full screen mode on a secondary monitor positioned in front of the participant. Each displayed image stayed on the screen until the trial concluded and the background was returned to black.

The application consists of two graphical windows (refer to **Figure 5.4**):

- Control Interface (primary window): This allows the experimenter to connect to the Trigger Box, select the direction for the upcoming stimulus (forward, left, or right), and synchronize the acquisition process.
- Stimulus Display (secondary window): This window is automatically initiated in full screen mode on a second monitor and shows the visual cue to the participant.

Specifically, when activated, the application:

- Initializes the session for data acquisition and verifies device connectivity.
- Remains in waiting mode for the incoming trigger signal, which corresponds to an unplanned stimulus event.
- Upon trigger detection, the app instantly presents the selected visual stimulus on the full-screen display.
- Maintains responsiveness in the GUI during the loop, enabling the experimenter to safely terminate or restore the display.
- Integrates a safety confirmation when closing to ensure the proper termination of all active figures and hardware sessions.

Simultaneously, the app transmitted a digital output signal back to the Trigger Box, prompting it to produce the appropriate analog square-wave output directed to the Vicon Lock.

This combined hardware-software system provided a precise method of correlating stimulus presentation with motion capture data. By recording the analog pulse within the kinematic data stream, it became possible to pinpoint the exact timing of stimulus onset and calculate reaction times as the interval between the presentation of the visual cue and the initiation of movement. Consequently, the system introduced a non-predictable, perceptual component to the task while ensuring high temporal accuracy across all synchronized signals.

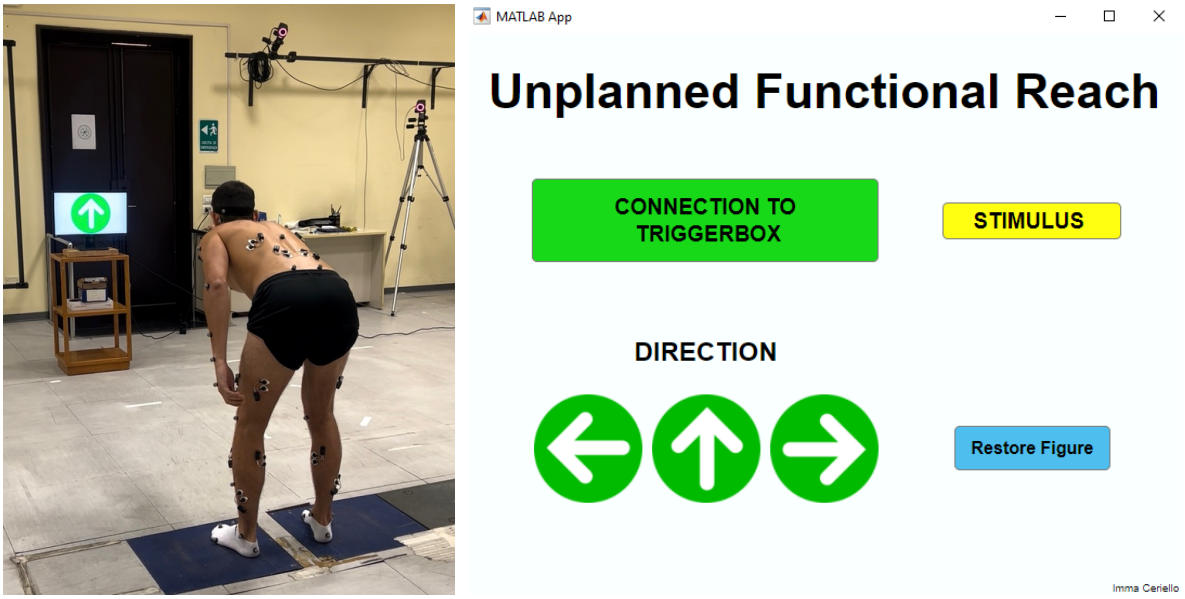

Figure 5.4. MATLAB application used for the presentation of unplanned visual stimuli during the unplanned Functional Reach (unplFR) task. Left panel: experimental setup showing the participant facing the stimulus monitor during task execution. Right panel: graphical user interface of the custom MATLAB App Designer application. The primary control interface allows the experimenter to connect to the Trigger Box, select the stimulus direction (forward, left, or right), and manage acquisition. Upon detection of a trigger signal, the application displays the corresponding directional cue in full-screen mode on a secondary monitor positioned in front of the participant, remaining visible until the end of the trial.

PART II

6. Study I: Muscle coordination strategies during Functional Reach across multiple directions in healthy individuals

Imma Ceriello[1,4] · Marco Ghislieri[2] · Lorenzo Rum[3,4] · Valentina Camomilla[1,4] · Andrea Macaluso[1] · Riccardo Borzuola[1]

[1]Laboratory of Bioengineering and Neuromechanics, Department of Movement, Human and Health Sciences, University of Rome "Foro Italico", Rome, Italy

[2]PolitoBIOMed Lab, Department of Electronics and Telecommunications, Politecnico di Torino, Torino, Italy

[3]Department of Biomedical Sciences, University of Sassari, Sassari, Italy

[4]Interuniversity Centre of Bioengineering of the Human Neuromusculoskeletal System, University of Rome "Foro Italico", Rome, Italy

Published on European Journal of Applied Physiology 2025,
https://doi.org/10.1007/s00421-025-05951-7

Author contributions: Imma Ceriello, Valentina Camomilla, Andrea Macaluso and Riccardo Borzuola conceived and designed research; Imma Ceriello and Riccardo Borzuola performed experiments; Imma Ceriello analyzed data; Imma Ceriello, Riccardo Borzuola and Marco Ghislieri interpreted results of experiments; Imma Ceriello prepared figures; Imma Ceriello, Riccardo Borzuola, Marco Ghislieri and Lorenzo Rum drafted the manuscript; Imma Ceriello, Riccardo Borzuola, Marco Ghislieri, Lorenzo Rum, and Valentina Camomilla edited and revised manuscript; Imma Ceriello, Marco Ghislieri, Lorenzo Rum, Valentina Camomilla, Andrea Macaluso and Riccardo Borzuola approved the final version of manuscript.

6.1. Rationale and Objectives

Maintaining postural stability is essential for safely performing everyday motor tasks and depends on the ability to manage the body's CoM within its base of support (Dunsky, 2019; Horak, 1987). The Functional Reach (FR) test offers a straightforward and effective way to assess this control since it requires individuals to intentionally shift their CoM towards their limits of stability while maintaining balance (Duncan et al., 1990; Tyson & DeSouza, 2004). Beyond its clinical applications, the FR task represents a valuable model for examining postural control strategies under increasing balance challenges. While previous research has looked into muscle activation patterns during reaching and postural adjustments (Maranesi et al. 2016a; Maranesi et al. 2016b; Marchesi et al. 2021), the specific coordination strategies used during the FR task are not well understood. Notably, there have been no studies on how muscle synergies are organized during FR tasks or how these strategies adapt to different directional challenges. Gaining insight into these mechanisms in healthy young adults is crucial for providing a reference framework against age- or pathology-related impairments can later be interpreted.

Objectives: This study aimed to characterize the muscle coordination strategies involved in the FR task among healthy young adults by extracting muscle synergies from surface EMG data. Additionally, we sought to determine if similar synergy structures are present across different FR variations (uniFR, biFR, and LR), even though each direction has its unique biomechanical and postural requirements. We hypothesized that a limited number of muscle synergies would effectively account for the performance of the FR tasks, indicating a shared modular control for

balance-related movements. We also believed that the general synergy structure would remain consistent across different FR task variations, preserving a similar overall organization in terms of the number of synergies and their functional roles, while task-dependent adaptations were expected to emerge in activation timing and relative muscle weightings according to the direction-specific balance demands.

6.2. Experimental Procedure

Participants and experimental setup followed the general framework detailed in **Chapter 5**. Specifically, data were collected during the uniFR, biFR, and LR task (see **Section 5.3.1**), each performed in blocks of 10 repetitions, from 17 healthy young volunteers (10 males and 7 females; average age: 27.5 ± 3 years; average height: 1.7 ± 0.1 m; average body mass: 64.9 ± 8.8 kg; 2 left-handed and 15 right-handed) (see **Section 5.2** for inclusion criteria).

The EMG recording and motion capture procedures followed the general setup described in **Section 5.3.4**. Specifically, this study included the acquisition of surface EMG signals and whole-body kinematics using the stereophotogrammetric system, while data from the force platforms were not considered in the present analyses.

6.3. Data Analysis

6.3.1. Identification of reaching phases

Kinematic data were mainly used for identifying FR repetitions and phases. Marker trajectories were initially filtered with a 4^{th}-order Butterworth filter with a 12 Hz cut-off frequency in Vicon Nexus software. Filtered data was then imported into MATLAB (R2022b, The MathWorks Inc., Natick, MA, USA) for the following additional processing and analyses. The velocities of the hand (marker on the middle knuckle) and the shoulder (acromion marker) were calculated and then used to divide each FR repetition into four distinct phases (Marchesi et al., 2021):

i. Arm Elevation: this phase begins when hand velocity (along the y-axis for forward direction and x-axis for lateral) reaches 10% of its peak speed and end when shoulder velocity (in the same directions) exceeds 10% of its peak speed.
ii. Reaching: this phase begins at the end of arm elevation (R1) and end when the Maximum hand trajectory Distance (MD) is reached, determined by identifying local maxima along the y-axis.
iii. Arm Returning: this phase begins after MD is reached and ends when shoulder velocity drops below 10% of its peak speed (R2).

iv. Arm Lowering: this phase begins at R2 and ends when hand velocity drops below 10% of its peak speed.

6.3.2. EMG pre-processing

The raw EMG signals were processed to remove impulse peaks and power-line peaks. Power-line interference was attenuated by applying a third-order Butterworth narrow band-stop (notch) filter centered at 50 Hz using a zero-phase forward–backward filtering procedure. Signals were then band-pass filtered (30-450 Hz) (De Luca et al., 2010; Marchesi et al., 2021), full wave rectified, and low-pass filtered at 4 Hz with a zero-lag 4^{th}-order Butterworth filter to obtain EMG linear envelopes (Marchesi et al., 2021). For each muscle, the EMG envelopes were normalized in amplitude to their global maximum to ensure equal weighting of all muscles during muscle synergy extraction, thereby addressing variations in signal amplitude across muscles due to factors such as electrode placement, muscle size, and skin impedance (Torricelli et al., 2016; Turpin et al., 2021), as each task consisted of multiple repetitions performed within a single continuous recording, allowing a well-defined and consistent maximum reference value. These envelopes were segmented based on the previously described reaching phases. To account for differences in phases' duration between participants, each EMG envelope was time-normalized to 100 points per repetition, where 0 corresponds to the start of the arm elevation phase and 100 corresponds to the end of the arm lowering phase. The R1, MD, and R2 events were consequently resampled and expressed as percentages relative to this normalized time scale, ranging from 0% (start of the task) to 100% (end of the task). This normalization enabled consistent comparison of temporal patterns across trials and participants, regardless of individual variability in absolute timing. Mean values for each phase were then computed for each participant based on all completed repetitions.

Additionally, to further reduce motion artifacts or residual noise beyond filtering, all EMG recordings were visually inspected. Trials showing evident contamination (e.g., abrupt amplitude shifts unrelated to muscle activity) were excluded. Overall, approximately 3% of trials were removed.

The normalized EMG envelopes of each recorded muscle, averaged across the sample population, are reported in the **Appendix – Supplementary Materials, Figure S6.1**. These envelopes serve as input for the factorization process (Lee & Seung, 1999) explained below. For each FR task, the normalized EMG envelopes extracted from all the repetitions (N_{rep}) were concatenated to obtain a single representative dataset for each subject (Oliveira et al., 2014).

This preliminary procedure provided a normalized (N_{rep}×100)×16 EMG matrix, which was later used for muscle synergy extraction.

6.3.3. Identification of muscle synergies

For each participant and task, muscle synergies were then extracted from the normalized EMG matrix, by using the Non-Negative Matrix Factorization (NNMF) algorithm (Lee & Seung, 1999). NNMF decomposes the original EMG envelope matrix (M(t)) into two components: time-dependent activation coefficients (C(t)) and time-independent weight vectors (W) (Zelik et al., 2014), as represented by Equation (6.1):

$$M(t) = \sum_{k=1}^{N_{syn}} C(t)_k \cdot W_k + e \tag{6.1}$$

where N_{syn} is the number of muscle synergies needed to model motor control and e is the reconstruction error. The activation coefficient $C(t)_k$ reflects the time-dependent modulation of muscles in the k-synergy reflecting the temporal pattern of muscle activity (temporal component). Meanwhile, the weight vector W_k represents the time-independent contribution of each muscle to the k-synergy, indicating the spatial involvement of each muscle in that synergy (spatial component).

The MATLAB function '*nnmf*' was used to factorize the EMG envelope matrix following the multiplicative update rules (Lee & Seung, 1999). To reduce the risk of the iterative algorithm converging to a local rather than a global minimum, the number of replicates was set to 50, with a maximum of 1000 iterations and a termination tolerance $1e^{-6}$ (Ghislieri, Agostini, et al., 2020). Synergy extraction was performed iteratively, starting from one muscle synergy and increasing up to the total number of recorded muscles. As a result, the function was run multiple times, varying N_{syn} from 1 to 16 for each subject and task.

6.3.4. Determining the optimal number of synergies

To determine the optimal number of synergies (N_{syn_opt}), two criteria were applied based on the computation of the Variance Accounted For (VAF) (D. J. Clark et al., 2010) and the Mean Squared Error (MSE) (Cheung et al., 2005), respectively. The first criterion identified the smallest N for which the VAF vs. number of synergies curve reached a value $\geq$ 90%, with the addition of another synergy resulting in a VAF increase of less than 5%. This approach has been widely adopted as a standard practice to ensure adequate reconstruction accuracy (Israely et

al., 2018; Roh et al., 2015; Scano et al., 2018). The choice of a 90% threshold reflects the empirical observation that, in many upper-limb and lower-limb tasks, this level of explained variance captures the principal patterns of muscle coordination while preserving the stability of the estimated number of synergies across experimental conditions (D. J. Clark et al., 2010; Ghislieri, Agostini, et al., 2020; Pale et al., 2020; Roh et al., 2013). The second criterion involved iteratively performing linear regressions on segments of the VAF vs. number of synergies curve. In each iteration, the regression was carried out by excluding the smallest N_{syn} value, with the process repeated for N_{syn} ranging from 1 The optimal N_{syn} was then defined as the minimum value where the MSE of the regression was below 10^{-4}, indicating that further increases in the number of synergies produced minimal reduction of residual variance and the VAF curve approached linearity. This threshold was set according to previous studies (d'Avella et al., 2006; Pellegrino et al., 2018; Pierella et al., 2022) and aims to objectively identify the "elbow point" beyond which additional synergies contribute negligibly to reconstruction quality. If the two criteria yielded different results, the larger N_{syn} was selected (Berger & d'Avella, 2014).

To streamline the analyses, an equal number of muscle synergies was considered within each FR task for all participants. This number was determined based on the rounded average value across participants (Coscia et al., 2014).

To visually represent the muscle synergies, the weight vectors (W) were normalized between 0 and 1 relative to their global maximum. The activation coefficient vectors (C(t)) were then scaled accordingly using these normalized weights.

6.3.5. Muscle synergy sorting

Since the NNMF algorithm was applied independently to each FR task per participant and because it does not consistently extract muscle synergies in the same order across subjects and tasks, both the weight vectors and activation coefficients were reordered based on their alignment with a reference set. The reference set was obtained by categorizing the synergies through a hierarchical clustering algorithm, minimizing the *Cityblock* distance between vectors (Danion & Latash, 2011). The hierarchical cluster analysis was applied separately for each FR task, with the number of clusters set equal to N_{syn_opt}. For each cluster, a reference weight vector ($W_{ref,i}$) was computed by averaging the weight vectors belonging to that cluster (Pellegrino et al., 2018). The corresponding reference activation coefficients ($C_{ref,i}$) were obtained by averaging the activation profiles associated with the weight vectors within the same cluster.

Unlike previous approaches, which typically sort muscle synergies by maximizing the scalar product based only on either the weight vectors or the activation coefficients (Banks et al., 2017; d'Avella & Bizzi, 2005; Santuz et al., 2017), this study aligned muscle synergies across tasks and participants by maximizing the combined normalized scalar product (M_{DOT}), as defined in Equation (6.2). This metric corresponds to the calculation of cosine similarity computed separately for the weight vectors and the activation coefficients:

$$M_{DOT} = \frac{W_{ref,i} \cdot W_j}{\| W_{ref,i} \| \| W_j \|} + \frac{C_{ref,i} \cdot C_j}{\| C_{ref,i} \| \| C_j \|} \tag{6.2}$$

where $W_{ref,i}$ and $C_{ref,i}$ represent the weight vectors and activation coefficients of the reference set of muscle synergies, created by pooling together the weight and activation coefficients from all participants, respectively. Meanwhile, W_j and C_j represent the weight and activation coefficients of an individual subject to be reordered, respectively.

This method simultaneously considers the similarity of both the weight vectors and the activation coefficients with respect to the reference set. A higher M_{DOT} value indicates a greater similarity between the participant's synergy components and the reference set (i.e., good alignment).

6.3.6. Muscle synergy analysis

Reaching tasks were analyzed separately in terms of muscle synergy composition, muscle synergy robustness, and muscle synergy consistency.

Muscle synergy composition. The muscle synergy composition was initially assessed by evaluating the primary contributions of muscles (i.e., weight values $W_k > 0.5$) and the activation coefficient patterns $C(t)_k$ associated with each muscle synergy, thereby enabling the association of specific biomechanical functions (Rimini et al., 2017). Comparisons between uniFR and biFR (i.e., uniFR vs. biFR), as well as that between uniFR and LR (i.e., uniFR vs. LR), were conducted independently, considering their respective directional characteristics and control strategies. Specifically, the uniFR vs. biFR analysis emphasized their shared directional component in the anterior-posterior direction, whereas the uniFR vs. LR analysis underscored the unilateral execution with the dominant limb, highlighting the transition from anterior-posterior to medio-lateral control demands.

Muscle synergy robustness. The robustness of the muscle synergies among all possible pairs of FR tasks was assessed for each subject through the Cross-Variance Accounted For ($CrossVAF$) (Ghislieri et al., 2023; Muceli et al., 2010) formulated as described in Equation (6.3):

$$CrossVAF^{i,j} = \left(1 - \frac{\sum_{k=1}^{m}\left(M_k^i - M_k^{R,j}\right)^2}{\sum_{k=1}^{m}\left(M_k^i\right)^2}\right) \cdot 100 \tag{6.3}$$

where M_k^i denotes the original EMG data of the k-muscle for the *i*-th FR task, while $M_k^{R,j}$ represents the reconstructed EMG data of the same muscles for the *j*-th task. $CrossVAF$ essentially quantifies the accuracy with which the muscle synergies derived from one FR task (e.g., the *i*-th FR task) can reproduce the EMG data of a different FR task (e.g., the *j*-th FR task). Subsequently, the average $CrossVAF$ ($CrossVAF_{avg}$) score was computed across all possible pairs of FR tasks for each subject. The $CrossVAF_{avg}$ ranges from 0% to 100%, indicating low to high similarity between the reconstructed and the original EMG data belonging to different FR tasks. This measure allows to evaluate the similarity in synergy-based muscle activation patterns between different FR tasks.

Intra- and inter-task consistency. The consistency of muscle synergies within each task across participants (i.e., intra-task consistency) and between tasks (i.e., inter-task consistency) was assessed by evaluating the similarity of the sorted weight vectors (W). Considering the intra-task consistency, this metric quantifies the similarity of weight vectors across participants within the same FR task for a given number of muscle synergies ($n = N_{syn\_opt}$). Cosine similarity (CS) was used to measure the similarity between each pair of weight vectors (d'Avella & Bizzi, 2005) as detailed in Equation (6.4):

$$CS_{W,n}^{i,j} = \frac{W_n^i \cdot W_n^j}{\| W_n^i \| \| W_n^j \|} \tag{6.4}$$

where $CS_{W,n}^{i,j}$ represents the cosine similarity calculated between the weight vectors W_n of the *i-th* and *j-th* participant. Specifically, the weight vectors of each participant were compared to those of all other participants, and the results were averaged across participants. To define an overall reference value for intra-subject similarity within each task, the same procedure was followed, with the results further averaged across all muscle synergies.

Considering the inter-task consistency, this parameter evaluates the similarity of the weight vectors across two different tasks for a given number of muscle synergies as detailed in Equation (6.5):

$$CS_{W,n}^{i,j}[t1,t2] = \frac{W_n^{i,t_1} \cdot W_n^{j,t_2}}{\| W_n^{i,t_1} \| \| W_n^{j,t_2} \|} \tag{6.5}$$

The W_n vectors of the *i*-th subject extracted during one FR task ($W_n^{i,t1}$) were compared to those of all the other subjects during a different FR task ($W_n^{j,t2}$). The mean values were then computed, first across muscle synergies and then across individuals.

The value of $CS_{W,n}^{i,j}$ and $CS_{W,n}^{i,j}$ $[t1,t2]$ ranges from 0 to 1, with higher values indicating greater similarity between the two vectors.

6.4. Statistical Analysis

The Shapiro-Wilk test was used to evaluate normality of data distribution for the reaching events, the optimal number of muscle synergies, and the muscle synergy robustness parameters. Depending on the results, repeated measures Analysis of Variance (rmANOVA) was applied for normally distributed data, while Friedman test was used for non-normal distributions. *Post-hoc* comparisons were conducted with Bonferroni corrections for multiple comparisons. A similar approach was followed to assess intra-task consistency. Depending on the results of the Shapiro-Wilk test, either the Wilcoxon signed-rank test (for non-normally distributed data) or the paired Student's *t*-test (for normally distributed data) was applied.

To further assess muscle synergy composition, statistically significant differences in temporal activation patterns ($C(t)$) between FR tasks were tested through Statistical Parametric Mapping (SPM) (Friston et al., 1994). SPM identified the time intervals in which statistically significant differences in activation timing emerged between tasks. SPM analyses were performed with the freely available spm1d toolbox (www.spm1d.org). When the assumption of normality was not met, the non-parametric alternative, Statistical non-Parametric Mapping (SnPM), was applied.

The effect size of statistically significant differences was determined using Hedges' g statistic (Hedges, 1981). According to this measure, g values of 0.2, 0.5, and 0.8 correspond to small, medium, and large effect sizes, respectively. An alpha level of 0.05 was set for all analyses, and parameter estimates were expressed as mean ± standard error (SE) over the sample population. Statistical analyses were performed using MATLAB's Statistical and Machine

Learning Toolbox (MATLAB version R2022b, The MathWorks Inc., Natick, Massachusetts, United States).

6.5. Results

Table 6.1 shows the average occurrence of the R1, MD, and R2 events for each task (uniFR, biFR, and LR) expressed as the percentage of the whole task duration (0 %: start of arm elevation; 100 %: end of arm lowering). Considering the R1 and R2 events, statistically significant differences were found between uniFR and LR tasks (R1: $p < 0.001$, $|g|=1.03$; R2: $p < 0.001$, $|g| = 0.89$) and between biFR and LR tasks (R1: $p = 0.001$, $|g| = 1.02$; R2: $p = 0.005$, $|g| = 0.77$). Instead, no statistically significant differences were found between the three FR tasks for the MD timing.

Table 6.1. The average percentage of the reaching events for each task.

Reaching tasks	Reaching events (%)		
	R1	MD	R2
uniFR	18.4 ± 0.8 ***	54.8 ± 1.0	86.5 ± 1.2 ***
biFR	18.9 ± 0.6 ††	54.6 ± 1.1	86.0 ± 1.2 ††
LR	21.9 ± 0.8 ***,††	53.3 ± 1.2	82.3 ± 1.1 ***,††

Reaching events expressed as the percentage of the task duration (0%: start of arm elevation; 100%: end of arm lowering) averaged across participants. All data are reported as mean ± SE over the sample population. Statistically significant differences among tasks are indicated by asterisks (***p < 0.001) and daggers (††p < 0.01).

6.5.1. Optimal number of muscle synergies

Figure 6.1 shows the variation in VAF (Fig. 3a) and MSE (Fig. 3b) values as a function of N_{syn}. Statistically significant differences in the optimal number of muscle synergies were found between uniFR and LR tasks ($p = 0.003$, $|g| = 1.13$) and between biFR and LR tasks ($p = 0.001$, $|g| = 1.23$). Specifically, fewer muscle synergies were required to account for muscle activation patterns during the uniFR and biFR tasks compared to LR task. On average, EMG data were accurately reconstructed using 3.0 ± 0.2 muscle synergies for the uniFR task and 2.9 ± 0.1 muscle synergies for the biFR task. These reconstructions achieved an average VAF of 92.3 ± 0.4% for uniFR and 93.2 ± 0.3% for biFR, with corresponding SE values of $(6.9 \pm 1.0)^{-5}$ and $(6.0 \pm 1.0)^{-5}$, respectively. For the LR task, 3.8 ± 0.3 muscle synergies were needed, with a VAF of 90.9 ± 0.4% and an MSE of $(6.5 \pm 0.8)^{-5}$.

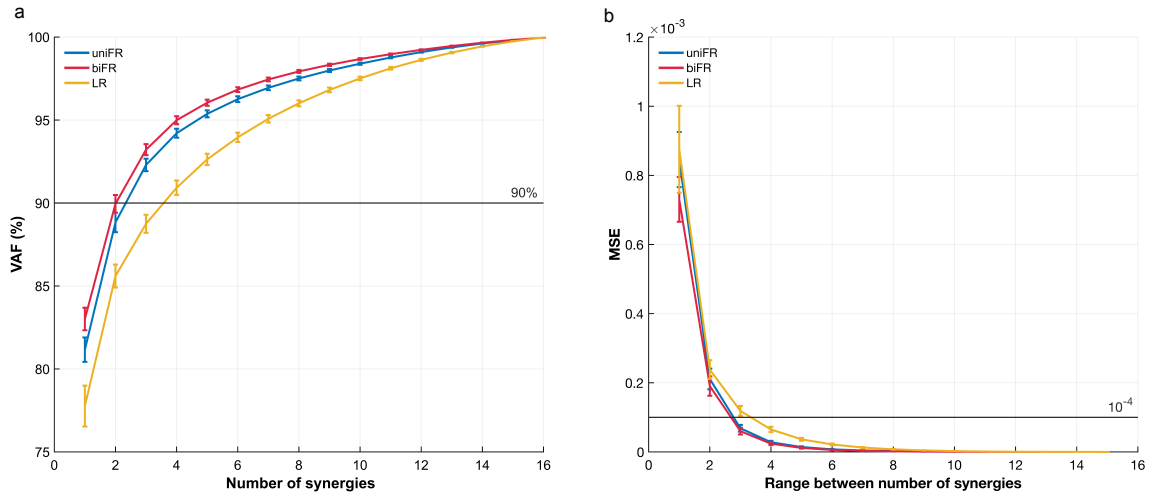

Figure 6.1. Selection of optimal number of synergies $N_{syn\ opt}$. The selection was performed considering two criteria applied to the Variance Accounted For (VAF) vs. number of synergies curve (Panel a) and the Mean Squared Error (MSE) vs. number of synergies curve (Panel b). The first criterion identified the smallest value where the VAF vs. number of synergies curve exceeded 90%, with any additional synergy resulting in less than a 5% increase in VAF. The second criterion involved iterative linear regressions on segments of the VAF curve, excluding the smallest value in each iteration, repeated for values from 1 to 15. The optimal value was the minimum point where the MSE was below 10^{-4}. If the two criteria differed, the larger value was chosen. All data are reported as mean ± SE over sample population. uniFR: unilateral Functional Reach; biFR: bilateral Functional Reach; LR: Lateral Reach.

6.5.2. Muscle synergy composition

Figure 6.2 illustrates the muscle synergies extracted from the uniFR, biFR, and LR tasks averaged over the sample population. By evaluating the muscles that are mainly enrolled in each muscle synergy and the corresponding activation coefficients pattern, the biomechanical functions associated with each muscle synergy during both uniFR and biFR tasks are as follows:

- The first synergy ($W1$ and $C1$) mainly involves the activation of the AD, ES, LD, GastM, and Sol muscles on both the dominant and non-dominant sides. This muscle synergy can be associated with the execution of the reaching movement, spanning from its initiation to completion, with peak activation occurring between ~30% and ~70% of the task duration. During this phase, the body is most "unbalanced". The ankle plantar flexors, GastM, and Sol muscles support the transition from a static posture to a forward-leaning position. The AD sustains arm elevation, while the ES and LD suggest a reliance on trunk extensors to maintain an upright posture. This is particularly evident as reaching in the forward direction induced greater anterior destabilization.
- The second synergy ($W2$ and $C2$) predominantly involves the bilateral activation of ES and BF muscles, with a minor contribution of the GastM. It can be associated with the lower limb stabilization, braking to control movement, and returning to an upright

posture. It shows an initial smaller activation peak between ~20% and ~40%, followed by a larger peak from ~55% to ~80%.

- The third synergy ($W3$ and $C3$) involves the activation of the VL and TA muscles, with the knee extensor VL stabilizing the knee and the ankle dorsiflexor TA supporting ankle stability. This muscle synergy can be associated with postural adjustments, primarily activating during the preparation and conclusion phases of the reaching movement. Its involvement diminishes as the body transitions into the reaching phase but increases once the body returns to an upright posture.

Conversely, when analyzing the muscle synergy composition of the LR task compared to the uniFR and biFR tasks, some distinct biomechanical functions emerged, reflecting the postural stability demands specific to lateral reaching:

- The first synergy ($W1$ and $C1$) is mainly described by the activity of the non-dominant LD, VL, and TA muscles, and requires less activation from anterior-posterior stabilizers compared to the uniFR and biFR tasks. It can be associated with a stabilizing synergy when the center of pressure shifts toward the ipsilateral side during the reaching movement. The activation profile is flatter and more evenly distributed across the cycle, with a more gradual rise and peak between ~40% and ~80%, reflecting a smoother and less dynamic activation pattern, likely due to the LR requiring more sustained control.
- The second synergy ($W2$ and $C2$) is primarily characterized by the activity of BF and ES muscles on the non-dominant side. The ES is mainly responsible for counteracting lateral lean and ensuring that the trunk returns to a stable upright position after the reach, while the BF counterbalances forces at the hip joint, providing stability to the lower limb. Notably, the Sol muscle on the dominant side shows greater involvement in LR compared to uniFR, highlighting its role in ankle stabilization. The activation profile of this synergy peaks between approximately 50% and 70% of the movement cycle, with a broader and lower peak, suggesting a more evenly distributed activation pattern to maintain medio-lateral stability for a prolonged period. Furthermore, activation in LR begins slightly earlier compared to uniFR and biFR tasks.
- The third synergy ($W3$ and $C3$) is characterized by a greater involvement of posterior muscles, particularly on the non-dominant side. It can be primarily associated with postural adjustments on the contralateral side, driven by the non-dominant ankle plantar flexors muscles (GastM and Sol muscles). These muscles play a supportive role and activate early to create a stable base from which to perform lateral movement.

During the final phase of the movement (post-reach), they help in returning the body to an upright posture by controlling ankle motion and generating force for re-centering the body. Additionally, higher and more sustained synergy engagement is required during both the early preparation and late recovery phases of the task.

The fourth synergy ($W4$ and $C4$) can be linked to arm elevation and reaching execution until the maximum distance is achieved. On the dominant side, the AD and LD muscles primarily control arm elevation and assist in trunk stabilization. In contrast, the non-dominant side generally exhibits lower muscle weights, with the LD showing the highest activation. The activation profile progressively increases, peaking around 40-50% of the movement, and then declines during the return phase.

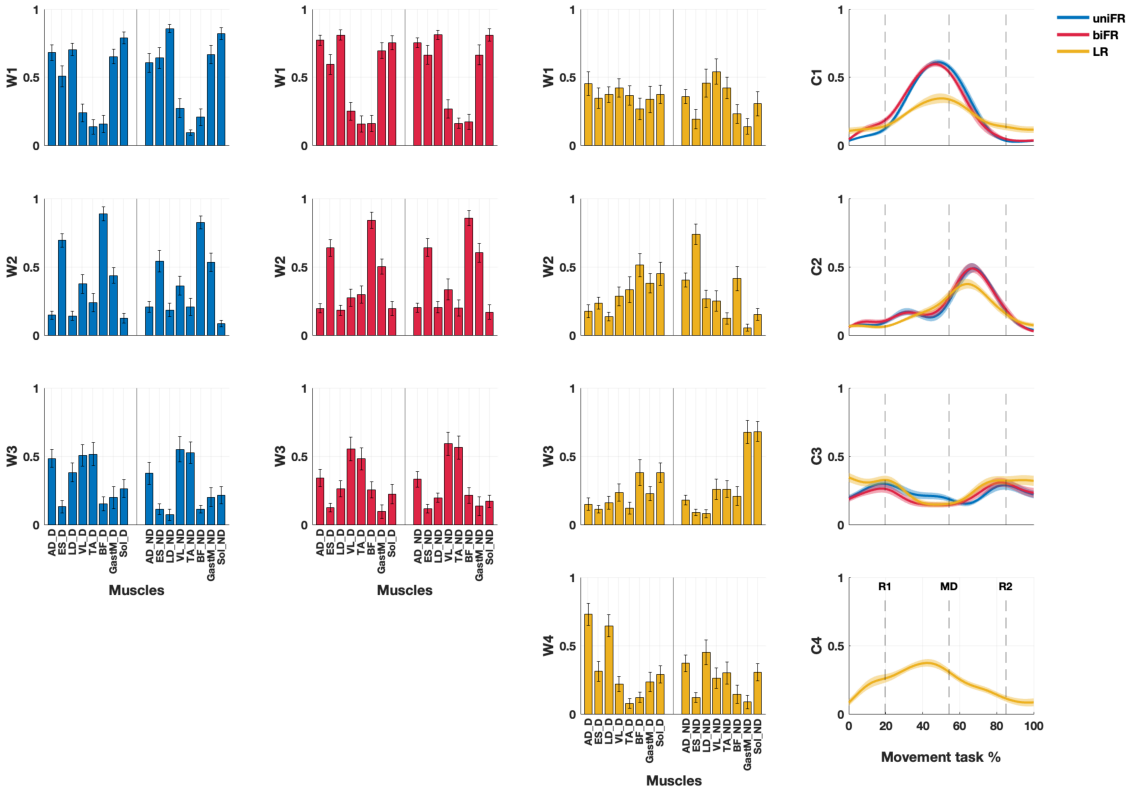

Figure 6.2. Muscle weights (W_k, first, second and third column) and activation coefficients (C_k, fourth column) of the muscle synergies averaged across participants during the uniFR, biFR, and LR tasks. For each synergy (k), W_k (bars indicating muscle contribution levels) and the corresponding C_k (neural command activation profiles) are shown in the same color. Blue, red, and yellow represent the uniFR, biFR, and LR tasks, respectively. Vertical dotted lines in the activation coefficient plots mark the reaching events as averaged across the tasks. uniFR: unilateral Functional Reach; biFR: bilateral Functional Reach; LR: Lateral Reach. AD: Anterior Deltoid, ES: Erector Spinae, LD: Latissimus Dorsi, VL: Vastus Lateralis, TA: Tibialis Anterior, BF: Biceps Femoris, GastM: Gastrocnemius Medialis, Sol: Soleus. Muscles are represented grouped by side (D = Dominant, ND = Non-Dominant). R1: End of arm elevation and start reaching; MD: Maximum distance reached and start of arm returning; R2: Stop of arm returning and start of arm lowering.

6.5.3. Muscle synergy composition

Table 6.2 presents the averaged $CrossVAF$ values. The $CrossVAF$ values were significantly lower when uniFR and biFR EMG data were reconstructed based on LR muscle synergies (LR to uniFR: $p < 0.001$, $|g| = 3.98$; LR to biFR: $p < 0.001$, $|g| = 3.42$), with no statistically significant difference between these two. Similarly, when reconstructing LR EMG data using muscle synergies extracted during uniFR and biFR tasks, the $CrossVAF$ values were significantly lower (uniFR to LR: $p < 0.001$, $|g| = 4.50$; biFR to LR: $p < 0.001$, $|g| = 4.60$). In contrast, reconstructions between uniFR and biFR conditions resulted in higher $CrossVAF$ values, although significantly different between each other (uniFR to biFR: $p = 0.011$, $|g| = 2.52$; biFR to uniFR: $p = 0.011$, $|g| = 2.23$).

Table 6.2. Cross-Variance Accounted For values averaged across participants ($\boldsymbol{CrossVAF_{avg}}$).

$\boldsymbol{CrossVAF_{avg}}$ (%)		Reconstructed		
		uniFR	**biFR**	**LR**
Extracted	**uniFR**	97.0 ± 0.2 *,†††	90.2 ± 0.9*,#	68.0 ± 1.2 †††,#
	biFR	90.6 ± 0.8 *,†	96.5 ± 0.4 *,###	68.3 ± 2.0 †,###
	LR	63.9 ± 2.6 †††	62.0 ± 3.3 ###	96.4 ± 0.6 †††,###

$\boldsymbol{CrossVAF_{avg}}$ values averaged across participants obtained when the muscle synergies extracted during a specific FR condition (i.e., Extracted) are used to reconstruct EMG data acquired during the remaining FR conditions (i.e., Reconstructed). Statistically significant differences among tasks are indicated as follows: uniFR vs. biFR by asterisks (*p < 0.05); uniFR vs. LR by daggers (†p < 0.05, †††p < 0.001); biFR vs. LR by sharp signs (#p < 0.05, ###p < 0.001).

6.5.4. Intra- and Inter-task consistency

Figure 6.3 shows the average intra- and inter-task consistency values. Specifically, **Figure 6.3a** demonstrates that uniFR and biFR exhibited high intra-task consistency, with average CS values of 0.75 ± 0.01 and 0.77 ± 0.01, respectively, while LR showed slightly lower intra-task consistency, with an average CS value of 0.61 ± 0.01. No statistically significant difference was detected between uniFR and biFR, while uniFR and LR presented a statistically significant difference ($p < 0.001$, $|g| = 1.68$).

With regard to inter-task consistency, as shown in **Figure 6.3b**, uniFR and biFR displayed a relatively high degree of similarity, with an average CS of 0.77 ± 0.01, comparable to the intra-task consistency of these tasks. Conversely, the similarity between uniFR and LR was much lower (average $CS = 0.54 \pm 0.01$) and statistically significant different ($p < 0.001$, $|g| = 2.42$).

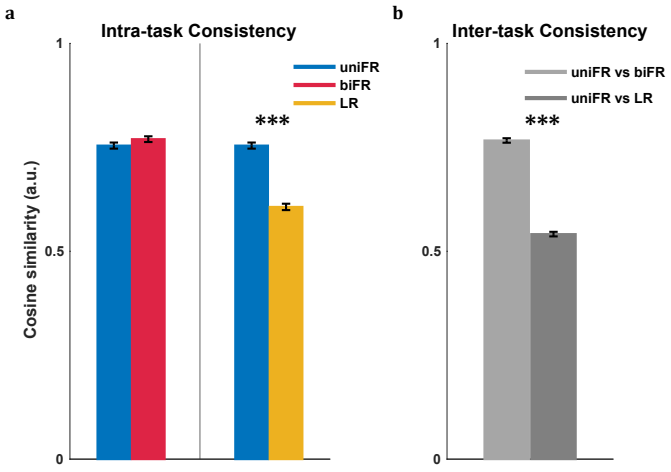

Figure 6.3. (a) Intra-task consistency averaged across all muscle synergies for each task. **(b)** Inter-task consistency between tasks averaged across all muscle synergies and across participants. All data are reported as mean ± SE. Statistically significant differences (***p < 0.001) are indicated by asterisks. uniFR: unilateral Functional Reach; biFR: bilateral Functional Reach; LR: Lateral Reach.

Figure 6.4 represents the intra-task consistency separately for each muscle synergy, comparing uniFR vs. biFR (**Figure 6.4a** and **Figure 6.4b**) and uniFR vs. LR (**Figure 6.4c** and **Figure 6.4d**). A statistically significant difference in intra-task consistency values between uniFR and biFR ($p < 0.001$, $|g| = 0.35$) was observed only for the first muscle synergy (see **Figure 6.4a**). No significant changes were observed in the temporal activation patterns of the muscle synergy extracted during uniFR and biFR tasks, as none of the SnPM curves exceeded the significance threshold (see **Figure 6.4b**).

Comparing intra-task consistency between uniFR and LR tasks, results revealed statistically significant differences for the first and the second muscle synergy (Syn_1: $p < 0.001$, $|g| = 2.25$; Syn_2: $p < 0.001$, $|g| = 1.29$) (see **Figure 6.4c**). SPM analysis revealed significant differences in activation coefficients between uniFR and LR for Syn_1 (around 30–60%) and Syn_2 (around 67–78%) (see **Figure 6.4d**). For Syn_3, a brief but significant difference was observed at the beginning of the reaching task, approximately within the 0-3% range.

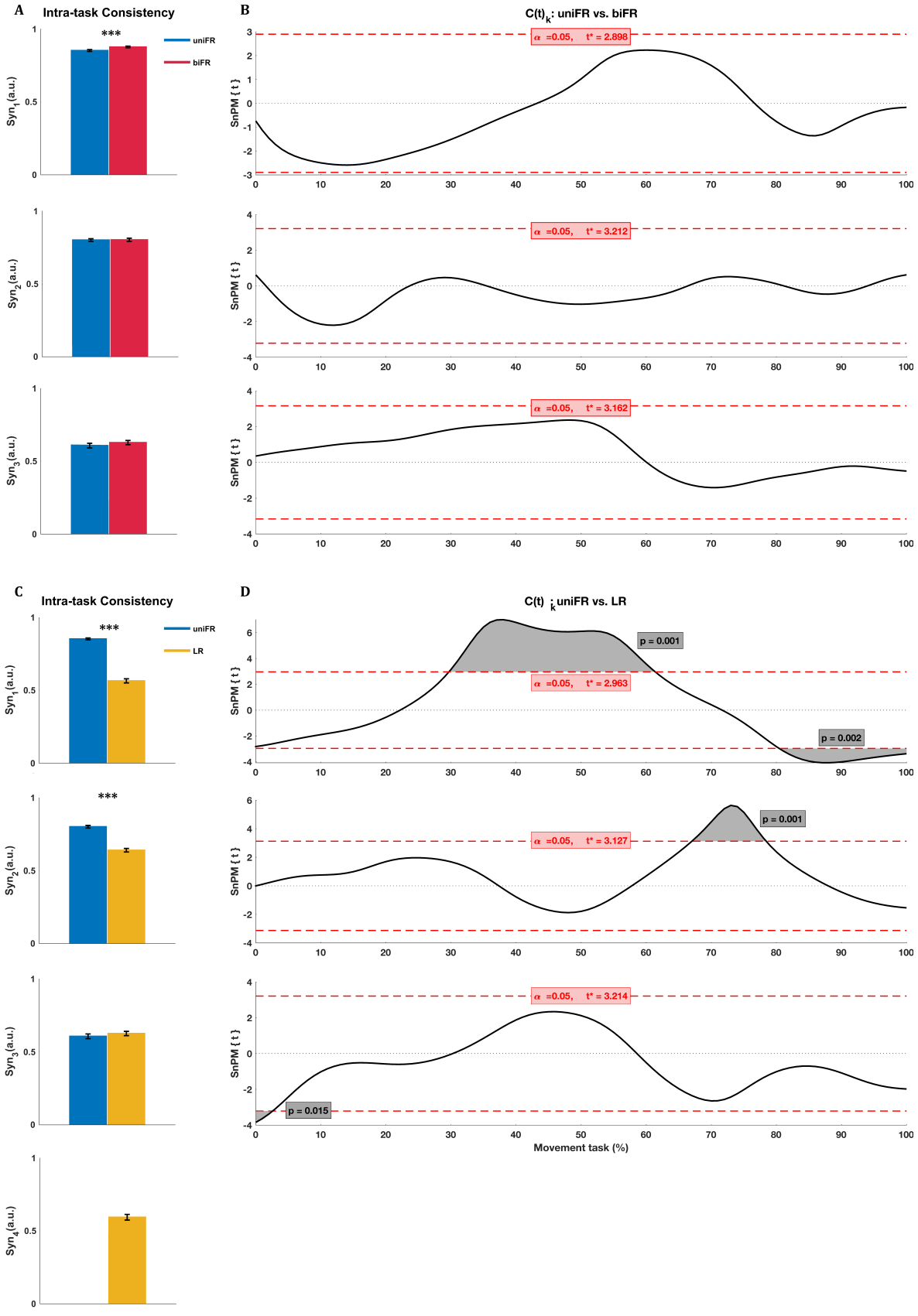
A
Intra-task Consistency
***
uniFR
biFR
Syn1(a.u.)
Syn2(a.u.)
Syn3(a.u.)
B
C(t)k: uniFR vs. biFR
α =0.05, t* = 2.898
α =0.05, t* = 3.212
α =0.05, t* = 3.162
SnPM{t}
C
Intra-task Consistency
***
uniFR
LR
Syn1(a.u.)
Syn2(a.u.)
Syn3(a.u.)
Syn4(a.u.)
D
C(t)k: uniFR vs. LR
p = 0.001
α =0.05, t* = 2.963
p = 0.002
α =0.05, t* = 3.127
p = 0.001
α =0.05, t* = 3.214
p = 0.015
SnPM{t}
Movement task (%)

1050

Figure 6.4. (a) Intra-task consistency of uniFR and biFR tasks for each muscle synergy (Syn_k), separately. **(b)** Statistical differences in activation coefficients as computed through SnPM between uniFR and biFR. **(c)** Intra-task consistency of uniFR and LR tasks for each muscle synergy (Syn_k), separately. **(d)** Statistical differences in activation coefficients as computed through the SnPM between uniFR and LR. In (b) and (d) the horizontal dashed red lines represent critical t-values (t*) at α=0.05, while the grey areas highlight intervals with statistically significant differences. Statistically significant differences in cosine similarity values between tasks (***p < 0.001) are indicated by asterisks. uniFR: unilateral Functional Reach; biFR: bilateral Functional Reach; LR: Lateral Reach. SnPM: Statistical nonParametric Mapping.

6.6. Discussion

The Functional Reach (FR) test and its recent variations across multiple directions assess voluntary reaching while standing, a complex motor action for daily life. These tests are commonly used by clinicians since they challenge dynamic balance and require whole-body coordination. This study advances the understanding of neuromuscular coordinative strategies underlying the control of postural stability across different variations of the FR tests. Additionally, it establishes a reference baseline for future assessments in elderly or pathological populations.

In agreement with our initial hypotheses, the present study show that a limited number of muscle synergies is sufficient to accurately model functional reach tasks, reinforcing current knowledge on the modular organization of motor control and the coordinated activation of muscle patterns, as hypothesized for a shared modular control across task variations. Specifically, on average, we identified three muscle synergies to model FR tasks in the forward direction performed with the dominant side only (uniFR) and both sides (biFR). In contrast, an additional muscle synergy was needed to describe the different biomechanical demands required by the LR task, indicating a partial divergence from our second hypothesis.

Our findings on the FR task partially align with the research conducted by Krishnamoorthy et al. (2003), who observed that the control of bipedal upright posture during voluntary sway or arm movement tasks is regulated by at least two distinct muscle synergies: one for forward shifts and another for backward shifts. They also suggested that the CNS utilizes specific combinations of these synergies depending on the direction of movement. The difference in the number of muscle synergies identified may be attributed to several factors: *i*) the more dynamic balance task involving both voluntary swaying and arm movements in our study; *ii*) the inclusion of a broader group of muscles in the muscle synergy analysis, extending beyond postural muscles; and *iii*) variations in EMG pre-processing procedures, such as filtering. This comprehensive approach likely contributed to the identification of three muscle synergies associated with these tasks.

In this study, we quantified and compared muscle synergies' robustness and consistency across different FR variations to provide insights into task generalizability and temporal variability, respectively. Despite the decrease in robustness when reconstructing LR EMG data, common muscle synergies were identified between lateral- and forward-reaching tasks. When considering muscle synergy variability over time, a slightly lower temporal variability (i.e., higher consistency) was observed in the forward-reaching tasks compared to the lateral-reaching task. These findings suggest that forward-reaching tasks share a more stable neuromuscular control strategy compared to lateral-reaching movements, which require more adaptive motor patterns, potentially reflecting greater functional complexity. This aligns with the findings of other authors (D. A. Winter et al., 1996), who demonstrated that during standing reach-to-target tasks, bilateral EMG activity is tuned to distinct reaching directions, with muscle groups being activated on similar reach directions, suggesting that pre-movement and pre-target muscle activation patterns correspond to a limited number of robust functional muscle synergies. Our study confirms this directional relationship, revealing greater similarity in muscle synergy composition between uniFR and biFR tasks compared to the LR task in which postural control requires a shift from the anterior-posterior to medial-lateral direction.

To gain an overall understanding of the motor control strategies adopted by the CNS during reaching tasks, EMG data recording included not only muscles of the lower leg but also thigh and trunk muscles that are involved in stabilizing the ankle, knee, and hip joints. In accordance with Monte et al. (2024), the muscle synergies identified in the present study exhibited a combination of lower leg muscles with either thigh or trunk muscles. This pattern suggests that muscle synergies are organized more by function than by strict anatomical grouping (Monte et al., 2024).

By evaluating the primary contributions of muscles within each muscle synergy, we proposed specific motor functions associated with each muscle synergy that were shared between uniFR and biFR. The first synergy was mainly related to the transition from a static posture to a forward-leaning posture during the execution of the reach. The involvement of calf and posterior trunk muscles is in line with Maranesi et al. (2016a), who reported that these muscles become active at approximately 20% of the FR period. Since anterior-posterior postural adjustments are mainly under ankle control (D. A. Winter et al., 1996), our findings appear to confirm the use of the "ankle" strategy in the forward direction due to an increased plantar-flexion torque at the ankle joint originating from the activation of GastM and Sol muscles. The second synergy, involving dorsal muscles (i.e., ES, BF, and GastM) was mainly associated to

counteracting the lean and stabilizing the lower limbs during the backward movement to return to the upright posture. Their recruitment at the point of maximum reach is consistent with the activation patterns described by (Crenna et al., 1987). The third and final synergy was primarily responsible for postural adjustments and was most active during the preparatory and final phases of the reaching task through the activation of VL and TA muscles. This finding aligns with those of Trivedi et al. (2010), who reported that activation of these muscles accompanies preparatory adjustments, while the Sol and GastM muscles are inhibited before reaching onset. Although the muscle synergy vectors and activation coefficients were similar between uniFR and biFR tasks, some differences were observed in terms of temporal variability, particularly regarding the first muscle synergy. Specifically, in the first synergy, the biFR task showed higher intra-task consistency than uniFR in muscle synergy weightings among participants. Similar differences in spatial composition of muscle synergies across individuals have been reported in other studies (Frère & Hug, 2012; Hilt et al., 2018; Hug et al., 2010; Torres-Oviedo et al., 2006), and could be related to subtle differences in biomechanical functions (Ting & Macpherson, 2005; Torres-Oviedo & Ting, 2007), suggesting a subject-specific modular organization of motor control. The higher consistency observed in biFR may also be due to the requirement for coordinated use of dominant and non-dominant sides. Interestingly, even the uniFR task entails a symmetrical muscle contribution, suggesting that, although the movement is unilateral and one side of the body is expected to be activated more than the other to counteract the unilateral load, the neuromuscular control strategy engages both sides of the body in a coordinated manner. One possible explanation for this symmetry is the need to maintain trunk stability during reaching movements to limit compensatory twisting. In young individuals with sufficient strength levels, this asymmetric load is likely well-regulated, allowing for an overall balanced neuromuscular response.

When analyzing the LR task, it was observed that the second and third synergies retained similar biomechanical functions to those identified in uniFR and biFR. In contrast, although the dominant was unilaterally employed for uniFR and LR tasks, the lateral body-weight shifting during LR exhibited different muscle contributions between the dominant and non-dominant sides, underscoring the asymmetric nature of the movement. The involvement of the non-dominant ES muscle during the contralateral sway of the body aligns with the research by Chvatal and Ting , who found that a muscle synergy that was characterized by a major activation of ES was recruited for medial-lateral perturbations. The third synergy was linked to postural adjustments on the contralateral side, driven by the GastM and Sol ankle muscles. These results

support the hypothesis proposed by Chvatal et al. (2011), who suggested that during bipedal balance control, the muscle activity of the contralateral leg (which was not recorded in their study) played a crucial role in generating the acceleration of CoM toward the side of the perturbation in response to the disturbance in that direction. Such mechanism would support the idea that postural control involves coordinated actions across both limbs, particularly when shifting weight laterally. In the LR task, as the body prepares to shift weight in the dominant direction, the non-dominant leg supports the body load, resulting in the activation of the ankle muscles first, followed by the thigh and trunk muscles. Consistently, the first synergy exhibited the recruitment of the non-dominant LD, VL, and TA, which are likely activated to stabilize the lateral leaning while the dominant side was loaded. The LD muscles appear to be responsible for trunk stabilization in the fourth synergy, particularly on the dominant side. The first synergy supported ipsilateral stabilization, while the fourth was associated with arm elevation and trunk control. The motor functions observed during these two synergies appeared to be grouped within the first synergy for both uniFR and biFR tasks. This pattern illustrates how the same core set of synergies can be flexibly reorganized across tasks, as their functions are selectively merged or separated to accommodate specific biomechanical demands. This interpretation is consistent with previous observations that the CNS preserves a stable repertoire of motor modules that can be adaptively combined in different contexts (Saito et al., 2021; Torres-Oviedo & Ting, 2007).

During the LR task, we observed increased co-contraction of muscles enrolled in the first muscle synergy, particularly in the dominant side. This finding aligns with established research on neural adaptations during postural control (Latash, 2018). In a study by Krishnamoorthy and colleagues (2004), they observed that the CNS dynamically adapts the muscle synergies during voluntary sway or arm movement tasks, drawing from a broader “menu” that includes both simultaneous activation of agonists and antagonists. In healthy individuals, such co-activation reflects task complexity and may confer stability benefits (Latash, 2018). Our observation of increased muscle co-contraction supports the established principle that greater instability results in higher co-activation to maintain postural stability.

Moreover, the LR task exhibited greater variability in both intra- and inter-task consistency compared to the similarly monoliteral and forward-directed FR task. Specifically, all synergies demonstrated moderate intra-task consistency across participants, with the exception of the third synergy, which did not differ from the third one in the uniFR task. Nevertheless, the overall intra-task consistency of the LR task was significantly lower than that of the uniFR task, and its

inter-task consistency was substantially lower than that observed between uniFR and biFR tasks. This could be attributed to the LR task being less standardized across participants, resulting in high execution variability and consequent greater variability in neural commands, reflecting a less consistent motor control strategy. Additionally, the lower robustness observed in the reconstruction of LR EMG patterns using uniFR and biFR muscle synergies may be due to the different biomechanical demands of the LR task. Specifically, postural control in the medial-lateral direction is essential for maintaining dynamic stability (Rogers & Mille, 2003) due to the specific strategies employed. Notably, the 'hip strategy' is used to manage mid-lateral oscillations (D. A. Winter et al., 1996), requiring the activation of stabilizing muscles in the hip and trunk to maintain balance. Future studies should incorporate the analysis of additional muscles involved in hip stabilization (i.e. gluteal muscles, rectus femoris) to enhance our understanding of neuromuscular strategies underlying medial-lateral postural control. However, it is clear that the increased variability observed in the LR task may be linked not only to lower standardization but also to the greater postural challenge it presents, which could vary among individuals.

Our findings also indicated that feedforward and feedback postural adjustments share common "motor primitives" as hypothesized by Leonard et al. (2009). Feedforward postural adjustments are initiated when the goal is to actively shift the CoM within the base of support. In contrast, when the task requires precise control of an end posture and a return to an upright position, feedback postural adjustments are employed. In our study, the third synergy encompassed these mechanisms. Voluntary arm raising movements are preceded by feedforward postural adjustments of leg muscles to counteract for the upcoming mechanical perturbation associated with the arm movement (Aruin & Latash, 1995; Belen'kiĭ et al., 1967; Massion, 1984; Zattara & Bouisset, 1988). In contrast, the feedback mechanism is activated following the self-generated perturbation in transitioning from a stable upright posture to a forward or lateral leaning position. Interestingly, the third synergy, which accounts for these aspects, exhibited a comparable level of intra-task consistency across all tasks. This indicates that, in young healthy individuals, feedforward and feedback mechanisms appear to be finely tuned to control postural changes and movement performance.

Some limitations of the present study should be acknowledged. First, the small sample size may limit the generalizability of the findings to broader healthy populations. Second, participants in the present study were instructed to perform FR tasks according to specific reaching execution strategies (i.e., avoiding torso rotation, knee bending, and heel lifting). It would be valuable to

explore how muscle synergies adapt when reaching strategies are unrestricted, as suggested by Wernick-Robinson et al. (1999), who reported that movement strategy influences FR distance. Furthermore, while kinematic data were collected, this study focused specifically on muscle synergy analysis through EMG data. This targeted analytical approach was chosen to thoroughly examine neuromuscular coordination patterns without the additional complexity of kinematic variables. Future studies could integrate movement kinematics and center of pressure excursion to better characterize these tasks and enhance understanding of the dynamic interaction between motor control, balance, and muscle activation. This integration would potentially enrich our understanding of the underlying mechanisms, though the current EMG-focused analysis provides valuable standalone insights into the neural control strategies employed during the tasks examined. Additionally, the fact that all participants were Caucasian may limit the generalizability of the findings to populations with broader ethnic representation. This homogeneity was due to the demographic composition of the recruitment area, rather than an a priori exclusion of other ethnic groups. Finally, although we chose not to explore the differences between the dominant and non-dominant sides in this study, the investigation of this aspect would help in better understanding the symmetry between uniFR and biFR tasks.

In conclusion, our findings suggest that anterior-posterior functional reaches rely on well-structured and consistent motor patterns, reflecting a high level of movement stability and reliability. In contrast, lateral reaching movements require more refined neuromuscular control, likely due to the increased complexity associated with medial-lateral weight shifting and intersegmental coordination. This distinction underlines the relevance of assessing not only the maximal reach distance but also the coordination patterns that sustain balance and movement.

By quantifying the composition and adaptability of muscle synergies, this study provides an objective framework to understand how the CNS organizes movement strategies in response to directional demands. This approach holds potential for early detection of age-related neuromuscular decline or differentiation of motor control deficits in neurological disorders. Identifying direction-specific alterations in synergies might guide targeted rehabilitation by highlighting muscle groups requiring focused intervention. Importantly, the higher specificity and variability of lateral reaching synergies suggest that training or rehabilitation protocols limited to anterior-posterior movements may not fully generalize to lateral postural control. Including multi-directional balance and reaching exercises could therefore enhance adaptability and functional outcomes. Overall, these findings lay the groundwork for creating

reference datasets of functional tasks in healthy young individuals, supporting future efforts to screen and monitor alterations in motor coordination associated with aging or neurological disorders.

7. Study II: Task-Dependent Intermuscular Coherence between Postural Muscles during Voluntary Upright Reaching

Imma Ceriello[1] · Riccardo Borzuola[1] · Valentina Camomilla[1] · Andrea Macaluso[1] · Madeleine Lowery[2]

[1]Laboratory of Bioengineering and Neuromechanics, Department of Movement, Human and Health Sciences, University of Rome "Foro Italico", Rome, Italy

[2]School of Electrical and Electronic Engineering, University College Dublin, Dublin, Ireland

Publication submitted to the Experimental Physiology Journal and currently in an advanced stage of peer review.

Author contributions: Imma Ceriello, Riccardo Borzuola, Valentina Camomilla, and Andrea Macaluso developed and planned the research; Imma Ceriello and Riccardo Borzuola conducted the experiments; Imma Ceriello analyzed the data; Imma Ceriello and Madeleine Lowery interpreted the experimental results; Imma Ceriello created the figures; Imma Ceriello and Riccardo Borzuola drafted the manuscript; Imma Ceriello, Riccardo Borzuola, Valentina Camomilla, Andrea Macaluso, and Madeleine Lowery reviewed and revised the manuscript; Imma Ceriello, Riccardo Borzuola, Valentina Camomilla, Andrea Macaluso, and Madeleine Lowery gave their approval for the final version of the manuscript.

7.1. Rationale and Objectives

While previous studies have characterized intermuscular coherence during static or isolated postural tasks (Danna-Dos-Santos et al., 2014; García-Massó et al., 2016; Konieczny et al., 2022; Nandi et al., 2019; Noé et al., 2017; Nojima et al., 2020; Tsiouri et al., 2024; Watanabe et al., 2018a, 2018b), the neural coordination underlying compound movements, which combine voluntary goal-directed actions and dynamic postural adjustments, remains largely unexplored. Gaining insight into how coherence patterns adapt during these movements is important for understanding how the CNS flexibly integrates automatic and voluntary components to maintain balance under varying mechanical constraints.

Objectives: The present study aimed to determine whether the coherence of oscillatory activity between postural trunk and lower-limb muscles during upright reaching reflects direction-dependent modulation or a common neural drive that generalizes across reaching directions.

Furthermore, the analysis evaluated how these neural coordination patterns interact with the biomechanical requirements of balance control, providing a comprehensive view of the interplay between neural and mechanical aspects of postural regulation. Understanding how neural coupling adapts, or fails to adapt, to distinct postural demands provides critical insight into the flexibility of CNS control and may constitute a physiological marker for impaired postural adaptability in clinical populations. It was hypothesized that intermuscular coherence would vary according to the direction of reaching, demonstrating task-specific neural adaptations to the biomechanical requirements of different directions. Additionally, functionally synergistic muscles were expected to exhibit synchronized activity, suggesting a common neural drive contributing to postural stability.

7.2. Experimental Procedure

Participants and experimental procedure adhered to the overall methodology outlined in **Chapter 5**. Data collection took place during the uniFR, biFR, and LR tasks (refer to **Section 5.3.1**) involving a total of 17 healthy young individuals (10 males and 7 females; mean age: 27.5 ± 3 years; mean height: 1.7 ± 0.1 m; mean body mass: 64.9 ± 8.8 kg; with 2 left-handed and 15 right-handed individuals) (see **Section 5.2** for criteria for inclusion).

The procedures for EMG recording and motion analysis were consistent with the established framework in **Section 5.3.4**. Specifically, this research encompassed the collection of surface EMG signals, full-body kinematic data via a stereophotogrammetric system, as well as measurements taken from the force platforms.

As the task was designed to assess dynamic balance rather than upper-limb performance, coherence analyses were limited to trunk and lower-limb muscles primarily contributing to postural stabilization. Accordingly, among the recorded muscles, erector spinae (ES), tibialis anterior (TA), gastrocnemius medialis (GastM), and soleus (Sol) were considered for the present analysis. This selection is consistent with previous studies on postural tasks investigating intermuscular coherence patterns (Boonstra et al., 2009; García-Massó et al., 2016; Konieczny et al., 2022; Nandi et al., 2019; Watanabe et al., 2018a).

7.3. Data Analysis

7.3.1. Identification of reaching repetitions

The process for identifying reaching repetitions was carried out as outlined in **Chapter 6, Section 6.3.1**. Reaching repetitions were segmented based on hand kinematics, with trial onset defined as the instant at which hand velocity exceeded 10% of its peak value and trial

termination defined as the instant at which hand velocity fell below 10% of its peak value. For coherence estimation, trials belonging to the same task for each participant were subsequently concatenated prior to analysis, as described in the following section (see **Section 7.3.3-7.3.4**). Visual inspection of task execution was performed a posteriori, and those repetitions which exhibited an incorrect execution of the reaching task were removed from further analysis.

7.3.2. Center of pressure

The center of pressure (CoP) was calculated using data from two force plates corresponding to the left CoP_L and right CoP_R sides. Vertical ground reaction forces (F_Z) were obtained for each plate and used to compute a weighted average of the individual CoPs, resulting in a global CoP trajectory. A zero-lag, 4th-order Butterworth low-pass filter with a cutoff frequency of 12 Hz was applied to remove high-frequency noise. The global CoP in both the AP and ML directions was estimated at each time point using a weighted average based on the vertical ground reaction forces (Exell et al., 2011):

$$CoP_{AP}(t) = \frac{CoP_{L,y}(t) \cdot F_{Z,L}(t) + CoP_{R,y}(t) \cdot F_{Z,R}(t)}{F_{Z,L}(t) + F_{Z,R}(t)} \quad (7.1)$$

$$CoP_{ML}(t) = \frac{CoP_{L,x}(t) \cdot F_{Z,L}(t) + CoP_{R,x}(t) \cdot F_{Z,R}(t)}{F_{Z,L}(t) + F_{Z,R}(t)} \quad (7.2)$$

where $CoP_{L,y}(t)$ and $CoP_{R,y}(t)$ are the AP positions from the left and right force plates, and $CoP_{L,x}(t)$ and $CoP_{R,x}(t)$ are the corresponding ML positions. $F_{Z,L}(t)$ and $F_{Z,R}(t)$ are the vertical ground reaction forces from the left and right plates, respectively. The resulting CoP trajectory was then offset-corrected by subtracting the mean position in each direction and segmented according to the previously identified reaching repetitions.

To quantify the displacement of the CoP, the pathlength (PL_{CoP}) of each trajectory was computed in the horizontal plane. PL_{CoP} was used to quantify the total amount of displacement, reflecting the cumulative distance travelled by the CoP. This metric was computed for each repetition and normalized by the participant's height to allow for inter-subject comparisons. PL_{CoP} was calculated as the cumulative Euclidean distance between consecutive sampling points in the AP and ML directions, based on the formulation originally proposed by Hufschmidt et al. (1980), and modified here to include height normalization:

$$PL_{CoP} = \frac{1}{h}\sum_{i=1}^{n-1}\sqrt{(x_{i+1}-x_i)^2+(y_{i+1}-y_i)^2} \quad (7.3)$$

where (x_i, y_i) represent the ML and AP coordinates, n is the number of samples, and h is the participant's height. For each condition, PL_{CoP} values across repetitions were then summarized by computing the median.

7.3.3. EMG pre-processing

EMG data were high-pass filtered using a 4th-order, zero-lag Butterworth filter with a cut-off at 10 Hz to remove movement artefacts. After filtering, EMG data were full-wave rectified, as indicated by previous studies (Boonstra & Breakspear, 2012; Halliday & Farmer, 2010; Myers et al., 2003; Ward et al., 2013), and concatenated across trials prior to the intermuscular coherence analysis. A sensitivity analysis using Hilbert-derived envelopes and unrectified EMG signals was also conducted to exclude possible rectification effects (see **Appendix – Supplementary Materials, Figures S7.1–S7.2**).

7.3.4. Intermuscular coherence analysis

The magnitude-squared coherence between EMG signals recorded from pairs of muscles was calculated to assess the frequency domain coupling between both bilateral and unilateral EMG signals for each reaching task. Bilateral EMG coherence was estimated between homologous muscles of the dominant and non-dominant limbs, specifically the TA, GastM, and Sol. Unilateral coherence was estimated between intra-limb muscle pairs, TA–GastM, GastM–Sol, ES–GastM, ES–Sol, and ES–TA, on both the dominant and non-dominant sides. In this context, the term "dominant" refers to the body side corresponding to the participant's dominant upper limb, which was used to perform the unilateral and lateral reaching tasks. This distinction was included to assess potential side-specific modulation related to the functional involvement of the dominant limb during task execution.

A surrogate data analysis, involving the cross-subject combination of EMG signals, was also employed to confirm that observed coherence between ES and ankle postural muscles (TA, GastM, and Sol) reflected correlated neural inputs (see **Appendix – Supplementary Materials, Figure S7.3**). Coherence was estimated using Welch's method with a Hanning window of 2048 samples and 75% overlap, yielding a frequency resolution of 0.98 Hz (Kattla & Lowery, 2010). For each EMG signal pair, *x(t)* and *y(t)*, the magnitude squared coherence at frequency *f* was estimated as

$$C_{xy}(f) = \frac{|S_{xy}(f)|^2}{S_{xx}(f)S_{yy}(f)} \tag{7.4}$$

where $S_{xy}(f)$ is the cross spectrum and $S_{xx}(f)$ and $S_{yy}(f)$ are the auto spectra of $x(t)$ and $y(t)$. The value of $C_{xy}(f)$ ranges from 0 to 1, where a value of 1 indicates a perfect linear relationship between $x(t)$ and $y(t)$, while a value of 0 indicates no linear relationship between the two signals at that frequency. For non-overlapping segments with taper, a coherence estimate is typically deemed significant at $P < a$ if the magnitude squared coherence exceeds $Z = 1 - \alpha^{1/(L-1)}$, where L represents the total number of disjoint segments utilized for calculating the coherence (Rosenberg et al., 1989) and a = 0.05, which corresponds to a confidence interval above 95%. To account for overlapping segments with taper, the significance level was modified according to the method described by Welch (1967) and adapted by Terry & Griffin (2008):

$$Z_{ovlp} = 1 - \alpha^{1/(wL^*-1)} \tag{7.5}$$

$$L^* = floor\left[\frac{(L-1)}{(1-ovlp)}\right] + 1 \tag{7.6}$$

where the variable *ovlp* is the percentage of overlap between segments, while L^* denotes the count of overlapping segments. The weighting factor, w, depends on the degree of overlap and taper type. For tapered segments, the calculation of w follows the method outlined by Kattla & Lowery (2010). To reduce the probability of detection of spurious or 'false' coherence, the probability of detection P_D was also determined using the approach described by Carter (1977). This quantity represents the probability that the estimated coherence $\hat{C}$ exceeds the threshold Z_{ovlp}, given a true underlying coherence value C:

$$P_D = \int_{Z_{ovlp}}^{1} p\left(\hat{C}|L^*, C\right)d\hat{C} = 1 - P(\hat{C} \leq Z_{ovlp}|L^*, C) \tag{7.7}$$

where $p\left(\hat{C}|L^*, C\right)d\hat{C}$ is the conditional probability density function of the estimated coherence. The cumulative distribution function $P(\hat{C} \leq Z_{ovlp}|L^*, C)$ expresses the probability that the estimated coherence does not exceed the threshold, for a given true coherence C and number of overlapping segments L^*. Accordingly, coherence at a given frequency was considered statistically significant only if two conditions were met: (1) $\hat{C} > Z_{ovlp}$, and (2) the probability of detecting such a coherence, P_D, exceeded 0.95 (Lowery et al., 2007). This dual criterion ensured both statistical significance and adequate detection power. The EMG-EMG coherence

values that met these two criteria were then integrated within each of the delta (0-5 Hz), alpha (8-12 Hz), beta (13-35 Hz), and low gamma (35-60 Hz) frequency bands.

7.3.5. Co-contraction index

Co-contraction was estimated using a modified version of the co-contraction index (CCI) originally proposed by Rudolph et al. (2000), introducing temporal normalization to allow direct comparison across subjects. The EMG signals were first band-pass filtered from 30–450 Hz using a 100th-order Finite Impulse Response (FIR) filter applied with zero-phase distortion, to remove movement artifacts and high-frequency noise. The signals were then full-wave rectified, and the linear envelope extracted using a 4th-order low-pass Butterworth filter with a cutoff frequency of 10 Hz, applied with zero-phase distortion. To ensure consistency with the coherence analysis, which was computed over concatenated repetitions, EMG envelopes were amplitude-normalized using the median of the maximum values observed for each repetition and each muscle. The CCI was then computed on these globally normalized signals, allowing for direct comparison with coherence values derived from the same time window.

The CCI was computed using the following discrete-time, duration-normalized equation:

$$CCI_{norm} = \frac{1}{T}\sum_{i=1}^{N}\left[\frac{EMGSi}{EMGLi} \cdot (EMGSi + EMGLi)\right] \cdot \Delta t \tag{7.8}$$

where $EMGS$ is the activity of the less-active muscle at each time point, $EMGL$ is the activity of the more active muscle, Δt is the time interval between samples, and T is the total duration of the FR repetition. This sample-by-sample formulation yields a time-averaged estimate of co-contraction intensity. CCI_{norm} was assessed between the TA and the GastM antagonist muscles and calculated separately for the dominant and non-dominant sides.

7.4. Statistical Analysis

Linear mixed-effects models were applied to evaluate the influence of frequency band, task, dominance, and muscle pair on coherence values. These factors and their interactions were incorporated as fixed effects, while participant was considered as a random factor to account for variability among subjects. Distinct models were developed for unilateral and bilateral conditions. Post-hoc pairwise comparisons were carried out on the estimated marginal means, applying Bonferroni correction to adjust for multiple comparisons. Comparisons were performed within combinations of the relevant fixed factors, and the resulting p-values were utilized to determine statistical significance. P-values were presented using heatmaps

organized by the relevant combinations of task, muscle pair, dominance, and frequency band. P-values below 0.05 were deemed statistically significant.

Correlation analyses were performed to investigate the relationships between intermuscular coherence and two outcome measures: the CCI_{norm}, which reflects neuromuscular coordination, and the PL_{CoP}, which serves as an indicator of postural stability. The analyses were carried out independently for each frequency band (delta, alpha, beta, and low gamma), task condition (biFR, uniFR, LR), and configuration (unilateral or bilateral). The Shapiro–Wilk test was used to evaluate the normality of coherence and each performance measure; based on those results, either Pearson or Spearman correlation coefficients were calculated. All obtained p-values were corrected for multiple comparisons using the Bonferroni method and reported separately according to dominance (for CCI_{norm}) or configuration (for CoP).

The effect size of statistically significant differences was determined using Hedges' g statistic (Hedges, 1981). According to this measure, g values below 0.2 are considered small, those around 0.5 indicate medium effects, and values above 0.8 represent large effects. Statistical analyses were performed using MATLAB's Statistical and Machine Learning Toolbox (MATLAB version R2022b, The MathWorks Inc., Natick, Massachusetts, United States) and RStudio (version 2025.05.0+496, Posit team (2025). RStudio: Integrated Development Environment for R. Posit Software, PBC, Boston, MA.).

7.5. Results

7.5.1. Task-related differences in intermuscular coherence

Overall, task-dependent modulation of intermuscular coherence was observed between bilateral lower-limb, unilateral lower-limb, and trunk–limb muscle pairs in the delta, beta and low gamma bands.

7.5.1.1. Bilateral muscle pairs

Figure 7.1 shows the integral of the significant coherence in each frequency band, capturing the extent of task-dependent modulation for each bilateral muscle pair. In the delta band, coherence was significantly higher during both biFR and uniFR compared to LR across all bilateral muscle pairs (GastM, Sol, TA), with all comparisons yielding $p < 0.0001$ ($g = 1.7654 – 3.7117$). In the beta band, coherence was greater in uniFR compared to LR for Sol ($p = 0.0462$ $g = 0.8335$) and TA ($p = 0.0433$, $g = 0.8417$), and in biFR compared to LR for Sol ($p = 0.0208$, $g = 0.9294$). In the low gamma band, a task-related difference emerged only for the TA, showing higher coherence in uniFR than LR ($p = 0.0036$, $g = 1.1153$), with no significant differences

observed for the GastM (p = 1) or Sol (p = 0.4204). Alpha-band coherence remained low across all muscle pairs and was unaffected by task.

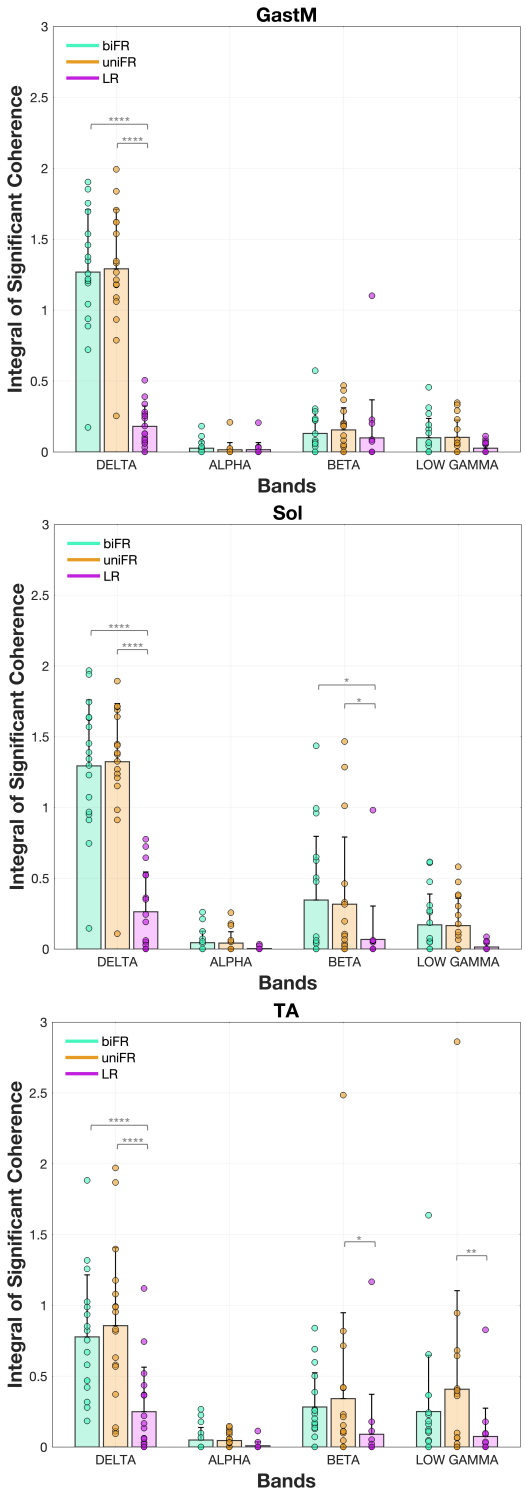

Figure 7.1. Mean values ± standard deviation (with individual data points overlaid) for bilateral muscle pairs of the integral of the coherence lying above the 5% significance threshold and satisfying the detection probability criterion, across the delta, alpha, beta,

and low gamma frequency bands, averaged over all subjects. Separate panels show results for gastrocnemius medialis (GastM), soleus (Sol), and tibialis anterior (TA) muscle pairs. Data are shown for the three Functional Reach conditions: bilateral Functional Reach (biFR, aqua green), unilateral Functional Reach (uniFR, ochre), and Lateral Reach (LR, purple). Individual points are depicted for each participant (n = 17). Asterisks indicate significant differences across tasks (*p < 0.05; **p < 0.01; ***p < 0.001; ****p < 0.0001). Exact p-values are reported in **Figure S7.4**.

The results of the statistical analysis of the effect of task on coherence within each frequency band for the bilateral muscle pairs are presented in **Appendix – Supplementary Materials, Figure S7.4**. The bilateral intermuscular coherence spectra averaged across all subjects are presented in **Figure 7.2**.

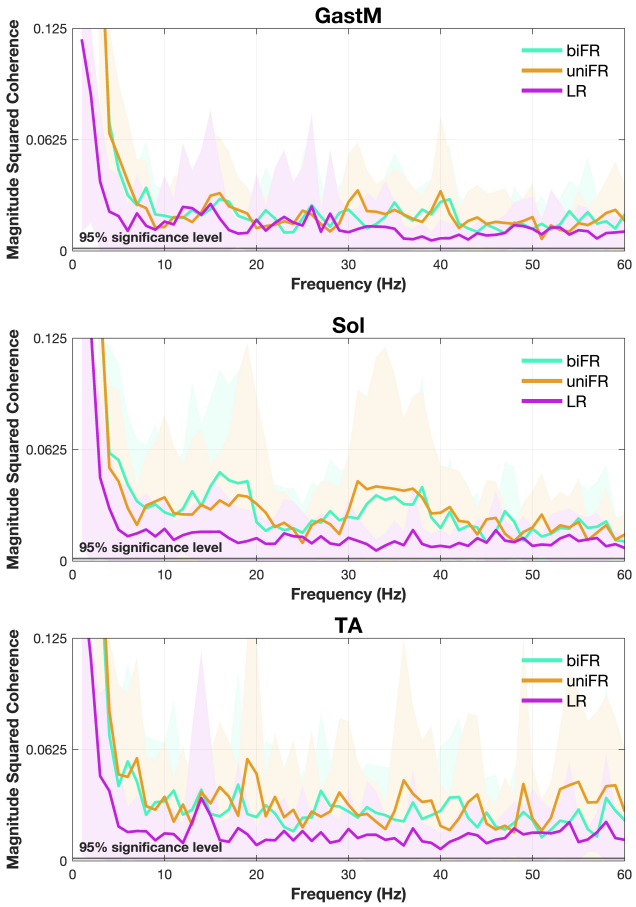

Figure 7.2. Average bilateral magnitude-squared intermuscular coherence spectra across participants for gastrocnemius medialis (GastM), soleus (Sol), and tibialis anterior (TA) muscle pairs (top to bottom panels). Coherence spectra are shown for the three Functional Reach conditions: bilateral Functional Reach (biFR, aqua green), unilateral Functional Reach (uniFR, ochre), and Lateral Reach (LR, purple). Shaded areas indicate the standard deviation across participants. The horizontal dashed line represents the 95% significance level. The y-axis was limited to 0.125 to enhance the visibility of condition-related differences in coherence.

7.5.1.2. Unilateral limb-limb muscle pairs

The integral of the significant coherence between unilateral muscle pairs within each frequency band is presented in **Figure 7.3**. In the delta band, coherence showed distinct task-related

modulations for specific muscle pairs. For the GastM–Sol pair on the dominant side, coherence was significantly higher in uniFR compared to LR ($p = 0.0226$, $g = 0.9176$). In contrast, the TA–GastM pair on the non-dominant side consistently showed greater coherence during LR compared to both uniFR and biFR, with significant differences observed across the delta ($p < 0.0001$, $g = 2.6007$ and $g = 2.5214$, respectively), beta ($p = 0.0004$, $g = 1.3083$, and $p = 0.0077$, $g = 1.0358$, respectively), and low gamma bands ($p = 0.0074$, $g = 1.0401$, and $p = 0.0368$, $g = 0.8596$, respectively). No significant task-related modulation was observed in the alpha band for any unilateral muscle pair.

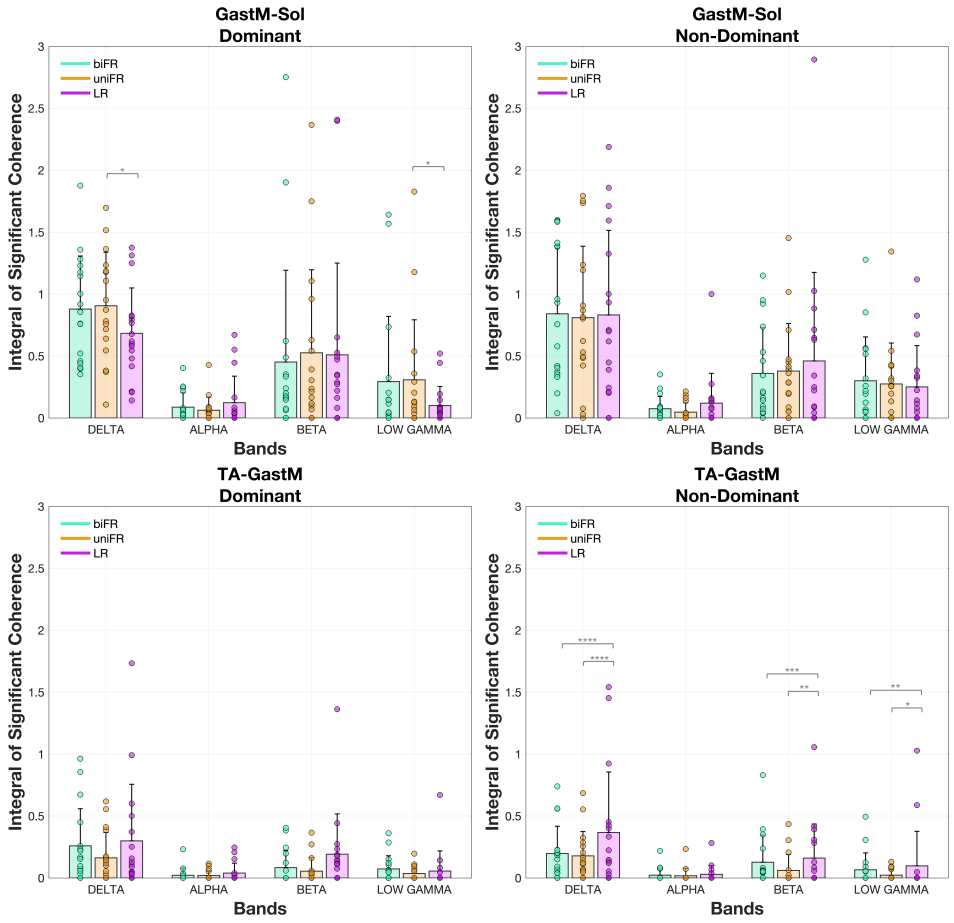

Figure 7.3. Mean values ± standard deviation (with individual data points overlaid) for unilateral muscle pairs of the integral of the coherence lying above the 5% significance threshold and satisfying the detection probability criterion, across the delta, alpha, beta, and low gamma frequency bands, averaged over all subjects. Upper panels show results for the gastrocnemius gedialis–Soleus (GastM–Sol) muscle pair, while lower panels show results for the tibialis anterior–gastrocnemius medialis (TA–GastM) muscle pair. For each muscle pair, data are presented separately for the dominant (left panels) and non-dominant (right panels) sides. Data are shown for the three Functional Reach conditions: bilateral Functional Reach (biFR, aqua green), unilateral Functional Reach (uniFR, ochre), and Lateral Reach (LR, purple). Individual points are depicted for each participant (n = 17). Asterisks indicate significant differences across tasks (*$p < 0.05$; **$p < 0.01$; ***$p < 0.001$; ****$p < 0.0001$). Exact p-values are reported in **Figure S7.4**.

The results of the statistical analysis of the effect of task on coherence within each frequency band for the unilateral limb-limb muscle pairs are presented in **Appendix – Supplementary Materials, Figure S7.4**. The bilateral intermuscular coherence spectra averaged across all participants are presented in **Figure 7.4**.

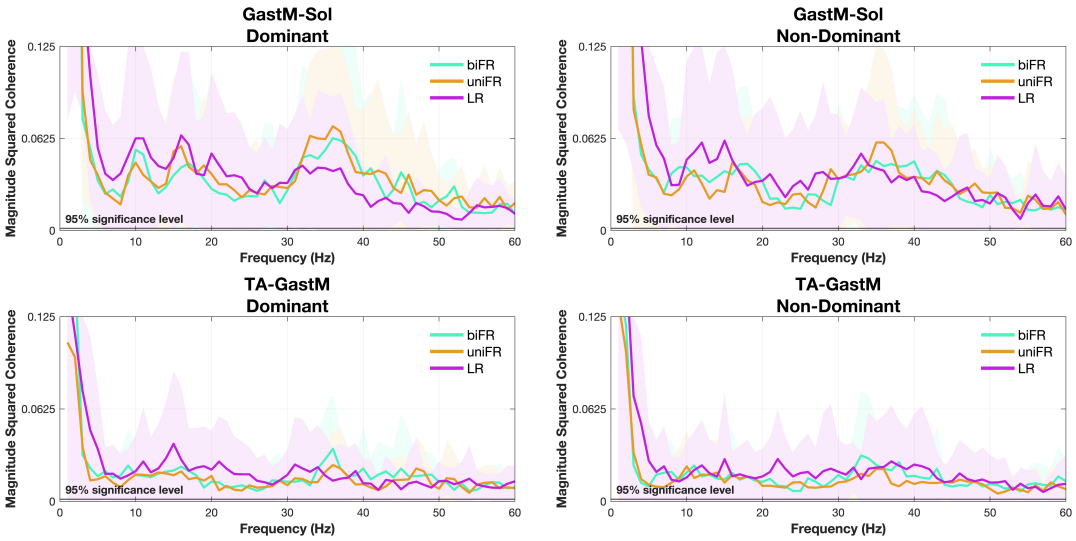

Figure 7.4. Average unilateral magnitude-squared intermuscular coherence spectra across participants. Upper panels show results for the gastrocnemius medialis–soleus (GastM–Sol) muscle pair, and lower panels for the tibialis anterior–gastrocnemius medialis (TA–GastM) muscle pair. For each muscle pair, coherence spectra are presented separately for the dominant (left panels) and non-dominant (right panels) sides. Coherence spectra are shown for the three Functional Reach conditions: bilateral Functional Reach (biFR, aqua green), unilateral Functional Reach (uniFR, ochre), and Lateral Reach (LR, purple). Shaded areas indicate the standard deviation across participants. The horizontal dashed line represents the 95% significance level. The y-axis was limited to 0.125 to enhance the visibility of condition-related differences in coherence.

7.5.1.3. Unilateral trunk-limb muscle pairs

The integral of the significant coherence between the unilateral trunk and limb muscle pairs involving the ES muscle examined is presented in **Figure 7.5** for each task and frequency band. In the delta band, task-related modulation was evident: coherence for ES–GastM and ES–Sol was significantly higher during biFR and uniFR compared to LR ($p < 0.0001$, $g = 2.0012 – 2.8329$, both sides), while no differences were observed across tasks for ES–TA ($p = 1$). No task-related effects emerged in the beta, low gamma, or alpha bands for any ES-involved pairing.

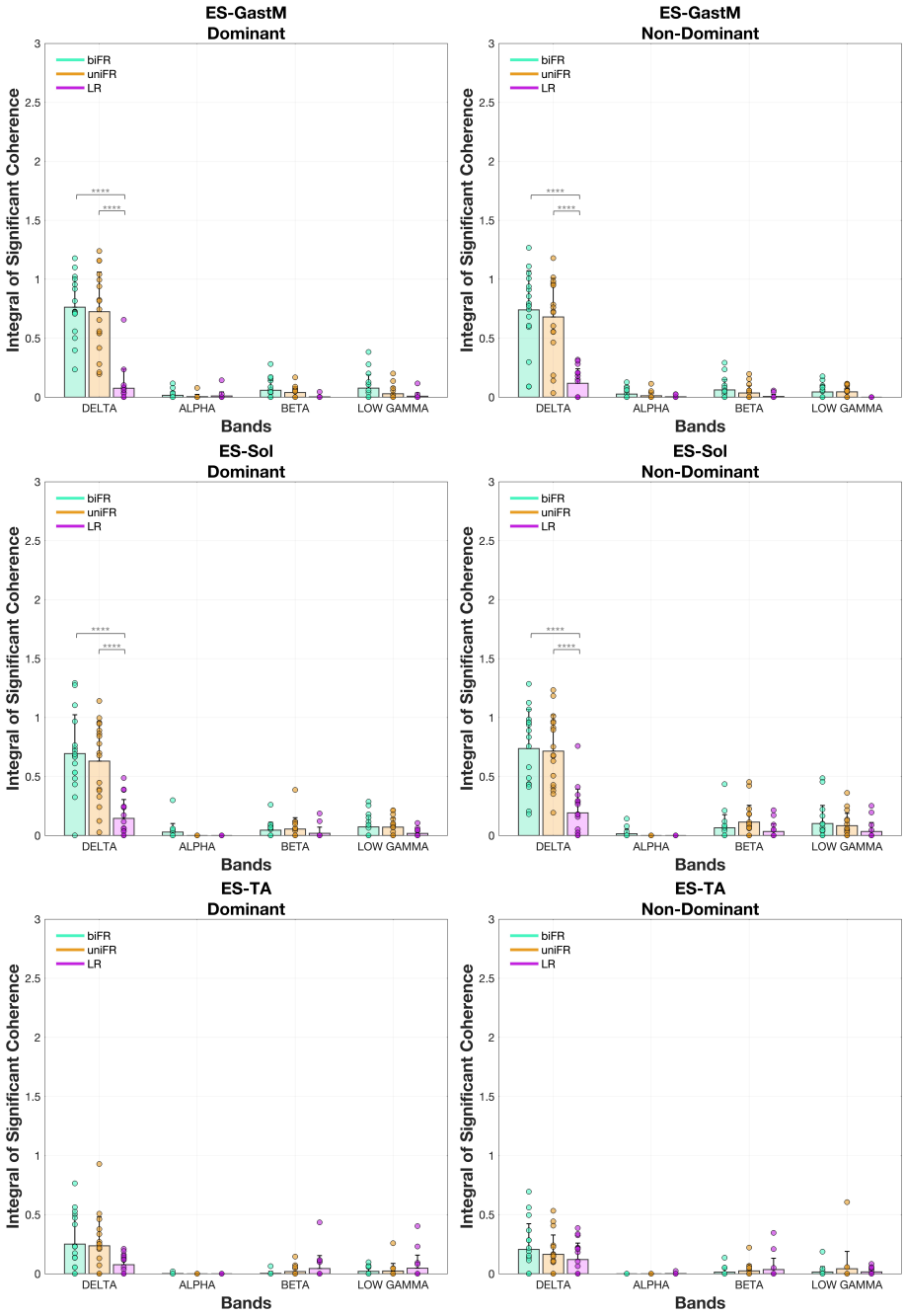

Figure 7.5. Mean values ± standard deviation (with individual data points overlaid) of the integral of intermuscular coherence exceeding the 5% significance threshold and satisfying the detection probability criterion, computed for unilateral erector spinae (ES)–ankle muscle pairs across the delta, alpha, beta, and low gamma frequency bands and averaged over all subjects. Upper panels show results for the erector spinae–gastrocnemius medialis (ES–GastM) muscle pair, middle panels for the erector spinae–Soleus (ES–Sol) muscle pair, and lower panels for the erector spinae–tibialis anterior (ES–TA) muscle pair. For each muscle pair, data are presented separately for the dominant (left panels) and non-dominant (right panels) sides. Data are shown for the three Functional Reach conditions: bilateral Functional Reach (biFR, aqua green), unilateral Functional Reach (uniFR, ochre), and Lateral Reach (LR, purple). Asterisks indicate significant differences across tasks (*p < 0.05; **p < 0.01; ***p < 0.001; ****p < 0.0001). Exact p-values are reported in **Figure S7.4.**

The results of the statistical analysis of the effect of task on coherence within each frequency band for the unilateral trunk-limb muscle pairs are presented in **Appendix – Supplementary Materials, Figure S7.4**. Intermuscular coherence spectra between the trunk and lower limb muscles on both the dominant and non-dominant sides, averaged across all subjects, are presented in **Figure 7.6**.

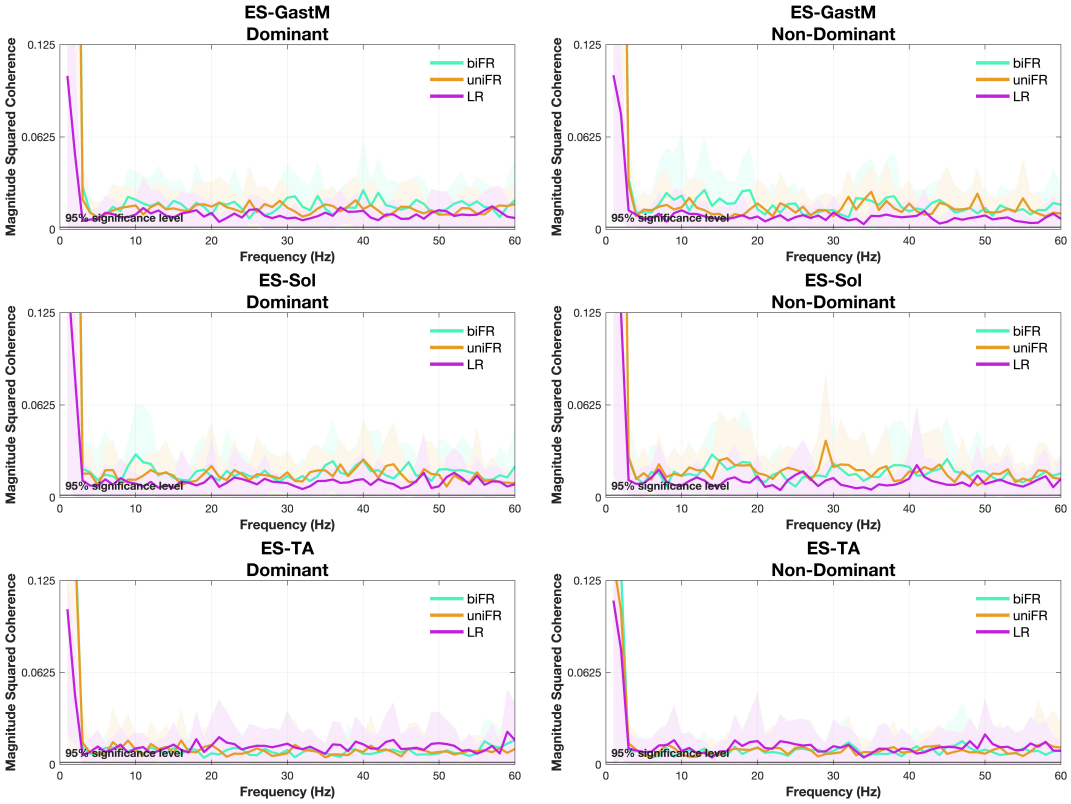

Figure 7.6. Average unilateral magnitude-squared intermuscular coherence spectra across participants for erector spinae (ES)–ankle muscle pairs. Upper panels show results for the erector spinae–gastrocnemius medialis (ES–GastM) muscle pair, middle panels for the erector spinae–soleus (ES–Sol) muscle pair, and lower panels for the erector spinae–tibialis anterior (ES–TA) muscle pair. For each muscle pair, coherence spectra are presented separately for the dominant (left panels) and non-dominant (right panels) sides. Coherence spectra are shown for the three Functional Reach conditions: bilateral Functional Reach (biFR, aqua green), unilateral Functional Reach (uniFR, ochre), and lateral Reach (LR, purple). Shaded areas indicate the standard deviation across participants. The horizontal dashed line represents the 95% significance level. The y-axis was limited to 0.125 to enhance the visibility of condition-related differences in coherence.

7.5.2. Muscle pair-related differences in intermuscular coherence

In addition to the task dependent differences in intermuscular coherence, significant differences were observed between muscle groups in the delta, beta and low gamma bands. During forward reaching (biFR and uniFR), delta-band coherence was significantly higher for the bilateral GastM and Sol muscle pairs compared to the TA ($p < 0.0001$, $g = 1.4504 – 1.7242$). No significant differences between bilateral muscle pairs were observed in the alpha or beta

bands. In the low gamma band, the TA pair exhibited higher coherence than the GastM during uniFR ($p = 0.0091$, $g = 1.0210$).

In the delta band, the agonist GastM–Sol pair exhibited significantly higher coherence than the antagonist TA–GastM pair across all tasks and on both limb sides ($p < 0.0001$, $g = 1.5826 – 3.0635$), with the effect being especially pronounced during biFR and uniFR (**Figure 7.3**). When comparing trunk–limb combinations, both ES–GastM and ES–Sol exhibited higher coherence than ES–TA during biFR and uniFR ($p < 0.0001$, $g = 1.6269 – 2.2728$) (**Figure 7.5**). There were no significant differences between ES–GastM and ES–Sol in any task or side ($p = 1$). When comparing limb–limb to trunk–limb pairings, GastM–Sol showed higher coherence than both ES–GastM and ES–Sol during LR ($p < 0.0001$, $g = 2.2165 – 2.9412$), while the latter two had higher coherence than TA–GastM in uniFR and biFR ($p < 0.0001$, $g = 1.7944 – 2.3153$), but lower coherence in LR on the non-dominant side ($p < 0.0001$, $g = -2.8522$ and $g = -2.5447$, respectively). Coherence for ES–TA was consistently lower than that of GastM–Sol across all tasks and sides ($p < 0.0001$, $g = -2.9282 – -2.4980$).

In the beta band, GastM–Sol coherence on the dominant side was significantly higher than that of all trunk–limb muscle pairs examined ($p < 0.0001$, $g = 1.6200 – 2.0896$). This difference was also present on the non-dominant side across tasks: in LR ($p < 0.0001$, $g = 1.7505 – 1.8727$), in biFR (e.g., vs. ES–GastM $p = 0.0036$, $g = 1.2261$; ES–Sol $p = 0.0042$, $g = 1.2117$; ES–TA $p = 0.0004$, $g = 1.4211$), and in uniFR (e.g., vs. ES–GastM $p = 0.0004$, $g = 1.4098$; ES–Sol $p = 0.0154$, $g = 1.0879$; ES–TA $p = 0.0002$, $g = 1.4571$). GastM–Sol also showed higher coherence than the antagonist TA–GastM pair in biFR ($p < 0.0001$, $g = 1.5170$, dominant side), uniFR ($p < 0.0001$, $g = 1.9434$, dominant side; $p = 0.0014$, $g = 1.3083$, non-dominant side), and LR ($p = 0.0014$, $g = 1.3110$, dominant side). No significant differences were observed between the ES–involved pairs themselves (all $p = 1$). During LR on the non-dominant side, TA–GastM coherence was significantly higher than ES–GastM ($p < 0.0001$, $g = 1.5334$), ES–Sol ($p = 0.0004$, $g = 1.4180$), and ES–TA ($p = 0.0004$, $g = 1.4111$).

In the low gamma band, GastM–Sol coherence was higher than that of TA–GastM in uniFR on both the dominant ($p = 0.0112$, $g = 1.1195$) and non-dominant ($p = 0.0246$, $g = 1.0401$) sides. In line with beta band findings, TA–GastM also showed greater coherence than ES–GastM ($p = 0.0098$, $g = 1.1324$), ES–Sol ($p = 0.0388$, $g = 0.9917$), and ES–TA ($p = 0.0191$, $g = 1.0662$) during LR on the non-dominant side. GastM–Sol was higher than ES–TA in biFR ($p = 0.0106$, $g = 1.1244$, dominant; $p = 0.0063$, $g = 1.1748$, non-dominant), in uniFR ($p = 0.0065$, $g = 1.1718$, dominant), and in LR ($p = 0.0480$, $g = 0.9685$, non-dominant). GastM–Sol coherence was also greater than

ES–GastM in uniFR (p = 0.0082, g = 1.1497, dominant), and in biFR (p = 0.0216, g = 1.0536) and LR (p = 0.0259, g = 1.0347) on the non-dominant side.

No significant differences were observed in the alpha band between any limb–limb or trunk–limb pairings.

Statistical results are reported in the supplementary information in **Appendix – Supplementary Materials, Figure S7.5**.

7.5.3. Limb dominance-related differences in intermuscular coherence

TA-GastM coherence was statistically higher during LR on the non-dominant side than the dominant side for the delta (p < 0.001, g = 2.1028), beta (p = 0.0252, g = 0.7683), and low gamma (p = 0.084, g = 0.9047) bands. No other significant differences were detected between sides for any other muscle pair or task examined.

Details of the statistical results are presented in the supplementary information in **Appendix – Supplementary Materials, Figure S7.6**.

7.5.4. Correlation of coherence with postural stability and co-contraction index

On the non-dominant side, a significant negative correlation was observed between delta-band coherence of the TA–GastM pair and PL_{CoP} during LR (p = 0.0456, r = -0.7065, g = -1.8953), as illustrated in **Figure 7.7A**. Additionally, on the dominant side, low gamma-band coherence between the ES–Sol pair showed a significant negative correlation with PL_{CoP} during biFR (p = 0.0147, r = -0.7697, g = -2.2887) (see **Figure 7.7B**). No other significant correlations were observed across frequency bands, tasks, and muscle pairings on either the dominant or non-dominant side (see **Appendix – Supplementary Materials, Figure S7.7**).

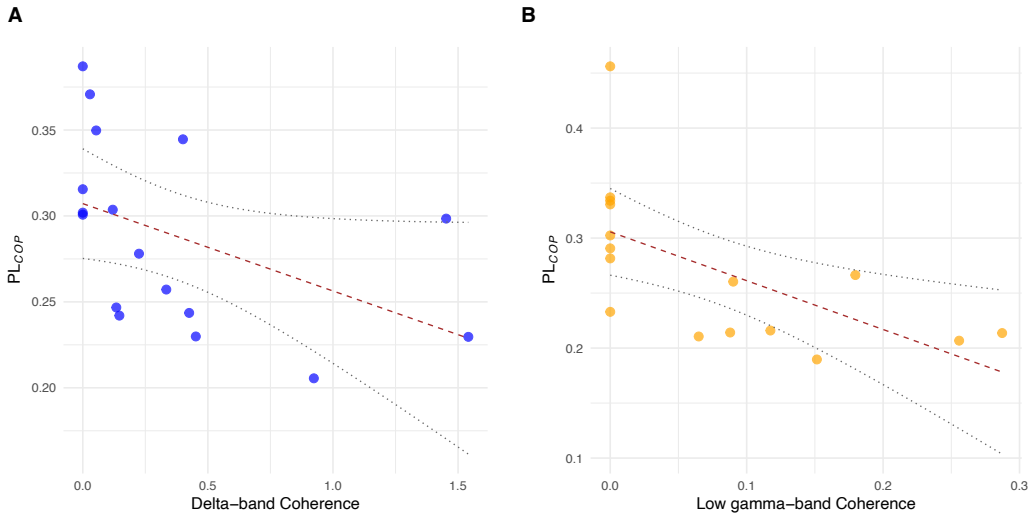

Figure 7.7. Scatter plots showing the associations between intermuscular coherence and the path length of the center of pressure ($\boldsymbol{PL_{CoP}}$). (**A**) Delta-band coherence of the tibialis anterior–gastrocnemius medialis (TA–GastM) muscle pair on the non-dominant side during Lateral Reach (LR). (**B**) Low gamma-band coherence of the erector spinae–soleus (ES–Sol) muscle pair on the dominant side during bilateral Functional Reach (biFR). Each point represents an individual participant. The dashed red line indicates the linear regression fit, and the dotted lines represent the 95% confidence intervals.

On the dominant side, a significant positive correlation was found between delta-band coherence and $\boldsymbol{CCI_{norm}}$ during LR (p = 0.0073, r = 0.7445, g = 2.1170) (**Figure 7.8A**), as well as between beta-band coherence and $\boldsymbol{CCI_{norm}}$ in the same condition (p = 0.0319, r = 0.6802, g = 1.7615) (**Figure 7.8B**).

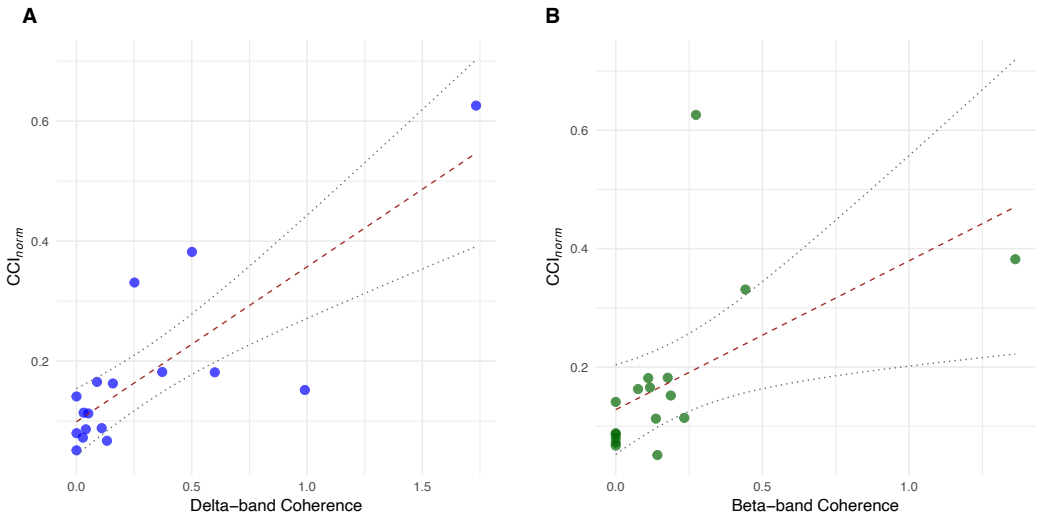

Figure 7.8. Scatter plots showing the associations between intermuscular coherence and the normalized co-contraction index ($\boldsymbol{CCI_{norm}}$). Panel **A** shows the relationship between delta-band intermuscular coherence and $\boldsymbol{CCI_{norm}}$ on the dominant side during Lateral Reach (LR). Panel **B** shows the relationship between beta-band intermuscular coherence and $\boldsymbol{CCI_{norm}}$ on the dominant side during Lateral Reach (LR). Each point represents an individual participant. The dashed red line indicates the linear regression fit, and the dotted lines represent the 95% confidence intervals.

7.6. Discussion

Consistent with our hypotheses, intermuscular coherence varied according to both the direction of reaching and the muscle combinations involved, demonstrating that neural coupling is flexibly tuned to the biomechanical requirements of each task. As participants transitioned from quiet standing to destabilized postures in the sagittal and frontal planes, the CNS adjusted the distribution and synchronization of shared neural inputs to coordinate trunk and lower-limb muscles in a directionally appropriate way. In parallel, functionally synergistic muscles showed synchronized activity, confirming the presence of a common neural drive that contributes to postural stability.

During forward reaching tasks (biFR and uniFR), coherence was significantly higher in the delta band, both among bilateral homologous muscles (TA, GastM, Sol) and between trunk-limb pairs of the posterior chain (ES–GastM, ES–Sol). Additionally, the synergistic ankle plantar-flexors (GastM–Sol) exhibited greater delta-band coherence compared to the antagonistic muscles (TA-GastM). The delta-band component is generally considered an index of the common neural drive to muscles, particularly during tasks involving low-force, static contractions and slow, steady force production such as postural maintenance (Borzuola et al., 2025; Farina & Negro, 2015). These low-frequency oscillations are thought to originate primarily from subcortical structures rather than the corticospinal system (Boonstra et al., 2009; De Luca & Erim, 1994; Kamen & and De Luca, 1992) and can also be modulated by shared afferent feedback and other subcortical mechanisms (Boonstra & Breakspear, 2012; Yamanaka et al., 2023). Our findings suggest a predominance of subcortical common drive, which promotes coordinated low-frequency activation of muscles that contribute to sagittal stability. Such organization is consistent with prior studies showing robust delta band among bilateral homologous muscle pairs and unilateral plantar flexors during static standing tasks (Boonstra et al., 2009; Mochizuki et al., 2006; Obata et al., 2014; Watanabe et al., 2018a, 2018b). The elevated coherence in trunk-limb extensors pairs indicates the integration of trunk and lower-limb extensors into a posterior-chain synergy, primarily driven by subcortical networks that stabilize the body in the sagittal plane. This finding supports the conclusions of Noé et al. (2017), suggesting that postural instability promotes functional integration between trunk and lower-limb extensors, supporting the idea that the CNS dynamically integrates proximal and distal muscles into unified coordination patterns when postural constraints increase. Furthermore, consistent with reports by Danna-Dos-Santos et al. (2014), the significant coherence between synergistic muscles in the posterior chain (e.g., GastM-Sol, ES-GastM) reflects a simplification of motor control by the CNS, which uses common neural inputs to stabilize posture through multi-muscle synergies. Notably, surrogate analysis (see **Appendix – Supplementary Materials**, Figure S7.**3**) confirmed that the observed coherence between ES and ankle muscles was not attributable to spurious coupling, but rather reflects true functional synchronization, underscoring the neural origin of these synergies.

Additionally, in all tasks, the synergistic plantar-flexor GastM-Sol pair consistently showed higher coherence than the antagonist TA-GastM pair. The limited modulation of beta- and low gamma-band coherence across tasks suggests that the GastM-Sol coupling is largely stable and reflects the automatic, subcortically mediated nature of the plantar-flexor synergy. However,

coherence within the GastM-Sol pair tended to be greater in the dominant limb during lateral reaching (LR), where the mechanical demands for fine balance adjustments increase. This enhancement likely reflects a cortical contribution to synergy control, consistent with evidence that beta-band coherence between synergistic muscles increases during complex standing tasks (Nandi et al., 2019; Nojima et al., 2020; Watanabe et al., 2018a, 2018b). Beta-band coherence has been associated with corticospinal common drive, particularly in dynamic or voluntary tasks such as gait (Jensen et al., 2018), bipedal squatting (Kenville et al., 2020), and forward leaning (Watanabe et al., 2018a). Fisher et al., (2012) further emphasized that intermuscular coherence in the beta range depends on the functional integrity of the corticospinal tract ,, which plays a central role in voluntary motor control (Welniarz et al., 2017). Furthermore, recent evidence has shown that beta-band coherence reflects not only corticospinal drive but also cortical-level coordination of functionally synergistic muscles (Laine & Valero-Cuevas, 2017; Reyes et al., 2017), supporting the idea that higher coherence in these frequencies may reflect active cortical control over multi-muscle synergies. In addition to the beta band, coherence in the low gamma band also showed the same pattern. Indeed, not only the beta-band but also the low gamma band has been associated with transcortical pathways (Conway et al., 1995; Fisher et al., 2012), and their joint presence suggests cortical involvement in the coordination of postural muscles during upright reaching. In this context, the elevated GastM-Sol coherence on the dominant side may represent a voluntary, transcortically mediated modulation that fine-tunes synergistic activation to maintain stability during asymmetric postural demands. Thus, while the plantar-flexor synergy operates primarily under subcortical common drive, it remains adaptively upregulated by cortical mechanisms when task complexity or directional instability increases.

Moreover, during lateral reaching, an asymmetric reorganization of coherence between limbs indicates a redistribution of neural control across subcortical and cortical pathways. Enhanced intra-limb coherence between plantar-flexor synergists, as well as between agonist–antagonist muscle pair, suggests that the CNS reinforces local neuromuscular coupling to stabilize load-bearing joints under asymmetric conditions. This is consistent with findings from Obata et al. (2014), who reported that both intra- and inter-limb coherence are modulated based on the distribution of effort and task-specific postural constraints. In the non-dominant side, the antagonist TA-GastM displayed higher coherence across delta, beta, and low gamma bands compared to both forward reaching conditions, as well as the TA-GastM pair on the dominant side. Higher delta-band coherence in this limb was negatively correlated with PL_{CoP}, suggesting

that enhanced antagonist coupling improved postural stability, likely through increased ankle joint stiffness (Baratto et al., 2002). Such predominance of low-frequency synchronization under medial-lateral instability supports previous evidence that antagonist coupling increases with postural challenge (Nandi et al., 2019; Nojima et al., 2020). In contrast, in the dominant side, coherence in TA-GastM did not show significant differences across tasks but was positively correlated with the CCI_{norm} in both delta and beta bands. This suggests that joint stability was achieved via voluntary modulation of stiffness through shared neural input. Antagonist co-contraction has been demonstrated to effectively enhance joint stiffness during motor tasks (Geertsen et al., 2013; Hansen et al., 2001), and in this scenario, it likely played a role in maintaining accuracy and control throughout the reaching movement without sacrificing postural stability. Together, these results confirm a clear asymmetry in neural control strategies between limbs. The non-dominant limb, which was responsible for stabilizing the body under lateral load, relied on increased low-frequency coherence, indicative of more automatic coordination. In contrast, the dominant limb employed a more refined and voluntary control through co-contraction mechanisms, with neural coherence reflecting the modulation of joint stiffness rather than a generalized response to postural demand. Notably, TA–GastM coherence on the non-dominant side exceeded that of all trunk–limb pairings across the same frequency bands during LR, reinforcing the importance of ankle-level coordination in medial-lateral stability. Altogether, this side-specific organization of neural control suggests the inter-limb independence as a strategy to counter lateral instability, also supporting the dual role of coherence in both automatic and voluntary components of postural control. This interpretation is consistent with findings by Mochizuki et al. (2006a), who demonstrated that standing postural control relies primarily on automatic, subcortical mechanisms rather than voluntary drive. Their results further suggest that low-frequency modulations in muscle activity during quiet stance may be closely related to CoP dynamics, which is consistent with the negative correlation observed in the present study between delta-band coherence and CoP path length in the non-dominant limb. In contrast, the presence of beta-band coherence in the dominant limb, especially ii association with antagonist co-contraction, may reflect a voluntary, cortically mediated strategy to modulate joint stiffness and enhance movement precision under postural constraint.

Finally, although alpha-band coherence was consistently present across all conditions, it remained low and unaltered, in line with previous literature. Alpha-band coherence is primarily associated with subcortical and spinal mechanisms (Baker & Baker, 2003; Conway et al., 1995;

McAuley & Marsden, 2000), which may play a limited role in dynamic postural regulation in healthy young adults. Supporting this, Obata et al. (2014) reported alpha-range coherence only in elderly individuals, while it was absent in younger participants, further suggesting that coherence in this frequency band may become more prominent under compensatory or age-related neuromuscular strategies.

Several limitations should be acknowledged in the present study. First, our sample was restricted to healthy young adults, which limits the generalizability of the findings to older adults or clinical populations with known deficits in postural control. Previous studies have shown age-related alterations in intermuscular coherence, particularly reductions in low-frequency synchronization and increased reliance on alpha-band activity (Mochizuki et al., 2006; Obata et al., 2014; Watanabe et al., 2018a), suggesting that aging may reshape the neural strategies underlying multi-muscle coordination. Future research should explore how age-related changes in the nervous system affect frequency-specific coherence patterns, especially in tasks that challenge balance in the frontal and sagittal planes. Moreover, the limited sample size should be acknowledged as a potential constraint, as it may have reduced the ability to detect smaller effects despite the consistent trends observed in the data. Second, the definition of frequency bands, particularly the beta range, was based on conventions adopted in recent literature, including the systematic scoping review by Yamanaka et al. (2023). However, discrepancies still exist across studies regarding the exact frequency boundaries, especially in the beta and low gamma ranges. These methodological differences could lead to variation in the detection and interpretation of coherence patterns and highlight the need for greater consensus on frequency band definitions in EMG-EMG coherence studies of upright motor control. Third, although we investigated multiple trunk–limb pairings, bilateral coherence between left and right ES was not analyzed due to the potential risk of signal cross-talk in surface EMG recordings of paraspinal muscles. This precludes us from making direct inferences about trunk-level bilateral coordination, which may also contribute significantly to postural stability. Moreover, extending the analysis to a larger set of trunk and limb muscles could provide a more integrated view of bilateral and intersegmental coordination mechanisms underlying postural control. Finally, while intermuscular coherence provides valuable insight into the presence of shared neural inputs, it does not reveal their precise origin—whether cortical, subcortical, or spinal. Future studies combining EMG coherence with neuroimaging or electrophysiological approaches, such as EEG or MEG, may help to disentangle the hierarchical contributions of central versus peripheral mechanisms to postural coordination. This would further clarify how

different frequency bands relate to distinct levels of neural control and refine our understanding of the neurophysiological basis of upright motor behavior.bIn conclusion, our findings underscore the value of intermuscular coherence as a window into the CNS's organization of postural strategies and provide new insights into the role of neural synchronization in coordinating muscle activity during reaching tasks. Delta-band coherence supports low-frequency coupling for automatic stabilization, particularly under sagittal and lateral postural loads. Beta- and low gamma-band coherence are commonly associated with corticospinal/transcortical contributions and thus are consistent with cortical involvement during unilateral or asymmetric conditions. However, it is important to acknowledge that intermuscular coherence alone cannot definitively identify the neural source, so any conclusions drawn should remain inferential. The CNS appears to flexibly organize intra- and inter-limb strategies to meet task-specific mechanical demands. Notably, the systematic modulation of coherence across tasks and muscle pairings suggests that muscle coordination is not merely a direct response to mechanical constraints but often reflects centrally guided strategies. In this sense, coherence analysis may offer a meaningful way to differentiate between functionally necessary muscle groupings and those shaped by shared neural control, providing insight into how the CNS builds and modulates synergies to meet postural demands.

eStudy III: Modular Motor Control of the Center of Mass Kinematic Patterns during Sit-to-Stand Tasks

Imma Ceriello[1,4] · Simone Ranaldi[2,4] · Giacomo Severini[3] · Valentina Camomilla[1,4] · Andrea Macaluso[1] · Riccardo Borzuola[1]

[1]Laboratory of Bioengineering and Neuromechanics, Department of Movement, Human and Health Sciences, University of Rome "Foro Italico", Rome, Italy

[2]Deparment of Industrial, Electronics and Mechanical Engineering, Roma Tre University, Rome, Italy

[3]School of Electrical and Electronic Engineering, University College Dublin, Dublin, Ireland

[4]Interuniversity Centre of Bioengineering of the Human Neuromusculoskeletal System, University of Rome "Foro Italico", Rome, Italy

Proceeding presented at the *12th Annual International Conference on Neural Engineering (IEEE EMBS NER 25)*, San Diego, California, on November 11–14, 2025.

Author contributions: Imma Ceriello, Riccardo Borzuola, Valentina Camomilla, and Andrea Macaluso developed and planned the research; Imma Ceriello and Riccardo Borzuola conducted the experiments; Imma Ceriello and Simone Ranaldi analyzed the data; Imma Ceriello and Simone Ranaldi interpreted the experimental results; Imma Ceriello and Simone Ranaldi created the figures; Imma Ceriello, Simone Ranaldi, and Riccardo Borzuola drafted the

manuscript; Imma Ceriello, Simone Ranaldi, Giacomo Severini, Riccardo Borzuola, Valentina Camomilla, and Andrea Macaluso reviewed and revised the manuscript; Imma Ceriello, Simone Ranaldi, Giacomo Severini, Riccardo Borzuola, Valentina Camomilla, and Andrea Macaluso gave their approval for the final version of the manuscript.

8.1. Rationale and Objectives

Previous research has indicated that unilateral lower-limb muscle synergies are reflective of the kinematic organization of the body's CoM during postural transitions (An et al., 2013; Ranaldi et al., 2025; Yang et al., 2017a). This study expands upon that framework by conducting a bilateral, whole-body analysis of the Sit-to-Stand (STS) task in healthy young adults. Instead of relying on time, synergy activation was examined in relation to the instantaneous CoM position in the sagittal plane, allowing for a more accurate representation of the task's functional progression.

Objectives: The objectives were to:

i. Characterize the bilateral muscle synergies involved in the STS task among healthy young adults.
ii. Evaluate whether correlating synergy activity with CoM displacement offers a more robust and interpretable understanding of motor organization, irrespective of limb dominance or movement timing.

8.2. Experimental Procedure

The participants and the experimental setup were based on the framework outlined in **Chapter 5**. Specifically, data were collected during the 30-Second STS task described in **Section 5.3.3**, which involved seventeen healthy young adults (10 males and 7 females; average age: 27.5 ± 3 years; average height: 1.7 ± 0.1 m; average body mass: 64.9 ± 8.8 kg; 2 left-handed and 15 right-handed) (see **Section 5.2** for inclusion criteria). The general acquisition protocol, including motion capture and surface EMG recording, was consistent with the setup presented in **Section 5.3.4**. The overall schematic representation of the experimental set-up is illustrated in **Figure 8.1**.

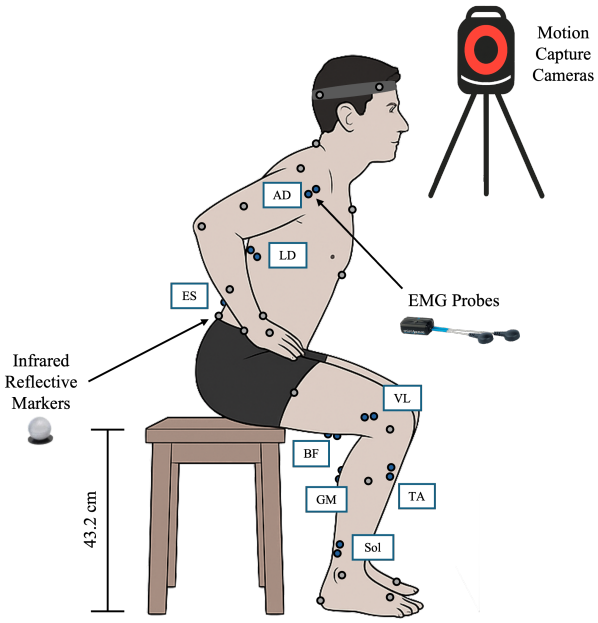

Figure 8.1. Schematic representation of the experimental set-up for the STS task. The figure illustrates the participant instrumented with reflective markers and surface electromyography (EMG) electrodes while seated on a standardized chair. EMG recordings were collected from the anterior deltoid (AD), erector spinae (ES), latissimus dorsi (LD), vastus lateralis (VL), biceps femoris (BF), tibialis anterior (TA), gastrocnemius medialis (GastM), and soleus (Sol) muscles. Whole-body kinematics were acquired using an optoelectronic motion capture system.

For the analyses in this study, only the kinematic data from the Plug-in Gait Full Body (PiG) markerset were considered.

8.3. Data Analysis

Kinematic data were filtered with a 4th-order Butterworth filter with a 12 Hz cut-off frequency. The velocity of the right posterior superior iliac spine marker was used to isolate the initial sit-to-stand phase of a complete sit to stand to sit cycle (i.e., the upward phase from sit to stand) to avoid the influence of passive, gravity-driven strategies that might be involved in the return-to-sit phases (Ranaldi et al., 2024). Specifically, movement onset was defined as the instant at which marker velocity exceeded 20% of its peak value, while movement offset was defined as the instant at which velocity dropped below 20% of its peak value.

EMG signals were pre-processed to remove impulse peaks and power-line peaks. Power-line interference was attenuated by applying a third-order Butterworth narrow band-stop (notch) filter centered at 50 Hz using a zero-phase forward–backward filtering procedure. Signals were then band-pass filtered (40-350 Hz), full wave rectified, and low-pass filtered at 10 Hz with a zero-lag 4th-order Butterworth filter to obtain linear envelopes (Ranaldi et al., 2023). For each muscle, EMG envelope was then normalized in amplitude to its median peak value across all

cycles maximum to ensure equal muscle contribution during synergy extraction by addressing the amplitude variations associated with anatomical and recording factors (Torricelli et al., 2016), as the analysis involved multiple cycles derived from three separate recordings, allowing a robust reference value and limiting the influence of extreme activation peaks across acquisitions. EMG envelopes were segmented based on the previously identified sitting-to-standing phase. To account for differences in phases' duration between participants, each EMG envelope was time-normalized to 100 points per cycle, where 0 corresponds to the start and 100 corresponds to the end of the sitting-to-standing phase. Amplitude and time-normalized EMG data were then concatenated and a randomized subset of cycles, representative of the 30-second STS duration, were selected for the synergy extraction (Ranaldi et al., 2023). The selected cycles were structured into an Ns-by-Nm matrix (with Ns denoting the number of samples and Nm the number of muscles), where each column represents the concatenated envelope of a given muscle across the various cycles.

8.3.1. Synergy extraction

Synergies were extracted from the Ns-by-Nm matrix for each participant using the NNMF algorithm described in **Chapter 6** (see **Section 6.3.3, Equation 6.1**). The decomposition followed the same multiplicative-update rules and parameter settings previously defined. Synergies were extracted iteratively, beginning with a single synergy and increasing up to the number of recorded muscles. The modified Akaike Information Criterion, as presented in (Ranaldi et al., 2023), (Ranaldi et al., 2021), was used to determine the optimal number of motor modules (*i.e.,* muscle synergies), which was then used to group participants. The criterion was applied on each side (Dominant [D] and Non-Dominant [N]) separately, and a common number of synergies was then defined as the median value for all the extractions for all the participants. Following the identification of the average number of synergies (N_{syn}), this fixed number of motor modules was extracted from all participants.

8.3.2. Synergy sorting

As the NNMF algorithm was applied independently to each participant and, given that it does not guarantee a consistent order of synergy extraction across individuals, the resulting weight vectors W were realigned based on their similarity to a reference set. This reference set was generated by grouping the extracted synergies based on the similarity of their muscle weight vectors, using a hierarchical clustering algorithm with the *Cityblock* distance as a metric (Danion & Latash, 2011). The number of clusters was set equal to N_{syn}, and the reference vectors

were computed as the average of the vectors within each cluster (Pellegrino et al., 2018). The individual W vectors were then reordered to maximize cosine similarity with the reference set:

$$CS_{ref} = \frac{W_{ref,i} \cdot W_j}{\| W_{ref,i} \| \| W_j \|} \quad (8.1)$$

Finally, an average representative set of synergies (W_{avg}) was computed across all participants. Data from each participant were projected onto the space defined by the average set of synergies by Non-Negative Reconstruction, and the Variance Accounted For (VAF) values, defined as uncentered Pearson correlation coefficients (Torres-Oviedo et al., 2006), were compared with the ones related to reconstruction with random surrogate W vectors, as in (De Marchis et al., 2019a).

8.3.3. Calculation of the Center of Mass

The whole-body CoM was estimated using the Vicon's Plug-in Gait Full Body model within the motion capture system. The model defines body segments based on marker placement and computes each segment's CoM as a fixed proportion along the line connecting the distal and proximal joint centers. The overall CoM is obtained as a weighted sum of the segmental CoMs, with weights proportional to the segment masses relative to total body mass.

The CoM trajectories were segmented according to the previously identified sit-to-stand phase and time-normalized to 100 points per cycle. The same cycles chosen for EMG analysis were employed for the CoM assessment. Only the anteroposterior and vertical components of the CoM were examined, as they reflect displacement in the sagittal plane, which represents the primary direction of movement during the task.

8.3.4. Extraction of the mapping

To investigate the mapping between the bi-lateral activity of the muscle synergies and the CoM position in the sagittal plane, the activity of each synergy was averaged as a function of the sagittal coordinates of the CoM itself, regardless of the time spent in each position.

8.4. Results

Participant-specific and side-specific number of synergies are shown in **Table 8.1**. On average, a four-synergy structure effectively coordinated both limbs, yielding an extracted VAF of 91.0% ± 0.4 (mean ± SE) and a reconstruction VAF of the average set of synergies of 88.0% ± 0.6. Based on these findings, a dimensionality of four synergies was selected to define a common W matrix.

Table 8.1. Number of participants exhibiting 3, 4, or 5 muscle synergies on each side.

	N=3	*N=4*	*N=5*
Dominant side	5	9	3
Non-Dominant side	4	11	2

Table 4 summarizes the distribution of participants according to the number of muscle synergies extracted on each side. Most participants exhibited four synergies on both the dominant and non-dominant sides, while fewer participants showed either three or five.

The average synergies coming from the identified Nsyn are shown in **Figure 8.2**. The identified synergies exhibit a high degree of symmetry between the two sides. Each synergy corresponds to a distinct functional phase of the STS task: W1 is active during stable standing, predominantly involving ankle plantar flexor muscles; W2 is linked to the transition to full knee and hip extension; W3 involves trunk flexion through the transitory knee extension point to maximal ankle dorsiflexion, reflecting the coordinated extension of the whole body; and W4 represents a separate synergy with respect to the others and primarily entails upper limb muscles activating during trunk forward transfer and final stabilization.

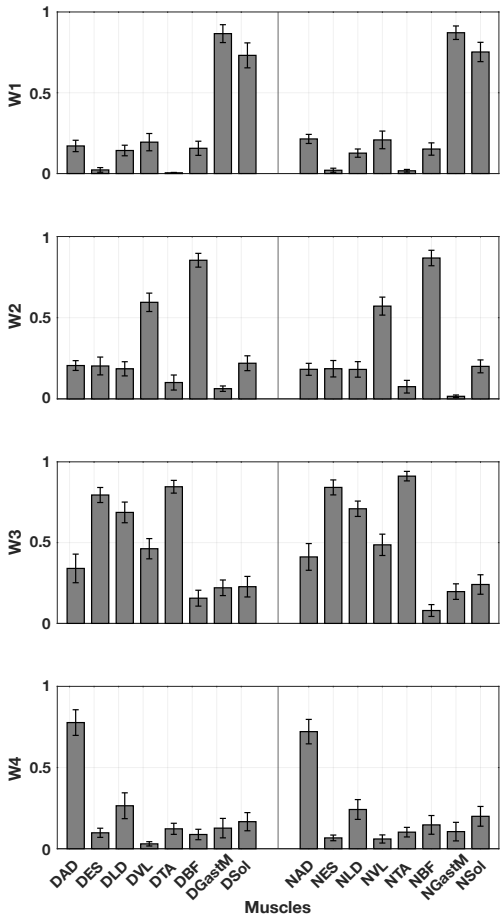

Figure 8.2. Mean and standard error of the averaged muscle weight vectors (Wavg) for each synergy (W1–W4), corresponding to the optimal number of motor modules identified across participants during the sit-to-stand task. Each panel shows the spatial distribution of muscle contributions for a single synergy. Muscle labels correspond to dominant-side (D, left group) and non-dominant-side (N, right group) muscles: anterior deltoid (DAD, NAD), erector spinae (DES, NES), latissimus dorsi (DLD, NLD), vastus lateralis (DVL, NVL), tibialis anterior (DTA, NTA), biceps femoris (DBF, NBF), gastrocnemius medialis (DGastM, NGastM), and soleus (DSol, NSol). Higher weights indicate a greater relative contribution of the muscle to the corresponding synergy. The functional interpretation of synergies W1–W4 is provided in the main text.

The mapping of the synergistic activity reported in **Figure 8.3** shows that the first synergy is managing the phase in which the CoM is at its maximum vertical position (i.e. full body extension), together with the synergy related to the fourth synergy involved in upper limb control.

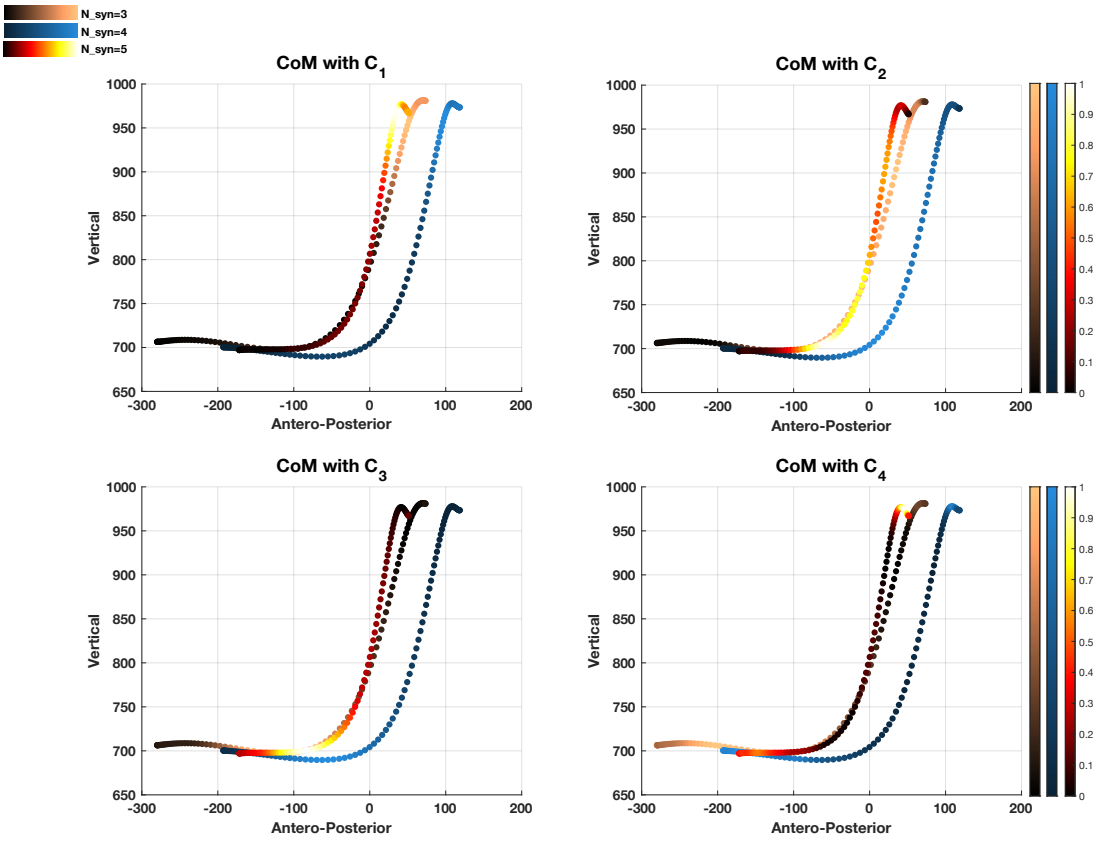

Figure 8.3. Center of mass (CoM) trajectories in the sagittal plane (antero–posterior vs vertical) associated with the activation of the four common motor modules (C1–C4) during the sit-to-stand task. Trajectories are color-coded to indicate the temporal activation of each motor module along the CoM path. Module C1 is primarily associated with peak vertical CoM displacement, C2 with upward propulsion, C3 with forward CoM transfer, and C4 with trunk and arm stabilization. Color saturation reflects the number of extracted synergies (Nsyn), with Nsyn = 3 indicating more diffuse activation (global control), Nsyn = 4 intermediate localization, and Nsyn = 5 more focused activation (fine control).

Vertical movement of the CoM is instead realized mainly through the activity of the second synergy, while the start of the movement (i.e. the horizontal portion of the CoM trajectory) is

managed by the third synergy. In all four cases, the distinction by the original number of synergies shows a more localized activation of the motor modules when the complexity of the control strategies is higher.

8.5. Discussion

The results presented here showed that it is possible to describe the STS movement through the activity of four muscle synergies, regardless of whether the problem is analyzed from a mono- or bi-lateral point of view. Moreover, the spatial structure of the synergy vectors is essentially equivalent between the two sides and across different subjects, proving that the movement itself is highly standardized on healthy individuals.

Recent studies adopting bilateral EMG acquisition further support the relevance of analyzing muscle synergies across both sides of the body. In upper-limb tasks, healthy individuals have been shown to exhibit symmetric synergy structures, whereas patients with cervical spinal cord injury display altered and asymmetric coordination patterns (Bellitto et al., 2023). In post-stroke gait, lower-limb recordings have revealed a reduced number of synergies and lower reconstruction accuracy on the paretic side compared to the non-paretic one (Barroso et al., 2017), highlighting the diagnostic value of side-by-side analysis. In the context of gait transitions, bilateral synergies have been shown to be functionally symmetric, with adaptations between walking and running primarily emerging from shifts in activation timing rather than from changes in spatial composition (Hagio et al., 2015).

The present results also demonstrate that it is possible to investigate the synergistic activity in a time-independent manner, by looking at the spatial mapping of the neuromuscular activation. This representation is simpler than the one presented in a previous work (Ranaldi et al., 2024) as it does not take into account time-derivatives and alternative coordinate systems. Despite this simplification, this model provides an equally robust framework for quantifying the relationship between the synergy activity and the biomechanical aspects of the movement. The general nature of this correlation is independent on the specific complexity of the control strategies (*i.e.,* the number of synergies) and can be summarized with a common set of W vectors and a fixed number of motor modules. These findings regarding the number of motor modules reinforce the features identified in (Ranaldi et al., 2024) while generalizing their applicability to a bi-lateral framework for the description of movement. Specifically, they revealed more peaked activation associated to generally more complex control patterns, as well as finer control of the timing of the different biomechanical functions.

This interpretation is supported by previous findings indicating that variations in movement strategy can emerge solely from temporal shifts in synergy activation, without altering the spatial structure of the motor modules. In particular, it was shown that modifying the onset timing of a single synergy was sufficient to reproduce distinct standing-up strategies, resulting in characteristic differences in the CoM trajectory, while the associated spatial patterns remained unchanged (Yang, An, Yamakawa, Tamura, Yamashita, & Asama, 2017). Moreover, in post-stroke individuals, the spatial composition of muscle synergies has been reported to remain largely consistent with that of healthy controls, whereas the main alterations involved prolonged or delayed activation profiles (Yang et al., 2019). These observations reinforce the hypothesis that synergy timing plays a central role in shaping biomechanical outputs and support the relevance of synergy-CoM mapping as a framework for detecting subtle impairments in motor coordination or compensatory control mechanisms.

Some limitations of the present study should be acknowledged. First, the relatively small sample size may affect the extent to which the findings can be generalized to the wider healthy population. Second, the CoM was estimated using the Vicon's Plug-in Gait Full Body model in Vicon Nexus, which calculates segmental CoMs based on individual anthropometric data such as height, weight, and limb lengths. While this method yields subject-specific and biomechanically plausible CoM trajectories, the resulting values are reported in global (millimeters) coordinates and are not scaled to account for differences in body size. As a result, inter-subject comparisons may be influenced by anthropometric variability. Future work should consider applying normalization approaches (*e.g.,* CoM height relative to stature or limb length) to enhance comparability across individuals. Third, although the seat used for the STS task had a fixed height of 43.2 cm (17 inches), in accordance with the standardized protocol, it was not adjusted for participants' individual anthropometric characteristics. This may have introduced varying mechanical demands across subjects of different stature, potentially affecting lower-limb joint kinematics, muscle activation patterns, and CoM trajectories. Fourth, the analysis focused on the overall upward phase of the STS movement without dividing it into detailed sub-phases. Future studies could benefit from a more refined segmentation to explore how synergies contribute across different stages of the task.

When included in rehabilitation protocols, the mapping presented here can be considered as a tool for stimulating the activity of different motor modules by asking for specific CoM trajectories in space. While this aspect has already been proposed for healthy movement by describing different phase-space regions as a function of the underlying synergies (Ranaldi et

al., 2024), the results of the present study indicate that this relationship is not side-dependent. This provides additional support for the use of such models in the treatment of unilateral motor impairments, such as hemiplegia or mono-lateral limb amputation.

Moreover, our findings reinforce the importance of bilateral EMG acquisition in capturing comprehensive neuromotor strategies across different functional contexts and highlight the potential of symmetric coordination patterns as normative references for rehabilitation assessment and the development of targeted therapeutic interventions.

8. Study IV: Age-Dependent Synergistic Control of Sit-to-Stand Motion

Imma Ceriello[1,3] · Simone Ranaldi[2,3] · Valentina Camomilla[1,3] · Andrea Macaluso[1] · Riccardo Borzuola[1]

[1]Laboratory of Bioengineering and Neuromechanics, Department of Movement, Human and Health Sciences, University of Rome "Foro Italico", Rome, Italy

[2]Deparment of Industrial, Electronics and Mechanical Engineering, Roma Tre University, Rome, Italy

[3]Interuniversity Centre of Bioengineering of the Human Neuromusculoskeletal System, University of Rome "Foro Italico", Rome, Italy

The study presented in this chapter is currently in preparation for submission.

9.1. Rationale and Objectives

The ability to transition from a seated to a standing position is a fundamental motor task that is essential for maintaining autonomy and daily functional independence (Inkster & Eng, 2004). This movement necessitates precise coordination among various joints and muscle groups to manage the trajectory of CoM and ensure postural stability (Mathiyakom et al., 2005; Y.-C. Pai et al., 1994; Yoshioka et al., 2009). Age-related declines in muscle strength, sensory feedback, and motor coordination can significantly impact the biomechanics and neural control of the STS movement, leading to altered strategies, decreased efficiency, and an increased risk of falls among older adults (An et al., 2013; Piano et al., 2020; Roebroeck et al., 1994; Sadeh et al., 2023). Relative to the preceding chapters, this study represents the first within the thesis to enable a direct comparison between young and older adults. In particular, it builds upon the neuromuscular characterization of the STS task presented in **Study III** (**Chapter 8**) in healthy young adults, which is used as a reference to examine age-related differences in movement strategies and neuromuscular coordination.

Objectives: The aim was to investigate the age-dependent modulation of bilateral muscle synergies and movement strategies during the STS task. Specifically, it seeks to:

- Identify and compare the muscle synergies involved in the Sit-to-Stand motion across young and older adults.
- Assess how the number, spatial composition, and temporal activation profiles of these synergies change with age.
- Examine the relationship between synergy modulation and CoM kinematics to determine whether age-related differences in neuromuscular coordination are associated with distinct movement strategies.

In accordance with previous findings (Yang et al., 2017b), we hypothesize that aging does not significantly alter the spatial organization of muscle synergies but instead leads to modifications in their temporal activation patterns, indicative of compensatory control strategies. Moreover, we expect that these neural-level adaptations will correspond with changes in CoM kinematics.

9.2. Experimental Procedure

The framework detailed in **Chapter 5** served as the basis for both participants and the experimental setup. Data collection took place during the 30-Second STS task described in **Section 5.3.3**, which included seventeen healthy young adults (10 males and 7 females; average age: 27.5 ± 3 years; average height: 1.7 ± 0.1 m; average body mass: 64.9 ± 8.8 kg; consisting of 2 left-handed and 15 right-handed individuals) and sixteen healthy older adults (6 males and 10 females; average age: 77.4 ± 7.4 years; average height: 1.7 ± 0.06 m; average body mass: 67.7 ± 10.4 kg; with 2 left-handed and 14 right-handed participants), as outlined in **Section 5.2**. for inclusion criteria. The overall acquisition protocol, which included motion capture and surface EMG recording, followed the methodology established in **Section 5.3.4**. Notably:

- The anterior deltoids were excluded from the current analysis among the muscles recorded (refer to **Section 5.3.4**).
- Only the kinematic data from the Plug-in Gait Full Body (PiG) markerset were considered.

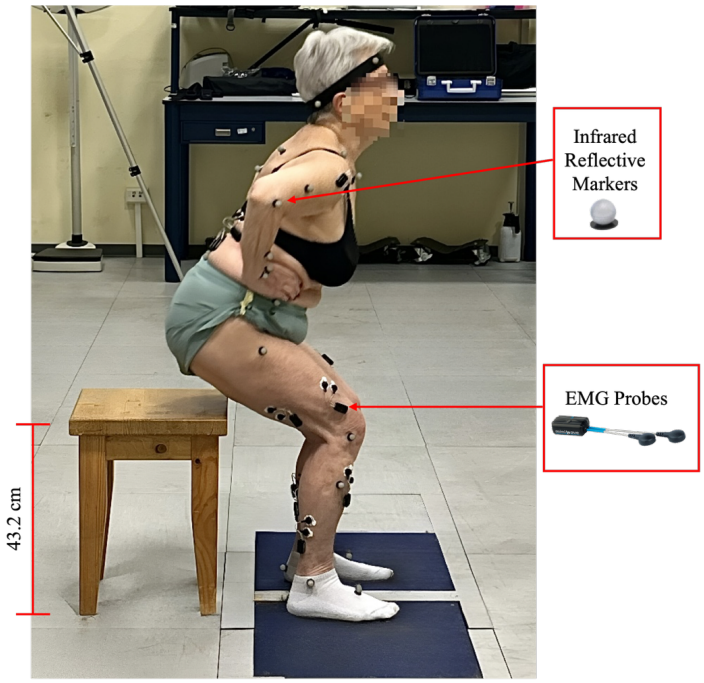

Figure 9.1. Experimental set-up for the sit-to-stand task. The figure shows a representative participant instrumented with surface electromyography (EMG) electrodes and infrared reflective markers. EMG electrodes were placed bilaterally over seven muscles: erector spinae (ES), latissimus dorsi (LD), vastus lateralis (VL), tibialis anterior (TA), biceps femoris (BF), gastrocnemius medialis (GastM), and soleus (Sol). A total of 39 infrared reflective markers were positioned according to the Plug-in Gait (PiG) kinematic model. The inset panels highlight the EMG probe and the reflective marker used in the experimental setup.

9.3. Data Analysis

9.3.1. Event identification

Kinematic data were processed using a 4th-order Butterworth filter with a cut-off frequency of 12 Hz. The velocity measured from the marker on the right posterior superior iliac spine was used to identify the initial sit-to-stand event (i.e., the upward phase from sit to stand) of a complete sit to stand to sit cycle (Ranaldi et al., 2025). The starting point of the movement from sitting to standing was defined as the point at which the velocity reached 20% of its maximum value, and the end as the point when it dropped below 20% (i.e., the same kinematic criteria described in **Study III, Chapter 8, Section 8.3**).

9.3.2. EMG pre-processing

The EMG signals were processed by applying a band-pass filter (40-350 Hz), full wave rectification, and low-pass filtering at 10 Hz with a zero-lag 4th-order Butterworth filter to obtain linear envelopes (Ranaldi et al., 2023). For each muscle, the EMG envelope was then normalized in amplitude to its median peak value across all cycles maximum to guarantee an equal contribution for each muscle during synergy extraction, addressing amplitude variations

associated with anatomical and recording factors (Torricelli et al., 2016). The EMG envelopes were segmented based on the previously identified sitting-to-standing phase. To accommodate for varying durations of phases among participants, each EMG envelope was time-normalized to 100 points per cycle, where 0 corresponds to the start and 100 corresponds to the end of the upward phase. The amplitude and time-normalized EMG data were then concatenated and a randomized subset of sixteen cycles, representative of the 30-second STS upward phase, were selected for the synergy extraction (Ranaldi et al., 2023). The selected cycles were then organized into an Ns-by-Nm matrix for each participant (with Ns indicating the number of samples and Nm denoting the number of muscles), where each column represents the concatenated envelope of a given muscle across multiple cycles (i.e., the same kinematic criteria described in **Study III, Chapter 8, Section 8.3**).

9.3.3. Muscle synergy analysis

9.3.3.1. Synergies extraction

Synergies were extracted from the Ns-by-Nm matrix for each participant, by using the NNMF algorithm, as described in **Chapter 6** (see **Section 6.3.3, Equation 6.1**). The same multiplicative-update algorithm and parameter settings were applied. Synergy extraction was performed iteratively, beginning with a single muscle synergy and increasing to encompass all recorded muscles. Consequently, the function was executed multiple times, adjusting between 1 and 14 for each individual.

The optimal number of muscle synergies (N_{syn_opt}) was determined according to the procedure detailed in **Chapter 6, Section 6.3.4**, which outlines the selection criteria based on the VAF and the MSE.

9.3.3.2. Synergy sorting

As in **Section 8.3.2**, the weight vectors and activation coefficients were reordered based on their similarity to a reference set of synergies, ensuring a consistent organization across participants.

9.3.3.3. Cross-validation analysis

The Variance Accounted For (VAF), defined as uncentered Pearson correlation coefficients (Torres-Oviedo et al., 2006), was first computed for each participant based on the optimal number of muscle synergies identified (extracted VAF). Subsequently, data from each participant were mapped onto the space defined by the average set of synergies by Non-Negative Reconstruction, and the corresponding VAF values were computed (reconstruction

VAF). The extracted and reconstruction VAF values were then compared with the ones related to reconstruction with random surrogate W vectors (surrogate VAF), as in (De Marchis et al., 2019b). This procedure was performed for both groups. The detailed results of this analysis are provided in the **Supplementary Materials (Appendix Figure S9.1)**.

9.3.3.4. Synergy-based parameters

Temporal features of each muscle synergy were analyzed to characterize both the duration and timing of their activation profiles. Specifically, for each synergy, the Full Width at Half Maximum (FWHM) of the activation coefficient was computed as the number of normalized time samples in which the activation exceeded 50% of its peak amplitude (Martino et al., 2015). Within this interval, the Root Mean Square (RMS) was calculated to quantify the overall magnitude of activation.

To further describe the temporal organization of the activation patterns, the Centre of Activity (CoA) was estimated using circular statistics (Batschelet, 1981; Berens, 2009; Sylos-Labini et al., 2014). For each synergy, the normalized activation coefficient was expressed as a function of angular position (0–360°), where the angle q represents the relative time within the movement cycle (corresponding to 0–100% of the cycle). The cosine and sine components of each time sample were first weighted by the corresponding activation amplitude and summed as:

$$A = \sum_{t=1}^{N} (\cos \theta_t \times C_t) \tag{9.1}$$

$$B = \sum_{t=1}^{N} (\sin \theta_t \times C_t) \tag{9.2}$$

where θ_t represents the angular position corresponding to each normalized time sample t (spanning 0–360°), C_t is the synergy activation coefficient at time t, and N is the total number of samples within one normalized movement cycle.

The CoA was then obtained as the angular position of the resultant vector:

$$CoA = \tan^{-1}(B/A) \tag{9.3}$$

The CoA therefore provides a compact representation of the central tendency of each synergy's activation timing, expressed as an angle within the cycle.

Inter-limb consistency, defined as $CS_{sbj,k}$, was quantified using cosine similarity between the muscle weight vectors associated with the dominant and non-dominant sides. For each subject sbj and each synergy k, two weight vectors were constructed: $W^{D}_{sbj,k} = [W^{D}_{sbj,1}, \dots, W^{D}_{sbj,M}]$, containing the weights of the muscles M belonging to the dominant side, and $W^{ND}_{sbj,k} = [W^{ND}_{sbj,1}, \dots, W^{ND}_{sbj,M}]$, containing the weights of the homologous muscles M of the non-dominant side. The inter-limb consistency $CS_{sbj,k}$ represents the degree of similarity in muscle weighting between the two sides and was computed as follows:

$$CS_{sbj,k} = \frac{W^{D}_{sbj,k} \cdot W^{ND}_{sbj,k}}{\| W^{D}_{sbj,k} \| \, \| W^{ND}_{sbj,k} \|} \quad (6)$$

This metric yields values ranging from 0 to 1, with higher values indicating greater inter-limb consistency.

9.3.4. Center of Mass

The whole-body CoM was calculated following the same procedure described in **Chapter 8, Section 8.3.3**, using the Vicon Plug-in Gait Full Body model (Vicon Nexus 2.12), with trajectories extracted for the upward phase, time-normalized to 100 points, and based on the same cycles used for the EMG analysis. Only the anteroposterior and vertical components of the CoM were analyzed, as the sagittal plane is the main direction of movement during this activity.

To explore the relationship between CoM dynamics and synergy activation, a state-to-synergy mapping was performed as outlined in Ranaldi et al. (2025). For each participant, position–velocity phase spaces were constructed from the normalized CoM trajectories expressed in Cartesian coordinates, considering both displacement and velocity components in the antero-posterior and vertical directions. At each time sample, the most active synergy was identified from the reconstructed activation profiles. A Gaussian Naive Bayes classifier was then trained to map CoM features to synergy states. The resulting probability maps illustrate the likelihood of each synergy being active within specific regions of the CoM phase space. CoM trajectories as averaged from young and elderly participants, respectively, were projected onto the synergy maps derived from the young group, allowing for a comparison of group-specific postural control strategies.

9.4. Statistical Analysis

Statistical analyses were conducted to evaluate differences between groups across all extracted metrics. The normality of data within each group for each parameter was assessed using the Shapiro Wilk test. Based on the results of the normality test, either independent samples t tests for normally distributed data or Mann Whitney U tests for non-normally distributed data were applied. The effect size for each comparison was quantified using Hedges' g statistic (Hedges, 1981). The N_{syn_opt}, the temporal features of the activation coefficients, namely FWHM, RMS, and CoA, as well as inter-limb consistency were compared between the groups. Statistical comparisons for inter-limb consistency, FWHM, RMS, and CoA were performed individually for each synergy. *P* values obtained for these parameters were adjusted using the Bonferroni correction to address multiple comparisons across the metrics.

All analyses were performed in MATLAB (version R2024b, The MathWorks, Natick, MA, USA) with the significance threshold established at $p < 0.05$.

All the parameters were expressed as mean ± standard error (SE) over the sample population.

9.5. Results

Figure 9.2 reports the VAF and MSE as a function of the number of extracted synergies N_{syn} for both groups. EMG reconstructions in the Young and Elderly participants required on average 3.6 ± 0.2 synergies, yielding mean VAF values of 92.1 ± 0.4% and 92.8 ± 0.3%, respectively, with corresponding MSEs of (4.7 ± 0.6) × 10^{-5} and (4.7 ± 0.7) × 10^{-5}. No significant differences were observed between groups.

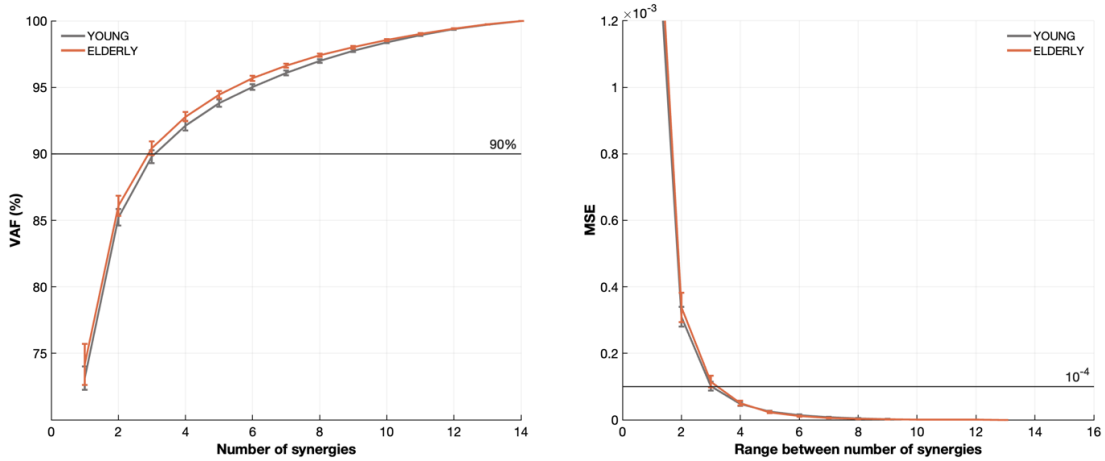

Figure 9.2. Optimal number of synergies for each group. Evaluation of two criteria: Variance Accounted For (VAF) versus number of synergies and Mean Squared Error (MSE) versus number of synergies. Data presented as mean ± SE across the sample population, with young adults represented in dark grey and older adults in orange. The first criterion identified the smallest number

of synergies for which the VAF exceeded 90%, with the addition of further synergies resulting in less than a 5% increase in VAF. The second criterion was based on iterative linear regressions applied to progressively shortened segments of the VAF curve (from 1 to 13 synergies), with the optimal value defined as the minimum number of synergies for which the MSE dropped below 10^{-4}. When the two criteria yielded different values, the larger number of synergies was selected.

The average muscle synergies identified through the optimal number of components (N_{syn_opt}) are illustrated in **Figure 9.3**. These synergies demonstrated a significant degree of bilateral symmetry in both groups, suggesting consistent coordination patterns across both sides of the body. Mean inter-limb consistency values and their standard errors for each synergy are reported in **Table 9.1**, and no statistically significant differences were observed between groups. Detailed results of this analysis, including individual subject distributions overlaid on group-level summaries, are provided in the Supplementary Materials (**Appendix Figure S9.2**). Each synergy can be interpreted in relation to a specific functional component of the STS. *W1* was primarily active during quiet standing, characterized by dominant ankle plantar flexor activity. *W2* was engaged during trunk flexion and the subsequent transition from knee extension to maximal ankle dorsiflexion, reflecting the coordinated extension of the entire body. Finally, *W3* and *W4* were mainly associated with the conclusion of the rising phase, facilitating full knee and hip extension.

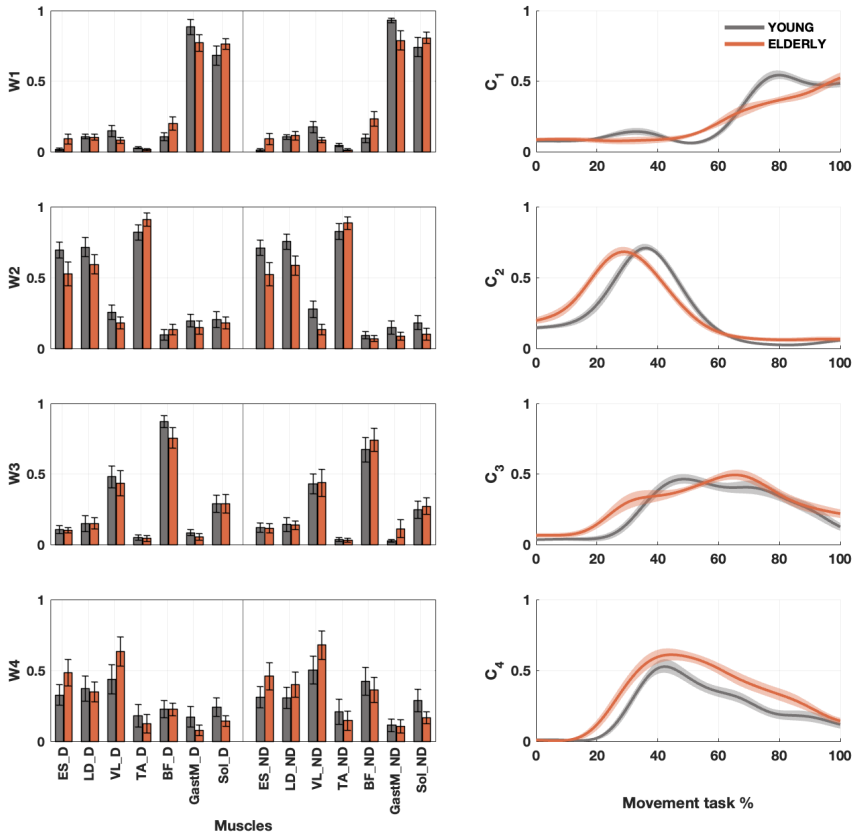

Figure 9.3. Averaged muscle synergy structure (W1–W4, left panels) and corresponding activation coefficients (C1–C4, right panels) during the sit-to-stand task in young (dark grey) and older (orange) adults. Bar plots show the mean muscle weightings (± standard error) for each synergy, while line plots illustrate the normalized activation profiles across the movement cycle (0–100%). Muscle labels correspond to erector spinae (ES), latissimus dorsi (LD), vastus lateralis (VL), tibialis anterior (TA), biceps femoris (BF), gastrocnemius medialis (GastM), and soleus (Sol), reported separately for the dominant (D) and non-dominant (ND) sides. Shaded areas around the activation curves indicate the standard error.

Table 9.1. Inter-limb consistency for each group and muscle synergy.

		Inter-limb Consistency	
		Young	**Elderly**
Synergies	**Syn1**	0.96 ± 0.02	0.96 ± 0.01
	Syn2	0.96 ± 0.007	0.96 ± 0.001
	Syn3	0.92 ± 0.02	0.93 ± 0.01
	Syn4	0.81 ± 0.05	0.93 ± 0.03

Inter-limb consistency values compared between young and elderly participants for each muscle synergy (Syn1–Syn4). No statistically significant differences were observed between groups.

The FWHM and RMS of the activation coefficients (C) for each synergy are illustrated in **Figure 9.4**. In terms of FWHM, elderly participants demonstrated significantly higher values compared

to young adults for C2 (p = 0.02, g = 0.97). No significant differences were found in RMS between groups.

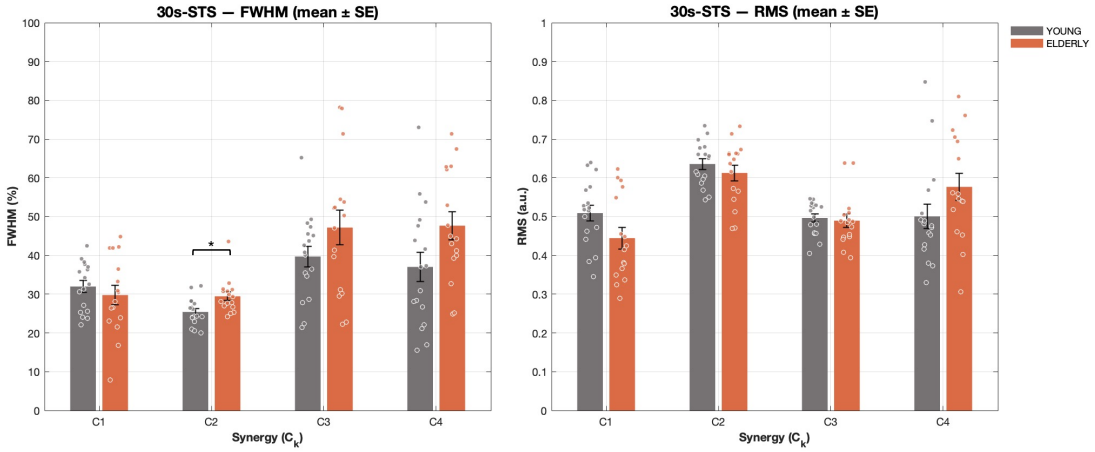

Figure 9.4. Mean ± standard error (SE) values of the full width at half maximum (FWHM) of the activation profiles (left panel) and root mean square (RMS) amplitude (right panel) computed for each synergy (C1–C4) during the 30-s sit-to-stand (30s-STS) task in young (dark grey) and older (orange) adults. Individual participant data points are overlaid on the bar plots. Asterisks indicate significant between-group differences (*p < 0.05).

Figure 9.5 presents the CoA values, expressed as a percentage of the movement cycle, for each synergy within the young and elderly groups. Overall, the CoA patterns displayed a consistent temporal sequence across synergies in both groups, indicating the orderly recruitment of muscle synergies during the STS. Notably, a significant difference emerged for C2 (p = 0.009, g = 1,23), with the elderly group showing earlier activation compared to the young group. However, no significant differences were observed for the other synergies.

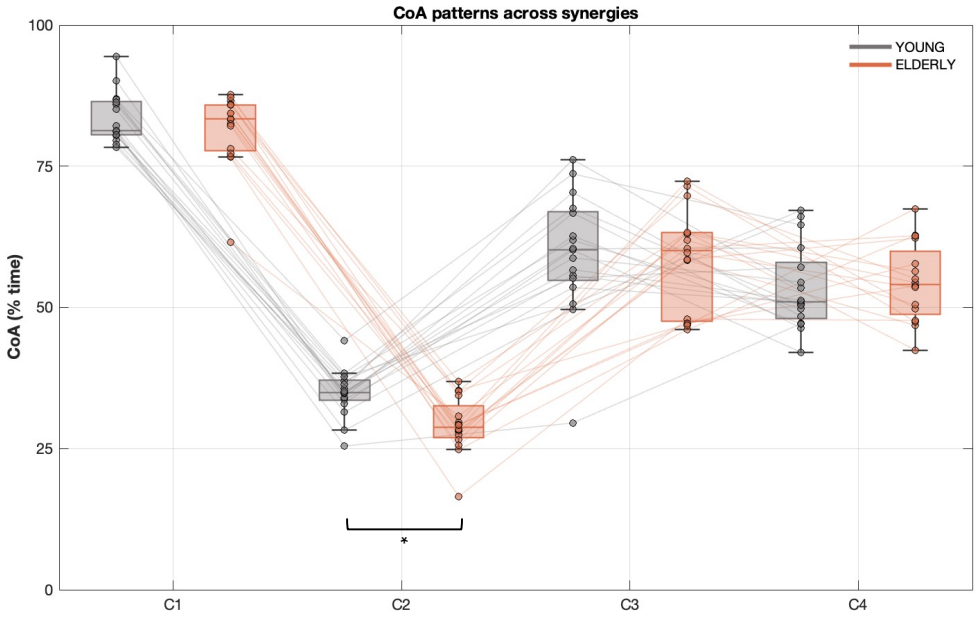

Figure 9.5. Boxplots show the center of activation (CoA) values (expressed as % of the movement cycle) for each synergy (C1–C4) in young (dark gray) and elderly (orange) participants. Dots represent individual subjects, and connecting lines indicate within-subject CoA patterns across synergies. The asterisk denotes a significant between-group difference (*$p < 0.05$).

The state-to-synergy probability maps depicted in **Figure 9.6** illustrate the relationship between the position–velocity dynamics of the CoM and the activation of individual muscle synergies in the anteroposterior (left panels) and vertical (right panels) directions. In the anteroposterior position–velocity space, both groups demonstrated consistent CoM–synergy relationships across most components. However, notable group differences were observed for C2 and C4. In the case of C2, the trajectory for the elderly group (dashed line) was notably shifted in comparison to the young group (solid line), passing through areas of lower activation probability. A similar, though less pronounced, displacement was noted for C4, where the elderly trajectory intersected the upper-left boundary of the region of maximal probability, suggesting a weaker correlation between CoM motion and synergy activation during this phase of movement. Conversely, in the vertical direction, the regions of maximal probability were distributed across distinct areas of the phase space, indicating the sequential activation of the synergies throughout the movement. In this direction, the CoM trajectories of both the young and elderly groups predominantly overlapped within the same high-probability regions, revealing no significant group-related deviations.

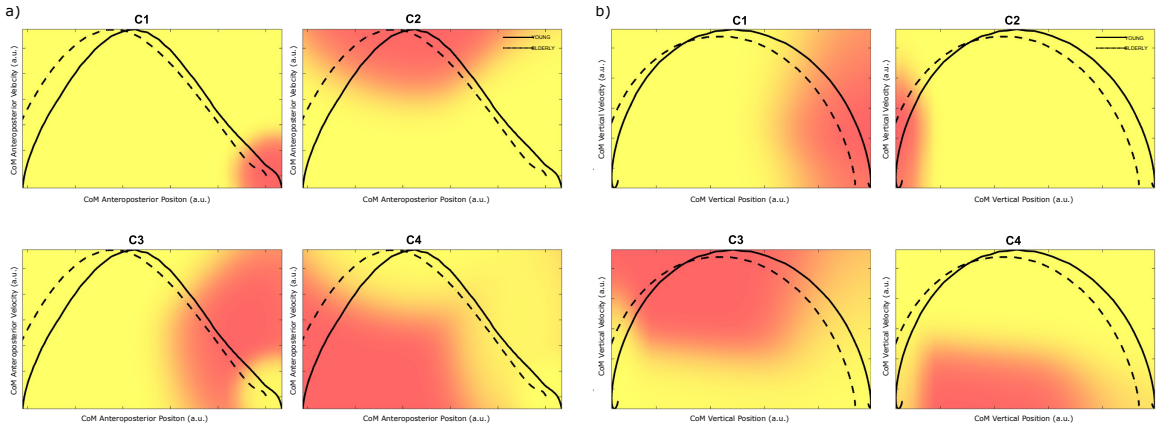

Figure 9.6. State-to-synergy mapping in the position–velocity phase space of the center of mass (CoM). Left panels **(a)** refer to the anteroposterior position–velocity space, while right panels **(b)** correspond to the vertical space. Each subplot represents one of the four synergy activity maps (C1-C4). The color scale indicates the probability of each synergy being the most active among the four, with darker shades corresponding to higher probabilities. Solid lines represent the young group, whereas dashed lines represent the elderly group.

9.6. Discussion

This study demonstrates that healthy aging does not substantially alter the modular organization of muscle synergies underlying the STS task, but it is associated with specific

temporal and biomechanical adaptations. Across young and older adults, STS execution relied on a consistent set of four bilateral muscle synergies, indicating a high degree of standardization in the neuromuscular control of this functional action. These findings are consistent with previous investigations of STS in older adults, which reported the presence of three to four muscle synergies based on unilateral muscle recordings (An et al., 2013; Hanawa et al., 2017; Yang et al., 2017b; Yang et al., 2019). Notably, our results indicate that age does not significantly alter the number of synergies required to reconstruct muscle activation, implying that the complexity of motor control in our healthy elderly cohort was not reduced (Allen & Franz, 2018; Baggen et al., 2020; Monaco et al., 2010).

Employing a bilateral framework allowed for the assessment of integrated control mechanisms of both body sides during this inherently symmetric task. The significant interlimb consistency observed in the synergy structures underscores that the neural organization governing postural transitions is predicated upon stable and symmetric motor modules. This methodological approach also addresses constraints highlighted by Steele et al. (2015), who noted that synergy structure can be affected by the number and selection of recorded muscles, leading to potential overestimation of VAF when fewer muscles are analyzed. By recording from a large set of bilateral trunk and lower-limb muscles, this study provided a comprehensive representation of the neuromuscular coordination underlying the STS task. The preservation of bilateral symmetry in synergy structure observed here is consistent with evidence from other symmetric whole-body tasks, in which bilateral synergies have been described (Bellitto et al., 2023; Ceriello et al., 2025; Saito, Yokoyama, Sasaki, & Nakazawa, 2023).

Moreover, the spatial structure of the synergy vectors exhibited remarkable comparability between young and older adults, suggesting that the fundamental architecture of motor modules remains preserved with advancing age. This finding aligns with previous studies reporting that elderly adults generally retain a similar number and composition of synergies as younger individuals during both the STS movement and gait (Monaco et al., 2010; Roelker et al., 2021; Yang et al., 2017b). While the overall spatial organization was conserved, aging was associated with subtle but meaningful adaptations in the temporal domain. The earlier and broader activation of the second synergy, which predominantly involves trunk flexors and ankle dorsiflexors responsible for momentum transfer, suggests a temporal reorganization of control objectives aimed at stabilizing the CoM prior to seat-off. This adjustment appears to reflect a compensatory strategy for generating forward momentum that occurs earlier in the movement. Similar temporal shifts toward prolonged or anticipatory synergy activation have

been documented in both STS and gait literature, indicating a redistribution of effort to uphold stability and safety amidst diminished neuromuscular efficiency (Allen & Franz, 2018; Guo et al., 2022; Santuz et al., 2022; Yang et al., 2017b).

The analysis of the relationship between synergy recruitment and CoM dynamics yielded additional insights into the coordination between neural and biomechanical control mechanisms. Although the general correspondence between CoM trajectories and synergies was maintained, older adults demonstrated reduced alignment, particularly concerning the synergies linked to trunk flexion (C2) and final stabilization (C4). Such discrepancies were most prominent along the anteroposterior axis, necessitating fine adjustments to effectively manage forward momentum, while the vertical control aspect remained largely unaffected. This directional specificity supports previous biomechanical findings suggesting that aging is correlated with increased trunk flexion, elevated anteroposterior CoM velocity, and greater postural sway during the transition phases of raising and stabilization (Papa & Cappozzo, 2000; Piano et al., 2020; Sadeh et al., 2023).

Some methodological considerations must be taken into account when interpreting the results of this study. The fixed seat height used, while consistent with standardized protocols, may have introduced variability in the mechanical demands experienced by participants of varying body sizes. Future studies that adjust seat height according to individual anthropometrics could yield a more accurate assessment of age-related neuromuscular adaptations under comparable mechanical conditions. Additionally, the temporal segmentation of the movement may require further development. The current analysis focused on the overall upward phase without dividing it into more detailed sub-phases. A finer subdivision of the STS movement into its classical sub-stages could help elucidate how each synergy contributes to the successive transitions of the task and whether aging affects these stages differently.

Despite these considerations, the combined use of bilateral synergy analysis and CoM-based evaluation provides a valuable framework for examining the interplay between neural and biomechanical coordination. This bilateral approach offers insights into interlimb symmetry and coordination, both of which are crucial for understanding normal and impaired postural control. Future research should aim to broaden this approach to include populations with compromised balance control. Extending this analysis to older individuals who have experienced previous falls and compare them with those who have not could help identify neuromuscular patterns associated with fall risk. Additionally, studying individuals with unilateral deficits, such as stroke survivors, individuals with Parkinson's disease, or those who

use lower-limb prostheses, could shed light on how asymmetries influence bilateral coordination strategies. Such investigations would yield valuable insights into the compensatory mechanisms that maintain stability in the presence of motor or structural asymmetries, informing the development of targeted interventions to enhance interlimb coordination and functional autonomy. Longitudinal studies could further determine whether targeted rehabilitation or balance training can restore the temporal precision of synergy recruitment and improve postural stability in older adults.

In conclusion, healthy aging appears not to significantly disrupt the overarching neuromuscular control strategy, though it may influence specific aspects of coordination. In particular, the temporal coupling with whole-body dynamics experiences a shift towards greater diffusion and overlap during specific phases of the STS movement, revealing an adaptive reorganization within a symmetric and resilient control architecture.

9. Study V: Aging Effects on Neuromuscular Coordination during Functional Reaching Movements

Imma Ceriello[1] · Marco Ghislieri[2] · Valentina Camomilla[1] · Andrea Macaluso[1] · Riccardo Borzuola[1]

[1]Laboratory of Bioengineering and Neuromechanics, Department of Movement, Human and Health Sciences, University of Rome "Foro Italico", Rome, Italy

[2]Polito[BIO]Med Lab, Department of Electronics and Telecommunications, Politecnico di Torino, Torino, Italy

The study presented in this chapter is currently in preparation for submission.

10.1. Rationale and Objectives

This study builds upon prior research (Ceriello et al., 2025) (**Study I**) examining muscle coordination during Functional Reach in various directions by exploring the influence of aging on neuromuscular control strategies essential for maintaining balance during voluntary reaching movements.

Reaching performance is determined not only by the distance of the reach but also by the coordination of multiple joints and muscles that regulate the CoM displacement. In older adults, this ability is often impaired due to factors such as reduced muscle strength, diminished sensory feedback, and compromised postural control, resulting in shorter reach distances and altered movement strategies (De Waroquier-Leroy et al., 2014; Duncan et al., 1990; Kozak et

al., 2003). Gaining insight into how age impacts the neuromuscular organization is crucial for understanding the mechanisms underlying postural adaptation and balance decline.

Objectives: The current study aims to investigate the effect of aging on muscle synergy organization during voluntary upright reaching movements. Specifically, it seeks to identify and compare the muscle synergies engaged in young and older adults, as well as evaluate how their quantity, spatial structure, and temporal activation profiles change with age.

Based on prior evidence in elderly populations (Allen & Franz, 2018; Baggen et al., 2020; Monaco et al., 2010; Roelker et al., 2021; Yang et al., 2017b), we hypothesize that aging would not significantly alter the spatial structure of muscle synergies but would lead to changes in their temporal activation patterns, reflecting compensatory mechanisms to sustain stability. Investigating these age-related adaptations in synergy organization during everyday tasks such as upright reaching may provide valuable insights into how the CNS reorganizes motor control to address potential declines in balance capabilities.

10.2. Experimental Procedure

Participants and experimental procedures adhered to the general framework outlined in **Chapter 5**. Specifically, data were collected during the uniFR, biFR, and LR tasks (see **Section 5.3.1**) from seventeen healthy young volunteers (10 males and 7 females; average age: 27.5 ± 3 years; average height: 1.7 ± 0.1 m; average body mass: 64.9 ± 8.8 kg; 2 left-handed and 15 right-handed) and seventeen healthy older adults (7 males and 10 females; average age: 77.7 ± 7.0 years; average height: 1.64 ± 0.07 m; average body mass: 67.8 ± 10.4 kg; 2 left-handed and 10 right-handed) (refer to **Section 5.2** for inclusion criteria). Data from Ceriello et al. (2025) were used as reference for the young group and re-analyzed together with the elderly dataset.

The EMG recording and motion capture procedures conformed to the general setup described in **Section 5.3.4**. This study specifically included the acquisition of surface EMG signals and whole-body kinematics via the stereophotogrammetric system; however, data from the force platforms were not included in the current analysis.

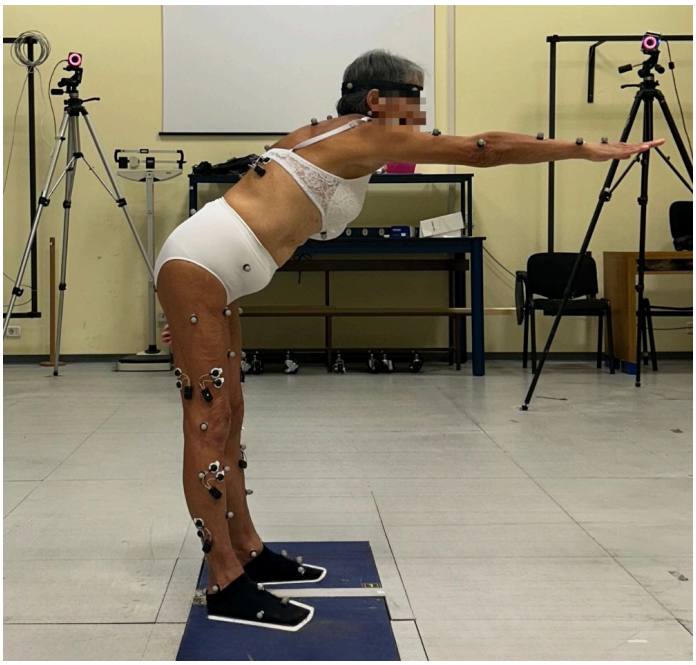

Figure 10.1. Experimental set-up for the Functional Reach task. The figure shows a representative older adult participant instrumented with surface electromyography (EMG) electrodes and infrared reflective markers. EMG electrodes were placed bilaterally over eight muscles: anterior deltoid (AD), erector spinae (ES), latissimus dorsi (LD), vastus lateralis (VL), tibialis anterior (TA), biceps femoris (BF), gastrocnemius medialis (GastM), and soleus (Sol). A total of 61 infrared reflective markers were positioned according to the Plug-in Gait and Conventional Gait Model 2.5 kinematic protocols. Whole-body kinematics were recorded using an optoelectronic motion capture system.

10.3. Data Analysis

The main data processing and analysis procedures were identical to those described in **Chapter 6 (Section 6.3)**. Briefly, kinematic data were used to identify movement phases (**Section 6.3.1**), EMG signals were pre-processed and time–normalized (**Section 6.3.2**), and muscle synergies were extracted and characterized following the same criteria for synergy number selection (**Section 6.3.4**), sorting (**Section 6.3.5**), and quantitative evaluation, including synergy robustness assessed via CrossVAF and intra-task consistency, both computed as described in **Section 6.3.6**.. The whole–body CoM was computed using the Plug–in Gait Full Body model, as described in **Chapter 9, Section 9.3.4**.

Only the additional analyses, which were introduced specifically in this study, are detailed below.

10.3.1. Kinematic Parameters

A series of kinematic metrics was computed to characterize reaching performance. All kinematic parameters were derived from the segment of movement occurring between the

onset of the reaching phase (R1) and the maximum distance (MD) event, after applying time normalization (t).

Maximum Distance Reached:

The maximum distance reached was defined as the absolute displacement of the hand marker along the reaching direction (marker on the middle knuckle; along the y-axis for forward direction and x-axis for lateral) between R1 and MD, normalized by the individual's body height (H):

$$D_{max} = \frac{|hand(\tau_{MD}) - hand(\tau_{R1})|}{H} \quad (10.1)$$

CoM Path Length:

To quantify the trajectory traveled by the CoM, the cumulative path length was determined by summing the three-dimensional point-to-point Euclidean distances between consecutive samples within the R1–MD interval:

$$PL_{CoM} = \sum_{k=1}^{N-1} \|CoM(\tau_{k+1}) - CoM(\tau_k)\|_2 \quad (10.2)$$

where N denotes the number of normalized samples within the R1–MD interval.

Center of Mass Displacement:

The total displacement of the CoM was calculated as the three-dimensional Euclidean distance between the CoM position at R1 and at MD:

$$Displ_{CoM} = \|CoM(\tau_{MD}) - CoM(\tau_{R1})\|_2 \quad (10.3)$$

10.3.2. Synergy-based parameters

Beyond the core synergy extraction procedure, additional synergy-based parameters were computed to quantify specific spatial and temporal features of the synergies.

In complement to the total VAF, the VAF explained by a single synergy (**VAF1**) was investigated. This metric quantifies how much variance of the original EMG dataset can be reconstructed using only one synergy (Bekius et al., 2021; Steele et al., 2015).

Temporal features were then investigated by computing, for each synergy, the Full Width at Half Maximum (**FWHM**) of the corresponding activation coefficient, defined as the number of normalized time samples in which the activation exceeded 50% of its peak amplitude (Martino et al., 2015). The magnitude of activity within this most relevant temporal interval was further quantified by computing the Root Mean Square (**RMS**) within the FWHM window.

Finally, to determine which muscles predominantly contributed to each synergy, an **adaptive thresholding** procedure was applied to the synergy weight vectors using Otsu's method. Originally developed for image processing, Otsu's method is an unsupervised threshold selection procedure that automatically distinguishes "foreground" from "background" based on the distribution of gray levels in an image's histogram (Otsu, 1979). In this context, we applied the same principle to the distribution of muscle weights within each synergy: weights exceeding the automatically determined threshold were labeled as active muscles, while those below the threshold were considered inactive contributors. This approach offers a fully data-driven and non-arbitrary means of identifying the dominant muscles for each synergy.

From a computational standpoint, Otsu's threshold corresponds to the value that maximizes the between-class variance of the two resulting clusters (active versus inactive). In our implementation, the threshold was evaluated at the individual subject level: for each participant and each synergy, Otsu's criterion was applied independently to determine a subject-specific optimal threshold. These subject-level thresholds were subsequently averaged across participants to establish a single adaptive threshold for that synergy. This process ensured that the identification of active muscles was not based on a fixed a priori cutoff but instead reflected a population-based estimate driven purely by the empirical distribution of muscle weights.

10.4. Statistical Analysis

Linear mixed-effects models were employed to investigate the effects of group and task. A single model that included the group × task interaction was fitted for each variable, allowing group effects to be tested within each task using post hoc contrasts instead of running separate models for each task. For each muscle synergy, individual models were fitted for the synergy-derived parameters, which included the FWHM and the RMS of activation profiles. The same statistical approach was applied to the VAF1 and the N_{syn}, calculated for each subject and task as indicators of reconstruction quality and dimensionality. The RMS values were logit-transformed to improve normality, while all other parameters were analyzed on their original scale. Kinematic parameters, such as D_{max}, PL_{CoM}, and $Displ_{CoM}$ were also analyzed using the same model

structure. Group, task, and their interaction were included as fixed effects, while participant variability was accounted for by including participant as a random factor. Post hoc pairwise comparisons were conducted on the estimated marginal means, with a Bonferroni correction applied to adjust for multiple comparisons. Comparisons were performed within combinations of the relevant fixed factors, and the resulting p-values were used to determine statistical significance, with p-values below 0.05 considered statistically significant.

The main text reports only the results related to group differences, while task-related and interaction effects are detailed in the Supplementary Material.

For the intra-task consistency, between-group comparisons were performed separately for each task. Data normality was assessed using the Shapiro–Wilk test. When normality was met, independent-samples t-tests were applied; otherwise, Mann–Whitney rank-sum tests were used. Bonferroni correction was applied to account for multiple comparisons across tasks and synergies.

The CrossVAF analysis was conducted separately for each group to assess the robustness of muscle synergies across all possible task pairs. The Shapiro–Wilk test was used to evaluate the normality of data distributions. Depending on the results, either a repeated-measures ANOVA (for normally distributed data) or a Friedman test (for non-normal data) was implemented. When significant effects were observed, post hoc comparisons were performed with Bonferroni correction for multiple testing.

The effect sizes of statistically significant differences were calculated using Hedges' g statistic (Hedges, 1981).

All the parameters were expressed as mean ± standard error (SE) over the sample population.

All statistical analyses were carried out using MATLAB (version R2024b, The MathWorks, Natick, MA, USA).

10.5. Results

10.5.1. Optimal number of synergies

Figure 10.2 illustrates the variation in VAF and the MSE as a function of the number of extracted synergies N_{syn} for both groups. On average, the young group showcased EMG activity reconstructed using 3.0 ± 0.2 muscle synergies during the uniFR task and 2.9 ± 0.1 synergies during the biFR task. These reconstructions yielded an average VAF of 92.3 ± 0.4% for uniFR and 93.2 ± 0.3% for biFR, with corresponding MSE values of (6.9 ± 1.0) × 10^{-5} and (6.0 ± 1.0) × 10^{-5}, respectively. For the LR task, the reconstruction required 3.8 ± 0.3 synergies, resulting in a mean VAF of 90.9 ± 0.4% and an MSE of (6.5 ± 0.8) × 10^{-5}.

In the elderly group, EMG activity was reconstructed using 2.9 ± 0.06 muscle synergies for the uniFR task, 2.9 ± 0.06 synergies for the biFR task, and 3.5 ± 0.2 synergies for the LR task. These reconstructions produced mean VAF values of 93.0 ± 0.2%, 93.8 ± 0.2%, and 90.1 ± 0.3%, along with corresponding MSE values of (5.9 ± 0.4) × 10^{-5}, (5.5 ± 0.4) × 10^{-5}, and (10.3 ± 1.1) × 10^{-5}, respectively.

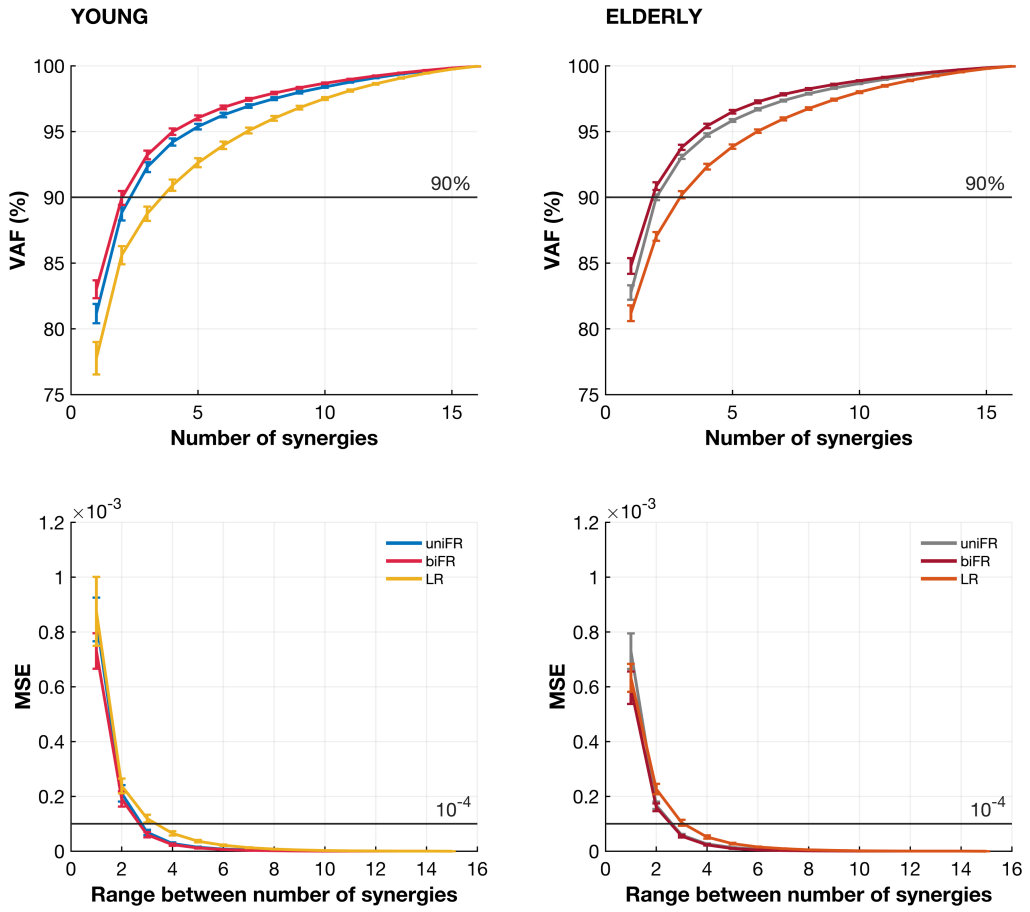

Figure 10.2. Determination of the optimal number of synergies, denoted as N_{syn_opt}, for each group was carried out by evaluating two criteria: the Variance Accounted For (VAF) versus the number of synergies curve, and the Mean Squared Error (MSE) versus the number of synergies curve. Results are presented separately for young (left column) and older (right column) adults. For young adults, curves correspond to unilateral Functional Reach (uniFR, blue), bilateral Functional Reach (biFR, red), and Lateral Reach (LR, yellow). For older adults, curves correspond to uniFR (grey), biFR (dark red), and LR (orange). All data are presented as mean ± SE across the sample population. The first criterion identified the smallest number of synergies for which the VAF exceeded 90%, with the addition of further synergies resulting in less than a 5% increase in VAF. The second criterion was based on iterative linear regressions applied to progressively shortened segments of the VAF curve (from 1 to 15 synergies), with the optimal value defined as the minimum number of synergies for which the MSE dropped below 10^{-4}. When the two criteria yielded different values, the larger number of synergies was selected as N_{syn_opt}.

When comparing the two groups, elderly adults demonstrated a significantly higher VAF1 (p = 0.0016, $|g|$ = 1.51) (**Figure 10.3**) and a lower number of extracted synergies N_{syn} (p = 0.046, $|g|$

= 0.79) during the LR task. In contrast, no significant group differences were observed for the uniFR and biFR tasks.

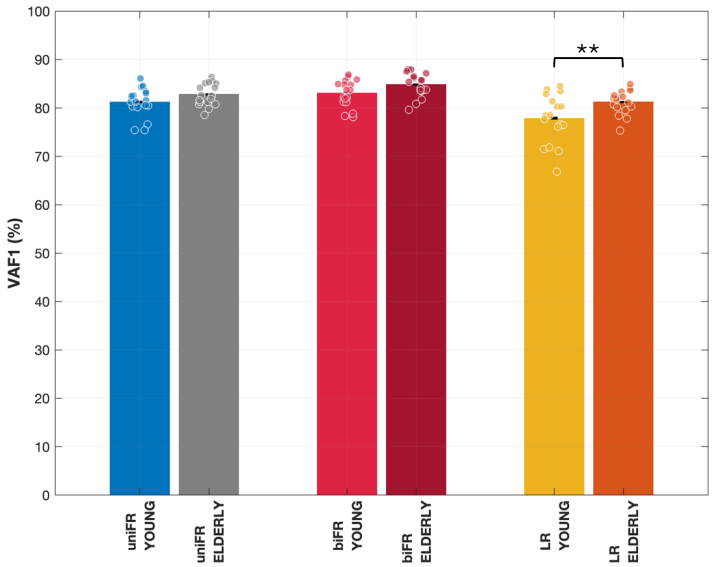

Figure 10.3. Group-averaged VAF1 (%) for the unilateral Functional Reach (uniFR), bilateral Functional Reach (biFR), and Lateral Reach (LR) tasks in young and older adults. For young adults, bars are shown in blue (uniFR), red (biFR), and yellow (LR); for older adults, bars are shown in grey (uniFR), dark red (biFR), and orange (LR). Bars represent mean values, circles indicate individual participants, and error bars denote the standard error. Statistically significant differences (**p < 0.01) are indicated by asterisks.

10.5.2. Muscle synergy composition

Figures 10.4, 10.5, and 10.6 illustrate the muscle synergies extracted from the uniFR, biFR, and LR tasks, respectively, averaged across participants within each group. Each row corresponds to a specific synergy, with the spatial muscle weightings (W) displayed on the left and the associated temporal activation coefficients (C) on the right. The red dashed line indicates the adaptive threshold determined using Otsu's method, with muscles above this threshold considered active contributors to the synergy. The bars represent the mean ± SE of muscle weights, while the shaded areas surrounding the activation profiles denote the standard error across participants. These group-level representations outline the characteristic spatial and temporal organization of the extracted synergies for each task, facilitating direct comparison of synergy structure between young and elderly adults.

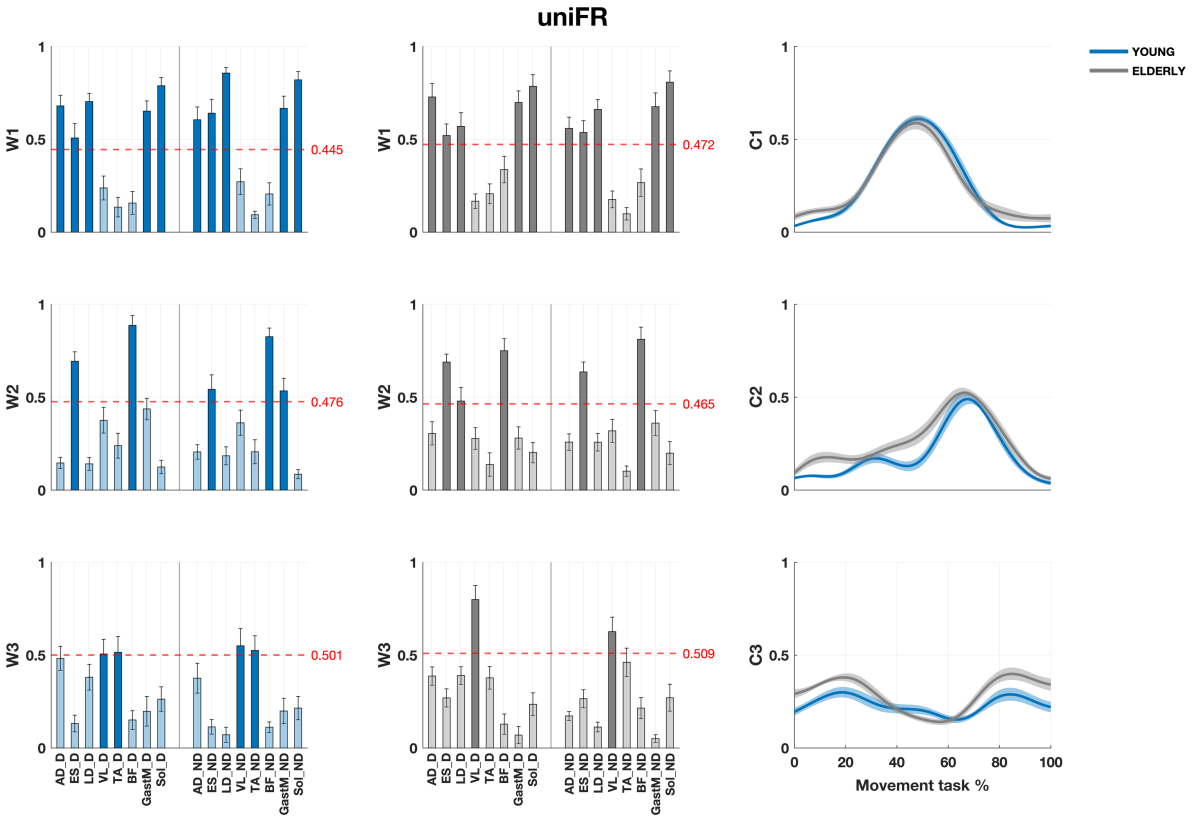

Figure 10.4. Average muscle synergy structures (W) and corresponding activation coefficients (C) for young (blue) and elderly (grey) participants during the unilateral Functional Reach (uniFR) task. Each row represents one synergy. The red dashed line indicates the adaptive threshold computed using the Otsu method; muscles with activation values exceeding this threshold were considered active within the synergy. Bars show mean ± SE muscle weights, and shaded areas in the activation profiles (C) represent standard errors across participants. Muscle labels correspond to anterior deltoid (AD), erector spinae (ES), latissimus dorsi (LD), vastus lateralis (VL), tibialis anterior (TA), biceps femoris (BF), gastrocnemius medialis (GastM), and soleus (Sol), reported separately for the dominant (D) and non-dominant (ND) sides.

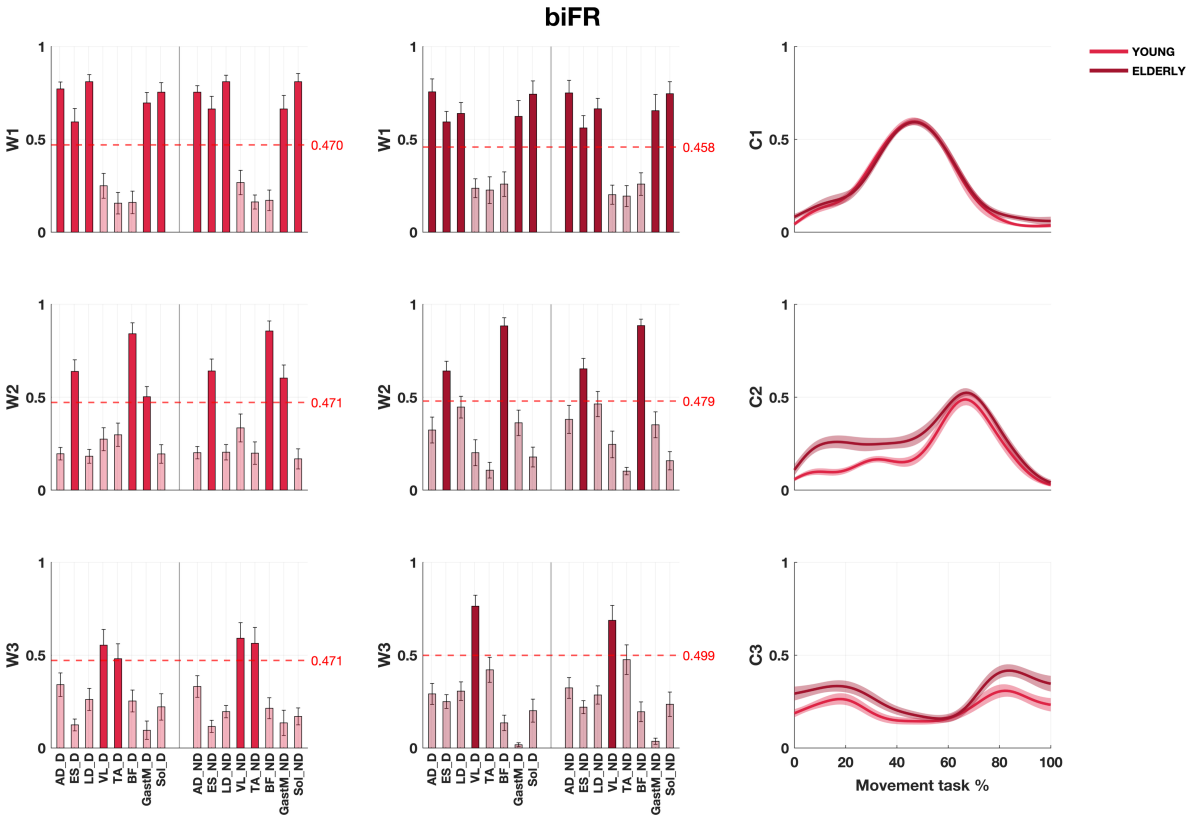

Figure 10.5. Average muscle synergy structures (W) and corresponding activation coefficients (C) for young (red) and elderly (burgundy) participants during the bilateral Functional Reach (biFR) task. Each row represents one synergy. The red dashed line indicates the adaptive threshold computed using the Otsu method; muscles with activation values exceeding this threshold were considered active within the synergy. Bars show mean ± SE muscle weights, and shaded areas in the activation profiles (C) represent standard errors across participants. Muscle labels correspond to anterior deltoid (AD), erector spinae (ES), latissimus dorsi (LD), vastus lateralis (VL), tibialis anterior (TA), biceps femoris (BF), gastrocnemius medialis (GastM), and soleus (Sol), reported separately for the dominant (D) and non-dominant (ND) sides.

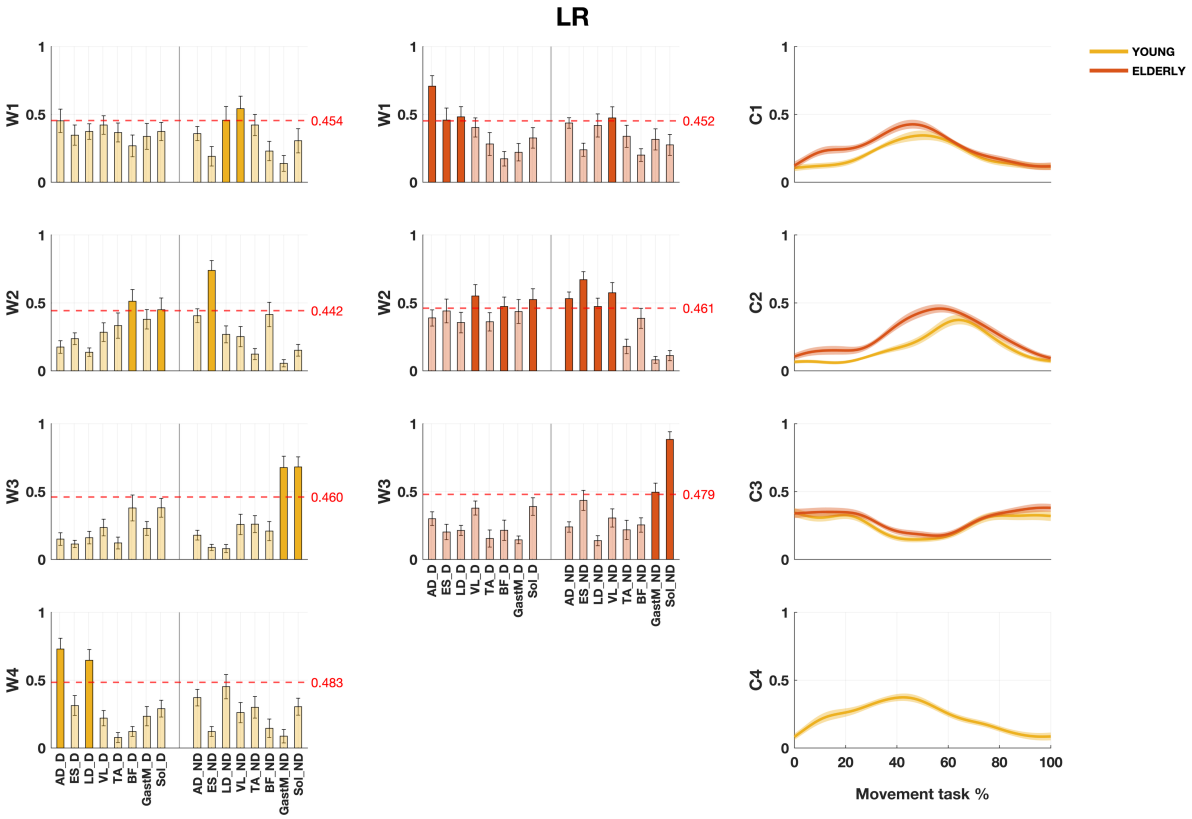

Figure 10.6. Average muscle synergy structures (W) and corresponding activation coefficients (C) for young (yellow) and elderly (orange) participants during the Lateral Reach (LR) task. Each row represents one synergy. The red dashed line indicates the adaptive threshold computed using the Otsu method; muscles with activation values exceeding this threshold were considered active within the synergy. Bars show mean ± SE muscle weights, and shaded areas in the activation profiles (C) represent standard errors across participants. Muscle labels correspond to anterior deltoid (AD), erector spinae (ES), latissimus dorsi (LD), vastus lateralis (VL), tibialis anterior (TA), biceps femoris (BF), gastrocnemius medialis (GastM), and soleus (Sol), reported separately for the dominant (D) and non-dominant (ND) sides.

10.5.3. Muscle synergy robustness and consistency

Tables 10.1 and **10.2** summarize the averaged $CrossVAF$ values for the young and elderly groups, respectively.

In the young group (**Table 10.1**), $CrossVAF$ values were significantly lower when uniFR and biFR EMG data were reconstructed using muscle synergies extracted during LR (LR to uniFR: $p < 0.001$, $|g| = 3.98$; LR to biFR: $p < 0.001$, $|g| = 3.42$), with no statistically significant difference between these two reconstructions. Similarly, when reconstructing LR EMG data using synergies extracted from the uniFR and biFR tasks, $CrossVAF$ values were markedly reduced (uniFR to LR: $p < 0.001$, $|g| = 4.50$; biFR to LR: $p < 0.001$, $|g| = 4.60$). Reconstructions between uniFR and biFR yielded higher $CrossVAF$ values, although the difference between directions remained significant (uniFR to biFR: $p = 0.011$, $|g| = 2.52$; biFR to uniFR: $p = 0.011$, $|g| = 2.23$).

Table 10.1. Cross-Variance Accounted For values averaged across participants ($\boldsymbol{CrossVAF_{avg}}$) for the young group.

$\boldsymbol{CrossVAF_{avg}}$ (%)		Reconstructed		
		YOUNG		
		uniFR	biFR	LR
Extracted	uniFR	97.0 ± 0.2*,†††	90.2 ± 0.9*,#	68.0 ± 1.2†††,#
	biFR	90.6 ± 0.8*,†	96.5 ± 0.4*,###	68.3 ± 2.0†,###
	LR	63.9 ± 2.6†††	62.0 ± 3.3###	96.4 ± 0.6†††,###

$\boldsymbol{CrossVAF_{avg}}$ values averaged across participants obtained when the muscle synergies extracted during a specific reaching condition (i.e., Extracted) are used to reconstruct EMG data acquired during the other reaching conditions (i.e., Reconstructed) in the young group. Statistically significant differences among tasks are indicated as follows: uniFR vs. biFR by asterisks (*p < 0.05); uniFR vs. LR by daggers (†p < 0.05, †††p < 0.001); biFR vs. LR by sharp signs (#p < 0.05, ###p < 0.001).

A comparable trend was observed in the elderly group (**Table 10.2**), where $CrossVAF$ values were significantly lower when uniFR and biFR EMG data were reconstructed from LR-derived synergies (LR to uniFR: $p < 0.001$, $|g| = 3.65$; LR to biFR: $p < 0.001$, $|g| = 4.46$). Similarly, reconstructing LR data from uniFR and biFR synergies resulted in reduced $CrossVAF$ values (uniFR to LR: $p < 0.001$, $|g| = 4.06$; biFR to LR: $p < 0.001$, $|g| = 5.25$), whereas reconstructions between uniFR and biFR again yielded the highest $CrossVAF$ values (uniFR to biFR: $p = 0.011$, $|g| = 4.13$; biFR to uniFR: $p < 0.001$, $|g| = 5.24$).

Table 10.2. Cross-Variance Accounted For values averaged across participants ($\boldsymbol{CrossVAF_{avg}}$) for the elderly group.

$\boldsymbol{CrossVAF_{avg}}$ (%)		Reconstructed		
		ELDERLY		
		uniFR	biFR	LR
Extracted	uniFR	97.1 ± 0.1*,†††	89.0 ± 0.7*,#	76.2 ± 1.7†††,#
	biFR	90.1 ± 0.4*,†††	97.2 ± 0.1*,###	75.8 ± 1.4†††,###
	LR	70.3 ± 2.4†††	66.7 ± 2.2###	96.5 ± 0.3†††,###

$\boldsymbol{CrossVAF_{avg}}$ values averaged across participants obtained when the muscle synergies extracted during a specific reaching condition (i.e., Extracted) are used to reconstruct EMG data acquired during the other reaching conditions (i.e., Reconstructed) in the elderly group. Statistically significant differences among tasks are indicated as follows: uniFR vs. biFR by asterisks (*p < 0.05); uniFR vs. LR by daggers (†††p < 0.001); biFR vs. LR by sharp signs (#p < 0.05, ###p < 0.001).

A notable group difference was observed in the uniFR task for Syn3, demonstrating greater intra-task consistency among elderly participants compared to the younger group ($p < 0.001$, $|g| = 0.63$). In the biFR task, Syn1 showed higher consistency in the younger group ($p < 0.001$, $|g| = 0.64$), while Syn3 exhibited higher consistency in the elderly group ($p < 0.001$, $|g| = 0.65$).

In the LR task, all three synergies (Syn1–3) revealed significantly greater intra-task consistency in elderly participants (Syn1: $p = 0.012$, $|g| = 0.37$; Syn2: $p < 0.001$, $|g| = 0.55$; Syn3: $p < 0.001$, $|g| = 0.57$). No additional significant effects were observed.

Table 10.3. Between-group comparison of intra-task consistency for each task

		Intra-task Consistency					
		uniFR		biFR		LR	
		Young	Elderly	Young	Elderly	Young	Elderly
Synergies	Syn1	0.85 ± 0.006	0.82 ± 0.01	0.88 ± 0.006***	0.80 ± 0.01***	0.57 ± 0.01*	0.62 ± 0.01*
	Syn2	0.80 ± 0.009	0.79 ± 0.009	0.80 ± 0.01	0.81 ± 0.008	0.64 ± 0.01***	0.71 ± 0.01***
	Syn3	0.61 ± 0.02***	0.73 ± 0.02***	0.63 ± 0.01***	0.73 ± 0.01***	0.63 ± 0.01***	0.72 ± 0.01***
	Syn4	/	/	/	/	0.59 ± 0.02	/

Intra-task consistency values compared between young and elderly participants for each task (uniFR, biFR, LR) and muscle synergy (Syn1–Syn3). Statistically significant differences among groups are indicated by asterisks (*p < 0.05, (***p < 0.001).

10.5.4. Synergy-based parameters

The FWHM and RMS of the activation coefficients (C) for each synergy and task are illustrated in **Figure 10.7**. In terms of FWHM, elderly participants demonstrated significantly higher values compared to young adults for C2 and C3 during both the uniFR (C2: p =0.007 , $|g| = 0.98$; C3: $p = 0.039$, $|g| = 0.71$) and biFR (C2: $p < 0.001$, $|g| = 1.62$; C3: $p = 0.019$, $|g| = 0.81$) tasks, as well as for C1 and C2 during the LR task (C1: $p = 0.013$, $|g| = 1.02$; C2: $p = 0.007$, $|g| = 0.98$). Regarding RMS, significant between-group differences were observed in C3 during the uniFR ($p = 0.035$, $|g| = 0.79$) and biFR ($p = 0.009$, $|g| = 0.98$) tasks, along with C1 and C2 in the LR task (C1: $p = 0.029$, $|g| = 0.76$; C2: $p = 0.006$, $|g| = 1.04$) with elderly participants exhibiting greater RMS values.

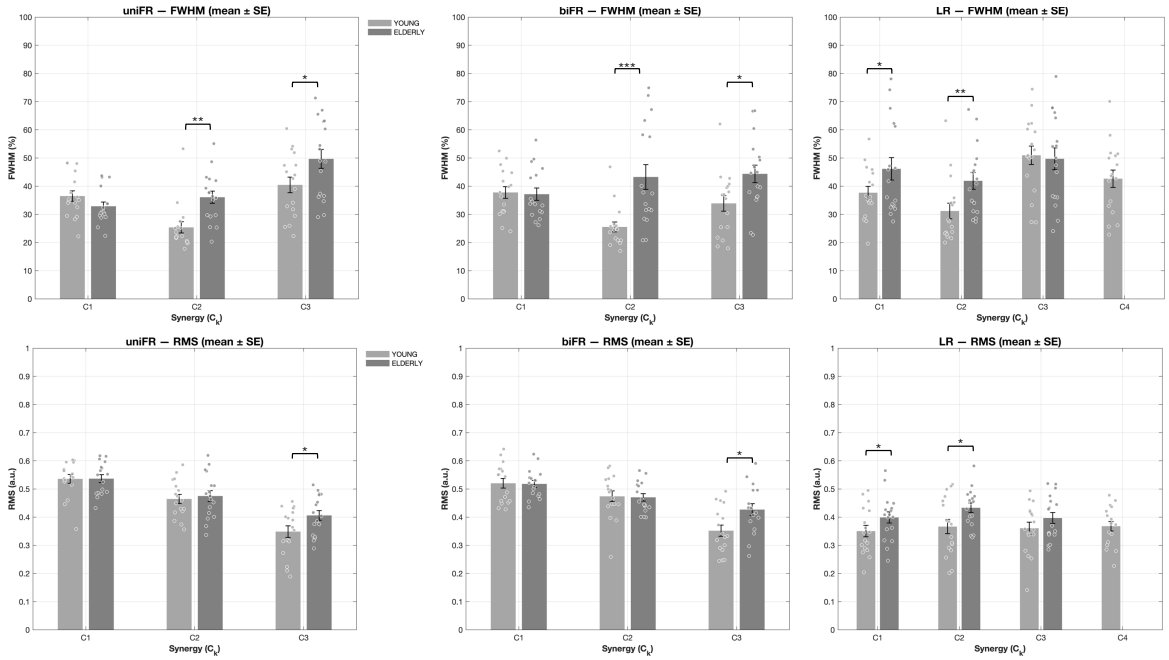

Figure 10.7. Mean ± standard error (SE) values of the full width at half maximum (FWHM) of the activation profiles (top panels) and root mean square (RMS) amplitude (bottom panels) of the synergy activation coefficients (C) for each synergy (C1–C4) and task—unilateral Functional Reach (uniFR), bilateral Functional Reach (biFR), and Lateral Reach (LR)—in young (light grey) and older (dark grey) adults. Individual participant data points are overlaid on the bar plots. Asterisks indicate significant between-group differences (*p < 0.05; **p < 0.01; ***p < 0.001).

10.5.5. Kinematics parameters

Table 10.4 presents the average occurrence of the R1, MD, and R2 events for each task (uniFR, biFR, and LR), expressed as a percentage of the total task duration (0%: start of arm elevation; 100%: end of arm lowering) for both young and elderly groups. Notably, for the R1 event, statistically significant differences were observed between the two groups across all tasks ($p < 0.001$, $|g| = 1.33–1.55$), with the elderly group exhibiting higher values. Similarly, significant differences for the R2 event were found across all tasks, with the young group showing greater values ($p < 0.001$, $|g| = 0.90$ - 1.12 for uniFR and biFR; $p = 0.02$, $|g| = 0.26$ for LR). Furthermore, in the LR task, the MD event also demonstrated a small significant difference between the groups ($p < 0.008$, $|g| = 0.29$), again indicating higher values in the elderly.

Table 10.4. The average percentage of the reaching events for each task within each group.

		Reaching tasks					
		uniFR		biFR		LR	
		Young	Elderly	Young	Elderly	Young	Elderly
Reaching events (%)	R1	18.4 ± 0.8***	24.3 ± 1.0***	18.9 ± 0.6***	23.9 ± 1.2***	21.9 ± 0.8***	27.1 ± 0.9***
	MD	54.8 ± 1.0	55.1 ± 1.2	54.6 ± 1.1	54.1 ± 1.7	53.3 ± 1.2**	56.0 ± 1.0**

	R2	86.5 ± 1.2***	81.8 ± 1.2***	86.0 ± 1.2***	82.0 ± 1.0***	82.3 ± 1.1*	81.6 ± 1.1*

Reaching events expressed as the percentage of the task duration (0%: start of arm elevation; 100%: end of arm lowering) averaged across participants for young and elderly participants. All data are reported as mean ± SE over the sample population. Statistically significant differences among groups for each task and event are indicated by asterisks (*p < 0.05; (**p < 0.01; ***p < 0.001).

Figure 10.8 presents a comparison of the kinematic parameters, D_{max}, PL_{CoM}, and $Displ_{CoM}$, between young and elderly participants across three tasks (uniFR, biFR, and LR). In all tasks, the young group exhibited significantly greater D_{max} compared to the elderly group ($p < 0.001$, $|g| = 0.54 – 1.32$). For the uniFR task, significant differences were also noted for both PL_{CoM} and $Displ_{CoM}$ ($p < 0.001$ for each, $|g| = 0.52$ and $|g| = 0.70$, respectively), with the young group showing higher values. Additionally, in the biFR task, young participants exhibited significant greater $Displ_{CoM}$ ($p = 0.002$, $|g| = 0.34$). Conversely, for the LR task, no significant differences between the groups were found in these two parameters.

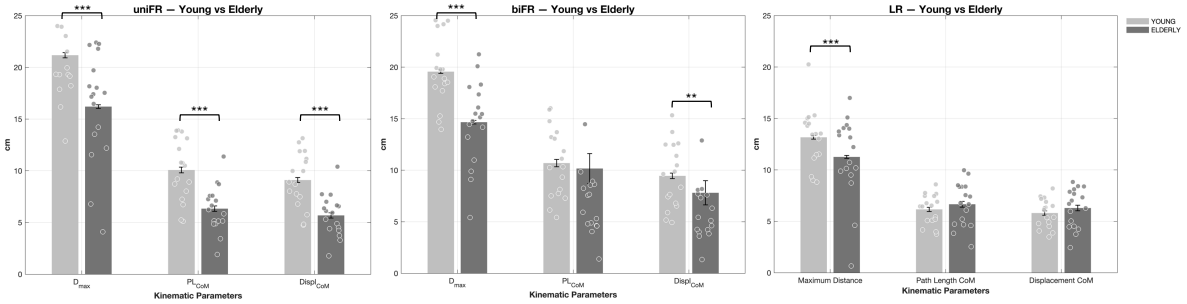

Figure 10.8. Mean (± SE) values of maximum reaching distance ($D_{\max}$), center of mass path length (PL_{CoM}), and center of mass displacement ($Displ_{CoM}$) for each Functional Reach task—unilateral (uniFR), bilateral (biFR), and Lateral (LR)—in young (light grey) and older (dark grey) adults. Individual participant data points are overlaid on the bar plots. Asterisks indicate significant between-group differences (**p < 0.01; ***p < 0.001).

10.6. Discussion

This study explored the impact of aging on the neuromuscular strategies involved in upright reaching across various directions. Both young and older adults carried out the tasks with similarly high EMG reconstruction accuracy from a small set of muscle synergies, indicating that upright reaching relies on a low-dimensional modular organization. Nevertheless, aging introduced selective yet meaningful modifications in how these modules were organized and recruited.

Across all reaching tasks, older adults generally exhibited higher VAF1 values compared to younger participants, suggesting a tendency towards more strongly coupled muscle activation patterns and a reduction in control complexity (Douaud et al., 2014). The elevated VAF1 values observed in older adults across tasks reflect previous findings related to gait and balance-

challenging locomotion, where elderly individuals display higher VAF1 and increased coactivation, while maintaining a similar number of synergies as their younger counterparts (Allen & Franz, 2018; da Silva Costa et al., 2020). However, our findings revealed a statistically significant difference only during the lateral reach, where older adults also demonstrated a reduced number of synergies. This notable reduction in the number of synergies required to reconstruct muscle activation may reflect diminished neuromuscular complexity in motor control (D. J. Clark et al., 2010; Dominici et al., 2011; Roemmich et al., 2014). This outcome contrasts with existing literature on other functional tasks, which indicates that the number of synergies does not change with aging (Allen & Franz, 2018; Baggen et al., 2020; Monaco et al., 2010). The combination of higher VAF1 and reduced modular dimensionality indicates a clear task-dependent simplification of neuromuscular control with age, particularly when postural demands increase in the mediolateral direction. Conversely, during forward reaches, either unilateral or bilateral, the number of synergies was comparable between groups, implying that aging did not alter the fundamental modular structure when the movement required primarily anterior–posterior control.

Synergy composition analyses further confirmed that the spatial organization of muscle synergies was highly comparable between groups in the forward-reaching tasks. As demonstrated in our previous study on young adults (Ceriello et al., 2025), these synergies represent well-defined biomechanical functions: the first synergy facilitates the transition from a quiet stance to a forward lean, the second manages braking and the return-to-upright actions, and the third coordinates both preparatory and final postural adjustments. The preservation of these spatial patterns in older adults indicates that aging does not significantly impact the fundamental coordination structure necessary for anterior–posterior reaching. On the contrary, the lateral reach task revealed a more significant reorganization of synergy structure in older adults. In young adults, this task typically engages four functionally distinct modules: the first synergy stabilizes the non-dominant side during an ipsilateral weight shift, the second supports trunk and hip control to counteract lateral leaning, the third provides contralateral ankle-driven postural adjustments during both the initiation and recovery phases, and the fourth is responsible for dominant-side arm elevation and trunk stabilization (Ceriello et al., 2025). In older adults, however, these biomechanical roles were not represented by separate, specialized synergies. Rather, the first synergy combined stabilizing functions that, in young adults, were divided between the non-dominant support synergy and the dominant arm/trunk synergy. Additionally, in older participants, the second synergy exhibited broader and less

selective coactivation. This reorganization indicates a loss of functional segregation among synergies and suggests that older adults rely on fewer, more generalized coordination patterns to meet the challenges of lateral reaching. This trend aligns with the increased coactivation often observed in older adults during gait, static standing, and dynamic postural control (Lo et al., 2017; Nagai et al., 2011; Peterson & Martin, 2010; Y. Wang et al., 2017), reflecting a compensatory stiffening strategy that may enhance stability, but potentially reduce adaptability and efficiency. Together, these findings indicate that our initial hypothesis of preserved spatial modularity holds for forward reaching but does not extend to the lateral reaching task. The lateral condition revealed a distinct reorganization of synergy composition in older adults, characterized by reduced dimensionality and merging of biomechanical functions, representing a deeper compensatory adjustment that emerges specifically when mediolateral stability is challenged.

Cross-reconstruction analyses further supported this interpretation. In both age groups, the similarity of synergistic patterns was highest for forward-reaching tasks and lowest for the combination of forward and lateral reaching. This confirms that task specificity, characterized by the distinction between anterior–posterior and mediolateral control, is maintained in older adults. These findings align with our earlier research on younger individuals (Ceriello et al., 2025), suggesting that the directional tuning of motor modules remains intact in older adults, despite a reduction in neuromuscular complexity within tasks. Consistency analyses revealed additional age-related adaptations. In forward-reaching tasks, differences between the groups were specific to certain synergies; however, the most pronounced differences emerged in lateral reaching, where all three synergies demonstrated significantly greater consistency in older adults. Given the reduction in the number of synergies and the evidence of merging in this task, the increased consistency likely indicates reduced variability, resulting from a more constrained modular organization. Consequently, older adults seem to rely on more stereotyped and less flexible coordination patterns when mediolateral balance demands increase.

Temporal features of synergy activation reinforced this interpretation and supported our hypothesis of age-related temporal adaptations. In the forward-reaching tasks, older adults exhibited significantly higher FWHM and RMS values, indicating prolonged and intensified activation during both the braking/return-to-upright phase and preparatory/final postural adjustments. In the lateral reach, these temporal differences were even more pronounced, with the first two synergies presenting substantially higher FWHM and RMS values. These extended

and more intense activation patterns align with the merging and widespread coactivation observed in the spatial domain, suggesting that older adults compensate for diminished neuromuscular precision by extending stabilizing actions. Comparable changes in timing toward extended or anticipatory synergy activation have been observed in other functional tasks in the literature, including sit-to-stand movements and walking. This indicates a redistribution of effort to maintain stability and safety in the face of reduced neuromuscular efficiency (Allen & Franz, 2018; Guo et al., 2022; Santuz et al., 2022; Yang et al., 2017b).

A complementary perspective on these temporal adaptations arises from the timing of the main movement events. Across all tasks, older adults exhibited a delayed onset of the R1 event (onset of reaching) within the task cycle, indicating a slower transition from quiet stance into movement initiation. In the lateral reach, the MD event (maximum distance) was also slightly delayed, suggesting a modest slowing in the progression of the task under higher postural demands. Conversely, the R2 event (start of the return phase) took place earlier for the elderly participants, indicating an anticipatory shift towards re-establishing stability. These alterations in R1, MD, and R2 correspond with the broader temporal dispersion observed in synergy activations, reinforcing the interpretation of a reorganized reach–return timing that aims to maintain stability.

Kinematic results further complement the neuromuscular findings. Across all tasks, older adults reached shorter distances and displayed reduced CoM excursions in forward reaching. This aligns with previous studies on Functional Reach, which indicate that elderly individuals prioritize postural safety over maximal reach amplitude (DeWaard et al., 2002). Interestingly, CoM displacement did not vary between the groups during lateral reaching, suggesting that older adults achieved similar movement amplitudes but at a higher neuromuscular "cost." This was evident through broader activation patterns and reduced modular complexity. Such a dissociation between maintained kinematic performance and increased neuromuscular effort highlights the compensatory strategies that often emerge with aging.

Supporting our findings, substantial evidence indicates that mediolateral stability is particularly susceptible to age-related decline. Older adults show a diminished capacity to actively control CoM displacement in the frontal plane (Cofré Lizama et al., 2014), a movement direction that relies heavily on coordinated hip and trunk actions as well as rapid sensory reweighting. Notably, impairments in mediolateral balance have emerged as one of the strongest predictors of future falls in older adults (S. G. Brauer et al., 2000; Hilliard et al., 2008; Lord et al., 1999; Tinetti et al., 1988).

Several limitations must be acknowledged. While synergy analyses offer valuable insights into neuromuscular coordination, they fail to encompass the full range of motor strategies. Specifically, this study did not investigate detailed kinematics or center of pressure strategies, which could provide further insights into age-related compensations. Future research that integrates joint kinematics, or center of pressure trajectories could yield a more comprehensive understanding of how aging influences movement execution and how the mechanical demands of balance relate to the neural control of muscle activation. Additionally, although the selected muscle set included key contributors to lower-limb and trunk stability, it did not account for all muscles involved in mediolateral control, such as the hip abductors and adductors. Expanding the muscle set could uncover additional patterns within the synergy organization. It should also be noted that temporal normalization was performed over the entire task duration, and R1, MD, and R2 were treated as discrete kinematic events rather than extended movement phases; therefore, potential differences in the relative duration of these events across groups were not explicitly accounted for in the temporal analysis of synergy activation. A phase-based time normalization could be considered in future studies to enable phase-specific comparisons of synergy timing when interpreting age-related differences. Lastly, the sample comprised healthy, high-functioning older adults, which may lead to an underestimation of neuromuscular adaptations in frail individuals or those with clinical pathologies. Future studies should expand this methodology to include older adults with impaired balance control. Analyzing both fallers and non-fallers could assist in identifying whether the compensatory characteristics observed here are effective adjustments or early signs of instability. Long-term studies could provide additional insights into whether specific rehabilitation or balance training can enhance the timing of synergy recruitment and improve postural stability among older individuals.

In conclusion, while evidence of age-related changes in muscle synergies during everyday movements is still limited, this study offers a direction-specific perspective on how aging influences neuromuscular control during upright reaching. In the context of forward reaching, aging was linked to prolonged and stronger activation of stabilizing synergies, which was accompanied by reduced reaching distances and smaller CoM excursions. This close relationship between temporal changes and kinematic constraints suggests that older adults cope with forward perturbations by extending the duration of stabilizing actions, adopting a more conservative strategy, despite maintaining a preserved modular structure. Conversely, the lateral reaching task revealed a different age-related pattern. Although older adults reached shorter distances, their CoM displacements were comparable to those of younger adults;

however, this was achieved by relying on fewer, less functionally distinct synergies, alongside a significant increase in coactivation and prolonged activation. This dissociation between maintained mediolateral CoM excursions and increased neuromuscular effort reflects the known vulnerability of mediolateral balance control in aging and underscores the substantial compensatory adjustments necessary to stabilize movements in the frontal plane.

10. Study VI: Characterization of Kinematic Synergies on Functional Reach Test

Imma Ceriello[2] · Ilaria Bufacchi[1] · Riccardo Borzuola[2] · Valentina Camomilla[2]

[1]Deparment of Industrial, Electronics and Mechanical Engineering, Roma Tre University, Rome, Italy

[2]Laboratory of Bioengineering and Neuromechanics, Department of Movement, Human and Health Sciences, University of Rome "Foro Italico", Rome, Italy

The study presented in this chapter is currently in preparation for submission. It was conducted as part of the Master's thesis of Ilaria Bufacchi and was carried out at the Laboratory of Bioengineering and Neuromechanics, University of Rome "Foro Italico", using data acquired within the present doctoral project.

Author contributions: Imma Ceriello, Riccardo Borzuola, and Valentina Camomilla developed and planned the research; Imma Ceriello and Riccardo Borzuola conducted the experiments; Imma Ceriello and Ilaria Bufacchi analyzed the data; Imma Ceriello, Ilaria Bufacchi, and Valentina Camomilla interpreted the experimental results; Imma Ceriello created the figures. Imma Ceriello and Ilaria Bufacchi drafted the work.

11.1. Rationale and Objectives

Previous work has shown that muscle synergies underlying multidirectional upright reaching tasks are directionally tuned, although some patterns are preserved across different directions (Ceriello et al., 2025) (**Study I**). Expanding on these results, the current research examines the kinematic aspects, exploring whether comparable coordination principles can be detected at the joint motion level.

Objectives: The aim of this study was to characterize the kinematic synergies involved in executing multidirectional upright reaching tasks in healthy young adults. Specifically, the study seeks to:

i. Identify and describe the kinematic synergies and related postural strategies that play a role in maintaining dynamic balance during upright reaching movements.

ii. Compare the extracted synergies across different task directions to determine whether the CNS employs similar coordination modules for performing analogous motor tasks.

11.2. Experimental Procedure

The participants and the experimental design were established based on the framework presented in **Chapter 5**. Data collection took place during the uniFR, biFR, and LR tasks described in **Section 5.3.1**., involving a total of fifteen healthy young adults (9 males and 6 females; average age: 27.5 ± 3.1 years; average height: 1.7 ± 0.1 m; average body mass: 65.7 ± 9.0 kg; consisting of 2 left-handed and 13 right-handed individuals) (see Section 5.2. for eligibility criteria). Kinematic data were recorded according to the method outlined in Section 5.3.4. For the analyses conducted in this research, we focused solely on the kinematic data derived from the Plug-in Gait Full Body (PiG) markerset.

11.3. Data Analysis

11.3.1. Identification of reaching repetitions

The process for identifying the reaching repetitions was carried out as detailed in **Chapter 6, Section 6.3.1**. To accommodate for variations in phase durations among different participants, each repetition was converted to a standardized scale of 100 points. On this scale, 0 signifies the beginning of the arm elevation phase, and 100 signifies the conclusion of the arm lowering phase. Accordingly, the events labelled R1, MD, and R2 were resampled and represented as percentages relative to this normalized time scale, which ranges from 0% (start of the task) to 100% (completion of the task).

11.3.2. Degree of freedom selection and gimbal lock problem

The joints examined in this analysis included the ipsilateral and contralateral shoulders, hips, knees, and ankles, along with the ipsilateral spine, which was treated as equivalent to the contralateral spine. In this context, "ipsilateral" refers to the side executing the movement, while "contralateral" pertains to the opposite side during unilateral actions. The primary focus for the shoulders and spine was their role in upper-body mobility, whereas the other joints were evaluated to assess lower-body function and postural dynamics throughout the activity.
To calculate angular displacement for each joint, YXZ Cardan angles represented the orientation of the distal segment in relation to the proximal segment. These angles were expressed across the three anatomical planes, which included sagittal, frontal, and transverse, as per the established PiG conventions.

Since the computation of Cardan angles can be influenced by axis alignment, Gimbal Lock can occur when one rotation approaches 90 degrees, leading to axis collinearity and a loss of one degree of freedom (Šenk & Chèze, 2006). This issue is less prevalent in lower-limb joints but can affect shoulder rotations, particularly when arm elevation angles approach 90 degrees. To reduce this effect, the standard PiG rotation sequence (YXZ) was replaced with a YZY Euler sequence. This adjustment was made by modifying the relevant .mod file in Vicon BodyBuilder (version 3.6.3). In the YZY sequence, the initial rotation sets the plane of elevation, the second defines arm elevation, and the third indicates internal–external rotation. This revised order yields a more precise depiction of shoulder movements while reducing sensitivity to Gimbal Lock.

From an anatomical and functional standpoint, specific degrees of freedom (DoFs) were chosen for the following analysis. For the shoulders, only the second component of the YZY sequence, which represents arm elevation, was included. In the case of the spine, both the first and second rotations, related to flexion–extension and lateral bending, were incorporated, as these movements contribute to control in the sagittal and frontal planes during forward and lateral reaching tasks. A similar approach was adopted for the hips, while for the knees and ankles, only the angles in the sagittal plane were analyzed due to the movement limitations imposed by the task and the anatomical predominance of flexion and extension in these joints. Accordingly, the analyzed DoFs were:

- Ipsilateral (ISh) and contralateral (CSh) shoulder elevation plane angles.
- Spine (Sp1 and Sp2) in the sagittal and frontal planes, respectively.
- Ipsilateral (IH1 and IH2) and contralateral (CH1 and CH2) hip angles in the sagittal and frontal planes, respectively.
- Ipsilateral (IK1) and contralateral (CK1) knee angles in the sagittal plane.
- Ipsilateral (IA1) and contralateral (CA1) ankle angles in the sagittal plane.

11.3.3. Kinematic synergy analysis

11.3.3.1. Synergy extraction

Kinematic synergies were extracted using the SynergyAnalyzer toolbox (Russo et al., 2024), implemented in MATLAB. This toolbox offers an object-oriented framework for synergy extraction utilizing various decomposition algorithms, including Non-Negative Matrix Factorization (NNMF), Principal Component Analysis (PCA), and Mixed Matrix Factorization (MMF) (Scano et al., 2022). For this analysis, only the PCA-based method was employed to extract kinematic synergies. PCA transforms the original multivariate space of strongly

correlated variables (DoF) into a smaller set of new variables that are uncorrelated. These new variables, called synergies, are linear combinations of the original variables and explain a significant proportion of the variability in the data (Gracia-Ibáñez et al., 2020).

The kinematic dataset was organized in accordance with the toolbox requirements, with each participant's data formatted as a 1 × 10 MATLAB structure, where each element represented one repetition of a given task. Each entry included: (i) the kinematic data matrix featuring the selected DoFs, (ii) task-related metadata (comprising the plane of motion, start and target conditions, and timing of repetitions), and (iii) the corresponding time vector. As noted in the previous section, each repetition was time-normalized to span 0–100% of the task duration, resulting in 101 samples in MATLAB.

For each DoF, joint angular displacements served as input signals. The kinematic data underwent filtering using a second-order zero-lag Butterworth filter with a cutoff frequency of 10 Hz. Repetitions that were part of the same task, start condition, and plane of motion were averaged to create a representative profile for each participant and task.

Synergies were subsequently extracted using PCA applied to the averaged, filtered data matrix (12 DoFs × 101 time points). The cumulative reconstruction quality was evaluated through the coefficient of determination (R^2). R^2 of the original signal was defined as 1 − SSE/SST, where SSE is the sum of the squared residuals and SST is the sum of the squared differences with the mean input vector (d'Avella et al., 2006). The optimal number of synergies (N_{syn}) was determined as the minimum number of components needed to surpass an R^2 threshold of 0.95. To streamline the analyses, an equal number of muscle synergies was considered within each task for all participants. This number was determined based on the rounded average value across participants (Coscia et al., 2014).

11.3.3.2. Synergy sorting

Since synergy extraction was carried out independently for each participant and task, the order of the extracted components was not inherently consistent across conditions. For this reason, the resulting weight vectors W were realigned based on their similarity to a reference set. A *k-means clustering* algorithm was utilized across all subjects and tasks to derive reference weight and corresponding activation profiles. The number of clusters was defined to be equal to N_{syn}, with reference vectors obtained by averaging the vectors within each cluster (Pellegrino et al., 2018). Then, to enhance cosine similarity with the reference set, the individual W vectors were reordered (see **Section 8.3.1, Equation 8.1**). Finally, an average representative set of synergies was created for each task across all participants.

The consistency of kinematic synergies within each task across participants was assessed by evaluating the similarity of the sorted weight vectors (W) through cosine similarity (CS) between each pair of weight vectors (**see Chapter 6, Paragraph 6.3.6, Equation 6.4**).

11.4. Statistical Analysis

The Shapiro–Wilk test was conducted to evaluate the normality of synergy weights (W), the normality of the optimal number of synergies (N_{syn}), and the normality of the consistency. When the data met the normality criteria, repeated-measures ANOVA was utilized to compare synergy weights; if not, the non-parametric Friedman test was used instead. Post hoc analysis utilized the Bonferroni correction for adjustments. All the parameters were expressed as mean ± standard error (SE) over the sample population.

The effect size of statistically significant differences was determined using Hedges' g statistic (Hedges, 1981).

Statistical analyses were performed using MATLAB's Statistical and Machine Learning Toolbox (MATLAB version R2024b, The MathWorks Inc., Natick, Massachusetts, United States).

11.5. Results

On average, two kinematic synergies were sufficient to reconstruct all three tasks (see **Figure 11.1**). Data were accurately reconstructed using 2 ± 0 synergies for both uniFR and biFR, and 1.93 ± 0.02 for LR. No significant difference was found in N_{syn} between tasks.

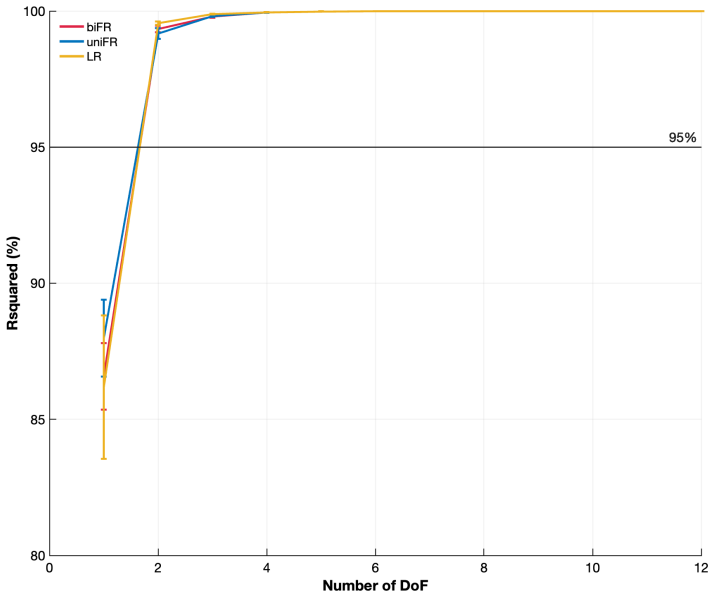

Figure 11.1. Selection of the optimal number of kinematic synergies. Variance explained (R^2, %) as a function of the number of degrees of freedom (DoF) for unilateral Functional Reach (uniFR), bilateral Functional Reach (biFR), and Lateral Reach (LR) tasks.

Curves are shown in blue (uniFR), red (biFR), and yellow (LR). Data are reported as mean ± standard error across participants. The horizontal line indicates the 95% variance-explained threshold used to determine the optimal number of kinematic synergies.

The overall kinematic synergies extracted are shown in **Figure 11.2**. W1 exhibits a positive component of shoulder elevation during LR (ISh), and a positive component of shoulder/s elevation during uniFR (ISh) and biFR (ISh and CSh). In contrast, in W2, the LR is characterized by a positive component in the frontal plane at the spine (Sp2), whereas uniFR and biFR are dominated by components in the sagittal plane at the hips (CH1 and IH1).

Several task-dependent modulations of kinematic synergy weights were observed across the DoFs. For the first synergy (W1), significant differences emerged mainly at the shoulder and trunk levels. The CSh exhibited markedly higher weights in biFR compared to both uniFR ($p = 6.2\times10^{-6}$, $g = 7.19$) and LR ($p = 0.0016$, $g = 6.67$), whereas the lSh showed the opposite trend, with lower weights in biFR relative to uniFR ($p = 8.0\times10^{-5}$, $g = -3.82$) and LR ($p = 0.0016$, $g = -3.28$). At the spine level, Sp2 displayed significantly lower weights in biFR than in LR ($p = 1.5\times10^{-5}$, $g = -2.85$) and in uniFR than in LR ($p = 0.00078$, $g = -2.74$). The CH1 showed higher contribution in biFR compared to LR ($p = 3.5\times10^{-5}$, $g = 2.46$), while the CH2 and IH2 were more involved during LR than biFR ($p = 0.0318$, $g = -1.13$). Finally, the IA1 presented greater weight in biFR compared to LR ($p = 0.0185$, $g = 1.31$). For the second synergy (W2), stronger task-related modulations were evident, involving both upper- and lower-body DoFs. The Sp2 showed substantially lower weights in biFR relative to LR ($p = 3.6\times10^{-7}$, $g = -9.78$) and uniFR–LR ($p = 0.0105$, $g = -8.95$). Similarly, CH2 and IH2 had reduced weights in biFR compared with LR ($p = 1.8\times10^{-4}$, $g = -1.39$ and -1.43, respectively). Conversely, CH1, IH1, and CA1 showed lower weights during LR compared to biFR, with large effect sizes for CH1 ($p = 0.0030$, $g = -6.17$), IH1 ($p = 0.0057$, $g = -4.58$), and CA1 ($p = 0.0105$, $g = -1.82$). Additionally, CH1 ($p = 2.47\text{x}10^{-6}$, $g = -7.69$) and IH1 ($p = 9.56\text{x}10^{-7}$, $g = -5.42$) exhibited reduced weights during LR when compared to uniFR. Finally, the IA1 displayed significantly higher values in biFR ($p = 9.5\times10^{-5}$, $g = 2.06$) and in uniFR ($p = 7.4\times10^{-5}$, $g = 2.03$) compared with LR.

The complete table reporting all pairwise comparisons between DoFs' weights, including *p*-values and Hedges' *g* effect sizes, is provided in **Appendix – Supplementary Materials, Table S11.1**.

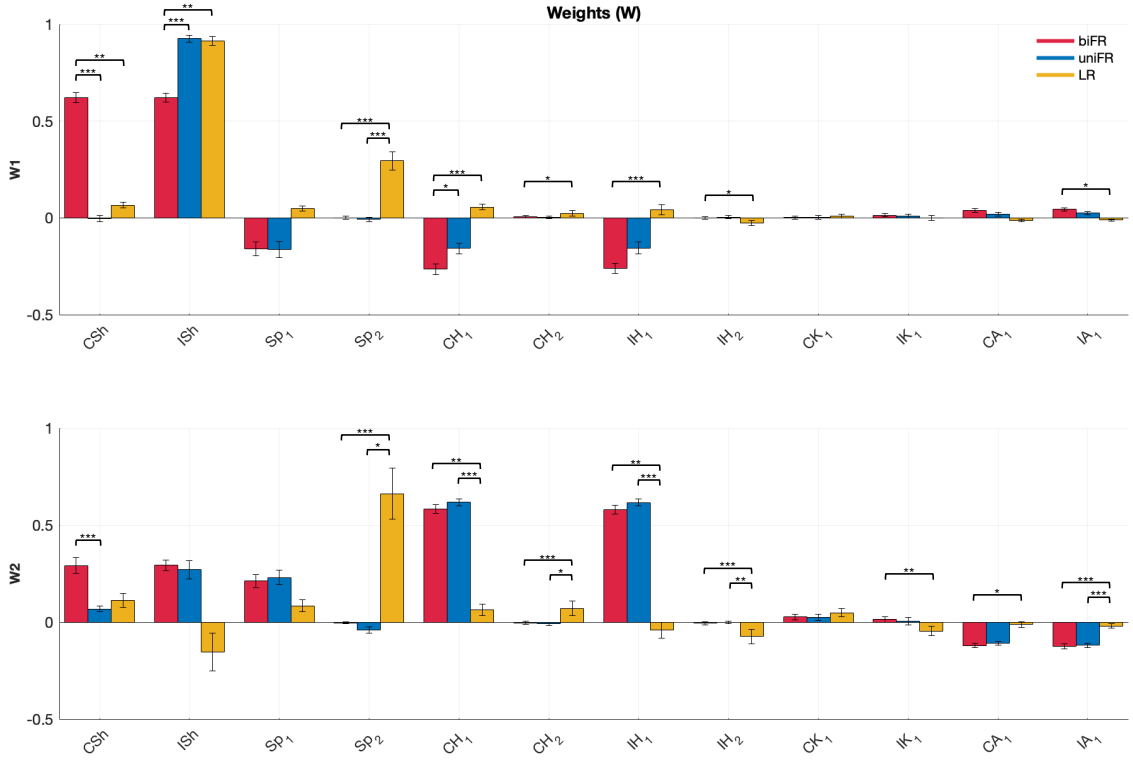

Figure 11.2. Average synergy weights (W) across participants (mean ± standard error) for the kinematic synergies identified during the Functional Reach tasks. Bars are shown for bilateral Functional Reach (biFR, red), unilateral Functional Reach (uniFR, blue), and Lateral Reach (LR, yellow). Each panel corresponds to a different synergy (W1–W2), and bars represent the contribution of individual kinematic variables to the synergy structure. Asterisks indicate significant differences across tasks (*p < 0.05; **p < 0.01; ***p < 0.001).

Figure 11.3 shows the activation profiles of the two kinematic synergies. Vertical dotted lines in the activation profiles plots mark the reaching events (R1, MD, and R2) as averaged across the tasks.

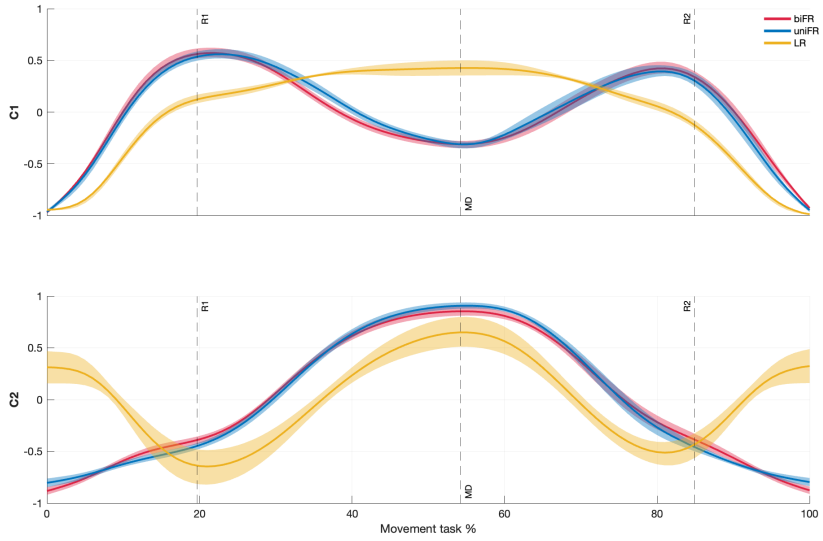

Figure 11.3. Activation profiles (C) of the kinematic synergies (Syn_k) across the movement cycle during the Functional Reach tasks. Top and bottom panels show the activation coefficients for the first and second kinematic synergies (C1 and C2), respectively. Curves represent the mean activation profiles, with shaded areas indicating the standard error across participants. Results are shown for bilateral Functional Reach (biFR, red), unilateral Functional Reach (uniFR, blue), and Lateral Reach (LR, yellow). Vertical dashed lines indicate key phases of the movement cycle (reach initiation, mid-movement, and return).

Figure 11.4 illustrates the CS on W computed for each kinematic synergy across all tasks to assess consistency. Overall, high levels of similarity were observed across participants, indicating that the extracted synergies were stable and representative of common coordination patterns. The only exception was found for the second synergy in the LR task, which showed lower consistency (0.47 ± 0.07).

No significant differences were detected across tasks for the first synergy, confirming that this synergy exhibited a comparable structure among participants in all conditions. In contrast, the second synergy exhibited significant differences between biFR and LR ($p = 1.50\times10^{-7}$, $g = 0.65$) and between uniFR and LR ($p = 3.06\times10^{-8}$, $g = 0.65$), while no significant difference was found between biFR and uniFR ($p = 1$, $g = 0.04$). These findings indicate that the consistency of the second synergy decreased during the LR, suggesting greater inter-individual variability in the organization of movement for this task. A summary table reporting all pairwise comparisons, *p*-values, and Hedges' *g* effect sizes is provided in **Appendix – Supplementary Materials, Table S11.2.**

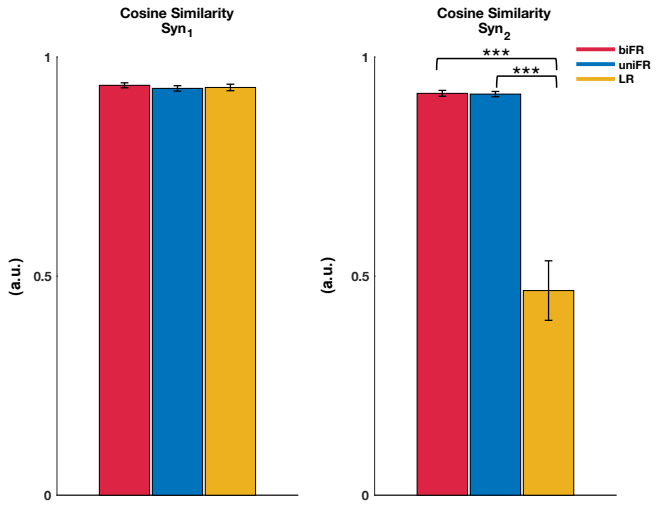

Figure 11.4. Cosine similarity of the synergy weight vectors (W) for each kinematic synergy (Syn1 and Syn2), computed separately for the Functional Reach tasks. Bars represent mean ± standard error of cosine similarity values. Results are shown for bilateral Functional Reach (biFR, red), unilateral Functional Reach (uniFR, blue), and lateral Reach (LR, yellow). Higher values indicate greater similarity between synergy structures across tasks. Asterisks denote significant differences across tasks (***p < 0.001).

11.6. Discussion

The present study explored the kinematic synergies involved in multidirectional upright reaching among healthy young adults, offering a complementary perspective to previous analyses of muscle synergies conducted during the same tasks (Ceriello et al., 2025). By employing PCA on joint angular displacements, two primary kinematic synergies were identified that effectively reconstructed the movements across all conditions, accounting for over 95% of the total variance. One of the main rationales for performing PCA on kinematic data is that the total variance can often be approximated with high accuracy using only a few principal components. PCA has been notably applied in the research of postural control in human movement (Esmaeili et al., 2022; P. Federolf et al., 2013; P. A. Federolf, 2016; Huang et al., 2021a, 2021b; Y.-Y. Tsai et al., 2018; S. Wang et al., 2022; Yamagata et al., 2019). In studies of postural control, applying PCA to kinematic data allows for the decomposition of intricate multi-segment whole-body movements into a set of simpler movement components. Consistent with this framework, our finding suggests that the dimensionality of kinematic coordination during upright reaching is notably low, aligning with the notion that the CNS simplifies motor control by combining multiple degrees of freedom into a limited number of coordinated modules (d'Avella et al., 2003).

Interestingly, when compared to the muscle synergy analysis conducted by Ceriello et al. (2025), notable differences appear in the dimensionality of the synergy set. In that study, three muscle synergies were necessary to reconstruct the forward-reaching tasks, while the lateral task required four. In contrast, the current kinematic analysis showed that only two synergies were sufficient for all tasks, including the lateral reach. This discrepancy suggests that although the neural control of muscle activation may become more complex to address the mechanical demands of balance, the resulting kinematic output remains organized within a lower-dimensional framework. This interpretation is consistent with prior research indicating that kinematic and muscle synergies, while interconnected, do not necessarily possess the same dimensionality or organizational structure (Lambert-Shirzad & Van Der Loos, 2017; Tagliabue et al., 2015). Specifically, the results of our study indicate that W1 primarily captured upper-body modulations, while W2 reflected coordinated adjustments across both trunk and lower-limb segments.

The high cosine similarity observed among participants confirms that the extracted synergies were both stable and representative of shared coordination patterns. The only exception was the second synergy during lateral reach, which exhibited reduced inter-participant similarity.

This finding likely reflects greater variability in the postural strategies adopted (P. Federolf et al., 2013). Therefore, the lower consistency of the second synergy may not signify noise or instability but rather functional flexibility in how different individuals manage balance under challenging conditions. Again, these findings confirm the previous reported in Ceriello et al. (2025), where it was suggested that forward-reaching tasks share a more stable neuromuscular control strategy compared to lateral-reaching movements, which require more adaptive motor patterns, potentially reflecting greater functional complexity.

From a functional perspective, the current findings provide valuable insights into the control of dynamic balance during whole-body reaching. The compact nature of kinematic synergies observed across all tasks indicates that the CNS relies on a limited set of coordination primitives, which are flexibly adjusted to meet both accuracy and stability demands. This efficiency may underlie the capacity to execute voluntary movements without compromising balance. Furthermore, the consistent organization of kinematic synergies across individuals suggests that these coordination modules represent standardized movement patterns, potentially serving as normative templates for evaluating pathological deviations.

These findings have significant implications for both research and rehabilitation. Identifying stable, low-dimensional kinematic synergies could aid in the development of diagnostic and training tools designed to enhance balance control, as deviations from the normative synergy structure may indicate compensatory or dysfunctional strategies. Additionally, synergy-informed models can inform the design of assistive or robotic devices, enabling the implementation of control architectures that replicate natural coordination and joint co-variation during upright movement (Garcia-Rosas et al., 2018; Lapresa et al., 2022).

Several limitations of this study should be acknowledged. A primary methodological limitation of this study pertains to the extraction method utilized for identifying synergies. To facilitate a direct comparison with the findings reported by Ceriello et al. (2025), it is essential to investigate whether the observed differences between muscle and kinematic synergies are influenced by the factorization techniques employed, specifically, NNMF for muscle data versus PCA for kinematic data. Given that these algorithms operate under different mathematical constraints and assumptions, they may produce varying synergy dimensionalities or component structures. Future studies could address this issue by implementing both PCA and NNMF on the same kinematic dataset or by exploring alternative hybrid approaches, such as MMF, to achieve a more comprehensive understanding of the kinematic and muscular synergies. Another limitation is the homogeneity of the sample, which is restricted to young

healthy adults. Future research should examine whether similar kinematic synergy structures are present in older adults. Expanding this approach to elderly populations could help determine whether kinematic synergy analysis can differentiate between age-related changes in balance control or uncover compensatory coordination patterns. Furthermore, the framework utilized in this study could be broadened to include pathological cohorts to evaluate its sensitivity in identifying altered coordination strategies in individuals with compromised postural stability or motor disorders.

In summary, multidirectional upright reaching under the demands of dynamic balance can be effectively represented by two kinematic synergies that encompass components of upper-body and postural control. The structural stability of these synergies across various tasks, combined with their capacity for flexible reweighting, suggests that human upright reaching is governed by a compact yet adaptive coordination architecture. Compared to the higher dimensionality observed in the muscular domain, these results underscore the efficiency of the motor system in producing low-dimensional kinematic outcomes from complex neural control, reinforcing synergy-based models of motor organization and providing translational insights for motor rehabilitation and robotics.

PART III

11. Conclusions and Future Perspectives

12.1. Summary of the findings

Study I: Muscle coordination strategies during Functional Reach across multiple directions in healthy individuals

This study examined the modular organization of muscle activation during multidirectional upright reaching in healthy young adults. Results showed that fewer synergies were required to stabilize the body during anterior–posterior tasks (uniFR and biFR), whereas mediolateral control in the LR task required an additional synergy, reflecting increased postural demands. Despite clear directional tuning of muscle contributions, the same underlying motor functions were consistently recruited across tasks, indicating that similar muscle synergies were flexibly combined to meet different stability requirements. A greater similarity in synergy structure and robustness emerged between uniFR and biFR compared to LR, supporting the presence of a shared neural control strategy for anterior–posterior balance. In contrast, the LR task exhibited higher variability and less standardized recruitment patterns, consistent with the greater

complexity of mediolateral weight shifting. Overall, these findings provide a comprehensive characterization of modular postural control during upright reaching and lay the groundwork for establishing reference datasets of functional tasks in healthy young individuals, enabling future comparisons with aging or clinical populations.

Study II: Task-Dependent Intermuscular Coherence between Postural Muscles during Voluntary Upright Reaching

This study explored how neural synchronization between postural muscles adapts to the directional demands of upright reaching in healthy young adults. Intermuscular coherence revealed a clear task-dependent organization, with forward reaching characterized by strong low-frequency coupling within bilateral and posterior-chain muscles, supporting automatic stabilization along the sagittal plane. In contrast, lateral reaching was associated with more asymmetric coherence patterns, particularly in ankle muscle pairs, reflecting the increased demands of mediolateral control. Specifically, delta-band coherence supported low-frequency coupling for automatic stabilization across both sagittal and lateral postural loads. At the same time, the increase in beta- and low-gamma-band coherence in the synergistic ankle plantar-flexors indicated a corticospinal/transcortical contribution, as expected during unilateral or asymmetric postural conditions. Overall, these results complement the findings of the previous study by reinforcing the link between neural coupling and modular organization during functional reaching.

Study III: Modular Motor Control of the Center of Mass Kinematic Patterns during Sit-to-Stand Tasks

This study examined the bilateral organization of muscle synergies during the STS task in healthy young adults and investigated how these synergies relate to CoM dynamics. A consistent four-synergy structure emerged across participants, each module corresponding to a distinct functional phase of the movement: one managing stable standing, one driving upward propulsion, one coordinating forward transfer of the trunk, and one stabilizing the trunk and arms during the transition to upright posture. These synergies displayed high bilateral symmetry, indicating that STS is supported by a stable and integrated modular architecture across limbs. The synergy–CoM mapping provided a functional interpretation of how each module contributes to the mechanical demands of the task, linking temporal activation to specific portions of the movement. As control complexity increased, activation patterns became more localized and selective, suggesting refined modulation of control without changes to the

underlying modular structure. In other words, the nervous system fine-tunes effort and timing while preserving the same fundamental motor functions. Overall, these findings support the existence of a generalized, side-independent muscle synergy framework for sit-to-stand control in healthy individuals.

Study IV: Age-Dependent Synergistic Control of Sit-to-Stand Motion

This study compared the bilateral organization of muscle synergies and their relationship with CoM dynamics during the STS task in young and older adults. Both groups expressed a consistent four-synergy structure with highly similar spatial patterns, indicating that the fundamental modular architecture supporting STS is preserved with age. Despite this shared structure, older adults exhibited clear temporal adaptations, including earlier and broader recruitment of the synergy responsible for forward trunk motion and momentum transfer. These timing differences suggest compensatory strategies aimed at ensuring stability during the most mechanically demanding phase of the task. The synergy–CoM mapping further highlighted age-related modifications: while vertical CoM control was largely comparable between groups, differences emerged primarily along the anteroposterior axis, where older adults showed less alignment between CoM trajectories and the typical activation regions of the corresponding synergies. This reduced temporal–mechanical coupling indicates that aging may affect the precision with which neuromuscular modules are engaged during forward transfer. Overall, these findings show that although the core modular framework for sit-to-stand control is maintained with age, older adults rely on temporally adjusted, more conservative strategies that reflect a reduced flexibility in coordinating CoM movement during the task.

Study V: Aging Effects on Neuromuscular Coordination during Functional Reaching Movements

This study expands on the analysis of multidirectional upright reaching by comparing the modular organization of muscle activation in young and older adults. Both groups demonstrated a reliance on a low-dimensional synergy structure, confirming that upright reaching retains a fundamental modular framework even with aging. However, aging introduced selective and direction-specific modifications in the organization and recruitment of these modules. Older adults exhibited reduced modular differentiation during lateral reaching, which aligns with increased muscle coactivation and a shift towards more simplified neuromuscular strategies when faced with high mediolateral stability demands. In contrast,

forward reaching was notably preserved, as both young and older adults displayed similar numbers and spatial structures of muscle synergies. Temporal characteristics further underscored age-related adaptations. Older adults showed broader and more prolonged synergy activations across tasks, indicative of compensatory stabilizing actions. These temporal changes were accompanied by modifications in movement execution, resulting in shorter reach distances and reduced CoM excursions during forward reaching. In the lateral direction, older adults achieved comparable CoM displacements but employed a less efficient coordination strategy, suggesting increased neuromuscular effort in response to frontal-plane (biomechanical?) demands. Collectively, these findings indicate that aging reshapes the recruitment and particularly the temporal organization of muscle synergies in a direction-dependent manner, with the most significant adaptations occurring when mediolateral balance is challenged.

Study VI: Characterization of Kinematic Synergies on Functional Reach Test

This study investigated the modular organization of whole-body kinematics during multidirectional upright reaching in healthy young adults, providing a complementary perspective to the muscle synergy findings obtained in the same tasks. Principal component analysis revealed a compact set of two kinematic synergies that consistently reconstructed reaching movements across conditions, indicating that the CNS coordinates posture and action through a low-dimensional set of movement primitives. Synergy patterns were highly consistent across participants. The only exception was the second synergy during lateral reaching, which showed reduced similarity between individuals and likely reflected increased variability in how participants managed the increased mediolateral balance demands. Compared with the higher dimensionality observed in muscle synergies, these findings suggest that although neuromuscular control may involve multiple specialized modules, the resulting whole-body movement is organized within a simpler kinematic framework. Overall, this study demonstrates that dynamic reaching relies on low-dimensional, direction-specific kinematic synergies that align with, yet do not fully mirror, the structure observed at the muscular level, offering a unified yet distinct perspective on modular motor organization.

12.2. Closing marks

The studies presented in this thesis provide a thorough understanding of how the CNS organizes neuromuscular coordination to maintain dynamic balance in both young and older adults. By integrating analyses of muscle synergies, intermuscular coherence, and whole-body

kinematic organization across a range of ecologically relevant, and clinically established, tasks, this research offers a comprehensive overview of the modular, neural, and biomechanical principles that govern postural control during voluntary destabilizing movements. A consistent finding emerged across all tasks and age groups: the spatial structure of motor modules is remarkably stable, suggesting that the central nervous system relies on a preserved repertoire of functional synergies to effectively coordinate movement.

In young adults, both muscle and kinematic data revealed low-dimensional structures capable of reconstructing complex whole-body behaviors using only a small set of modules. Despite variations in task demands, directions, or biomechanical constraints, the spatial structure of muscle synergies and the core components of kinematic coordination remained remarkably consistent. These findings suggest that the CNS relies on a shared repertoire of functional motor building blocks, adjusting their timing, amplitude, and neural coupling to accommodate the specific mechanical requirements of each task. This principle was further reinforced by intermuscular coherence results, which showed that shared neural inputs are systematically reconfigured based on task direction while preserving consistent underlying patterns across synergistic muscles. The convergence of these approaches indicates that modularity is not just an analytical construct but reflects a fundamental aspect of motor organization.

The assessment of older adults offered further insights into how this modular system evolves throughout the lifespan. Our findings suggest that aging did not alter the core synergy structures during upright reaching or sit-to-stand movements, reinforcing the notion that the fundamental repertoire of motor modules remains intact. Instead, age-related changes emerged in the recruitment of these modules: synergy activations became broader, prolonged, and occasionally merged, particularly when mediolateral balance was challenged. These temporal and organizational adaptations, combined with increased coactivation and reduced modular differentiation, indicate a shift toward more conservative and less flexible strategies that elderly use to enhance stability. Notably, these neuromuscular adjustments did not always result in significant differences in whole-body kinematics, suggesting that older adults can maintain functional performance at the expense of greater neuromuscular effort. This dissociation between preserved movement outcomes and altered underlying control strategies offers valuable insights into the compensatory mechanisms characteristic of healthy aging.

A significant conceptual contribution of this thesis is the integration of neural, muscular, and kinematic levels of analysis, demonstrating that balance control emerges from the interaction of multiple interdependent systems. Coherence analysis exposed the neural drives that support

modular muscle activation; synergy extraction revealed how these drives translate into organized patterns of muscle coordination; kinematic synergies and CoM mapping showed how these patterns shape whole-body behavior. The consistency observed across these levels underscores the robustness of modular control, whereas the differences between domains highlight the functional transformations that occur between neural inputs, muscular outputs, and resultant movements.

By establishing baseline synergy and coherence profiles in young adults and characterizing their selective reshaping in older adults, this thesis provides reference frameworks that enhance our understanding of motor control in healthy populations and serve as a foundation for detecting atypical or compensatory coordination patterns. These integrated perspectives clarify why certain tasks, particularly those requiring mediolateral stability, are disproportionately impacted by aging. Furthermore, they illustrate how the nervous system prioritizes safety and stability while maintaining functional performance.

In summary, the collective findings of this thesis demonstrate that dynamic balance during functional tasks is governed by a low-dimensional, robust, and direction-specific modular architecture. This architecture remains largely preserved with age but is adjusted temporally to compensate for reduced neuromuscular precision. Through a combination of neural, muscular, and kinematic analyses, this work advances our understanding of how the CNS organizes movement and postural control, shedding light on the mechanisms through which these processes adapt throughout adulthood and aging.

12.3. Directions for Future Research and Development

Future research should build upon the methodological and conceptual foundations established in this thesis to further illuminate how the neuromuscular system organizes dynamic balance under increasingly realistic and challenging conditions. A natural and essential continuation of this work is the analysis of the Unplanned Functional Reach task, which remains unexplored. Unlike its planned counterpart, unplanned reaching necessitates the rapid integration of sensory cues, immediate decision-making, and the swift modulation of both anticipatory and compensatory mechanisms in response to unexpected changes in task demands. Importantly, this task can be interpreted as an intrinsic sensorimotor perturbation providing an ideal functional framework to investigate how the neuromuscular system adapts to unpredictability. Investigating this task will provide valuable insights into how the CNS reorganizes synergy timing, neural coupling, and biomechanical strategies when confronted with unpredictable postural demands that more accurately reflect everyday scenarios. , extending beyond the

corticospinal output typically captured by muscle synergy analysis. Future work could further extend this approach by incorporating targeted perturbations of specific sensorimotor interaction sites, such as sensory feedback pathways or spinal interneuronal circuits, to more directly probe system compliance and age-related changes.

Another important direction for future research involves extending intermuscular coherence analyses to older adults. The current study has revealed clear, direction-specific patterns of neural synchronization in young adults, demonstrating how various frequency bands contribute to balance control during both forward and lateral movements. However, it remains unclear how aging affects the distribution of shared neural inputs, especially in tasks that require rapid stabilization or involve lateral instability. By expanding coherence analyses to include elderly participants and, ideally, incorporating a broader range of muscles, we can ascertain whether the compensatory strategies seen in their synergy activation patterns are accompanied by changes in cortical and subcortical drives. A particularly promising direction, in this respect, involves the integration of intermuscular coherence with muscle synergy analysis. By combining the functional groupings provided by synergies with coherence-based measures of shared neural input, including coherence network approaches, we could more directly investigate whether muscles working together within a synergy receive common neural drives and how these drives may change with task difficulty or age. In this context, incorporating cortico-muscular coherence measures (EEG–EMG) would provide an additional layer of insight by capturing the contribution of cortical activity to the shared neural drives identified at the muscular level, allowing a more direct assessment of how aging affects central motor pathways during postural control.

Further refinement can be achieved by extending the modular approach to the kinematic domain. Exploring kinematic synergies in older adults and relating them to the muscle synergies identified in this study would enhance our understanding of whether age-related changes in neuromuscular control reflect alterations in motor strategies or different mechanical solutions. This information would shed light on how the CNS balances neural control and biomechanical constraints, and whether the compensations observed in older adults stem from shifts in movement coordination, muscle recruitment, or both.

Beyond these directions, future research should also focus on expanding the investigation to include frail or pathological populations, where deficits in neuromuscular coordination and balance control may uncover unique adaptations or vulnerabilities that are not evident in

healthy individuals. Incorporating such populations would enhance the translational relevance of this work, particularly in the context of fall-risk assessment and rehabilitation.

Overall, these directions outline a coherent pathway for advancing current research, aiming for a more comprehensive characterization of the neural, muscular, and mechanical factors that interact to support dynamic balance across various populations and task demands.

12. Bibliography

Albalwi, A. A., & Alharbi, A. A. (2023). Optimal procedure and characteristics in using five times sit to stand test among older adults: A systematic review. *Medicine*, *102*(26), e34160. https://doi.org/10.1097/MD.0000000000034160

Allen, J. L., & Franz, J. R. (2018). The motor repertoire of older adult fallers may constrain their response to balance perturbations. *Journal of Neurophysiology*, *120*(5), 2368–2378. https://doi.org/10.1152/jn.00302.2018

An, Q., Ikemoto, Y., Asama, H., & The University of Tokyo, 7-3-1 Hongo, Bunkyou-ku, Tokyo 113-8656, Japan. (2013). Muscle Synergy Analysis Between Young and Elderly People in Standing-Up Motion. *Journal of Robotics and Mechatronics*, *25*(6), 1038–1049. https://doi.org/10.20965/jrm.2013.p1038

Aruin, A. S., & Latash, M. L. (1995). The role of motor action in anticipatory postural adjustments studied with self-induced and externally triggered perturbations. *Experimental Brain Research*, *106*(2), 291–300. https://doi.org/10.1007/BF00241125

Baggen, R. J., Van Dieën, J. H., Van Roie, E., Verschueren, S. M., Giarmatzis, G., Delecluse, C., & Dominici, N. (2020). Age-Related Differences in Muscle Synergy

Organization during Step Ascent at Different Heights and Directions. *Applied Sciences*, *10*(6), 1987. https://doi.org/10.3390/app10061987

Baker, M. R., & Baker, S. N. (2003). The effect of diazepam on motor cortical oscillations and corticomuscular coherence studied in man. *The Journal of Physiology*, *546*(Pt 3), 931–942. https://doi.org/10.1113/jphysiol.2002.029553

Baker, S. N., Olivier, E., & Lemon, R. N. (1997). Coherent oscillations in monkey motor cortex and hand muscle EMG show task-dependent modulation. *The Journal of Physiology*, *501*(1), 225–241. https://doi.org/10.1111/j.1469-7793.1997.225bo.x

Banks, C. L., Pai, M. M., McGuirk, T. E., Fregly, B. J., & Patten, C. (2017). Methodological Choices in Muscle Synergy Analysis Impact Differentiation of Physiological Characteristics Following Stroke. *Frontiers in Computational Neuroscience*, *11*, 78. https://doi.org/10.3389/fncom.2017.00078

Baratto, L., Morasso, P. G., Re, C., & Spada, G. (2002). A new look at posturographic analysis in the clinical context: Sway-density versus other parameterization techniques. *Motor Control*, *6*(3), 246–270. https://doi.org/10.1123/mcj.6.3.246

Barroso, F. O., Torricelli, D., Molina-Rueda, F., Alguacil-Diego, I. M., Cano-de-la-Cuerda, R., Santos, C., Moreno, J. C., Miangolarra-Page, J. C., & Pons, J. L. (2017). Combining muscle synergies and biomechanical analysis to assess gait in stroke patients. *Journal of Biomechanics*, *63*, 98–103. https://doi.org/10.1016/j.jbiomech.2017.08.006

Batschelet, E. (with Internet Archive). (1981). *Circular statistics in biology*. London ; New York : Academic Press. http://archive.org/details/circularstatisti0000bats

Bekius, A., Bach, M. M., Van De Pol, L. A., Harlaar, J., Daffertshofer, A., Dominici, N., & Buizer, A. I. (2021). Early Development of Locomotor Patterns and Motor Control in Very Young Children at High Risk of Cerebral Palsy, a Longitudinal Case Series. *Frontiers in Human Neuroscience*, *15*, 659415. https://doi.org/10.3389/fnhum.2021.659415

Belen'kiĭ, V. E., Gurfinkel', V. S., & Pal'tsev, E. I. (1967). [Control elements of voluntary movements]. *Biofizika*, *12*(1), 135–141.

Bellitto, A., De Luca, A., Gamba, S., Losio, L., Massone, A., Casadio, M., & Pierella, C. (2023). Clinical, Kinematic and Muscle Assessment of Bilateral Coordinated Upper-Limb Movements Following Cervical Spinal Cord Injury. *IEEE Transactions on Neural Systems and Rehabilitation Engineering*, *31*, 3607–3618. https://doi.org/10.1109/TNSRE.2023.3309539

Berens, P. (2009). CircStat: A MATLAB Toolbox for Circular Statistics. *Journal of Statistical Software*, *31*, 1–21. https://doi.org/10.18637/jss.v031.i10

Berger, D. J., & d'Avella, A. (2014). Effective force control by muscle synergies. *Frontiers in Computational Neuroscience*, *8*. https://doi.org/10.3389/fncom.2014.00046

Beurskens, R., & Bock, O. (2012). Age-Related Deficits of Dual-Task Walking: A Review. *Neural Plasticity*, *2012*, 131608. https://doi.org/10.1155/2012/131608

Bizzi, E., & Cheung, V. C. K. (2013). The neural origin of muscle synergies. *Frontiers in Computational Neuroscience*, *7*. https://doi.org/10.3389/fncom.2013.00051

Bohannon, R. W., Myers, B. J., Tudini, F. T., Clark, J. T., & Manor, J. P. (2020). Kinematics of shoulder, trunk, pelvis, and hip while reaching forward to progressively distant targets. *Journal of Bodywork and Movement Therapies*, *24*(3), 221–226. https://doi.org/10.1016/j.jbmt.2020.03.003

Boonstra, T. W., & Breakspear, M. (2012). Neural mechanisms of intermuscular coherence: Implications for the rectification of surface electromyography. *Journal of Neurophysiology*, *107*(3), 796–807. https://doi.org/10.1152/jn.00066.2011

Boonstra, T. W., Daffertshofer, A., Roerdink, M., Flipse, I., Groenewoud, K., & Beek, P. J. (2009). Bilateral motor unit synchronization of leg muscles during a simple dynamic balance task. *European Journal of Neuroscience*, *29*(3), 613–622. https://doi.org/10.1111/j.1460-9568.2008.06584.x

Boonstra, T. W., Danna-Dos-Santos, A., Xie, H.-B., Roerdink, M., Stins, J. F., & Breakspear, M. (2015). Muscle networks: Connectivity analysis of EMG activity during postural control. *Scientific Reports*, *5*(1), 17830. https://doi.org/10.1038/srep17830

Borzuola, R., Nuccio, S., Del Vecchio, A., Bazzucchi, I., Felici, F., De Vito, G., & Macaluso, A. (2025). Acute modulation of common synaptic inputs and motor unit discharge rates following neuromuscular electrical stimulation superimposed onto voluntary contractions. *Frontiers in Physiology*, *16*. https://doi.org/10.3389/fphys.2025.1590949

Bouisset, S., & Do, M.-C. (2008). Posture, dynamic stability, and voluntary movement. *Neurophysiologie Clinique/Clinical Neurophysiology*, *38*(6), 345–362. https://doi.org/10.1016/j.neucli.2008.10.001

Bouisset, S., Richardson, J., & Zattara, M. (2000). Do anticipatory postural adjustments occurring in different segments of the postural chain follow the same organisational rule for different task movement velocities, independently of the inertial load value? *Experimental Brain Research*, *132*(1), 79–86. https://doi.org/10.1007/s002219900228

Brauer, S., Burns, Y., & Galley, P. (1999). Lateral reach: A clinical measure of medio-lateral postural stability. *Physiotherapy Research International*, *4*(2), 81–88. https://doi.org/10.1002/pri.155

Brauer, S. G., Burns, Y. R., & Galley, P. (2000). A prospective study of laboratory and clinical measures of postural stability to predict community-dwelling fallers. *The Journals of Gerontology. Series A, Biological Sciences and Medical Sciences*, *55*(8), M469-476. https://doi.org/10.1093/gerona/55.8.m469

Budini, F., McManus, L. M., Berchicci, M., Menotti, F., Macaluso, A., Di Russo, F., Lowery, M. M., & De Vito, G. (2014). Alpha Band Cortico-Muscular Coherence Occurs in Healthy Individuals during Mechanically-Induced Tremor. *PLoS ONE*, *9*(12), e115012. https://doi.org/10.1371/journal.pone.0115012

Carter, G. (1977). Receiver operating characteristics for a linearly thresholded coherence estimation detector. *IEEE Transactions on Acoustics, Speech, and Signal Processing*, *25*(1), 90–92. https://doi.org/10.1109/TASSP.1977.1162898

Caruthers, E. J., Thompson, J. A., Chaudhari, A. M. W., Schmitt, L. C., Best, T. M., Saul, K. R., & Siston, R. A. (2016). Muscle Forces and Their Contributions to Vertical and Horizontal Acceleration of the Center of Mass During Sit-to-Stand Transfer in Young, Healthy Adults. *Journal of Applied Biomechanics*, *32*(5), 487–503. https://doi.org/10.1123/jab.2015-0291

Ceriello, I., Ghislieri, M., Rum, L., Camomilla, V., Macaluso, A., & Borzuola, R. (2025). Muscle coordination strategies during Functional Reach across multiple directions in healthy individuals. *European Journal of Applied Physiology*. https://doi.org/10.1007/s00421-025-05951-7

Charalambous, C. C., Bowden, M. G., Liang, J. N., Kautz, S. A., & Hadjipapas, A. (2024). Alpha and beta/low-gamma frequency bands may have distinct neural origin and function during post-stroke walking. *Experimental Brain Research*, *242*(10), 2309–2327. https://doi.org/10.1007/s00221-024-06906-8

Cheung, V. C. K., d'Avella, A., Tresch, M. C., & Bizzi, E. (2005). Central and Sensory Contributions to the Activation and Organization of Muscle Synergies during Natural Motor Behaviors. *The Journal of Neuroscience*, *25*(27), 6419–6434. https://doi.org/10.1523/JNEUROSCI.4904-04.2005

Chvatal, S. A., & Ting, L. H. (2012). Voluntary and Reactive Recruitment of Locomotor Muscle Synergies during Perturbed Walking. *The Journal of Neuroscience*, *32*(35), 12237–12250. https://doi.org/10.1523/JNEUROSCI.6344-11.2012

Chvatal, S. A., & Ting, L. H. (2013). Common muscle synergies for balance and walking. *Frontiers in Computational Neuroscience*, *7*. https://doi.org/10.3389/fncom.2013.00048

Chvatal, S. A., Torres-Oviedo, G., Safavynia, S. A., & Ting, L. H. (2011). Common muscle synergies for control of center of mass and force in nonstepping and stepping postural behaviors. *Journal of Neurophysiology*, *106*(2), 999–1015. https://doi.org/10.1152/jn.00549.2010

Clark, D. J., Ting, L. H., Zajac, F. E., Neptune, R. R., & Kautz, S. A. (2010). Merging of Healthy Motor Modules Predicts Reduced Locomotor Performance and Muscle Coordination Complexity Post-Stroke. *Journal of Neurophysiology*, *103*(2), 844–857. https://doi.org/10.1152/jn.00825.2009

Clark, S., Iltis, P. W., Anthony, C. J., & Toews, A. (2005). Comparison of Older Adult Performance during the Functional-Reach and Limits-of-Stability Tests. *Journal of Aging and Physical Activity*, *13*(3), 266–275. https://doi.org/10.1123/japa.13.3.266

Cofré Lizama, L. E., Pijnappels, M., Faber, G. H., Reeves, P. N., Verschueren, S. M., & Van Dieën, J. H. (2014). Age Effects on Mediolateral Balance Control. *PLoS ONE*, *9*(10), e110757. https://doi.org/10.1371/journal.pone.0110757

Conway, B. A., Halliday, D. M., Farmer, S. F., Shahani, U., Maas, P., Weir, A. I., & Rosenberg, J. R. (1995). Synchronization between motor cortex and spinal motoneuronal pool during the performance of a maintained motor task in man. *The Journal of Physiology*, *489*(3), 917–924. https://doi.org/10.1113/jphysiol.1995.sp021104

Coscia, M., Cheung, V. C., Tropea, P., Koenig, A., Monaco, V., Bennis, C., Micera, S., & Bonato, P. (2014). The effect of arm weight support on upper limb muscle synergies during reaching movements. *Journal of NeuroEngineering and Rehabilitation*, *11*(1), 22. https://doi.org/10.1186/1743-0003-11-22

Crenna, P., Frigo, C., Massion, J., & Pedotti, A. (1987). Forward and backward axial synergies in man. *Experimental Brain Research*, *65*(3). https://doi.org/10.1007/BF00235977

Criswell, E., & Cram, J. R. (Eds.). (2011). *Cram's introduction to surface electromyography* (2nd ed). Jones and Bartlett.

Csuka, M., & McCarty, D. J. (1985). Simple method for measurement of lower extremity muscle strength. *The American Journal of Medicine*, *78*(1), 77–81. https://doi.org/10.1016/0002-9343(85)90465-6

d'Avella, A., & Bizzi, E. (2005). Shared and specific muscle synergies in natural motor behaviors. *Proceedings of the National Academy of Sciences*, *102*(8), 3076–3081. https://doi.org/10.1073/pnas.0500199102

d'Avella, A., Portone, A., Fernandez, L., & Lacquaniti, F. (2006). Control of Fast-Reaching Movements by Muscle Synergy Combinations. *The Journal of Neuroscience*, *26*(30), 7791–7810. https://doi.org/10.1523/JNEUROSCI.0830-06.2006

d'Avella, A., Saltiel, P., & Bizzi, E. (2003). Combinations of muscle synergies in the construction of a natural motor behavior. *Nature Neuroscience*, *6*(3), 300–308. https://doi.org/10.1038/nn1010

da Silva Costa, A. A., Moraes, R., Hortobágyi, T., & Sawers, A. (2020). Older adults reduce the complexity and efficiency of neuromuscular control to preserve walking balance. *Experimental Gerontology*, *140*, 111050. https://doi.org/10.1016/j.exger.2020.111050

Danion, F., & Latash, M. L. (2011). *Motor Control: Theories, Experiments, and Applications*. Oxford University Press. https://doi.org/10.1093/acprof:oso/9780195395273.001.0001

Danna-Dos-Santos, A., Boonstra, T. W., Degani, A. M., Cardoso, V. S., Magalhaes, A. T., Mochizuki, L., & Leonard, C. T. (2014). Multi-muscle control during bipedal stance: An EMG–EMG analysis approach. *Experimental Brain Research*, *232*(1), 75–87. https://doi.org/10.1007/s00221-013-3721-z

De Luca, C. J., Donald Gilmore, L., Kuznetsov, M., & Roy, S. H. (2010). Filtering the surface EMG signal: Movement artifact and baseline noise contamination. *Journal of Biomechanics*, *43*(8), 1573–1579. https://doi.org/10.1016/j.jbiomech.2010.01.027

De Luca, C. J., & Erim, Z. (1994). Common drive of motor units in regulation of muscle force. *Trends in Neurosciences*, *17*(7), 299–305. https://doi.org/10.1016/0166-2236(94)90064-7

De Marchis, C., Ranaldi, S., Serrao, M., Ranavolo, A., Draicchio, F., Lacquaniti, F., & Conforto, S. (2019a). Modular motor control of the sound limb in gait of people with trans-femoral amputation. *Journal of NeuroEngineering and Rehabilitation*, *16*(1), 132. https://doi.org/10.1186/s12984-019-0616-7

De Marchis, C., Ranaldi, S., Serrao, M., Ranavolo, A., Draicchio, F., Lacquaniti, F., & Conforto, S. (2019b). Modular motor control of the sound limb in gait of people with trans-femoral amputation. *Journal of Neuroengineering and Rehabilitation*, *16*(1), 132. https://doi.org/10.1186/s12984-019-0616-7

De Waroquier-Leroy, L., Bleuse, S., Serafi, R., Watelain, E., Pardessus, V., Tiffreau, A.-V., & Thevenon, A. (2014). The Functional Reach Test: Strategies, performance and the influence of age. *Annals of Physical and Rehabilitation Medicine*, *57*(6–7), 452–464. https://doi.org/10.1016/j.rehab.2014.03.003

Degani, A. M., Leonard, C. T., & Danna-dos-Santos, A. (2017). The use of intermuscular coherence analysis as a novel approach to detect age-related changes on postural muscle synergy. *Neuroscience Letters*, *656*, 108–113. https://doi.org/10.1016/j.neulet.2017.07.032

Degani, A. M., Leonard, C. T., & Danna-dos-Santos, A. (2020). The effects of aging on the distribution and strength of correlated neural inputs to postural muscles during unperturbed bipedal stance. *Experimental Brain Research*, *238*(6), 1537–1553. https://doi.org/10.1007/s00221-020-05837-4

Dehail, P., Bestaven, E., Muller, F., Mallet, A., Robert, B., Bourdel-Marchasson, I., & Petit, J. (2007). Kinematic and electromyographic analysis of rising from a chair during a "Sit-to-Walk" task in elderly subjects: Role of strength. *Clinical Biomechanics*, *22*(10), 1096–1103. https://doi.org/10.1016/j.clinbiomech.2007.07.015

DeWaard, B. P., Bentrup, B. R., Hollman, J. H., & Brasseur, J. E. (2002). Relationship of the Functional Reach and Lateral Reach Tests in Elderly Females: *Journal of Geriatric Physical Therapy*, *25*(3), 4–9. https://doi.org/10.1519/00139143-200225030-00002

Doherty, T. J. (2003). Invited review: Aging and sarcopenia. *Journal of Applied Physiology (Bethesda, Md.: 1985)*, *95*(4), 1717–1727. https://doi.org/10.1152/japplphysiol.00347.2003

Dominici, N., Ivanenko, Y. P., Cappellini, G., d'Avella, A., Mondì, V., Cicchese, M., Fabiano, A., Silei, T., Di Paolo, A., Giannini, C., Poppele, R. E., & Lacquaniti, F. (2011). Locomotor Primitives in Newborn Babies and Their Development. *Science*, *334*(6058), 997–999. https://doi.org/10.1126/science.1210617

Douaud, G., Groves, A. R., Tamnes, C. K., Westlye, L. T., Duff, E. P., Engvig, A., Walhovd, K. B., James, A., Gass, A., Monsch, A. U., Matthews, P. M., Fjell, A. M., Smith, S. M., & Johansen-Berg, H. (2014). A common brain network links development, aging, and vulnerability to disease. *Proceedings of the National Academy of Sciences of the United States of America*, *111*(49), 17648–17653. https://doi.org/10.1073/pnas.1410378111

Duncan, P. W., Studenski, S., Chandler, J., & Prescott, B. (1992). Functional reach: Predictive validity in a sample of elderly male veterans. *Journal of Gerontology*, *47*(3), M93-98. https://doi.org/10.1093/geronj/47.3.m93

Duncan, P. W., Weiner, D. K., Chandler, J., & Studenski, S. (1990). Functional Reach: A New Clinical Measure of Balance. *Journal of Gerontology*, *45*(6), M192–M197. https://doi.org/10.1093/geronj/45.6.M192

Dunsky, A. (2019). The Effect of Balance and Coordination Exercises on Quality of Life in Older Adults: A Mini-Review. *Frontiers in Aging Neuroscience*, *11*, 318. https://doi.org/10.3389/fnagi.2019.00318

Ennis, K., Sizer, P. S., Sargent, E., Brismée, J.-M., Drusch, A., Kapila, J., & Hooper, T. L. (2021). Abdominal bracing changes lower quarter muscle activity but not reach distances during active forward reach on an unstable surface. *Journal of Bodywork and Movement Therapies*, *28*, 391–396. https://doi.org/10.1016/j.jbmt.2021.07.024

Esmaeili, S., Karami, H., Baniasad, M., Shojaeefard, M., & Farahmand, F. (2022). The association between motor modules and movement primitives of gait: A muscle and kinematic synergy study. *Journal of Biomechanics*, *134*, 110997. https://doi.org/10.1016/j.jbiomech.2022.110997

Exell, T., Kerwin, D., Irwin, G., & Gittoes, M. (2011). CALCULATING CENTRE OF PRESSURE FROM MULTIPLE FORCE PLATES FOR KINETIC ANALYSES OF SPRINT RUNNING. *ISBS - Conference Proceedings Archive*. https://ojs.ub.uni-konstanz.de/cpa/article/view/4973

Falaki, A., Cuadra, C., Lewis, M. M., Prado-Rico, J. M., Huang, X., & Latash, M. L. (2023). Multi-muscle synergies in preparation for gait initiation in Parkinson's disease. *Clinical Neurophysiology*, *154*, 12–24. https://doi.org/10.1016/j.clinph.2023.06.022

Farina, D., & Negro, F. (2015). Common synaptic input to motor neurons, motor unit synchronization, and force control. *Exercise and Sport Sciences Reviews*, *43*(1), 23–33. https://doi.org/10.1249/JES.0000000000000032

Farmer, S. F., Bremner, F. D., Halliday, D. M., Rosenberg, J. R., & Stephens, J. A. (1993). The frequency content of common synaptic inputs to motoneurones studied during voluntary isometric contraction in man. *The Journal of Physiology*, *470*(1), 127–155. https://doi.org/10.1113/jphysiol.1993.sp019851

Farmer, S. F., Gibbs, J., Halliday, D. M., Harrison, L. M., James, L. M., Mayston, M. J., & Stephens, J. A. (2007). Changes in EMG coherence between long and short thumb abductor muscles during human development. *The Journal of Physiology*, *579*(2), 389–402. https://doi.org/10.1113/jphysiol.2006.123174

Federolf, P. A. (2016). A novel approach to study human posture control: "Principal movements" obtained from a principal component analysis of kinematic marker data. *Journal of Biomechanics*, *49*(3), 364–370. https://doi.org/10.1016/j.jbiomech.2015.12.030

Federolf, P., Roos, L., & Nigg, B. M. (2013). Analysis of the multi-segmental postural movement strategies utilized in bipedal, tandem and one-leg stance as quantified by a principal component decomposition of marker coordinates. *Journal of Biomechanics*, *46*(15), 2626–2633. https://doi.org/10.1016/j.jbiomech.2013.08.008

Fisher, K. M., Zaaimi, B., Williams, T. L., Baker, S. N., & Baker, M. R. (2012). Beta-band intermuscular coherence: A novel biomarker of upper motor neuron dysfunction in

motor neuron disease. *Brain*, *135*(9), 2849–2864. https://doi.org/10.1093/brain/aws150

Frère, J., & Hug, F. (2012). Between-subject variability of muscle synergies during a complex motor skill. *Frontiers in Computational Neuroscience*, *6*. https://doi.org/10.3389/fncom.2012.00099

Friston, K. J., Holmes, A. P., Worsley, K. J., Poline, J.-P., Frith, C. D., & Frackowiak, R. S. J. (1994). Statistical parametric maps in functional imaging: A general linear approach. *Human Brain Mapping*, *2*(4), 189–210. https://doi.org/10.1002/hbm.460020402

Frykberg, G. E., & Häger, C. K. (2015). Movement analysis of sit-to-stand–research informing clinical practice. *Physical Therapy Reviews*, *20*(3), 156–167.

Galli, M., Cimolin, V., Crivellini, M., & Campanini, I. (2008). Quantitative analysis of sit to stand movement: Experimental set-up definition and application to healthy and hemiplegic adults. *Gait & Posture*, *28*(1), 80–85. https://doi.org/10.1016/j.gaitpost.2007.10.003

García-Massó, X., Pellicer-Chenoll, M., Gonzalez, L. M., & Toca-Herrera, J. L. (2016). The difficulty of the postural control task affects multi-muscle control during quiet standing. *Experimental Brain Research*, *234*(7), 1977–1986. https://doi.org/10.1007/s00221-016-4602-z

Garcia-Rosas, R., Oetomo, D., Manzie, C., Tan, Y., & Choong, A. P. (2018). On the Relationship Between Human Motor Control Performance and Kinematic Synergies

in Upper Limb Prosthetics. *Annual International Conference of the IEEE Engineering in Medicine and Biology Society. IEEE Engineering in Medicine and Biology Society. Annual International Conference*, *2018*, 3194–3197. https://doi.org/10.1109/EMBC.2018.8512992

Geertsen, S. S., Kjær, M., Pedersen, K. K., Petersen, T. H., Perez, M. A., & Nielsen, J. B. (2013). Central common drive to antagonistic ankle muscles in relation to short-term cocontraction training in nondancers and professional ballet dancers. *Journal of Applied Physiology*, *115*(7), 1075–1081. https://doi.org/10.1152/japplphysiol.00707.2012

Ghahramani, M., Rojas, R. F., & Stirling, D. (2022). Chest and pelvis coordination during functional reach test: A possible indication of balance deficiency in older adults. *Journal of Biomechanics*, *141*, 111177. https://doi.org/10.1016/j.jbiomech.2022.111177

Ghislieri, M., Agostini, V., & Knaflitz, M. (2020). Muscle Synergies Extracted Using Principal Activations: Improvement of Robustness and Interpretability. *IEEE Transactions on Neural Systems and Rehabilitation Engineering*, *28*(2), 453–460. https://doi.org/10.1109/TNSRE.2020.2965179

Ghislieri, M., Knaflitz, M., Labanca, L., Barone, G., Bragonzoni, L., Benedetti, M. G., & Agostini, V. (2020). Muscle Synergy Assessment During Single-Leg Stance. *IEEE Transactions on Neural Systems and Rehabilitation Engineering*, *28*(12), 2914–2922. https://doi.org/10.1109/TNSRE.2020.3030847

Ghislieri, M., Lanotte, M., Knaflitz, M., Rizzi, L., & Agostini, V. (2023). Muscle synergies in Parkinson's disease before and after the deep brain stimulation of the bilateral subthalamic nucleus. *Scientific Reports*, *13*(1), 6997. https://doi.org/10.1038/s41598-023-34151-6

Gracia-Ibáñez, V., Sancho-Bru, J. L., Vergara, M., Jarque-Bou, N. J., & Roda-Sales, A. (2020). Sharing of hand kinematic synergies across subjects in daily living activities. *Scientific Reports*, *10*(1), 6116. https://doi.org/10.1038/s41598-020-63092-7

Grinyagin, I. V., Biryukova, E. V., & Maier, M. A. (2005). Kinematic and dynamic synergies of human precision-grip movements. *Journal of Neurophysiology*, *94*(4), 2284–2294. https://doi.org/10.1152/jn.01310.2004

Grosse, P., & Brown, P. (2003). Acoustic startle evokes bilaterally synchronous oscillatory EMG activity in the healthy human. *Journal of Neurophysiology*, *90*(3), 1654–1661. https://doi.org/10.1152/jn.00125.2003

Guo, X., He, B., Lau, K. Y. S., Chan, P. P. K., Liu, R., Xie, J. J., Ha, S. C. W., Chen, C.-Y., Cheing, G. L. Y., Cheung, R. T. H., Chan, R. H. M., & Cheung, V. C. K. (2022). Age-Related Modifications of Muscle Synergies and Their Temporal Activations for Overground Walking. *IEEE Transactions on Neural Systems and Rehabilitation Engineering*, *30*, 2700–2709. https://doi.org/10.1109/TNSRE.2022.3206887

Hagio, S., Fukuda, M., & Kouzaki, M. (2015). Identification of muscle synergies associated with gait transition in humans. *Frontiers in Human Neuroscience*, *9*. https://doi.org/10.3389/fnhum.2015.00048

Halliday, D. M., & Farmer, S. F. (2010). On the need for rectification of surface EMG. *Journal of Neurophysiology*, *103*(6), 3547; author reply 3548-3549. https://doi.org/10.1152/jn.00222.2010

Hanawa, H., Kubota, K., Kokubun, T., Marumo, T., Hoshi, F., Kobayashi, A., & Kanemura, N. (2017). Muscle synergies underlying sit-to-stand tasks in elderly people and their relationship with kinetic characteristics. *Journal of Electromyography and Kinesiology*, *37*, 15–20. https://doi.org/10.1016/j.jelekin.2017.08.004

Hansen, N. L., Hansen, S., Christensen, L. O., Petersen, N. T., & Nielsen, J. B. (2001). Synchronization of lower limb motor unit activity during walking in human subjects. *Journal of Neurophysiology*, *86*(3), 1266–1276. https://doi.org/10.1152/jn.2001.86.3.1266

Hay, L., Bard, C., Fleury, M., & Teasdale, N. (1996). Availability of visual and proprioceptive afferent messages and postural control in elderly adults. *Experimental Brain Research*, *108*(1), 129–139. https://doi.org/10.1007/BF00242910

Hedges, L. V. (1981). Distribution theory for Glass's estimator of effect size and related estimators. *Journal of Educational Statistics*, *6*(2), 107–128. https://doi.org/10.2307/1164588

Hermens, H. J., & Merletti, R. (1996). *European Activities on Surface Electromyography*.

Hilliard, M. J., Martinez, K. M., Janssen, I., Edwards, B., Mille, M.-L., Zhang, Y., & Rogers, M. W. (2008). Lateral balance factors predict future falls in community-living older adults. *Archives of Physical Medicine and Rehabilitation*, *89*(9), 1708–1713. https://doi.org/10.1016/j.apmr.2008.01.023

Hilt, P. M., Delis, I., Pozzo, T., & Berret, B. (2018). Space-by-Time Modular Decomposition Effectively Describes Whole-Body Muscle Activity During Upright Reaching in Various Directions. *Frontiers in Computational Neuroscience*, *12*, 20. https://doi.org/10.3389/fncom.2018.00020

Horak, F. B. (1987). Clinical Measurement of Postural Control in Adults. *Physical Therapy*, *67*(12), 1881–1885. https://doi.org/10.1093/ptj/67.12.1881

Horak, F. B. (2006). Postural orientation and equilibrium: What do we need to know about neural control of balance to prevent falls? *Age and Ageing*, *35*(suppl_2), ii7–ii11. https://doi.org/10.1093/ageing/afl077

Horak, F. B. (2009). Postural Control. In *Encyclopedia of Neuroscience* (pp. 3212–3219). Springer, Berlin, Heidelberg. https://doi.org/10.1007/978-3-540-29678-2_4708

Horak, F. B., Diener, H. C., & Nashner, L. M. (1989). Influence of central set on human postural responses. *Journal of Neurophysiology*, *62*(4), 841–853. https://doi.org/10.1152/jn.1989.62.4.841

Horak, F. B., Henry, S. M., & Shumway-Cook, A. (1997). Postural perturbations: New insights for treatment of balance disorders. *Physical Therapy*, *77*(5), 517–533. https://doi.org/10.1093/ptj/77.5.517

Horak, F. B., & Macpherson, J. M. (2011). Postural Orientation and Equilibrium. In *Comprehensive Physiology* (pp. 255–292). John Wiley & Sons, Ltd. https://doi.org/10.1002/cphy.cp120107

Horak, F. B., & Nashner, L. M. (1986). Central programming of postural movements: Adaptation to altered support-surface configurations. *Journal of Neurophysiology*, *55*(6), 1369–1381.

Horak, F. B., Shupert, C. L., & Mirka, A. (1989). Components of postural dyscontrol in the elderly: A review. *Neurobiology of Aging*, *10*(6), 727–738. https://doi.org/10.1016/0197-4580(89)90010-9

Hortobágyi, T., Zheng, D., Weidner, M., Lambert, N. J., Westbrook, S., & Houmard, J. A. (1995). The influence of aging on muscle strength and muscle fiber characteristics with special reference to eccentric strength. *The Journals of Gerontology. Series A, Biological Sciences and Medical Sciences*, *50*(6), B399-406. https://doi.org/10.1093/gerona/50a.6.b399

Huang, B., Xiong, C., Chen, W., Liang, J., Sun, B.-Y., & Gong, X. (2021a). Common kinematic synergies of various human locomotor behaviours. *Royal Society Open Science*, *8*(4), rsos.210161, 210161. https://doi.org/10.1098/rsos.210161

Huang, B., Xiong, C., Chen, W., Liang, J., Sun, B.-Y., & Gong, X. (2021b). Common kinematic synergies of various human locomotor behaviours. *Royal Society Open Science*, *8*(4), rsos.210161, 210161. https://doi.org/10.1098/rsos.210161

Hufschmidt, A., Dichgans, J., Mauritz, K.-H., & Hufschmidt, M. (1980). Some methods and parameters of body sway quantification and their neurological applications. *Archiv Für Psychiatrie Und Nervenkrankheiten*, *228*(2), 135–150. https://doi.org/10.1007/BF00365601

Hug, F., Turpin, N. A., Guével, A., & Dorel, S. (2010). Is interindividual variability of EMG patterns in trained cyclists related to different muscle synergies? *Journal of Applied Physiology (Bethesda, Md.: 1985)*, *108*(6), 1727–1736. https://doi.org/10.1152/japplphysiol.01305.2009

Hughes, M. A., Weiner, D. K., Schenkman, M. L., Long, R. M., & Studenski, S. A. (1994). Chair rise strategies in the elderly. *Clinical Biomechanics (Bristol, Avon)*, *9*(3), 187–192. https://doi.org/10.1016/0268-0033(94)90020-5

Inkster, L. M., & Eng, J. J. (2004). Postural control during a sit-to-stand task in individuals with mild Parkinson's disease. *Experimental Brain Research*, *154*(1), 33–38. https://doi.org/10.1007/s00221-003-1629-8

Iosa, M., Fusco, A., Morone, G., & Paolucci, S. (2014). Development and decline of upright gait stability. *Frontiers in Aging Neuroscience*, *6*, 14. https://doi.org/10.3389/fnagi.2014.00014

Israely, S., Leisman, G., Machluf, C. C., & Carmeli, E. (2018). Muscle Synergies Control during Hand-Reaching Tasks in Multiple Directions Post-stroke. *Frontiers in Computational Neuroscience*, *12*, 10. https://doi.org/10.3389/fncom.2018.00010

Janssen, W. G. M., Bussmann, H. B. J., & Stam, H. J. (2002). Determinants of the sit-to-stand movement: A review. *Physical Therapy*, *82*(9), 866–879.

Jensen, P., Jensen, N. J., Terkildsen, C. U., Choi, J. T., Nielsen, J. B., & Geertsen, S. S. (2018). Increased central common drive to ankle plantar flexor and dorsiflexor muscles during visually guided gait. *Physiological Reports*, *6*(3), e13598. https://doi.org/10.14814/phy2.13598

Jones, C. J., Rikli, R. E., & Beam, W. C. (1999). A 30-s chair-stand test as a measure of lower body strength in community-residing older adults. *Research Quarterly for Exercise and Sport*, *70*(2), 113–119. https://doi.org/10.1080/02701367.1999.10608028

Kage, H., Okuda, M., Nakamura, I., Kunitsugu, I., Sugiyama, S., & Hobara, T. (2009). Measuring Methods for Functional Reach Test: Comparison of 1-Arm Reach and 2-Arm Reach. *Archives of Physical Medicine and Rehabilitation*, *90*(12), 2103–2107. https://doi.org/10.1016/j.apmr.2009.07.021

Kamen, G., & and De Luca, C. J. (1992). Firing Rate Interactions Among Human Orbicularis Oris Motor Units. *International Journal of Neuroscience*, *64*(1–4), 167–175. https://doi.org/10.3109/00207459209000542

Kandel, E. R., Schwartz, J. H., Jessell, T. M., Siegelbaum, S. A., & Hudspeth, A. J. (2012). *Principles of Neural Science, Fifth Edition*. McGraw Hill Professional.

Kattla, S., & Lowery, M. M. (2010). Fatigue related changes in electromyographic coherence between synergistic hand muscles. *Experimental Brain Research*, *202*(1), 89–99. https://doi.org/10.1007/s00221-009-2110-0

Kenville, R., Maudrich, T., Vidaurre, C., Maudrich, D., Villringer, A., Ragert, P., & Nikulin, V. V. (2020). Intermuscular coherence between homologous muscles during dynamic and static movement periods of bipedal squatting. *Journal of Neurophysiology*, *124*(4), 1045–1055. https://doi.org/10.1152/jn.00231.2020

Kılınç, Ö. O., De Ridder, R., Kılınç, M., & Van Bladel, A. (2023). Trunk and lower extremity biomechanics during sit-to-stand after stroke: A systematic review. *Annals of Physical and Rehabilitation Medicine*, *66*(3), 101676.

Kogami, H., An, Q., Yang, N., Wang, R., Yoshida, K., Hamada, H., Yamakawa, H., Tamura, Y., Shimoda, S., Yamasaki, H., Yokoyama, M., Alnajjar, F., Hattori, N., Takahashi, K., Fujii, T., Otomune, H., Miyai, I., Yamashita, A., & Asama, H. (2021). Analysis of muscle synergy and kinematics in sit-to-stand motion of hemiplegic patients in subacute period. *Advanced Robotics*, *35*(13–14), 867–877. https://doi.org/10.1080/01691864.2021.1928547

Konieczny, M., Domaszewski, P., Skorupska, E., Borysiuk, Z., & Słomka, K. J. (2022). Age-Related Differences in Intermuscular Coherence EMG-EMG of Ankle Joint Antagonist Muscle Activity during Maximal Leaning. *Sensors*, *22*(19), 7527. https://doi.org/10.3390/s22197527

Kozak, K., Ashton-Miller, J. A., & Alexander, N. B. (2003). The effect of age and movement speed on maximum forward reach from an elevated surface: A study in

healthy women. *Clinical Biomechanics*, *18*(3), 190–196. https://doi.org/10.1016/S0268-0033(02)00205-X

Krishnamoorthy, V., Latash, M. L., Scholz, J. P., & Zatsiorsky, V. M. (2003). Muscle synergies during shifts of the center of pressure by standing persons. *Experimental Brain Research*, *152*(3), 281–292. https://doi.org/10.1007/s00221-003-1574-6

Krishnamoorthy, V., Latash, M. L., Scholz, J. P., & Zatsiorsky, V. M. (2004). Muscle modes during shifts of the center of pressure by standing persons: Effect of instability and additional support. *Experimental Brain Research*, *157*(1), 18–31. https://doi.org/10.1007/s00221-003-1812-y

Laine, C. M., & Valero-Cuevas, F. J. (2017). Intermuscular coherence reflects functional coordination. *Journal of Neurophysiology*, *118*(3), 1775–1783. https://doi.org/10.1152/jn.00204.2017

Lambert-Shirzad, N., & Van Der Loos, H. F. M. (2017). On identifying kinematic and muscle synergies: A comparison of matrix factorization methods using experimental data from the healthy population. *Journal of Neurophysiology*, *117*(1), 290–302. https://doi.org/10.1152/jn.00435.2016

Lapresa, M., Zollo, L., & Cordella, F. (2022). A user-friendly automatic toolbox for hand kinematic analysis, clinical assessment and postural synergies extraction. *Frontiers in Bioengineering and Biotechnology*, *10*. https://doi.org/10.3389/fbioe.2022.1010073

Latash, M. L. (1993). *Control of Human Movement*. Human Kinetics Publishers.

Latash, M. L. (2018). Muscle coactivation: Definitions, mechanisms, and functions. *Journal of Neurophysiology*, *120*(1), 88–104. https://doi.org/10.1152/jn.00084.2018

Latash, M. L. (2024). Chapter 2 - Synergic control of movement: From single muscles to the whole body. In M. F. Levin, M. Petrarca, D. Piscitelli, & S. Summa (Eds.), *Progress in Motor Control* (pp. 25–47). Academic Press. https://doi.org/10.1016/B978-0-443-23987-8.00010-9

Latash, M. L., Krishnamoorthy, V., Scholz, J. P., & Zatsiorsky, V. M. (2005). Postural Synergies and Their Development. *Neural Plasticity*, *12*(2–3), 119–130. https://doi.org/10.1155/NP.2005.119

Lee, D. D., & Seung, H. S. (1999). Learning the parts of objects by non-negative matrix factorization. *Nature*, *401*(6755), 788–791. https://doi.org/10.1038/44565

Leo, A., Handjaras, G., Bianchi, M., Marino, H., Gabiccini, M., Guidi, A., Scilingo, E. P., Pietrini, P., Bicchi, A., Santello, M., & Ricciardi, E. (n.d.). A synergy-based hand control is encoded in human motor cortical areas. *eLife*, *5*, e13420. https://doi.org/10.7554/eLife.13420

Leonard, J. A., Brown, R. H., & Stapley, P. J. (2009). Reaching to Multiple Targets When Standing: The Spatial Organization of Feedforward Postural Adjustments. *Journal of Neurophysiology*, *101*(4), 2120–2133. https://doi.org/10.1152/jn.91135.2008

Liao, C.-F., & Lin, S.-I. (2008). Effects of different movement strategies on forward reach distance. *Gait & Posture*, *28*(1), 16–23. https://doi.org/10.1016/j.gaitpost.2007.09.009

Lo, J., Lo, O.-Y., Olson, E. A., Habtemariam, D., Iloputaife, I., Gagnon, M. M., Manor, B., & Lipsitz, L. A. (2017). Functional implications of muscle co-contraction during gait in advanced age. *Gait & Posture*, *53*, 110–114. https://doi.org/10.1016/j.gaitpost.2017.01.010

Loram, I. D. (2015, June 23). *Postural Control and Sensorimotor Integration*. https://www.semanticscholar.org/paper/Postural-Control-and-Sensorimotor-Integration-Loram/8226b359ba414551d0473284306973d8e7f13446

Lord, S. R., Clark, R. D., & Webster, I. W. (1991a). Physiological factors associated with falls in an elderly population. *Journal of the American Geriatrics Society*, *39*(12), 1194–1200. https://doi.org/10.1111/j.1532-5415.1991.tb03574.x

Lord, S. R., Clark, R. D., & Webster, I. W. (1991b). Postural stability and associated physiological factors in a population of aged persons. *Journal of Gerontology*, *46*(3), M69-76. https://doi.org/10.1093/geronj/46.3.m69

Lord, S. R., Rogers, M. W., Howland, A., & Fitzpatrick, R. (1999). Lateral Stability, Sensorimotor Function and Falls in Older People. *Journal of the American Geriatrics Society*, *47*(9), 1077–1081. https://doi.org/10.1111/j.1532-5415.1999.tb05230.x

Lord, S. R., & Ward, J. A. (1994). Age-associated differences in sensori-motor function and balance in community dwelling women. *Age and Ageing*, *23*(6), 452–460.

Lowery, M. M., Myers, L. J., & Erim, Z. (2007). Coherence between motor unit discharges in response to shared neural inputs. *Journal of Neuroscience Methods*, *163*(2), 384–391. https://doi.org/10.1016/j.jneumeth.2007.03.011

Maki, B. E., Holliday, P. J., & Fernie, G. R. (1990). Aging and postural control. A comparison of spontaneous- and induced-sway balance tests. *Journal of the American Geriatrics Society*, *38*(1), 1–9. https://doi.org/10.1111/j.1532-5415.1990.tb01588.x

Maki, B. E., & McIlroy, W. E. (1997). The role of limb movements in maintaining upright stance: The "change-in-support" strategy. *Physical Therapy*, *77*(5), 488–507. https://doi.org/10.1093/ptj/77.5.488

Manchester, D., Woollacott, M., Zederbauer-Hylton, N., & Marin, O. (1989). Visual, vestibular and somatosensory contributions to balance control in the older adult. *Journal of Gerontology*, *44*(4), M118-127. https://doi.org/10.1093/geronj/44.4.m118

Maranesi, E., Di Nardo, F., Rabini, R. A., Ghetti, G. G., Burattini, L., Mercante, O., & Fioretti, S. (2016). Muscle activation patterns related to diabetic neuropathy in elderly subjects: A Functional Reach Test study. *Clinical Biomechanics*, *32*, 236–240. https://doi.org/10.1016/j.clinbiomech.2015.11.005

Maranesi, E., Fioretti, S., Ghetti, G. G., Rabini, R. A., Burattini, L., Mercante, O., & Di Nardo, F. (2016). The surface electromyographic evaluation of the Functional Reach in elderly subjects. *Journal of Electromyography and Kinesiology*, *26*, 102–110. https://doi.org/10.1016/j.jelekin.2015.12.002

Marchesi, G., Ballardini, G., Barone, L., Giannoni, P., Lentino, C., De Luca, A., & Casadio, M. (2021). Modified Functional Reach Test: Upper-Body Kinematics and Muscular Activity in Chronic Stroke Survivors. *Sensors*, *22*(1), 230. https://doi.org/10.3390/s22010230

Martino, G., Ivanenko, Y. P., d'Avella, A., Serrao, M., Ranavolo, A., Draicchio, F., Cappellini, G., Casali, C., & Lacquaniti, F. (2015). Neuromuscular adjustments of gait associated with unstable conditions. *Journal of Neurophysiology*, *114*(5), 2867–2882. https://doi.org/10.1152/jn.00029.2015

Massion, J. (1984). Postural changes accompanying voluntary movements. Normal and pathological aspects. *Human Neurobiology*, *2*(4), 261–267.

Massion, J. (1992). Movement, posture and equilibrium: Interaction and coordination. *Progress in Neurobiology*, *38*(1), 35–56. https://doi.org/10.1016/0301-0082(92)90034-c

Massion, J. (1994). Postural control system. *Current Opinion in Neurobiology*, *4*(6), 877–887. https://doi.org/10.1016/0959-4388(94)90137-6

Mathiyakom, W., McNitt-Gray, J. L., Requejo, P., & Costa, K. (2005). Modifying center of mass trajectory during sit-to-stand tasks redistributes the mechanical demand across the lower extremity joints. *Clinical Biomechanics (Bristol, Avon)*, *20*(1), 105–111. https://doi.org/10.1016/j.clinbiomech.2004.08.005

McAuley, J. H., & Marsden, C. D. (2000). Physiological and pathological tremors and rhythmic central motor control. *Brain*, *123*(8), 1545–1567. https://doi.org/10.1093/brain/123.8.1545

Melzer, I., Benjuya, N., & Kaplanski, J. (2001). Age-related changes of postural control: Effect of cognitive tasks. *Gerontology*, *47*(4), 189–194. https://doi.org/10.1159/000052797

Mochizuki, G., Semmler, J. G., Ivanova, T. D., & Garland, S. J. (2006). Low-frequency common modulation of soleus motor unit discharge is enhanced during postural control in humans. *Experimental Brain Research*, *175*(4), 584–595. https://doi.org/10.1007/s00221-006-0575-7

Monaco, V., Ghionzoli, A., & Micera, S. (2010). Age-Related Modifications of Muscle Synergies and Spinal Cord Activity During Locomotion. *Journal of Neurophysiology*, *104*(4), 2092–2102. https://doi.org/10.1152/jn.00525.2009

Monte, A., Benamati, A., Pavan, A., d'Avella, A., & Bertucco, M. (2024). Muscle synergies for multidirectional isometric force generation during maintenance of upright standing posture. *Experimental Brain Research*, *242*(8), 1881–1902. https://doi.org/10.1007/s00221-024-06866-z

Muceli, S., Boye, A. T., d'Avella, A., & Farina, D. (2010). Identifying Representative Synergy Matrices for Describing Muscular Activation Patterns During Multidirectional Reaching in the Horizontal Plane. *Journal of Neurophysiology*, *103*(3), 1532–1542. https://doi.org/10.1152/jn.00559.2009

Myers, L. J., Erim, Z., & Lowery, M. M. (2004). Time and frequency domain methods for quantifying common modulation of motor unit firing patterns. *Journal of NeuroEngineering and Rehabilitation*, *1*(1), 2. https://doi.org/10.1186/1743-0003-1-2

Myers, L. J., Lowery, M., O'Malley, M., Vaughan, C. L., Heneghan, C., St Clair Gibson, A., Harley, Y. X. R., & Sreenivasan, R. (2003). Rectification and non-linear pre-processing of EMG signals for cortico-muscular analysis. *Journal of Neuroscience Methods*, *124*(2), 157–165. https://doi.org/10.1016/S0165-0270(03)00004-9

Nagai, K., Yamada, M., Uemura, K., Yamada, Y., Ichihashi, N., & Tsuboyama, T. (2011). Differences in muscle coactivation during postural control between healthy older and young adults. *Archives of Gerontology and Geriatrics*, *53*(3), 338–343. https://doi.org/10.1016/j.archger.2011.01.003

Nandi, T., Hortobágyi, T., van Keeken, H. G., Salem, G. J., & Lamoth, C. J. C. (2019). Standing task difficulty related increase in agonist-agonist and agonist-antagonist common inputs are driven by corticospinal and subcortical inputs respectively. *Scientific Reports*, *9*(1), 2439. https://doi.org/10.1038/s41598-019-39197-z

Newton, R. A. (2001). Validity of the Multi-Directional Reach Test: A Practical Measure for Limits of Stability in Older Adults. *The Journals of Gerontology Series A: Biological Sciences and Medical Sciences*, *56*(4), M248–M252. https://doi.org/10.1093/gerona/56.4.M248

Noé, F., García-Massó, X., & Paillard, T. (2017). Inter-joint coordination of posture on a seesaw device. *Journal of Electromyography and Kinesiology*, *34*, 72–79. https://doi.org/10.1016/j.jelekin.2017.04.003

Nojima, I., Suwa, Y., Sugiura, H., Noguchi, T., Tanabe, S., Mima, T., & Watanabe, T. (2020). Smaller muscle mass is associated with increase in EMG–EMG coherence of the leg muscle during unipedal stance in elderly adults. *Human Movement Science*, *71*, 102614. https://doi.org/10.1016/j.humov.2020.102614

Nonaka, H., Mita, K., Watakabe, M., Akataki, K., Suzuki, N., Okuwa, T., & Yabe, K. (2002). Age-related changes in the interactive mobility of the hip and knee joints: A geometrical analysis. *Gait & Posture*, *15*(3), 236–243. https://doi.org/10.1016/S0966-6362(01)00191-6

Obata, H., Abe, M. O., Masani, K., & Nakazawa, K. (2014). Modulation between bilateral legs and within unilateral muscle synergists of postural muscle activity changes with development and aging. *Experimental Brain Research*, *232*(1), 1–11. https://doi.org/10.1007/s00221-013-3702-2

Okada, S., Hirakawa, K., Takada, Y., & Kinoshita, H. (2001). Relationship between fear of falling and balancing ability during abrupt deceleration in aged women having similar habitual physical activities. *European Journal of Applied Physiology*, *85*(6), 501–506. https://doi.org/10.1007/s004210100437

Oliveira, A. S., Gizzi, L., Farina, D., & Kersting, U. G. (2014). Motor modules of human locomotion: Influence of EMG averaging, concatenation, and number of step

cycles. *Frontiers in Human Neuroscience*, *8*, 335. https://doi.org/10.3389/fnhum.2014.00335

Otsu, N. (1979). A Threshold Selection Method from Gray-Level Histograms. *IEEE Transactions on Systems, Man, and Cybernetics*, *9*(1), 62–66. https://doi.org/10.1109/tsmc.1979.4310076

Pai, Y. C., & Rogers, M. W. (1991). Segmental contributions to total body momentum in sit-to-stand. *Medicine and Science in Sports and Exercise*, *23*(2), 225–230.

Pai, Y.-C., Naughton, B., Chang, R., & Rogers, M. (1994). Control of body centre of mass momentum during sit-to-stand among young and elderly adults. *Gait & Posture*, *2*(2), 109–116. https://doi.org/10.1016/0966-6362(94)90100-7

Pai, Y.-C., Yang, F., Wening, J. D., & Pavol, M. J. (2006). Mechanisms of limb collapse following a slip among young and older adults. *Journal of Biomechanics*, *39*(12), 2194–2204. https://doi.org/10.1016/j.jbiomech.2005.07.004

Pale, U., Atzori, M., Müller, H., & Scano, A. (2020). Variability of Muscle Synergies in Hand Grasps: Analysis of Intra- and Inter-Session Data. *Sensors*, *20*(15), Article 15. https://doi.org/10.3390/s20154297

Papa, E., & Cappozzo, A. (2000). Sit-to-stand motor strategies investigated in able-bodied young and elderly subjects. *Journal of Biomechanics*, *33*(9), 1113–1122. https://doi.org/10.1016/S0021-9290(00)00046-4

Papegaaij, S., Taube, W., Baudry, S., Otten, E., & Hortobágyi, T. (2014). Aging causes a reorganization of cortical and spinal control of posture. *Frontiers in Aging Neuroscience*, *6*, 28. https://doi.org/10.3389/fnagi.2014.00028

Pellegrino, L., Coscia, M., & Casadio, M. (2020). Muscle activities in similar arms performing identical tasks reveal the neural basis of muscle synergies. *Experimental Brain Research*, *238*(1), 121–138. https://doi.org/10.1007/s00221-019-05679-9

Pellegrino, L., Coscia, M., Muller, M., Solaro, C., & Casadio, M. (2018). Evaluating upper limb impairments in multiple sclerosis by exposure to different mechanical environments. *Scientific Reports*, *8*(1), 2110. https://doi.org/10.1038/s41598-018-20343-y

Peterka, R. J., & Black, F. O. (1990). Age-related changes in human posture control: Sensory organization tests. *Journal of Vestibular Research: Equilibrium & Orientation*, *1*(1), 73–85.

Peterson, D. S., & Martin, P. E. (2010). Effects of age and walking speed on coactivation and cost of walking in healthy adults. *Gait & Posture*, *31*(3), 355–359. https://doi.org/10.1016/j.gaitpost.2009.12.005

Piano, L., Geri, T., & Testa, M. (2020). Raising and stabilization phase of the sit-to-stand movement better discriminate healthy elderly adults from young subjects: A pilot cross-sectional study. *Archives of Physiotherapy*, *10*, 7. https://doi.org/10.1186/s40945-020-00078-8

Pierella, C., Pellegrino, L., Muller, M., Inglese, M., Solaro, C., Coscia, M., & Casadio, M. (2022). Upper Limb Sensory-Motor Control During Exposure to Different Mechanical Environments in Multiple Sclerosis Subjects With No Clinical Disability. *Frontiers in Neurorobotics*, *16*, 920118. https://doi.org/10.3389/fnbot.2022.920118

Pollock, A. S., Durward, B. R., Rowe, P. J., & Paul, J. P. (2000). What is balance? *Clinical Rehabilitation*, *14*(4), 402–406. https://doi.org/10.1191/0269215500cr342oa

Prochazka, A. (2009). Reflexes. In *Encyclopedia of Neuroscience* (pp. 3400–3403). Springer, Berlin, Heidelberg. https://doi.org/10.1007/978-3-540-29678-2_5005

Ranaldi, S., De Marchis, C., Severini, G., & Conforto, S. (2021). An objective, information-based approach for selecting the number of muscle synergies to be extracted via non-negative matrix factorization. *IEEE Transactions on Neural Systems and Rehabilitation Engineering*, *29*, 2676–2683.

Ranaldi, S., Gizzi, L., Severini, G., & De Marchis, C. (2023). Optimal Identification of Muscle Synergies From Typical Sit-to-Stand Clinical Tests. *IEEE Open Journal of Engineering in Medicine and Biology*, *4*, 31–37. https://doi.org/10.1109/OJEMB.2023.3263123

Ranaldi, S., Gizzi, L., Severini, G., & De Marchis, C. (2024). Synergy-dependent centre-of-mass control strategies during sit-to-stand movements. *IEEE Open Journal of Engineering in Medicine and Biology*.

Ranaldi, S., Gizzi, L., Severini, G., & De Marchis, C. (2025). Synergy-Dependent Center-of-Mass Control Strategies During Sit-to-Stand Movements. *IEEE Open Journal of Engineering in Medicine and Biology*, *6*, 28–34. https://doi.org/10.1109/OJEMB.2024.3454970

Reyes, A., Laine, C. M., Kutch, J. J., & Valero-Cuevas, F. J. (2017). Beta Band Corticomuscular Drive Reflects Muscle Coordination Strategies. *Frontiers in Computational Neuroscience*, *11*. https://doi.org/10.3389/fncom.2017.00017

Rimini, D., Agostini, V., & Knaflitz, M. (2017). Intra-Subject Consistency during Locomotion: Similarity in Shared and Subject-Specific Muscle Synergies. *Frontiers in Human Neuroscience*, *11*, 586. https://doi.org/10.3389/fnhum.2017.00586

Roach, K. E., & Miles, T. P. (1991). Normal hip and knee active range of motion: The relationship to age. *Physical Therapy*, *71*(9), 656–665. https://doi.org/10.1093/ptj/71.9.656

Roebroeck, M. E., Doorenbosch, C. A. M., Harlaar, J., Jacobs, R., & Lankhorst, G. J. (1994). Biomechanics and muscular activity during sit-to-stand transfer. *Clinical Biomechanics*, *9*(4), 235–244. https://doi.org/10.1016/0268-0033(94)90004-3

Roelker, S. A., Koehn, R. R., Caruthers, E. J., Schmitt, L. C., Chaudhari, A. M. W., & Siston, R. A. (2021). Effects of age and knee osteoarthritis on the modular control of walking: A pilot study. *PLOS ONE*, *16*(12), e0261862. https://doi.org/10.1371/journal.pone.0261862

Roemmich, R. T., Fregly, B. J., & Hass, C. J. (2014). Neuromuscular Complexity During Gait is not Responsive to Medication in Persons with Parkinson's Disease. *Annals of Biomedical Engineering*, *42*(9), 1901–1912. https://doi.org/10.1007/s10439-014-1036-2

Rogers, M. W., & Mille, M.-L. (2003). Lateral Stability and Falls in Older People: *Exercise and Sport Sciences Reviews*, *31*(4), 182–187. https://doi.org/10.1097/00003677-200310000-00005

Roh, J., Rymer, W. Z., & Beer, R. F. (2015). Evidence for altered upper extremity muscle synergies in chronic stroke survivors with mild and moderate impairment. *Frontiers in Human Neuroscience*, *9*. https://doi.org/10.3389/fnhum.2015.00006

Roh, J., Rymer, W. Z., Perreault, E. J., Yoo, S. B., & Beer, R. F. (2013). Alterations in upper limb muscle synergy structure in chronic stroke survivors. *Journal of Neurophysiology*, *109*(3), 768–781. https://doi.org/10.1152/jn.00670.2012

Rosenberg, J. R., Amjad, A. M., Breeze, P., Brillinger, D. R., & Halliday, D. M. (1989). The Fourier approach to the identification of functional coupling between neuronal spike trains. *Progress in Biophysics and Molecular Biology*, *53*(1), 1–31. https://doi.org/10.1016/0079-6107(89)90004-7

Row, B. S., & Cavanagh, P. R. (2007). Reaching upward is more challenging to dynamic balance than reaching forward. *Clinical Biomechanics*, *22*(2), 155–164. https://doi.org/10.1016/j.clinbiomech.2006.06.003

Rudolph, K. S., Axe, M. J., & Snyder-Mackler, L. (2000). Dynamic stability after ACL injury: Who can hop? *Knee Surgery, Sports Traumatology, Arthroscopy*, *8*(5), 262–269. https://doi.org/10.1007/s001670000130

Russo, M., Scano, A., Brambilla, C., & d'Avella, A. (2024). SynergyAnalyzer: A Matlab toolbox implementing mixed-matrix factorization to identify kinematic-muscular synergies. *Computer Methods and Programs in Biomedicine*, *251*, 108217. https://doi.org/10.1016/j.cmpb.2024.108217

Sadeh, S., Gobert, D., Shen, K.-H., Foroughi, F., & Hsiao, H.-Y. (2023). Biomechanical and neuromuscular control characteristics of sit-to-stand transfer in young and older adults: A systematic review with implications for balance regulation mechanisms. *Clinical Biomechanics*, *109*, 106068. https://doi.org/10.1016/j.clinbiomech.2023.106068

Saito, H., Yokoyama, H., Sasaki, A., Kato, T., & Nakazawa, K. (2021). Flexible Recruitments of Fundamental Muscle Synergies in the Trunk and Lower Limbs for Highly Variable Movements and Postures. *Sensors*, *21*(18), 6186. https://doi.org/10.3390/s21186186

Saito, H., Yokoyama, H., Sasaki, A., Matsushita, K., & Nakazawa, K. (2023). Variability of trunk muscle synergies underlying the multidirectional movements and stability trunk motor tasks in healthy individuals. *Scientific Reports*, *13*(1), 1193. https://doi.org/10.1038/s41598-023-28467-6

Saito, H., Yokoyama, H., Sasaki, A., & Nakazawa, K. (2023). Muscle synergy patterns as altered coordination strategies in individuals with chronic low back pain: A cross-

sectional study. *Journal of NeuroEngineering and Rehabilitation*, *20*(1), 69. https://doi.org/10.1186/s12984-023-01190-z

Santello, M., Baud-Bovy, G., & Jörntell, H. (2013). Neural bases of hand synergies. *Frontiers in Computational Neuroscience*, *7*, 23. https://doi.org/10.3389/fncom.2013.00023

Santuz, A., Ekizos, A., Janshen, L., Baltzopoulos, V., & Arampatzis, A. (2017). On the Methodological Implications of Extracting Muscle Synergies from Human Locomotion. *International Journal of Neural Systems*, *27*(5), 1750007. https://doi.org/10.1142/S0129065717500071

Santuz, A., Janshen, L., Brüll, L., Munoz-Martel, V., Taborri, J., Rossi, S., & Arampatzis, A. (2022). Sex-specific tuning of modular muscle activation patterns for locomotion in young and older adults. *PloS One*, *17*(6), e0269417. https://doi.org/10.1371/journal.pone.0269417

Scano, A., Chiavenna, A., Malosio, M., Molinari Tosatti, L., & Molteni, F. (2018). Robotic Assistance for Upper Limbs May Induce Slight Changes in Motor Modules Compared With Free Movements in Stroke Survivors: A Cluster-Based Muscle Synergy Analysis. *Frontiers in Human Neuroscience*, *12*. https://doi.org/10.3389/fnhum.2018.00290

Scano, A., Mira, R. M., & d'Avella, A. (2022). Mixed matrix factorization: A novel algorithm for the extraction of kinematic-muscular synergies. *Journal of Neurophysiology*, *127*(2), 529–547. https://doi.org/10.1152/jn.00379.2021

Schenkman, M., Berger, R. A., Riley, P. O., Mann, R. W., & Hodge, W. A. (1990). Whole-body movements during rising to standing from sitting. *Physical Therapy*, *70*(10), 638–648; discussion 648-651. https://doi.org/10.1093/ptj/70.10.638

Šenk, M., & Chèze, L. (2006). Rotation sequence as an important factor in shoulder kinematics. *Clinical Biomechanics*, *21*, S3–S8. https://doi.org/10.1016/j.clinbiomech.2005.09.007

Shirley Ryan Ability Lab. (2013, May 20). *30 Second Sit to Stand Test*. https://www.sralab.org/rehabilitation-measures/30-second-sit-stand-test

Shukla, B., Bassement, J., Vijay, V., Yadav, S., & Hewson, D. (2020). Instrumented Analysis of the Sit-to-Stand Movement for Geriatric Screening: A Systematic Review. *Bioengineering (Basel, Switzerland)*, *7*(4), 139. https://doi.org/10.3390/bioengineering7040139

Shumway-Cook, A., & Woollacott, M. H. (2017). *Motor control: Translating research into clinical practice* (Fifth edition). Wolters Kluwer.

Smith, S. H. L., Reilly, P., & Bull, A. M. J. (2020). A musculoskeletal modelling approach to explain sit-to-stand difficulties in older people due to changes in muscle recruitment and movement strategies. *Journal of Biomechanics*, *98*, 109451. https://doi.org/10.1016/j.jbiomech.2019.109451

Smith, T. M., Hester, G. M., Ha, P. L., Olmos, A. A., Stratton, M. T., VanDusseldorp, T. A., Feito, Y., & Dalton, B. E. (2020). Sit-to-Stand Kinetics and Correlates of

Performance in Young and Older Males. *Archives of Gerontology and Geriatrics*, *91*, 104215. https://doi.org/10.1016/j.archger.2020.104215

Steele, K. M., Rozumalski, A., & Schwartz, M. H. (2015). Muscle synergies and complexity of neuromuscular control during gait in cerebral palsy. *Developmental Medicine & Child Neurology*, *57*(12), 1176–1182. https://doi.org/10.1111/dmcn.12826

Sylos-Labini, F., La Scaleia, V., Cappellini, G., Fabiano, A., Picone, S., Keshishian, E. S., Zhvansky, D. S., Paolillo, P., Solopova, I. A., d'Avella, A., Ivanenko, Y., & Lacquaniti, F. (2020). Distinct locomotor precursors in newborn babies. *Proceedings of the National Academy of Sciences*, *117*(17), 9604–9612. https://doi.org/10.1073/pnas.1920984117

Sylos-Labini, F., La Scaleia, V., d'Avella, A., Pisotta, I., Tamburella, F., Scivoletto, G., Molinari, M., Wang, S., Wang, L., van Asseldonk, E., van der Kooij, H., Hoellinger, T., Cheron, G., Thorsteinsson, F., Ilzkovitz, M., Gancet, J., Hauffe, R., Zanov, F., Lacquaniti, F., & Ivanenko, Y. P. (2014). EMG patterns during assisted walking in the exoskeleton. *Frontiers in Human Neuroscience*, *8*. https://doi.org/10.3389/fnhum.2014.00423

Tagliabue, M., Ciancio, A. L., Brochier, T., Eskiizmirliler, S., & Maier, M. A. (2015). Differences between kinematic synergies and muscle synergies during two-digit grasping. *Frontiers in Human Neuroscience*, *9*. https://doi.org/10.3389/fnhum.2015.00165

Takakusaki, K. (2017). Functional Neuroanatomy for Posture and Gait Control. *Journal of Movement Disorders*, *10*(1), 1–17. https://doi.org/10.14802/jmd.16062

Takasaki, K., Tanino, Y., Yoneda, H., Suzuki, T., Watanabe, M., & Kono, K. (2011). Comparison of Motion Strategies in the Functional Reach Test between Elderly Persons and Young Persons. *Journal of Physical Therapy Science*, *23*(5), 773–776. https://doi.org/10.1589/jpts.23.773

Tang, P.-F., & Woollacott, M. H. (2004). Balance control in older adults. In *Clinical Disorders of Balance, Posture and Gait, 2Ed* (2nd ed.). CRC Press.

Tang, S., Chen, L., Barsotti, M., Hu, L., Li, Y., Wu, X., Bai, L., Frisoli, A., & Hou, W. (2019). Kinematic Synergy of Multi-DoF Movement in Upper Limb and Its Application for Rehabilitation Exoskeleton Motion Planning. *Frontiers in Neurorobotics*, *13*, 99. https://doi.org/10.3389/fnbot.2019.00099

Terry, K., & Griffin, L. (2008). How computational technique and spike train properties affect coherence detection. *Journal of Neuroscience Methods*, *168*(1), 212–223. https://doi.org/10.1016/j.jneumeth.2007.09.014

Thompson, M., & Medley, A. (2007). Forward and Lateral Sitting Functional Reach in Younger, Middle-aged, and Older Adults: *Journal of Geriatric Physical Therapy*, *30*(2), 43–48. https://doi.org/10.1519/00139143-200708000-00002

Tinetti, M. E., Speechley, M., & Ginter, S. F. (1988). Risk Factors for Falls among Elderly Persons Living in the Community. *New England Journal of Medicine*, *319*(26), 1701–1707. https://doi.org/10.1056/NEJM198812293192604

Ting, L. H., & Macpherson, J. M. (2005). A Limited Set of Muscle Synergies for Force Control During a Postural Task. *Journal of Neurophysiology*, *93*(1), 609–613. https://doi.org/10.1152/jn.00681.2004

Ting, L. H., & McKay, J. L. (2007). Neuromechanics of muscle synergies for posture and movement. *Current Opinion in Neurobiology*, *17*(6), 622–628. https://doi.org/10.1016/j.conb.2008.01.002

Torres-Oviedo, G., Macpherson, J. M., & Ting, L. H. (2006). Muscle Synergy Organization Is Robust Across a Variety of Postural Perturbations. *Journal of Neurophysiology*, *96*(3), 1530–1546. https://doi.org/10.1152/jn.00810.2005

Torres-Oviedo, G., & Ting, L. H. (2007). Muscle Synergies Characterizing Human Postural Responses. *Journal of Neurophysiology*, *98*(4), 2144–2156. https://doi.org/10.1152/jn.01360.2006

Torres-Oviedo, G., & Ting, L. H. (2010). Subject-Specific Muscle Synergies in Human Balance Control Are Consistent Across Different Biomechanical Contexts. *Journal of Neurophysiology*, *103*(6), 3084–3098. https://doi.org/10.1152/jn.00960.2009

Torricelli, D., Barroso, F., Coscia, M., Alessandro, C., Lunardini, F., Bravo Esteban, E., & d'Avella, A. (2016). Muscle Synergies in Clinical Practice: Theoretical and Practical Implications. In J. L. Pons, R. Raya, & J. González (Eds.), *Emerging Therapies in Neurorehabilitation II* (Vol. 10, pp. 251–272). Springer International Publishing. https://doi.org/10.1007/978-3-319-24901-8_10

Tresch, M. C., Cheung, V. C. K., & d'Avella, A. (2006). Matrix Factorization Algorithms for the Identification of Muscle Synergies: Evaluation on Simulated and Experimental Data Sets. *Journal of Neurophysiology*, *95*(4), 2199–2212. https://doi.org/10.1152/jn.00222.2005

Tresch, M. C., & Jarc, A. (2009). The case for and against muscle synergies. *Current Opinion in Neurobiology*, *19*(6), 601–607. https://doi.org/10.1016/j.conb.2009.09.002

Trivedi, H., Leonard, J. A., Ting, L. H., & Stapley, P. J. (2010). Postural responses to unexpected perturbations of balance during reaching. *Experimental Brain Research*, *202*(2), 485–491. https://doi.org/10.1007/s00221-009-2135-4

Tsai, Y.-C., Hsieh, L.-F., & Yang, S. (2014). Age-related changes in posture response under a continuous and unexpected perturbation. *Journal of Biomechanics*, *47*(2), 482–490. https://doi.org/10.1016/j.jbiomech.2013.10.047

Tsai, Y.-J., & Lin, S.-I. (2015). Reaching forward: Effects of a preceding task and aging. *AGE*, *37*(1), 1. https://doi.org/10.1007/s11357-014-9739-8

Tsai, Y.-Y., Chang, G.-C., & Hwang, I.-S. (2018). Adaptation of kinematic synergy and postural control to mechanical ankle constraint on an unsteady stance surface. *Human Movement Science*, *60*, 10–17. https://doi.org/10.1016/j.humov.2018.04.010

Tsiouri, C., Amiridis, I. G., Kannas, T., Varvariotis, N., Sahinis, C., Hatzitaki, V., & Enoka, R. M. (2024). EMG coherence of foot and ankle muscles increases with a

postural challenge in men. *Gait & Posture*, *113*, 238–245. https://doi.org/10.1016/j.gaitpost.2024.06.019

Turpin, N. A., Uriac, S., & Dalleau, G. (2021). How to improve the muscle synergy analysis methodology? *European Journal of Applied Physiology*, *121*(4), 1009–1025. https://doi.org/10.1007/s00421-021-04604-9

Turvey, M. T. (1990). Coordination. *American Psychologist*, *45*(8), 938–953. https://doi.org/10.1037/0003-066X.45.8.938

Tyson, S. F., & DeSouza, L. H. (2004). Reliability and validity of functional balance tests post stroke. *Clinical Rehabilitation*, *18*(8), 916–923. https://doi.org/10.1191/0269215504cr821oa

Van Der Kruk, E., Silverman, A. K., Reilly, P., & Bull, A. M. J. (2021). Compensation due to age-related decline in sit-to-stand and sit-to-walk. *Journal of Biomechanics*, *122*, 110411. https://doi.org/10.1016/j.jbiomech.2021.110411

Veale, J. F. (2014). Edinburgh Handedness Inventory – Short Form: A revised version based on confirmatory factor analysis. *Laterality: Asymmetries of Body, Brain and Cognition*, *19*(2), 164–177. https://doi.org/10.1080/1357650X.2013.783045

Volkman, K. G., Stergiou, N., Stuberg, W., Blanke, D., & Stoner, J. (2007). Methods to Improve the Reliability of the Functional Reach Test in Children and Adolescents With Typical Development. *Pediatric Physical Therapy*, *19*(1), 20–27. https://doi.org/10.1097/01.pep.0000247173.14969.5a

Wang, S., Pai, Y.-C., & Bhatt, T. (2022). Kinematic synergies in over-ground slip recovery outcomes: Distinct strategies or a single strategy? *Gait & Posture*, *95*, 270–276. https://doi.org/10.1016/j.gaitpost.2021.01.025

Wang, Y., Watanabe, K., & Asaka, T. (2017). Aging effect on muscle synergies in stepping forth during a forward perturbation. *European Journal of Applied Physiology*, *117*(1), 201–211. https://doi.org/10.1007/s00421-016-3514-8

Ward, N. J., Farmer, S. F., Berthouze, L., & Halliday, D. M. (2013). Rectification of EMG in low force contractions improves detection of motor unit coherence in the beta-frequency band. *Journal of Neurophysiology*, *110*(8), 1744–1750. https://doi.org/10.1152/jn.00296.2013

Watanabe, T., Saito, K., Ishida, K., Tanabe, S., & Nojima, I. (2018a). Age-Related Declines in the Ability to Modulate Common Input to Bilateral and Unilateral Plantar Flexors During Forward Postural Lean. *Frontiers in Human Neuroscience*, *12*, 254. https://doi.org/10.3389/fnhum.2018.00254

Watanabe, T., Saito, K., Ishida, K., Tanabe, S., & Nojima, I. (2018b). Coordination of plantar flexor muscles during bipedal and unipedal stances in young and elderly adults. *Experimental Brain Research*, *236*(5), 1229–1239. https://doi.org/10.1007/s00221-018-5217-3

Weiner, D. K., Duncan, P. W., Chandler, J., & Studenski, S. A. (1992). Functional Reach: A Marker of Physical Frailty. *Journal of the American Geriatrics Society*, *40*(3), 203–207. https://doi.org/10.1111/j.1532-5415.1992.tb02068.x

Welch, P. (1967). The use of fast Fourier transform for the estimation of power spectra: A method based on time averaging over short, modified periodograms. *IEEE Transactions on Audio and Electroacoustics*, *15*(2), 70–73. https://doi.org/10.1109/TAU.1967.1161901

Welniarz, Q., Dusart, I., & Roze, E. (2017). The corticospinal tract: Evolution, development, and human disorders. *Developmental Neurobiology*, *77*(7), 810–829. https://doi.org/10.1002/dneu.22455

Wernick-Robinson, M., Krebs, D. E., & Giorgetti, M. M. (1999). Functional reach: Does it really measure dynamic balance? *Archives of Physical Medicine and Rehabilitation*, *80*(3), 262–269. https://doi.org/10.1016/S0003-9993(99)90136-3

Winter, D. (1995). Human balance and posture control during standing and walking. *Gait & Posture*, *3*(4), 193–214. https://doi.org/10.1016/0966-6362(96)82849-9

Winter, D. A., Prince, F., Frank, J. S., Powell, C., & Zabjek, K. F. (1996). Unified theory regarding A/P and M/L balance in quiet stance. *Journal of Neurophysiology*, *75*(6), 2334–2343. https://doi.org/10.1152/jn.1996.75.6.2334

Woollacott, M. H., Shumway-Cook, A., & Nashner, L. M. (1986). Aging and posture control: Changes in sensory organization and muscular coordination. *International Journal of Aging & Human Development*, *23*(2), 97–114. https://doi.org/10.2190/VXN3-N3RT-54JB-X16X

World Medical Association. (2025). World Medical Association Declaration of Helsinki: Ethical Principles for Medical Research Involving Human Participants. *JAMA*, *333*(1), 71–74. https://doi.org/10.1001/jama.2024.21972

Xiong, Q., Liu, Y., Mo, J., Chen, Y., Zhang, L., Xia, Z., Yi, C., Jiang, S., & Xiao, N. (2023). Gait asymmetry in children with Duchenne muscular dystrophy: Evaluated through kinematic synergies and muscle synergies of lower limbs. *Biomedical Engineering Online*, *22*(1), 75. https://doi.org/10.1186/s12938-023-01134-7

Xiong, Q., Wan, J., Jiang, S., & Liu, Y. (2022). Age-related differences in gait symmetry obtained from kinematic synergies and muscle synergies of lower limbs during childhood. *BioMedical Engineering OnLine*, *21*(1), 61. https://doi.org/10.1186/s12938-022-01034-2

Yamagata, M., Tateuchi, H., Pataky, T., Shimizu, I., & Ichihashi, N. (2021). Relation between frontal plane center of mass position stability and foot elevation during obstacle crossing. *Journal of Biomechanics*, *116*, 110219. https://doi.org/10.1016/j.jbiomech.2020.110219

Yamagata, M., Tateuchi, H., Shimizu, I., & Ichihashi, N. (2019). The effects of fall history on kinematic synergy during walking. *Journal of Biomechanics*, *82*, 204–210. https://doi.org/10.1016/j.jbiomech.2018.10.032

Yamanaka, E., Horiuchi, Y., & Nojima, I. (2023). EMG-EMG coherence during voluntary control of human standing tasks: A systematic scoping review. *Frontiers in Neuroscience*, *17*, 1145751. https://doi.org/10.3389/fnins.2023.1145751

Yang, N., An, Q., Kogami, H., Yamakawa, H., Tamura, Y., Takahashi, K., Kinomoto, M., Yamasaki, H., Itkonen, M., Shibata-Alnajjar, F., Shimoda, S., Hattori, N., Fujii, T., Otomune, H., Miyai, I., Yamashita, A., & Asama, H. (2019). Temporal Features of Muscle Synergies in Sit-to-Stand Motion Reflect the Motor Impairment of Post-Stroke Patients. *IEEE Transactions on Neural Systems and Rehabilitation Engineering*, *27*(10), 2118–2127. https://doi.org/10.1109/tnsre.2019.2939193

Yang, N., An, Q., Yamakawa, H., Tamura, Y., Yamashita, A., & Asama, H. (2017). Muscle synergy structure using different strategies in human standing-up motion. *Advanced Robotics*, *31*(1–2), 40–54. https://doi.org/10.1080/01691864.2016.1238781

Yang, N., An, Q., Yamakawa, H., Tamura, Y., Yamashita, A., Takahashi, K., Kinomoto, M., Yamasaki, H., Itkonen, M., Alnajjar, F. S., Shimoda, S., Asama, H., Hattori, N., & Miyai, I. (2017a). Clarification of muscle synergy structure during standing-up motion of healthy young, elderly and post-stroke patients. *IEEE ... International Conference on Rehabilitation Robotics: [Proceedings]*, *2017*, 19–24. https://doi.org/10.1109/ICORR.2017.8009215

Yang, N., An, Q., Yamakawa, H., Tamura, Y., Yamashita, A., Takahashi, K., Kinomoto, M., Yamasaki, H., Itkonen, M., Alnajjar, F. S., Shimoda, S., Asama, H., Hattori, N., & Miyai, I. (2017b). Clarification of muscle synergy structure during standing-up motion of healthy young, elderly and post-stroke patients. *2017 International Conference on Rehabilitation Robotics (ICORR)*, 19–24. https://doi.org/10.1109/ICORR.2017.8009215

Yokoyama, H., Kato, T., Kaneko, N., Kobayashi, H., Hoshino, M., Kokubun, T., & Nakazawa, K. (2021). Basic locomotor muscle synergies used in land walking are finely tuned during underwater walking. *Scientific Reports*, *11*(1), 18480. https://doi.org/10.1038/s41598-021-98022-8

Yoshida, K., An, Q., Yozu, A., Chiba, R., Takakusaki, K., Yamakawa, H., Tamura, Y., Yamashita, A., & Asama, H. (2019). Visual and Vestibular Inputs Affect Muscle Synergies Responsible for Body Extension and Stabilization in Sit-to-Stand Motion. *Frontiers in Neuroscience*, *12*, 1042. https://doi.org/10.3389/fnins.2018.01042

Yoshioka, S., Nagano, A., Hay, D. C., & Fukashiro, S. (2009). Biomechanical analysis of the relation between movement time and joint moment development during a sit-to-stand task. *BioMedical Engineering OnLine*, *8*(1), 27. https://doi.org/10.1186/1475-925X-8-27

Zattara, M., & Bouisset, S. (1988). Posturo-kinetic organisation during the early phase of voluntary upper limb movement. 1. Normal subjects. *Journal of Neurology, Neurosurgery & Psychiatry*, *51*(7), 956–965. https://doi.org/10.1136/jnnp.51.7.956

Zelik, K. E., La Scaleia, V., Ivanenko, Y. P., & Lacquaniti, F. (2014). Can modular strategies simplify neural control of multidirectional human locomotion? *Journal of Neurophysiology*, *111*(8), 1686–1702. https://doi.org/10.1152/jn.00776.2013

Zhao, K., Zhang, Z., Wen, H., Wang, Z., & Wu, J. (2019). Modular Organization of Muscle Synergies to Achieve Movement Behaviors. *Journal of Healthcare Engineering*, *2019*, 1–9. https://doi.org/10.1155/2019/8130297

PART IV

APPENDIX

Supplementary Materials

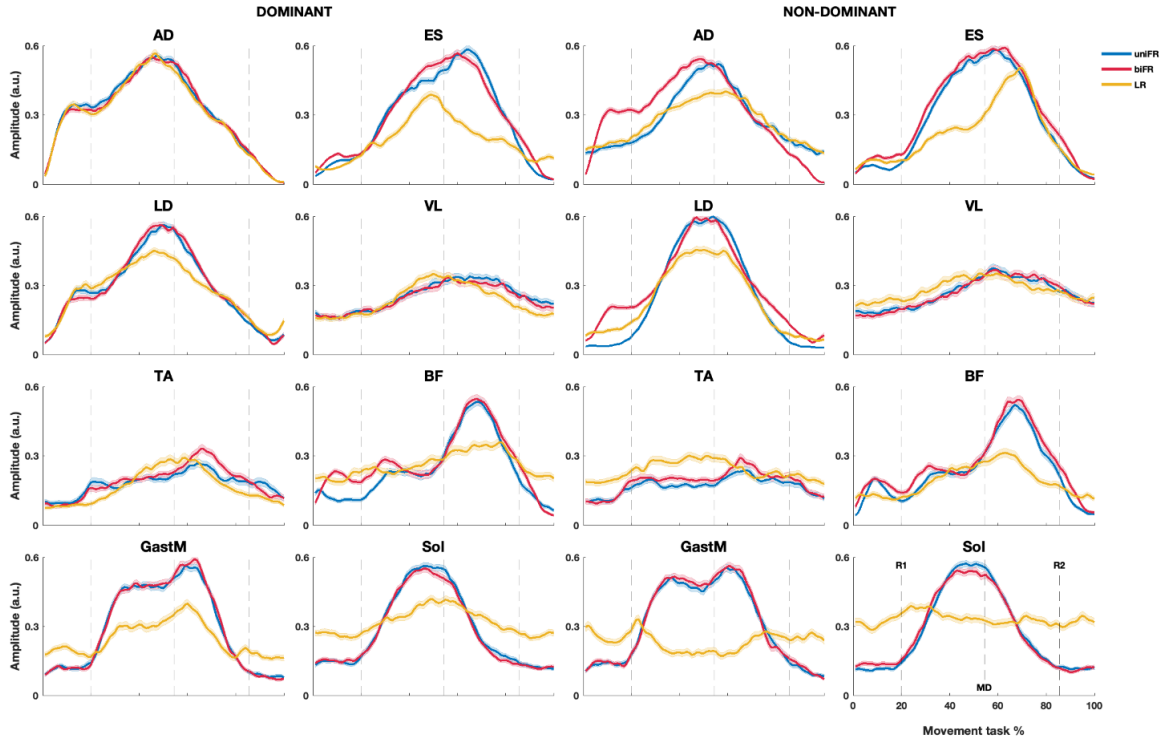

Figure S6.1. Average EMG envelopes (mean ± standard error) extracted during each reaching task (uniFR: unilateral Functional Reach; biFR: bilateral Functional Reach; LR: Lateral Reach). Each color represents a different motor task. Vertical dotted lines in the plots mark the reaching timings obtained by averaging the reaching events across the tasks. Muscles analyzed include: AD: Anterior Deltoid, ES: Erector Spinae, LD: Latissimus Dorsi, VL: Vastus Lateralis, TA: Tibialis Anterior, BF: Biceps Femoris, GastM: Gastrocnemius Medialis, Sol: Soleus. R1: End of arm elevation and start reaching; MD: Maximum distance reached and start of arm returning; R2: Stop of arm returning and start of arm lowering.

Assessment of Rectification Effects on Coherence Estimation

To evaluate the influence of rectification on coherence estimation, we performed a sensitivity analysis based on two alternative preprocessing approaches: coherence computed from Hilbert-derived envelopes following the procedure of Myers et al. (2003), and coherence computed from unrectified EMG signals that were only high-pass filtered at 10 Hz prior to analysis. For each muscle pair and task, intermuscular coherence was estimated from either the analytic signal (Hilbert) or the unrectified high-pass filtered signal, thereby bypassing the rectification step. Representative results are presented in **Figures S7.1** and **S7.2**. Both

approaches preserved the low-frequency features and task-dependent modulations observed in the rectified-signal analysis, with delta-band coherence remaining clearly expressed. This persistence supports the interpretation that the reported low-frequency coherence reflects genuine shared neural input rather than preprocessing artefacts.

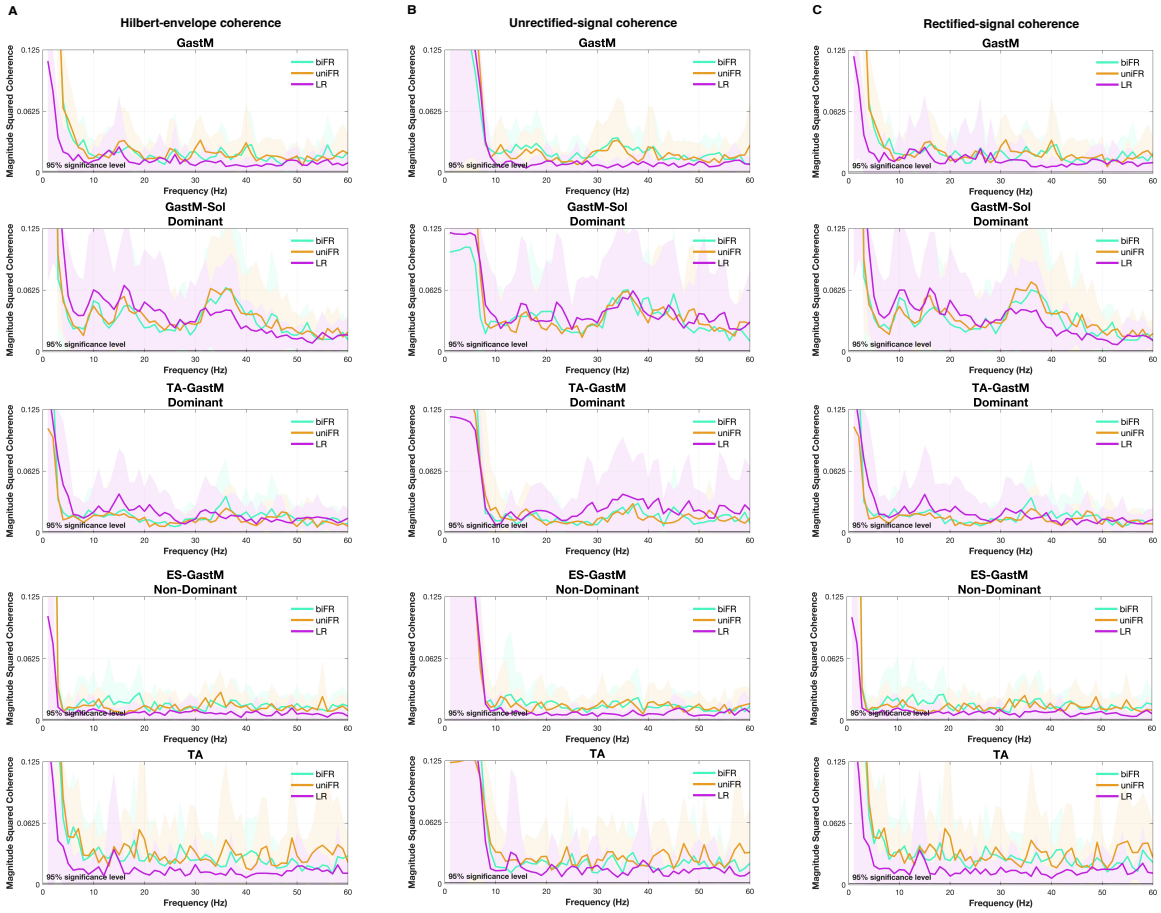

Figure S7.1. Comparison of intermuscular coherence estimates obtained using different EMG preprocessing approaches. Panel (**A**) shows coherence computed from Hilbert-derived EMG envelopes as part of the rectification sensitivity analysis. Panel (**B**) shows coherence estimated from unrectified EMG signals that were only high-pass filtered at 10 Hz prior to analysis. Panel (**C**) reports coherence computed from rectified EMG signals, corresponding to the main analysis presented in the thesis. For each panel, representative coherence spectra are shown for selected muscle pairs across tasks. Muscles include gastrocnemius medialis (GastM), soleus (Sol), tibialis anterior (TA), and erector spinae (ES). Curves correspond to bilateral Functional Reach (biFR, aqua green), unilateral Functional Reach (uniFR, ochre), and Lateral reach (LR, purple). Solid lines represent group-averaged magnitude-squared coherence, shaded areas indicate the standard deviation across participants, and the horizontal dashed line denotes the 95% significance threshold.

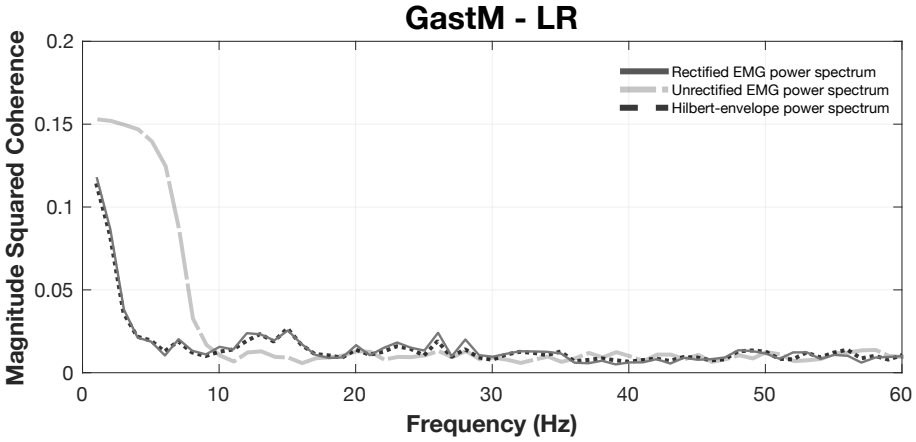

Figure S7.2. Power spectra of the gastrocnemius medialis (GastM) EMG signal during the Lateral reach (LR) task, computed using three different preprocessing approaches: rectified EMG (solid dark grey line), unrectified EMG (solid light grey line), and Hilbert-derived EMG envelope (dashed black line). Spectra are shown as magnitude squared coherence across frequencies (0–60 Hz) to illustrate the effect of EMG preprocessing on spectral content.

Surrogate-based validation of trunk-limb muscle pairs coherence

For every muscle pair that included the ES (ES–TA, ES–GastM, and ES–Sol, on both the dominant and non-dominant sides), a surrogate coherence spectrum was estimated between the ES EMG signal from one participant and a corresponding ankle EMG signal randomly selected from another participant, guaranteeing that there was no shared neural influence. This procedure was repeated 17 times for each muscle pair to create a surrogate dataset that corresponded to the number of subjects recorded, facilitating a direct comparison with the experimental coherence estimates. To enhance the robustness of the surrogate analysis, this procedure was further extended by repeating the random pairing process 100 times for each muscle pair. Surrogate coherence spectra were calculated using the same spectral parameters that were used for the experimental coherence analysis. Statistical significance benchmarks were applied to each of the 100 surrogate coherence spectra, and the results were subsequently averaged to obtain a stable reference distribution for each muscle pair. This approach enabled the evaluation of whether the observed ES–ankle muscle coherence reflected true functional coupling or could instead be attributed to spurious synchrony.

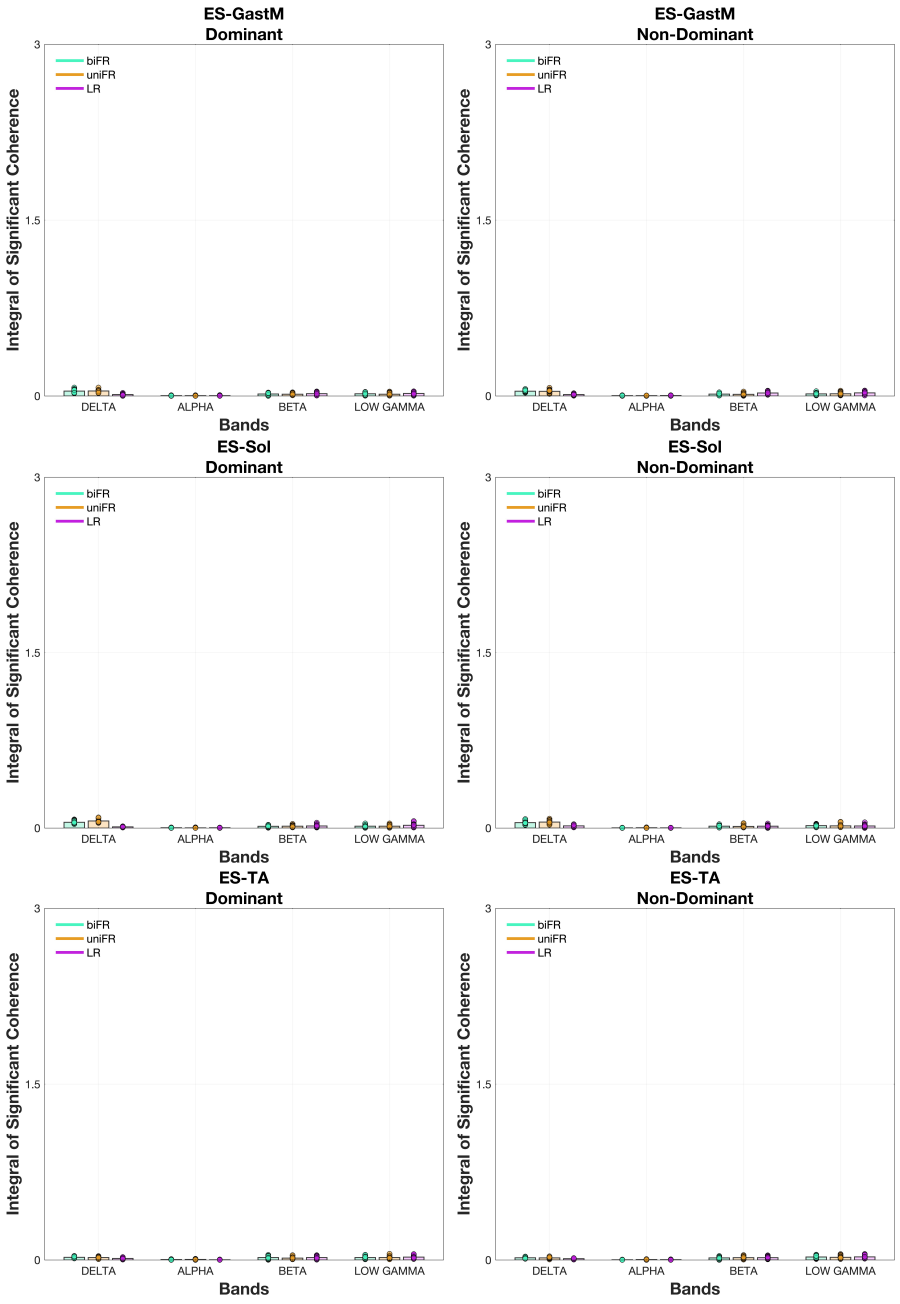

Figure S7.3. Mean ± standard deviation of surrogate intermuscular coherence values computed for erector spinae (ES)–ankle muscle pairs. Upper panels show results for the erector spinae–gastrocnemius medialis (ES–GastM) muscle pair, middle panels for the erector spinae–soleus (ES–Sol) muscle pair, and lower panels for the erector spinae–tibialis anterior (ES–TA) muscle pair. For each muscle pair, data are presented separately for the dominant (left panels) and non-dominant (right panels) sides, across the delta, alpha, beta, and low gamma frequency bands. Data are shown for the three Functional Reach conditions: bilateral Functional Reach (biFR, aqua green), unilateral Functional Reach (uniFR, ochre), and Lateral Reach (LR, purple). Individual data points are overlaid on the group means.

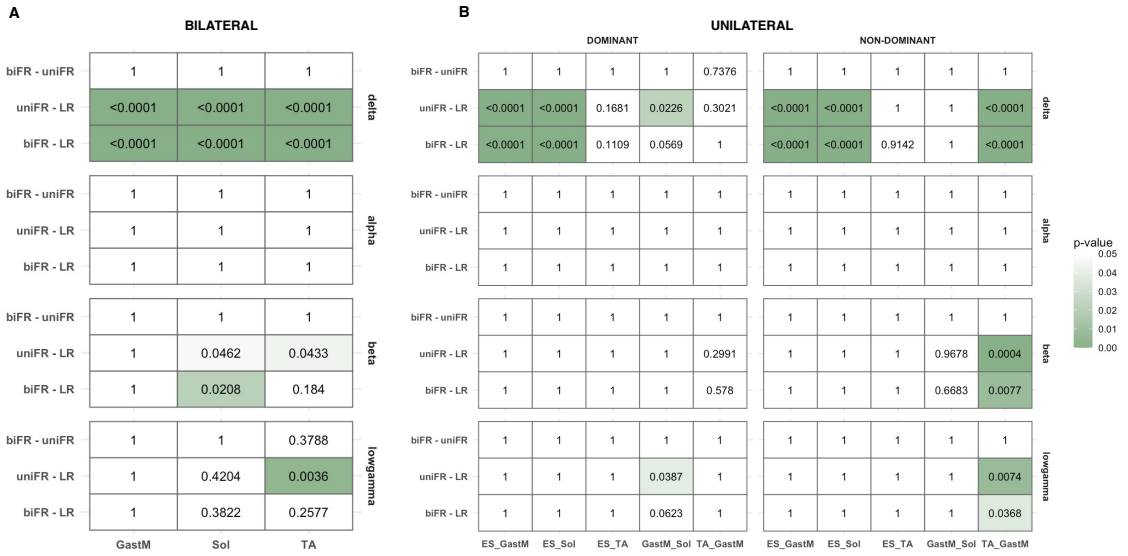

Figure S7.4. Heatmaps of p-values for pairwise comparisons between Functional Reach tasks—bilateral Functional Reach (biFR), unilateral Functional Reach (uniFR), and Lateral Reach (LR)—across frequency bands, muscle pairs, and dominance sides. Panel A shows results for bilateral intermuscular coherence, while panel B shows results for unilateral intermuscular coherence, reported separately for the dominant and non-dominant sides. Color intensity reflects the magnitude of the p-values, with darker shades indicating lower values. Statistically significant differences ($p < 0.05$, Bonferroni-corrected) are highlighted.

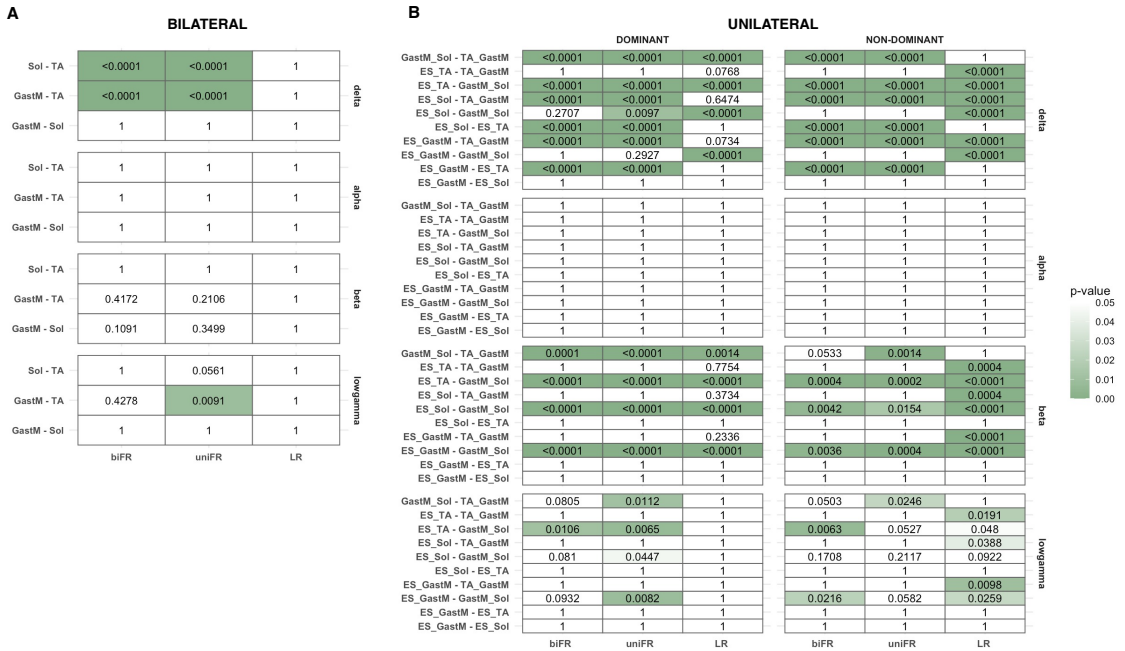

Figure S7.5. Heatmaps of p-values for pairwise comparisons between muscle pairs across frequency bands, Functional Reach tasks, and dominance sides. Comparisons are shown for bilateral Functional Reach (biFR), unilateral Functional Reach (uniFR), and Lateral Reach (LR). Panel A shows results for bilateral intermuscular coherence, while panel B shows results for unilateral intermuscular coherence, reported separately for the dominant and non-dominant sides. Color intensity reflects the magnitude of the p-values, with darker shades indicating lower values. Statistically significant differences ($p < 0.05$, Bonferroni-corrected) are highlighted.

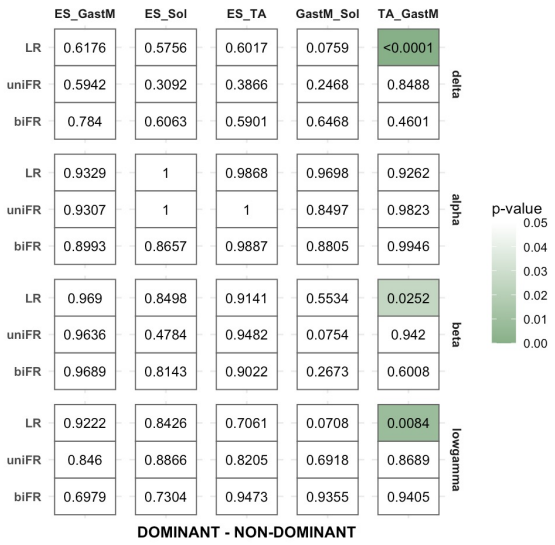

Figure S7.6. Heatmap of p-values for pairwise comparisons between dominant and non-dominant sides (dominant – non-dominant) across frequency bands and muscle pairs. Results are shown separately for the Functional Reach tasks—bilateral Functional Reach (biFR), unilateral Functional Reach (uniFR), and Lateral Reach (LR). Each cell reports the p-value of the dominant–non-dominant contrast for a given task and muscle pair. Color intensity reflects the magnitude of the p-values, with lower values indicated by darker shading. Statistically significant differences ($p < 0.05$, Bonferroni-corrected) are highlighted in green.

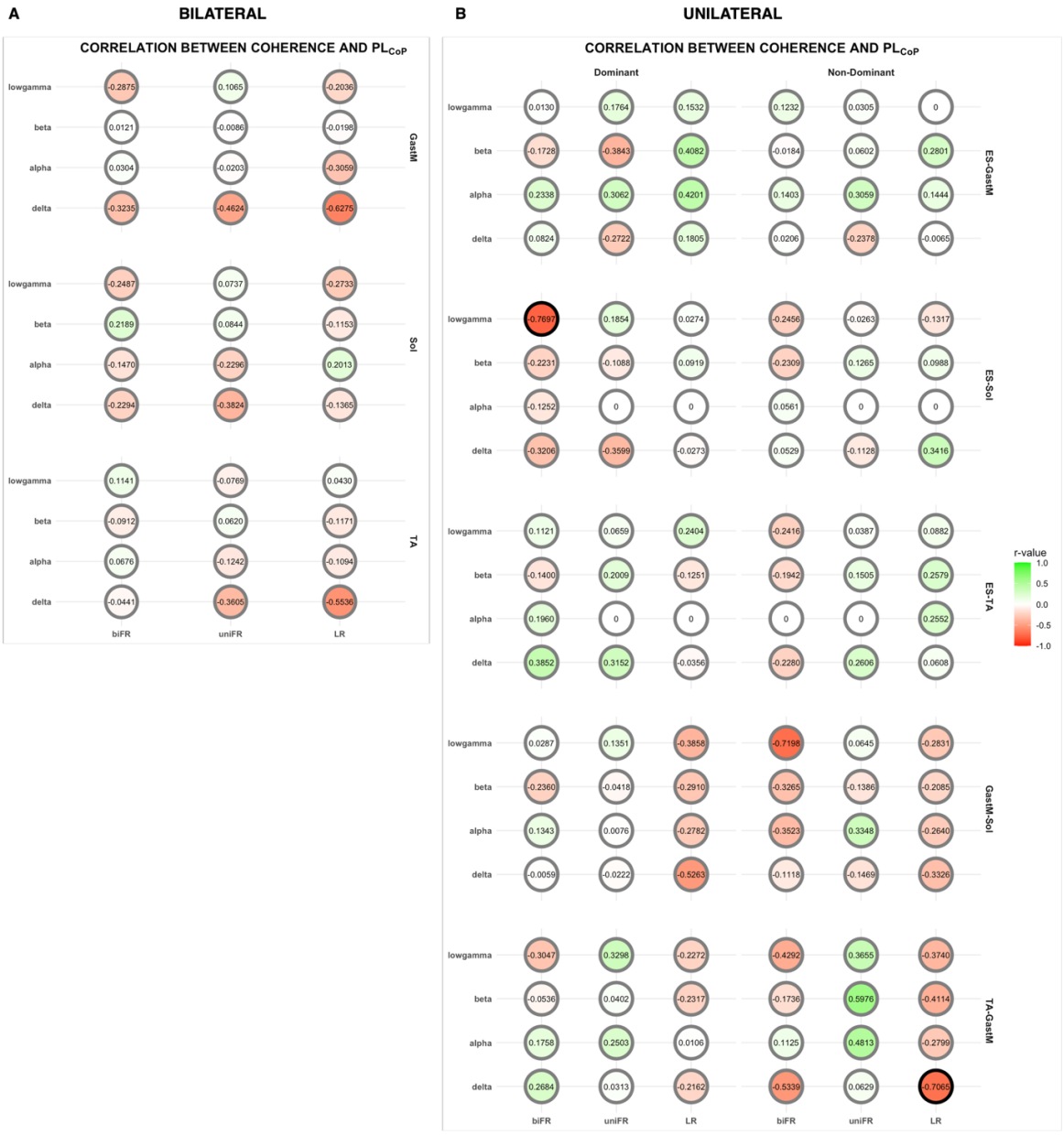

Figure S7.7. Heatmaps of Spearman's correlation coefficients (r) between intermuscular coherence and the center of pressure path length (PL_{CoP}) across frequency bands, Functional Reach tasks, and muscle pairs. Panel A shows correlations obtained from the bilateral coherence analysis, while panel B reports results for unilateral coherence, presented separately for the dominant and non-dominant sides. Each circle represents the correlation coefficient for a given task—bilateral Functional Reach (biFR), unilateral Functional Reach (uniFR), and lateral Reach (LR)—and frequency band (delta, alpha, beta, and low gamma). Circle color indicates the direction and magnitude of the association (green: positive; red: negative), while bold outlines denote statistically significant correlations ($p < 0.05$).

Figure S9.1. Violin plots illustrating the distribution of variance accounted for (VAF, %) values for extracted, reconstruction, and surrogate conditions in young (left panel) and older (right panel) adults. Extracted VAF refers to the variance explained by the participant-specific synergy set, reconstruction VAF to the variance obtained by projecting individual data onto the group-average synergy set, and surrogate VAF to the variance obtained using randomly generated surrogate W vectors. Black markers and error bars indicate the mean ± standard error.

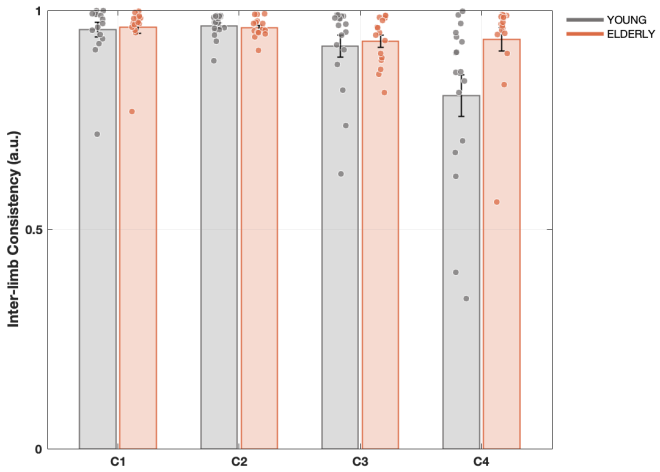

Figure S9.2. Inter-limb consistency across muscle synergies in Young and Elderly groups. Bar plots show mean inter-limb consistency values (± SE) for each synergy (C1–C4) in the Young (grey) and Elderly (orange) groups. Individual subject values are overlaid as filled circles. Values range from 0 to 1, with higher values indicating greater similarity in muscle weighting across limbs. Across all synergies, inter-limb consistency values were comparable between groups, and no statistically significant between-group differences were observed.

Table S11.1. Task-dependent pairwise comparisons between degrees of freedom (DoFs).

DoF	Contrast	Synergy	p_adjust	Hedges_g
CSh	**biFR-uniFR**	1	6.19585738837863e-06	7.19402141412440
CSh	**biFR-LR**	1	0.00156772618537274	6.67492066864047
CSh	**uniFR-LR**	1	0.603727862873172	-0.558021001232528
ISh	**biFR-uniFR**	1	8.03556702762334e-05	-3.81564952772127
ISh	**biFR-LR**	1	0.00156772618537274	-3.28440340575070

ISh	**uniFR-LR**	1	1	0.144137059319134
Sp1	**biFR-uniFR**	1	1	-0.0357581580264474
Sp1	**biFR-LR**	1	0.133829154074819	1.02828814500366
Sp1	**uniFR-LR**	1	0.203667464585487	0.916024481128401
Sp2	**biFR-uniFR**	1	1	-0.192998711303404
Sp2	**biFR-LR**	1	1.50309958691713e-05	-2.84787733890564
Sp2	**uniFR-LR**	1	0.000782188898565950	-2.73777632212637
CH1	**biFR-uniFR**	1	0.0185096979616325	0.966320252068613
CH1	**biFR-LR**	1	3.53140172928450e-05	2.46095500804567
CH1	**uniFR-LR**	1	0.301044739386872	1.34551393154078
CH2	**biFR-uniFR**	1	1	0.0553526853205523
CH2	**biFR-LR**	1	0.0317614120021708	-1.12730215526887
CH2	**uniFR-LR**	1	0.0528662728869734	-1.11006016194827
IH1	**biFR-uniFR**	1	0.0853792107489317	0.869776408441577
IH1	**biFR-LR**	1	0.000378139350362441	2.01565027886598
IH1	**uniFR-LR**	1	0.301044739386872	1.17841492021720
IH2	**biFR-uniFR**	1	1	-0.114353093284042
IH2	**biFR-LR**	1	0.0317614120021708	-1.28047354097118
IH2	**uniFR-LR**	1	0.0528662728869734	-1.13194916637428
CK1	**biFR-uniFR**	1	1	-0.0497503314376920
CK1	**biFR-LR**	1	1	-0.285294012303013
CK1	**uniFR-LR**	1	1	-0.220668171612186
IK1	**biFR-uniFR**	1	1	-0.138204516974866
IK1	**biFR-LR**	1	0.432381104448046	-0.162035560959158
IK1	**uniFR-LR**	1	1	-0.0396116740096339
CA1	**biFR-uniFR**	1	1	0.249012035423885
CA1	**biFR-LR**	1	0.301044739386873	0.665364337983533
CA1	**uniFR-LR**	1	0.819965034876894	0.539715345070346
IA1	**biFR-uniFR**	1	0.301044739386873	0.604366329523130
IA1	**biFR-LR**	1	0.0185096979616325	1.31120294140372
IA1	**uniFR-LR**	1	0.819965034876895	0.583115033995996
CSh	**biFR-uniFR**	2	8.03556702762334e-05	1.84232469976493
CSh	**biFR-LR**	2	0.203667464585487	1.08190659948267
CSh	**uniFR-LR**	2	0.0528662728869732	-1.07689890056037
ISh	**biFR-uniFR**	2	1	0.152328635594643
ISh	**biFR-LR**	2	0.791566259112816	-0.460588332286929
ISh	**uniFR-LR**	2	0.663809829993688	-0.498529255313287

Sp1	**biFR-uniFR**	2	0.839367608701258	-0.121598280379820
Sp1	**biFR-LR**	2	0.100903862703938	0.851226970024726
Sp1	**uniFR-LR**	2	0.0485048648018698	0.950541421312683
Sp2	**biFR-uniFR**	2	0.0528662728869734	-2.38265906687993
Sp2	**biFR-LR**	2	3.57731005632503e-07	-9.78142166688069
Sp2	**uniFR-LR**	2	0.0104610146764241	-8.94900365974904
CH1	**biFR-uniFR**	2	0.301044739386873	-0.442989864760190
CH1	**biFR-LR**	2	0.00304500284133920	6.17104874682377
CH1	**uniFR-LR**	2	2.47317187146507e-06	7.68619172824899
CH2	**biFR-uniFR**	2	0.432381104448046	-0.0547280807342183
CH2	**biFR-LR**	2	0.000177107341487640	-1.39168590907312
CH2	**uniFR-LR**	2	0.0317614120021709	-1.37589820183984
IH1	**biFR-uniFR**	2	0.133829154074819	-0.461048175749870
IH1	**biFR-LR**	2	0.00573232541209332	4.58011134899002
IH1	**uniFR-LR**	2	9.55906638854072e-07	5.42099701138457
IH2	**biFR-uniFR**	2	1	-0.0404224724350967
IH2	**biFR-LR**	2	0.000177107341487639	-1.42993131250058
IH2	**uniFR-LR**	2	0.00573232541209332	-1.43823651491001
CK1	**biFR-uniFR**	2	0.603727862873172	-0.0997214002280468
CK1	**biFR-LR**	2	1	-0.667737790043830
CK1	**uniFR-LR**	2	1	-0.559248333898915
IK1	**biFR-uniFR**	2	0.603727862873172	-0.201667847158094
IK1	**biFR-LR**	2	0.00573232541209331	-0.765289287702780
IK1	**uniFR-LR**	2	0.203667464585487	-0.571684606978767
CA1	**biFR-uniFR**	2	1	0.255260508251602
CA1	**biFR-LR**	2	0.0104610146764241	1.81692197070478
CA1	**uniFR-LR**	2	0.133829154074819	1.62398494586068
IA1	**biFR-uniFR**	2	1	0.0769963066592025
IA1	**biFR-LR**	2	9.54140502796204e-05	2.05987036478502
IA1	**uniFR-LR**	2	7.42594505302635e-05	2.03077978199021

Summary of the pairwise comparisons between degrees of freedom (DoFs) for each synergy and task comparison. The table reports the *p*-values (Bonferroni-corrected) and Hedges' *g* effect sizes for all pairwise contrasts. Significant *p*-values ($p < 0.05$) are highlighted in red.

Table S11.2. Pairwise statistical comparisons of cosine similarity (CS) values across tasks for each kinematic synergy.

Contrast	Synergy	p_adjust	Hedges_g
biFR-uniFR	1	1	0.129151178909500

biFR-LR	1	1	0.0551151202933061
uniFR-LR	1	1	-0.0255113082343128
biFR-uniFR	2	1	0.0398020456850410
biFR-LR	2	1.49825065285231e-07	0.647035715086195
uniFR-LR	2	3.05684786934568e-08	0.649824521389090

The table reports *p*-values (Bonferroni-corrected) and Hedges' *g* effect sizes for all task contrasts (biFR–uniFR, biFR–LR, uniFR–LR). Significant *p*-values ($p < 0.05$) are highlighted in red.

MATLAB GUI Code

```
classdef UNPLANNED_TRIGGERBOX < matlab.apps.AppBase

    % Properties that correspond to app components
    properties (Access = public)
        UIFigure                    matlab.ui.Figure
        ImmaCerielloLabel           matlab.ui.control.Label
        DIRECTIONLabel              matlab.ui.control.Label
        Image3                      matlab.ui.control.Image
        RestoreFigureButton         matlab.ui.control.Button
        Image2                      matlab.ui.control.Image
        STIMULUSButton              matlab.ui.control.Button
        CONNECTIONTOTRIGGERBOXButton   matlab.ui.control.Button
        UnplannedFunctionalReachLabel  matlab.ui.control.Label
        Image                       matlab.ui.control.Image
    end

    properties (Access = public)
        Property % Description
        secondwindow;
        imagetoshow;
        dq;
    end

    % Callbacks that handle component events
    methods (Access = private)

        % Code that executes after component creation
        function startupFcn(app)
            app.secondwindow = uifigure;
%           p = get(0, "MonitorPositions");
            app.secondwindow.Units = "normalized";
%           app.secondwindow.Position=p(2, :); %second display
            app.secondwindow.WindowState = "fullscreen"; % "maximized" sul secondo schermo così funziona anche la
chiusura delle finestre
            app.secondwindow.Color="k";
        end

        % Button pushed function: RestoreFigureButton
        function RestoreFigureButtonPushed(app, event)
            gl = uigridlayout(app.secondwindow,[1 1]);
            gl.BackgroundColor = "k";
        end

        % Button pushed function: CONNECTIONTOTRIGGERBOXButton
        function CONNECTIONTOTRIGGERBOXButtonPushed(app, event)
            fprintf( 'Connecting to Trigger Box...' );
            d=daqlist("ni");
            deviceInfo=d{1,"DeviceInfo"};
            app.dq=daq("ni");
            %Add channels
```

```
            [~,~]=addinput(app.dq,"TriggerBox","port1/line0","Digital");
            [~,~]=addinput(app.dq,"TriggerBox","port1/line1","Digital");
            app.dq.Channels
            fprintf( 'done\n' );
        end

        % Button pushed function: STIMULUSButton
        function STIMULUSButtonPushed(app, event)
            Message=msgbox('Reading Data','Data from TriggerBox','Icon','info');
            idx=1;
            while ishandle(Message)
                drawnow;
                tabledata=read(app.dq); %read the data
                port1_0=timetable2table(tabledata(1,1));
                port1_1=timetable2table(tabledata(1,2));

                P1_0(idx,1)=table2array(port1_0(1,2));
                P1_1(idx,1)=table2array(port1_1(1,2));

                if P1_1(idx,1) == 0 %fai quello che c'è scritto qui sotto
                    gl = uigridlayout(app.secondwindow,[1 1]);
                    gl.BackgroundColor = [0.98,1.00,1.00];
                    im = uiimage(gl);
                    im.ImageSource = [cd,filesep, app.imagetoshow];
                    im.ScaleMethod = 'fit';
%                    elseif P1_1(idx,1) == 0
%                        gl = uigridlayout(app.secondwindow,[1 1]);
%                        gl.BackgroundColor = "k";
                end
                idx=idx+1;
            end
        end

        % Image clicked function: Image, Image2, Image3
        function ImageClicked(app, event)
            switch event.Source
                case app.Image % Execution code related to Image
                    app.imagetoshow=app.Image.ImageSource;
                    disp(app.imagetoshow);
                case app.Image2 % Execution code related to Image2
                    app.imagetoshow=app.Image2.ImageSource;
                    disp(app.imagetoshow);
                case app.Image3 % Execution code related to Image3
                    app.imagetoshow=app.Image3.ImageSource;
                    disp(app.imagetoshow);
            end
        end

    end

    % Component initialization
    methods (Access = private)

        % Create UIFigure and components
        function createComponents(app)

            % Create UIFigure and hide until all components are created
            app.UIFigure = uifigure('Visible', 'off');
            app.UIFigure.Color = [0.9804 1 1];
            app.UIFigure.Position = [100 100 664 519];
            app.UIFigure.Name = 'MATLAB App';

            % Create UnplannedFunctionalReachLabel
            app.UnplannedFunctionalReachLabel = uilabel(app.UIFigure);
            app.UnplannedFunctionalReachLabel.HorizontalAlignment = 'center';
```

```
4481            app.UnplannedFunctionalReachLabel.FontSize = 45;
4482            app.UnplannedFunctionalReachLabel.FontWeight = 'bold';
4483            app.UnplannedFunctionalReachLabel.Position = [14 438 638 60];
4484            app.UnplannedFunctionalReachLabel.Text = 'Unplanned Functional Reach';
4485
4486            % Create CONNECTIONTOTRIGGERBOXButton
4487            app.CONNECTIONTOTRIGGERBOXButton = uibutton(app.UIFigure, 'push');
4488            app.CONNECTIONTOTRIGGERBOXButton.ButtonPushedFcn = createCallbackFcn(app,
4489    @CONNECTIONTOTRIGGERBOXButtonPushed, true);
4490            app.CONNECTIONTOTRIGGERBOXButton.BackgroundColor = [0.0941 0.851 0.0941];
4491            app.CONNECTIONTOTRIGGERBOXButton.FontSize = 20;
4492            app.CONNECTIONTOTRIGGERBOXButton.FontWeight = 'bold';
4493            app.CONNECTIONTOTRIGGERBOXButton.Position = [63 309 320 77];
4494            app.CONNECTIONTOTRIGGERBOXButton.Text = {'CONNECTION TO'; ' TRIGGERBOX'};
4495
4496            % Create STIMULUSButton
4497            app.STIMULUSButton = uibutton(app.UIFigure, 'push');
4498            app.STIMULUSButton.ButtonPushedFcn = createCallbackFcn(app, @STIMULUSButtonPushed, true);
4499            app.STIMULUSButton.BackgroundColor = [1 1 0.0667];
4500            app.STIMULUSButton.FontSize = 20;
4501            app.STIMULUSButton.FontWeight = 'bold';
4502            app.STIMULUSButton.Position = [442 330 165 34];
4503            app.STIMULUSButton.Text = 'STIMULUS ';
4504
4505            % Create Image
4506            app.Image = uiimage(app.UIFigure);
4507            app.Image.ImageClickedFcn = createCallbackFcn(app, @ImageClicked, true);
4508            app.Image.Tag = 'forward';
4509            app.Image.Position = [174 87 100 100];
4510            app.Image.ImageSource = 'Forward.png';
4511
4512            % Create Image2
4513            app.Image2 = uiimage(app.UIFigure);
4514            app.Image2.ImageClickedFcn = createCallbackFcn(app, @ImageClicked, true);
4515            app.Image2.Tag = 'lateraldx';
4516            app.Image2.Position = [283 87 100 100];
4517            app.Image2.ImageSource = 'Lateraldx.png';
4518
4519            % Create Image3
4520            app.Image3 = uiimage(app.UIFigure);
4521            app.Image3.ImageClickedFcn = createCallbackFcn(app, @ImageClicked, true);
4522            app.Image3.Tag = 'lateralsx';
4523            app.Image3.Position = [63 87 103 100];
4524            app.Image3.ImageSource = 'Lateralsx.png';
4525
4526            % Create RestoreFigureButton
4527            app.RestoreFigureButton = uibutton(app.UIFigure, 'push');
4528            app.RestoreFigureButton.BackgroundColor = [0.302 0.7451 0.9333];
4529            app.RestoreFigureButton.FontSize = 16;
4530            app.RestoreFigureButton.FontWeight = 'bold';
4531            app.RestoreFigureButton.Position = [453 117 144 41];
4532            app.RestoreFigureButton.Text = 'Restore Figure';
4533            app.RestoreFigureButton.ButtonPushedFcn = createCallbackFcn(app, @RestoreFigureButtonPushed, true);
4534
4535            % Create DIRECTIONLabel
4536            app.DIRECTIONLabel = uilabel(app.UIFigure);
4537            app.DIRECTIONLabel.HorizontalAlignment = 'center';
4538            app.DIRECTIONLabel.FontSize = 24;
4539            app.DIRECTIONLabel.FontWeight = 'bold';
4540            app.DIRECTIONLabel.Position = [154 212 139 31];
4541            app.DIRECTIONLabel.Text = 'DIRECTION';
4542
4543            % Create ImmaCerielloLabel
4544            app.ImmaCerielloLabel = uilabel(app.UIFigure);
4545            app.ImmaCerielloLabel.HorizontalAlignment = 'center';
```

```
            app.ImmaCerielloLabel.FontSize = 10;
            app.ImmaCerielloLabel.Position = [596 1 67 14];
            app.ImmaCerielloLabel.Text = 'Imma Ceriello';

            % Show the figure after all components are created
            app.UIFigure.Visible = 'on';
            app.UIFigure.CloseRequestFcn = @app.closeAPP;
        end
    end

    % App creation and deletion
    methods (Access = public)

        % Construct app
        function app = UNPLANNED_TRIGGERBOX

            % Create UIFigure and components
            createComponents(app)

            % Register the app with App Designer
            registerApp(app, app.UIFigure)

            % Execute the startup function
            runStartupFcn(app, @startupFcn)

            if nargout == 0
                clear app
            end
        end

        function closeAPP(app,src,event)
            selection = uiconfirm(app.UIFigure,'Close the APP?',...
                'Confirmation');

            switch selection
                case 'OK'
                    all_fig = findall(0, 'type', 'figure');
                    delete(all_fig)
                case 'Cancel'
                    return
            end
        end
    end
end
```

List of Related Publications and Conference Abstracts

Journal Articles

I. Ceriello, M. Ghislieri, L. Rum, V. Camomilla, A. Macaluso, and R. Borzuola,"Muscle coordination strategies during functional reach across multiple directions in healthy individuals", European Journal of Applied Physiology, pp. 1–19, 08 2025. https://doi.org/10.1007/s00421-025-05951-7 [Published]

I. Ceriello, S. Ranaldi, G. Severini, V. Camomilla, A. Macaluso, and R. Borzuola, "Modular Motor Control of the Center of Mass Kinematic Patterns during Sit-to-Stand Tasks". 2025 12th

International IEEE/EMBS Conference on Neural Engineering (NER), San Diego, CA, USA, 2025. In press.

I. Ceriello, R. Borzuola, V. Camomilla, A. Macaluso, and M. Lowery, "Task-Dependent Intermuscular Coherence between Postural Muscles during Voluntary Upright Reaching", Experimental Physiology. In press [Accepted 2 January 2026]

I. Ceriello, S. Ranaldi, V. Camomilla, A. Macaluso, and R. Borzuola," Age-Dependent Synergistic Control of Sit-to-Stand Motion". [Submitted to the European Journal of Applied Physiology]

Conference Abstracts

I. Ceriello, R. Borzuola, L. Rum, V. Camomilla, and A. Macaluso, "Directional variations in muscle coordination during functional reach". Abstracts of the 74th Congress of the Italian Society of Physiology, Rome, Italy, 11-13 September 2024. [Presented by I. Ceriello]

I. Ceriello, R. Borzuola, L. Rum, V. Camomilla, and A. Macaluso, "Investigating muscle coordination during dynamic functional reach assessment," Gait & Posture, vol. 114, p. S16, 2024. Abstracts of the 24th National Congress of SIAMOC, Stresa, Italy, 2-5 October 2024. 10.1016/j.gaitpost.2024.08.034. [Presented by I. Ceriello]

I. Ceriello, R. Borzuola, A. Macaluso, and V. Camomilla, "Impact of Hip Joint Centre Estimation on Lower Limb Kinematics During Functional Reach: A Comparison of CGM2 and PiG Models". Abstracts of the 18th International Symposium on 3D Analysis of Human Movement (3DAHM 2024), Montevideo, Uruguay, on December 3–6, 2024. [Presented by V. Camomilla]

I. Ceriello, R. Borzuola, V. Camomilla, A. Macaluso, and M. Lowery, "Intermuscular coherence in plantar- and dorsiflexor muscles during standing reaching tasks". Abstracts of the 75th Congress of the Italian Society of Physiology, Turin, Italy, 17-19 September 2025. [Presented by I. Ceriello]

I. Ceriello, R. Borzuola, V. Camomilla, A. Macaluso, and M. Lowery, "Intermuscular Coherence during Upright Reaching Tasks". Abstracts of the 25th National Congress of SIAMOC, Cagliari, Italy, 1-4 October 2025. [Presented by I. Ceriello]

I. Ceriello, S. Ranaldi, R. Borzuola, V. Camomilla, and A. Macaluso, “Bilateral Muscle Synergies During the 30-Second Sit-to-Stand Test”. Gait & Posture, Volume 122, Supplement, 2025, https://doi.org/10.1016/j.gaitpost.2025.08.006. Abstracts of the 25th National Congress of SIAMOC, Cagliari, Italy, 1-4 October 2025. [Presented by I. Ceriello]

I. Bufacchi, I. Ceriello, R. Borzuola, and V. Camomilla, “Organizing Degrees of Freedom through Kinematic Synergies in Functional Reaching”. Abstracts of the 25th National Congress of SIAMOC, Cagliari, Italy, 1-4 October 2025. [Presented by I. Bufacchi]

I. Ceriello, S. Ranaldi, G. Severini, V. Camomilla, A. Macaluso, and R. Borzuola, “Modular Motor Control of the Center of Mass Kinematic Patterns during Sit-to-Stand Tasks”. 12th Annual International Conference on Neural Engineering, San Diego, California, 11-14 November 2025. [Presented by I. Ceriello]

I. Ceriello, M. Ghislieri, V. Camomilla, A. Macaluso, and R. Borzuola, “Compensatory Neuromuscular Reorganization with Aging Revealed Through Muscle Synergies in Voluntary Upright Reaching”. Submitted to the ISEK XXVI Congress, Jyväskylä, Finland, June 24–27, 2026.

LIST OF FIGURES

LIST OF TABLES